STRUCTURAL PERFORMANCE OF BOX BASED CROSS LAMINATED TIMBER SYSTEM USED IN FLOOR APPLICATIONS

by

Yue Chen

B.A.Sc., Shanghai Jiao Tong University, China, 1999
M.A.Sc, Shanghai Jiao Tong University, China, 2001
M.A.Sc, The University of British Columbia, 2004

A THESIS SUBMITTED IN PARTIAL FULFILLMENT OF THE REQUIREMENTS FOR THE DEGREE OF

DOCTOR OF PHILOSOPHY

in

The Faculty of Graduate Studies

(Forestry)

THE UNIVERSITY OF BRITISH COLUMBIA
(Vancouver)

April 2011

ABSTRACT

The current outbreak of Mountain Pine Beetle (MPB) in the province of British Columbia (B.C.) is the most extensive disturbance event occurring in North American forests in recorded history. The concept of converting the beetle killed wood into engineered wood products by defect removal and reconstitution is employed to maximize value recovery from the material. Cross Laminated Timber (CLT), which is produced in modular form and can be utilized as part of a structural system for floor, wall or roof elements, is considered as an excellent application of the concept. CLT originates from Europe. Such products have been developed as a proprietary product by individual companies aimed at servicing specific markets. There is a need to investigate different ways of making CLT and to define its structural performance suitable for North America. The main focus of this study is to investigate the structural performance of box based CLT system used in floor applications.

Comprehensive three dimensional finite element models, which can be used to analyze the mechanical and vibration behavior of the plate and box type structures, were developed. Four prototype box elements, each having five replicates, were designed and manufactured locally. Third point bending tests were conducted on the specimens in the Timber Engineering and Applied Mechanics (TEAM) Laboratory at the University of British Columbia. The numerical analysis agreed well with experimental data in terms of vertical deflection and bending stiffness. Vibration, which is critical to floor serviceability, was also studied. Three types of excitation were applied to measure the fundamental frequency of the twenty specimens. Finite element analysis provided good predictions of fundamental frequency values comparing to the experimental results. A local built demonstration

building, L41home, was presented and analyzed as an example using the tools developed in this study for CLT applications.

As a pioneer research of CLT materials in North America, this work has contributed to the understanding of the structural performance of floor systems using CLT panels for the commercial and residential applications.

TABLE OF CONTENTS

LIST OF TABLES

LIST OF FIGURES

ACKNOWLEDGEMENTS

First and foremost, I would like to gratefully and sincerely thank my supervisors, Dr. Frank Lam and Dr. J. David Barrett, for their excellent guidance, encouragement, understanding, and support during my doctoral studies at the University of British Columbia. I feel very fortunate to be given the opportunity to explore the real beauty of timber engineering and truly enjoy working under their supervision. I would never have been able to finish my dissertation without their help. Also, I would like to thank Dr. Ricardo O. Foschi for his valuable suggestions and advice throughout my studies.

Thanks to members past and present of the Timber Engineering and Applied Mechanics group at UBC for their help and support over the years. Special thanks go to Mr. George Lee, Dr. Dominggus Yawalata, Mr. Larry Tong and Mr. Miao Hu for helping me with my test.

Thanks to the Forestry Innovation Investment Ltd. for providing financial support for this research work. Also, I want to thank CST Innovations Ltd. for the collaboration in terms of manufacturing CLT plate specimens.

Thanks to Professor Hans Joachim Blaß from Lehrstuhl für Ingenieurholzbau und Baukonstruktionen at Karlsruher Institut für Technologie (KIT) for the hosting and work collaboration during my research visitorship in Germany.

Last but not least, I would like to thank my family and friends for all their love and encouragement. For my parents who have been a constant source of emotional and moral support which is essential to me during the ups and downs of my graduate life. For my friends who are helping, supportive and on my side all the time.

To my parents

CHAPTER 1   INTRODUCTION

1.1 Background and objective

British Columbia (B.C.) is currently experiencing the largest Mountain Pine Beetle (MPB), *Dendroctonus ponderosae*, outbreak recorded in North American history (Figure 1-1). This ecosystem altering epidemic is causing widespread mortality of the lodgepole pine forest, the province's most abundant commercial tree species, and seriously damaging their ability to store carbon and protect against global warming. The extent of the epidemic in the interior of B.C. has passed the point where it is just a forestry issue. The Ministry of Forests and Range estimates that the cumulative area of B.C. affected (including red-attack and grey-attack) is about 16.3 million hectares which is more than four times the size of Vancouver Island (B.C. Ministry of Forests and Range, 2010).

Figure 1-1 Mountain pine beetle killed trees in B.C..

This epidemic has killed, and is killing the lodgepole pine trees much more quickly than they can be harvested. Depending on different local conditions, the dead timber is expected to remain its commercial value for 5-18 years. This is timber that the forest industry and forest dependent communities are relying upon for their longer-term future harvest, but the dead and dying trees must be recovered in a timely manner. The epidemic puts significant forest values at risk and threatens the stability and sustainability of forest ecosystems. In order to recover the greatest value from the dead timber before it burns or decays, the government encourages emerging and alternate timber processing and value-added industries to utilize the beetle killed wood that would otherwise be either chipped or used in low quality non-structural applications.

Thick cross laminated timber (CLT) elements in floor, wall, and roof components offer a significant new alternative for medium-rise timber buildings. These products could consume a significant quantity of beetle killed wood fibre for production of competitive and environmentally friendly construction materials. They have been developed to add value to the low quality wood. The concept is to convert the material into engineered wood products by defect removal and reconstitution. This alternative for building construction has already emerged during the past 10 years with good results. These products have been used in Austria (multi-storey family dwelling, Judenburg), in Germany (Canteen, Karlsruhe), in Switzerland (School, St. Peter), in the Scandinavian countries ("Vetenskapsstaden" multi-storey family dwelling, Stockholm, Sweden; "Kv. Lotsen" multi-storey office building, Ursviken, Sweden; one-family house, Ebeltoft, Denmark), and even in the Latin countries with a cultural tradition rather oriented towards brick and breeze block materials (Hotel, Kastelruph, Italy). It is very important to point out that Stadthaus – Murray Grove Tower, the nine-storey high-rise located in the London suburb of Hackney, is the tallest timber residential building in the world and has been assembled using CLT system.

The literature survey shows that humans are best suited to and feel most comfortable at certain humidity and temperatures. Excessively high or low humidity or temperatures cause discomfort (ANSI/ASHRAE 55, 1992; ASHRAE, 1997; Toftum et al., 1998; Rodriguez et al., 2000a; Rodriguez et al., 2000b; Hameury and Lundstrom, 2004). The use of massive wood structures leads to more freedom in dealing with the possibility to keep a comfortable indoor climate. This is because of the good dimensional stability of the cross laminated timber allows for more tolerance of moisture content variations within the wood material.

If MPB wood can be made into novel engineered wood products with the desirable cost structure and attributes, these products can help wood penetrate building sectors where performance is of prime importance. This includes low-rise commercial, industrial and multi-family residential building market in North America, Japan, and emerging markets such as China and Taiwan. There can be a pull through effect to help other wood products gain acceptance into the emerging markets where experience with wood structures is limited or lacking.

In order to introduce and promote thick laminated wood plate products to the North American building material market, it is very important to understand the characteristics of these structures and then provide advice on what should be considered during the design process to improve their performance and reduce cost. Experimental investigations can be a good strategy for critically examining the structure performance of CLT, but such experiments are time consuming, expensive and on occasions practically difficult to perform. In this situation, the use of computer aided numerical modeling can be a realistic scientific option. However, this option is only useful if the model is an accurate representation of the system. Therefore, the main objective of this study is to develop three dimensional finite element models, which can be used to analyze the mechanical and vibration behavior of thick laminated wood plate and box type structures using MPB wood, and verify the models by comparing predicted results with measured data obtained from experimental studies.

1.2 Introduction to the laminated wood plate products

Multi-layer timber plate products can be produced in a great variety of designs for specific uses. Each layer is composed of individual pieces of lumber, in which the grain of all members runs in the same direction. Different layers can all be oriented in one direction or in two or more different directions. The layer thickness may vary. Softwood is normally used. Species that are used in Germany, Austria and Switzerland are larch and white spruce and in Sweden, Norwegian spruce and Scots pine are commonly used. The connections between layers can be created using adhesives, nails, screws or dowels. Oak or other species may be chosen for visible surface layers to vary the visual appearance of the plate elements.

The most widely used multi-layer timber plate products are CLT which is manufactured using low-grade timber off-cuts, and then jointed in cross layers with either glue or mechanical connections. The manufacturing processes, combined with the effects of cross-lamination, minimize swelling and shrinkage, and give particularly stable timber elements.

1.2.1 History

The history of CLT goes back to the 1980's. Dröge and Stoy (1981) studied CLT as web-material of solid-web girder. Schickhofer (1994) presented rigid and flexible composite in area-covering laminated wood structures. In 1995, multi-storey residential buildings were built with a CLT material called Merk-Dickholz (MDH) from Finnforest Merk GmbH. In 1998, the first national technical approvals for CLT was approved by the Austrian Technical Approval (ÖTZ) authorities (Schickhofer and Hasewend, 2000). The term "Cross Laminated Timber (CLT)" was branded based on the German to English translation of "BrettSperrHolz" at the COST E5-Meeting in 2000 (Schickhofer, 2009). In the same year, CLT was approved for use in Germany on the basis of an expert's statement (Schickhofer and Hasewend, 2000). The first European Technical Approval (ETZ) for CLT was established in 2006 and in 2009, Technischen Universität Graz launched the CLT handbook (Schickhofer, 2009).

1.2.2 Applications

CLT can be employed in the construction of a wide variety of structural elements. A few examples are listed as follows (Contemporary timber construction, 2010),

- Structural and non-structural wall elements
- Multi-storey structures with or without concrete sub-structure
- Solid partitions with or without linings
- Floor/ceiling, parapet wall and roof elements

- Pre-insulated wall and roof cassettes
- Cantilevered floors/balconies
- Load bearing lift shafts
- Stairs

Depending on its intended use, CLT can be used for either visible or hidden construction applications. Elements from different manufacturers are supplied with either sanded or planed surfaces which can be used in natural color or color-treated. According to BS EN 13017-1 (2001), CLTs are divided into three classes, i.e. visible residential, visible industrial and standard grade, based on surface qualities. Visible residential grade is suitable for exposed internal use in residential and commercial structures; visible industrial grade is for exposed internal use in industrial structures; and standard grade is non-visible quality suitable for lining. Openings such as doors, windows, slots, and holes in the structural elements can be realized using common timber processing machines.

Combined with other engineered wood products, such as I-beams, Laminated Veneer Lumber (LVL) and Structural Plywood, CLT demonstrates great potential of serving as crucial elements in the construction of buildings made entirely from timber. Its applications are limited only by the imagination. As the market for and manufacture of CLT increases with the global demand for low-cost, sustainable and attractive residential and non-residential buildings, CLT's many possible applications will be revealed.

1.2.3 Advantages

1.2.3.1 Structure

CLT is comprised of adhesive bonded or mechanically connected, cross layered wood panels. An odd number of layers (3, 5, 7, 9…) are assembled cross-wise to guarantee structural integral stability and the arrangement of the lengthwise and crosswise wood members helps to increase dimensional stability considerably. In comparison to other commonly used timber construction materials, CLT offers completely new possibilities of load transfer. Load may not only be transferred in one direction (as is the case with columns, beams, etc.), but to all sides. This feature offers construction-relevant benefits and ensures problem-free connections. The large-scale components enable fast construction and lead to very few joints between the elements. The lack of joints results in better hermetic sealing, as well as lower heat transmission, water vapor diffusion, acoustic and fireproofing properties. Therefore, CLT presents new opportunities for architectural, residential or utility building projects. In addition, the high load-bearing property increases its popularity in the construction of bridges, carports, ancillary buildings, wood/concrete composite ceilings and in many other fields. This is a major factor for its success in the construction of detached and multi-tenant residential properties or in the construction of commercial and industrial premises.

1.2.3.2 Environment

Constructions move towards being carbon neutral as more wood is used. Harnessing the power of thermal mass, a CLT building reduces energy consumption for heating and cooling by 50 percent and coupled with Passive House Standards can achieve net-zero energy consumption in addition to potential for achieving negative carbon footprint. The term "passive house" refers to a specific energy standard, where a comfortable internal space temperature is achieved in a largely "passive" way with the free heat gains of solar irradiation through openings (windows, etc.) as well as the heat emissions of the occupants and household appliances. The rated useful life of a CLT house is about 100 years if interior and exterior finishing materials are properly chosen. At the end of the building's life, the CLT elements may be reused or recycled. Therefore, this material provides an asset value throughout its life cycle.

The CLT panels make a significant contribution towards lowering the building's carbon footprint. Taking the nine-storey Stadthaus in London as an example, the designers calculated that had the building been of conventional reinforced concrete construction, an additional 124 tonnes of carbon generated during construction. Adding this to the 188 tonnes of carbon sequestered (locked away) in the 900 m^3 of timber in the structure results in a total offset of 312 tonnes of carbon. This gain, combined with the building being better insulated and more airtight than the Building Regulations demand, convinced the local planning authority to grant a dispensation from the "Merton" rule that normally requires at least 10% of the energy used during occupation to be generated onsite. Thus, the designers avoided having an in-house combined heat and power plant or ground source heat pump (which would have occupied part of the basement) and left most of the roof space as an amenity (TRADA, 2009).

1.2.3.3 Economy

This new technology contributes to saving natural reserves of merchantable wood by using both sawmill wastes and wood stock that is not traditionally used in timber construction to produce CLT panels. Lumber qualities are often varied within the plate and species and lumber dimensions can also be changed to match the structural requirements of the laminations.

CLT is factory manufactured to exceptional levels of accuracy to ensure minimal defects and increase product quality while reducing construction time and cost. Depending on the strength, they can be processed with conventional timber processing machinery which is a decisive advantage in terms of construction. The construction elements, which are prefabricated and packed in factories, are delivered to sites in a suitable form for immediate placement. The panels are installed with a crane and lightweight power tools. On-site erection and assembly time is very short and the dependency on weather-related delays is considerably reduced due to the high degree of prefabrication. Site storage time prior to installation and/or operation can be reduced by just-in-time delivery scheduling. Still using the Stadthaus as an example, the entire building process of an equivalent concrete building was estimated to take 72 weeks, whereas the CLT solution required only 49 weeks. The erectors brought a large mobile crane, which eliminated the need for a tower crane that would normally be needed for a concrete structure. The four-man Austrian crew was on site three days a week and accomplished the entire superstructure erection in 27 working days, over nine weeks (TRADA, 2009). Therefore, CLT brought tremendous overall savings through a significant cut in the building program.

1.2.3.4 Utility

Compling with the strictest environmental and hygienic requirements, a CLT house could have walls, bridging and roofing made of 100% pure wood. A large number of adhesion bonds do not decrease moisture permeability of the structures through careful selection of the adhesive composition and bonding mode. The panel, which is almost uniform, has the same moisture permeability across its thickness.

While dominant in the homebuilding sector, the use of wood has been severely limited in large scale industrial/commercial/institutional (ICI) sector because of its flammability. CLT offers significant advantages in terms of fire protection compared to reinforced concrete or steel materials. In a fire, a charred layer forms around an undestroyed core which retains its load bearing capacity. It reduces the entry of oxygen and heat from outside and thus delays significantly the further spread of flame. For example, CLT panels from Binderholz Bausysteme GmbH, an Austrian CLT manufacturer, burned at a rate of 0.67 mm per minute and therefore the duration of the fire can be calculated. The excellent fire resistance property of CLT together with changes of the B.C. provincial building code to allow for wood-frame residential building of up to six storeys since April, 2009 has opened doors for the Canadian wood products industry to increase market share in the ICI sector of the construction industry.

1.2.3.5 Architectural design

CLT offers opportunities to use timber in situations where designers would otherwise choose traditional materials such as steel, concrete or masonry. Using CLT elements in construction drastically changes a traditional perception of architectural design of timber houses. CLT panels can be manufactured in various shapes and their construction properties allow for freedom of design, both in the building layout and style.

CLT panels are extremely versatile and perfectly compatible with steel, glass, aluminum and all conventional construction materials. With today's technology, research and the range of modern wooden products, it is possible to achieve delicate, transparent wooden construction with the best climatic conditions.

With the added components of wood windows, doors, floors, cabinets, etc., CLT constructions bring carbon-negative building solutions for the most forward-thinking architects from around the world.

1.2.4 Manufacturing process

1.2.4.1 Log cutting and drying

The boards are normally taken from the outer zone of the log where wood materials are often removed and wasted in the production of sawn timber.

Boards are dried to a moisture content of 12 ± 2 % before gluing. It is also important to adapt the moisture content to the intended service conditions because if the wood moisture content is very different from the relative humidity in the intended environment, deformations and stresses will occur. The moisture content is important for the end use and in some cases for the glue curing process because some adhesives cure through loss of or chemical reaction with water.

1.2.4.2 Lumber grading

Lumber grading is a complex process by which lumber is sorted into groups with ideally, similar appearance or structural properties in each group. The sorting of appearance products is quite different to the sorting used for structural products because of different set of criteria.

When lumber is used as a structural material in construction, it has to be strong enough, stiff enough, dry enough, etc. to meet the required performance levels. In Canada, a sophisticated system including different product standards, engineering design guidelines, government regulations, education, reviews, and check and balances have evolved over the years to help designers and builders determine what lumber they need for a specific building project, and what grade of lumber they are receiving. The main two methods of structural grading are visual grading and machine stress grading. Visual grading is based on the fact that mechanical properties of lumber differ from mechanical properties of clear wood because many growth characteristics affect properties and these characteristics can be seen and judged by eye. Growth characteristics, such as knots, slope of grain, checks and splits, shake, density, decay, heartwood and sapwood, pitch pockets and wane, are used to sort lumber into stress grades. In machine stress grading, lumber is passed through a machine which measures a property such as bending stiffness nondestructively and then assigns a grade on the basis of predetermined relationships between strength and stiffness.

Depending on the field of application, CLT panels can be built up using different grading classes. A wider range of board qualities can be used by employing low grade lumber for inner layers and higher grade pieces for highly stressed laminations at outer layers.

1.2.4.3 Finger jointing

To manufacture CLT panels in lengths beyond those commonly available for lumber, laminations must be made by end jointing lumber to the proper length. The most common end joint technique is finger jointing which consists of cutting finger profiles into the ends of wood pieces and joining them into longer pieces with an adhesive. Combined with careful grading and removal of bad defects, finger jointing is a good way to convert short wood lengths and low grade lumber into high performance and high value products. There are three main types of structural finger joints: vertical (finger profile visible on the wide face of lamination), horizontal (finger profile visible on the narrow face of lamination) and inclined at 45 degrees. The vertical profile, which is generally stronger than the horizontal profile under normal production conditions, is used for glued laminated timber; while the horizontal profile tends to be used for finger jointed lumber. Careful control at each stage of the process – determining lumber quality, cutting the joint, applying the adhesive, mating, applying end pressure, and curing – is crucial to produce consistent high strength joints. Just prior to manufacture, the ends of the lumber are inspected to ensure that there are no defects, such as knots or other features, that would impair joint strength. Then, joints are cut on both ends of the lumber with special knives. After application of adhesive, the joints in adjacent pieces of lumber are mated, and the adhesive is cured under pressure.

1.2.4.4 Planing

The assembly of laminations into CLT plates is another critical stage in manufacture. Laminations must be planed to strict tolerances in order to obtain clear, parallel, and gluable surfaces. In addition, surface cleanliness cannot be overlooked. Oil, grease, dirt, dust and even polluted air can contaminate a wood surface and prevent proper adhesion, which could lead to a low quality product. Therefore, industry production standards usually call for "same-day" machining and gluing. Freshly machining surfaces just before gluing is especially important for species high in resinous or oily extractives. This ensures that the final assembly will be rectangular and that the pressure will be applied evenly (Hoadley, 2000).

1.2.4.5 Connection

Connections, which are one of the most important, but least understood components in wood structures, provide continuity to the members and strength and stability to the system. Selection of a connection for a specific design application depends on the type of construction and the required strength capacity. Each connection must be designed to transmit forces adequately and provide satisfactory performance for the life of the structure without causing splitting, cracking, or excessive deformation of the wood members (ASCE, 1996). In CLT plate products, connections between different layers can be constructed using either mechanical fasteners or glue.

1.2.4.5.1 **Mechanical connection**

Mechanical connections in CLT panels consist of dowel type fasteners, such as nails, screws and wood dowels, which transmit either lateral or withdrawal loads. Lateral loads are transmitted by bearing stresses developed between the fastener and the wood members. Withdrawal loads are axial loads parallel to the fastener axis transmitted through friction or bearing to the wood materials (ASCE, 1996). Aluminum nails are a good option to avoid damaging cutting tools during machining structural elements from CLT panels.

1.2.4.5.2 **Glue connection**

Glue should be spread on the wood surface as evenly as possible, even though some degree of self-distribution will of course result when pressure is applied. Paint rollers and paint trays or glue application machines can be used. However, proper glue spreading can be difficult to control. Too little glue leads to a starved joint and a poor bond. A little excess glue can be tolerated, but too much results in wasteful and messy squeeze-out. Spreads are usually given in terms of pounds of glue per thousand square feet of single glue line, or MSGL (Hoadley, 2000). Usually adhesives based on polyurethane (PU), phenolic and melamine resins are applied.

Phenol Resorcinol Formaldehyde (PRF) adhesives are classified as thermosetting polymers and are produced by a condensation polymerization between formaldehyde, phenol and resorcinol (DGR Industrial Products Inc., 2010). They are dark red in color and are generally supplied in liquid form. A filled liquid or powdered hardener is added to the liquid prior to use. Because of their cost, they are used as assembly glues in solid wood products which must resist exposure to the weather and to water (Malanit, 2009).

Polyurethane adhesives can be classified either as thermoplastic or thermosetting polymers depending on how the adhesives are formulated. They are produced in many grades such as one-component, two-component, dispersion and solvent-based, for use in different application areas (Dynea, 2010).

- Face gluing

Pressure is applied after the adhesive is distributed on the wide faces between adjacent layers. The pressure is applied with either a mechanical or hydraulic system. The object of applying pressure is to press the glue line into a continuous, uniformly thin film, and to bring the wood surfaces into intimate contact with the glue and hold them undisturbed until setting or cure is complete. Since loss of solvent causes some glue shrinkage, an internal stress often develops in the glue line during setting. This stress becomes intolerably high if glue lines are too thick. Successful glue joints depend on the right correlation of glue consistency and pressure applied. Press time must be long enough to allow the glue to set well enough so that the joint will not be disturbed by pressure removal.

- Edge gluing (optional)

The edges of boards in a single layer can be glued for optimal tightness to achieve better mechanical and physical properties. Finger joints in different layers should be staggered at an appropriate distance. However, the element surfaces exposed to indoor climates will swell or shrink due to varying air humidity. For wide edge glued plates, the deformation of each board can cause significant shrinkage of the element, which will introduce large tensile stresses during drying process and lead to cracking of the surface layers. This problem could be avoided by either reducing the element width or only edge gluing middle layers which are not exposed to the varying climates.

1.2.4.6 Fabrication of structural elements

The fabrication of structural elements from CLT panels is carried out in production buildings, i.e. in an indoor climate which offers optimum working conditions. Computer numerical control (CNC) woodworking facilities are available to ensure accurate fabrication. Appropriate and powerful lifting and transport equipment is used for transport and erection processes. Therefore, prefabricated elements with dimensions significantly greater than those of the past are now possible. However, transport conditions should be considered at the planning stage because it limits the maximum sizes of elements that can be delivered by road (Kolb, 2008).

1.3 Conclusions

This chapter gave a general overview of the background and goals of this research work. A complete and brief introduction of CLT products, including their history, application and manufacturing process, was presented to provide a basic understanding of these innovative building materials.

CHAPTER 2 LITERATURE REVIEW

2.1 Introduction

In order to achieve the objective of this research, i.e. developing computer models to study the mechanical and vibration behavior of thick laminated plates, it is important and essential to gain a deep insight into the design and analysis methods of these materials. Numerous research work has been done on various aspects of this topic, such as exact theoretical solutions, numerical simulations and experimental applications of thick laminated wood plates, especially CLT elements. These researches contribute significantly to develop safe and reliable design guidelines for these products. In the following sections, detailed reviews of the previous work will be presented, which cover different subjects, such as design methods, analytical solution theories, vibration properties of CLT plates, etc.

2.2 Design methods

In Europe, CLT panels are proprietary engineered wood products; i.e., an industry based manufacturing standard for CLT is not available. Because of the increasing number of different types of solid wood panel from various producers, a general design method and a classification system are needed for engineering design practice. Some important theories, e.g. classical laminate plate theory, mechanically jointed beam theory and shear analogy method will be described later in sections 2.6.1, 2.6.2 and 2.6.3 of this chapter.

Since the classical composite theory does not consider shear deformation in laminated plates, it cannot give precise solutions to plates with a low span-to-depth ratio. To consider shear effect, Blaß and Görlacher (2003) used the theory of mechanically jointed beams which included shear deformation effect of cross layers by the reduction parameter γ_i. In this theory, the perpendicular to beam axis orientated layers were assumed as flexible connections between layers orientated parallel to the main axis and the factor γ_i was employed to consider the flexibility between layers parallel to the beam axis. The major parameter of the inner layers perpendicular to the beam axis, which influences the mechanical properties of CLT elements loaded in bending, was the rolling shear modulus. However, this calculation method according to Eurocode 5 only gave an accurate solution for simply supported beams with a sinusoidal load distribution (Blaß and Fellmoser, 2004).

For continuous beams loaded by concentrated loads or for CLT elements with more than five layers, the theory of mechanically jointed beams is not adequate. Kreuzinger (1999) proposed a more precise calculation method called shear analogy method (German: Schubanalogieverfahren) which was accepted in the German code for timber structures (DIN1052, 2004-08). To determine the load carrying capacity perpendicular to the element surface, the surface structure was divided into two fictitious elements A and B. Element A considered only the main part of the bending stiffness for each layer and element B represented the second part of the bending stiffness and the shear deflection for each layer as well as stiffness of connections between different layers. This method, in which both different modulus of elasticity and shear modulus values of single layers may be considered, was quite reliable for different statics systems with any load distribution and for various types of CLT configurations loaded in the out-of-plane direction.

Guggenberger and Moosbrugger (2006) and Moosbrugger (2010) analyzed the transverse bending behavior considering the specific internal structure of CLT plate elements. Three analytical models were presented to consider the interaction behavior of adjacent single plate layers. It was found that these three models were completely equivalent and exchangeable by applying suitable transformation relationships. Deformation-based formulae of the basic plate equations were then derived for the general case of bi-axial bending. However, because it was very difficult to establish theoretical models considering different properties within the same layer which had discrete parallel contact interfaces, the presented work was based on an assumption that every single layer was continuous and homogeneous with rigid connections on the contact interfaces.

Jöbstl et al. (2006) evaluated an improved design model, bearing model for CLT plates in bending, for the homogenized CLT products. Boards which were used to manufacture CLT elements were visually graded and then some of them were subjected to tension test to obtain the tension characteristics of the population. Bending test was conducted on CLT and glulam specimens with different dimensions to establish a relationship between these two products. Three methods which lead to comparable results were employed to calculate the bending MOE values of CLT members. Then, a design method for CLT plates which took into account both the laminating effect and the system effect was proposed based on a similar concept for glulam design. The difference between this design concept and the German design code DIN 1052:2004 was about 50% with the German code on the conservative side.

More studies aiming to derive a general design method for solid wood panels were conducted (Blaß and Fellmoser, 2004). The dynamic method of measuring the frequencies of a bending vibration was used to determine the rolling shear modulus (Görlacher, 2002). The shear influence in solid wood panels was analyzed using the shear analogy method.

According to this study, for span to depth ratios of at least 30, the influence of shear may be neglected for loading perpendicular to the plane. In this case, the composite theory was taken as a basis for the design of solid wood panels. Finally a strength class system for solid wood panels was given in order to simplify the design method. In this system characteristic strength, stiffness and density values of solid wood panels were given depending on type of stress and direction of stress with regard to the grain direction of the outer layers.

Bejtka and Lam (2008) discussed calculation methods for CLT elements used for floors loaded in the out-of-plane direction and for walls loaded in the in-plane direction. In the out-of-plane loading scenario, the theory of mechanically jointed beams and the shear analogy method, both of which required rolling shear modulus of cross layers, were compared. Two different types of load, i.e. axial and shear load, were considered for CLT panels loaded in the in-plane direction. They also briefly introduced the use of dowel type fasteners to transfer loads between CLT elements by overviewing connection load carrying capacity predicting method based on the well known European Yield Model.

In most CLT elements, wood members are only face glued, i.e. no connection between boards within the same layer, therefore shear forces have to be transferred via torsional resistance of bonding surfaces between adjacent layers. Jöbstl et al. (2004) carried out torsion tests on individual glued connections of two orthogonally glued boards to determine ultimate limit loads, torsional parameters (torsional strength, modulus of rotation) and stress distributions on the glued surfaces.

Because all these methods were very time consuming in practice, a simplified design process which offered practical, adequate, easy and quick solutions for engineers, was developed especially for the one dimensional CLT element (Schickhofer et al., 2009) based on the "bearing model for CLT-plates in bending" (Jöbstl et al., 2006). In addition, a software, CLTdesigner, was created to provide the design verification process of CLT elements loaded out-of-plane (Thiel and Schickhofer, 2010). This software, valid for European situations, can be used for bending and shear stresses in ultimate limit state design, structural fire design, as well as bending deflection and vibration used for serviceability limit state design. Later, CLT elements under in-plane loading and conventional connection types of CLT elements will be implemented in the software (Holz.Bau Forschungs GmbH, 2010).

Mestek et al. (2008) focused on stresses in CLT elements subjected to concentrated loads. Normal and shear stress distribution in the area of a concentrated load was calculated and evaluated for uniaxial spanned systems according to the shear analogy method and by a two dimensional finite element model using quadratic shell elements. Then a simplified method was developed to consider the influence of the shear deformation on the longitudinal strain of a simply supported beam under a concentrated load. Theoretical considerations and experimental investigations of the twisting stiffness of CLT elements and its influence on load bearing behavior were presented.

2.3 Rolling shear

Aicher and Dill-Langer (2000) reported numerical calculations concerning rolling shear modulus in wood. They founded that rolling shear modulus is not an intrinsic material property but an apparent smeared shear stiffness of structural elements depending on many factors such as wood properties in different (i.e. longitudinal, radial and tangential) directions, board sawing patterns (e.g. pith locations and annual ring curvatures) and geometry of board cross sections. They concluded that rolling shear modulus had a lower bound almost equal to the shear modulus in the radial-tangential growth plane and all realistic macro-scale configurations showed much higher apparent stiffness values by a factor of about 4.

2.4 Mechanical connection

Other than adhesives, another option for the connections between wood members is mechanical fasteners, such as nails, screws and dowels. In order to better understand the behavior of these dowel type connections in CLT plates, Schickhofer and Guggenberger (1996) established a theoretical model taking into account the flexibility of the joint interfaces of arbitrarily laminated timber structures. In this model the total flexibility of the joint interface was defined as the arithmetic mean value of the partial flexibilities relating to each of the two connected board layers. The constitutive relations of both wood and joint interfaces were assumed to be anisotropic elastic. To carry out more realistic analyses, it was suggested to take into account the nonlinear material behavior of wood and especially of the flexible joints.

Krämer (2004) presented design equations for the effective bending stiffness of the elements, resulting bending stresses of the lamellas and the action effects of nails in nail-laminated timber elements (NLTE) which were plane structural components composed of single, edgewise-oriented lamellas.

2.5 Evaluation of CLT stiffness properties

The stiffness properties of CLT elements are either calculated from properties of single layers (Bodig and Jayne, 1982; Kreuzinger, 1999; Blass and Görlacher, 2003) or evaluated by testing specimens cut from CLT panels (CEN, 2003b; CEN, 2004a; CEN, 2004b). However, stress compensation as well as homogenizing effects of the cross laminated layout are not taken into account properly using the former method and the listed test procedures are only valid for products with specific set of layers, geometrical properties and some other characteristics (adhesives, grooves, materials, etc.). Gsell et al. (2007), Steiger et al. (2008) and Gsell et al. (2008) developed a fully automated procedure to determine global elastic properties, i.e. two in-plane elastic moduli and three shear moduli, of full-scale CLT panels. The stiffness parameters obtained by matching experimental and theoretical modal analysis were proven to be correct by means of static bending tests.

2.6 Analytical solution theories

2.6.1 Classical laminate plate theory

The Classical Laminate Plate Theory (CLPT) is based on the Kirchhoff-Love hypothesis which involves the following assumptions: straight lines perpendicular to the mid-plane before deformation remain (1) straight, (2) inextensible, and (3) normal to the mid-surface after deformation. In this theory, the in-plane displacements are assumed to vary linearly through the thickness and the transverse displacement is assumed to be constant through the thickness (i.e., transverse normal strain is zero). This leads to assuming that plates are "infinitely" rigid in the transverse direction, whereas in reality they are weaker in that direction.

Consider a plate of total thickness h composed of N orthotropic layers with their principal material coordinates $(\bar{x}_1, \bar{x}_2, \bar{x}_3)$ oriented at angles $(\theta_1, \theta_2, \theta_3)$ to the laminate coordinate (x, y, z) (Figure 2-1). It is convenient to take the xy-plane of the problem in the undeformed mid-plane of the laminate (Figure 2-2). The z-axis is taken positive upward from the mid-plane. We assume that

- The layers are perfectly bonded together,
- The material of each layer is linearly elastic and has three planes of material symmetry (i.e., orthotropic),
- Each layer is of uniform thickness,
- The strains and displacements are small.

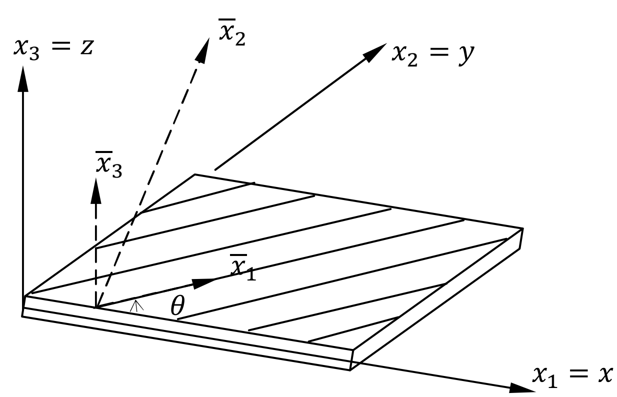

Figure 2-1 Coordinate system used for the description of the structure and the fiber direction.

A point P, located at the point (x, y, z) in the undeformed plate, moves after deformation to the position $(x + u_1, y + u_2, z + u_3)$ where (u_1, u_2, u_3) are the components of the displacement vector

$$u = u_1 \hat{e}_x + u_y \hat{e}_y + u_3 \hat{e}_z \tag{2-1}$$

and $(\hat{e}_x, \hat{e}_y, \hat{e}_z)$ are the unit vectors along the (x, y, z) coordinates. The first two assumptions of the Kirchhoff hypothesis require that the displacements (u_1, u_2, u_3) to be such that

$$u_1(x, y, z, t) = u(x, y, t) + z\phi_1(x, y, t)$$

$$u_2(x, y, z, t) = v(x, y, t) + z\phi_2(x, y, t)$$

$$u_3(x, y, z, t) = w(x, y, t) \tag{2-2}$$

where (u, v, w) are the displacements of a point on the xy-plane (i.e., the mid-plane of the laminate), ϕ_1 is the rotation of a transverse normal about the y-axis, and ϕ_2 is the rotation of a transverse normal about the x-axis and t denotes time.

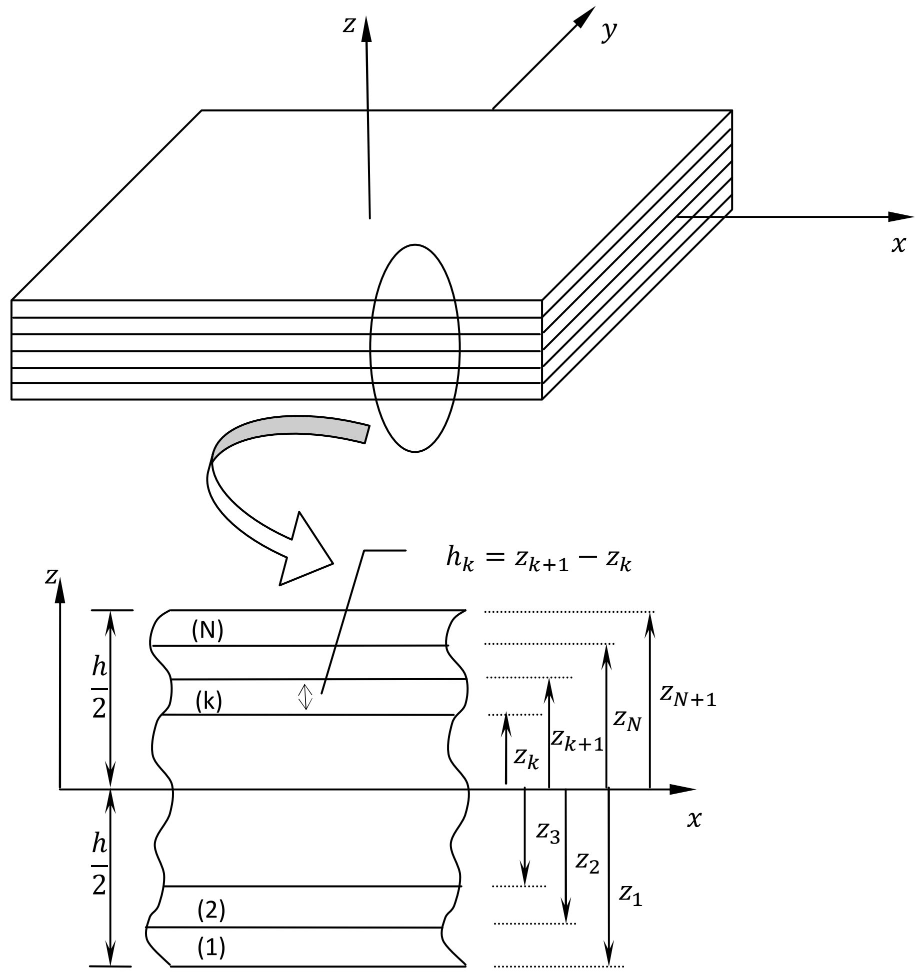

Figure 2-2 Coordinate system and layer numbering used for a typical laminated plate.

The third assumption of the Kirchhoff hypothesis implies that the rotations ϕ_1 and ϕ_2 are equal to $-\partial w/\partial x$ and $-\partial w/\partial y$, respectively.

$$\phi_1 = -\partial w/\partial x \text{ and } \phi_2 = -\partial w/\partial y \tag{2-3}$$

Thus the displacement field of the classical plate theory becomes

$$u_1(x,y,z,t) = u(x,y,t) - z\frac{\partial w}{\partial x}$$

$$u_2(x,y,z,t) = v(x,y,t) - z\frac{\partial w}{\partial y}$$

$$u_3(x,y,z,t) = w(x,y,t) \tag{2-4}$$

It is important to note that in using the kinematic assumptions of a single layer theory to model a laminated plate composed of multiple layers of possibly dissimilar-material layers, we assume that the strains are continuous through the thickness, including the interfaces of dissimilar-material layers. This assumption plays a significant role in developing laminate theories; it allows us to replace a laminate with an equivalent single layer whose material coefficients are averaged over the laminate thickness. However, the assumption restricts the use of the theory to model global response characteristics, and it does not represent the interlaminar stresses (i.e., stresses at the lamina interfaces) accurately.

Once the displacement field of a continuous body is known, the strains in the body can be computed using the strain-displacement relations

$$\varepsilon_1 = \frac{\partial u}{\partial x} - z\frac{\partial^2 w}{\partial x^2}$$

$$\varepsilon_2 = \frac{\partial v}{\partial y} - z\frac{\partial^2 w}{\partial y^2}$$

$$\varepsilon_6 = \frac{\partial u}{\partial y} + \frac{\partial v}{\partial x} - 2z\frac{\partial^2 w}{\partial x \partial y}$$

$$\varepsilon_3 = \varepsilon_4 = \varepsilon_5 = 0 \tag{2-5}$$

The strains in the above equations are of the general form,

$$\varepsilon_i = \varepsilon_i^{(0)} + z\varepsilon_i^{(1)} \qquad (i = 1, 2, 6) \tag{2-6}$$

Here $\varepsilon_i^{(0)}$ denote the strains associated with the stretching and in-plane shearing of the mid-plane and are called the membrane strains. The quantities $\varepsilon_i^{(1)}$ are the curvatures. Both $\varepsilon_i^{(0)}$ and $\varepsilon_i^{(1)}$ are functions of (x, y) only. It is clear that the strains vary linearly through the laminate thickness, and they are independent of the lamination scheme. For a fixed value of z, the strains vary only with respect to the x and y coordinates.

However, the CLPT is inadequate for the analysis of thick laminates as the theory is based on a linear displacement across the entire laminate with shear deformation neglected. The work presented by Pagano (1969, 1970, 1970) serves as a guide in defining the precision of CLPT calculations for the response of composite laminates under static bending. It is found that

(a) The CLPT stresses generally converge more rapidly to the exact solution than plate deflection,

(b) The CLPT leads to a very poor description of laminate response at low span-to-depth ratios, but converges to the exact solution as this ratio increases,

(c) In addition to span-to-depth ratios, the accuracy of the CLPT solution of a particular problem also depends upon material properties, lamination geometry.

To take into account shear deformation, some other theories introduced in the following sections may be used (Chen, 2006).

2.6.2 Theory of mechanically jointed beams

For CLT elements subjected to bending, load carrying capacity and also deflection are governed by the moment of inertia of the plate. The effective moment of inertia of a multiply beam can be calculated by,

$$I_{ef} = \sum_{i=1}^{3}(I_i + \gamma_i \cdot A_i \cdot a_i^2) \tag{2-7}$$

where $A_i = b_i \cdot h_i$ and $I_i = \frac{b_i \cdot h_i^3}{12}$.

The shear deformation of cross layers is taken into account by the reduction factor γ_i which represents flexible connections between layers oriented in the beam axis. γ_i can be obtained by,

$$\gamma_1 = 1/\left(1 + \frac{\pi^2 \cdot E_0 \cdot A_1 \cdot \overline{h_1}}{G_R \cdot b \cdot l^2}\right)$$

$$\gamma_2 = 1$$

$$\gamma_3 = 1/\left(1 + \frac{\pi^2 \cdot E_0 \cdot A_3 \cdot \overline{h_2}}{G_R \cdot b \cdot l^2}\right) \tag{2-8}$$

The distances between each center of gravity for the corresponding parallel layer and the center of gravity for the whole solid wood panel are,

$$a_1 = \left(\frac{h_1}{2} + \overline{h_1} + \frac{h_2}{2}\right) - a_2$$

$$a_3 = \left(\frac{h_2}{2} + \overline{h_2} + \frac{h_3}{2}\right) + a_2$$

$$a_2 = \left(\gamma_1 \cdot A_1 \cdot \left(\frac{h_1}{2} + \overline{h_1} + \frac{h_2}{2}\right) - \gamma_3 \cdot A_3 \cdot \left(\frac{h_2}{2} + \overline{h_2} + \frac{h_3}{2}\right)\right) / \sum_{i=1}^{3}(\gamma_i \cdot A_i) \tag{2-9}$$

where

h_i thickness of layer i parallel to the beam main axis direction (mm)

$\overline{h_i}$ thickness of layer i perpendicular to the beam main axis direction (mm)

b width of the element (mm)

n number of layers

L beam span

G_R rolling shear modulus (N/mm^2)

Therefore, the bending stress at the edge of each layer and the shear stress in the middle of each layer can be predicted as,

$$\sigma_i = \pm \frac{M}{I_{ef}} \cdot \left(\gamma_i \cdot a_i + \frac{h_i}{2}\right) \qquad (2\text{-}10)$$

$$\tau = \frac{V \cdot \gamma_i \cdot S_i}{I_{ef} \cdot b} \qquad (2\text{-}11)$$

where S_i is first moment of area of layer i. V and M are internal shear and moment, respectively.

Detailed information about this calculation method is referred to the European Technical Approval ETA-08/0242 (2009). By including the shear deformation, this method works for small span-to-depth ratio. However, as mentioned earlier this approach only gives an accurate solution for simply supported beams with a sinusoidal load distribution. For continuous beams loaded by concentrated loads or for CLT elements with more than five layers, this theory is not adequate. Therefore, a more precise design method called shear analogy method by Kreuzinger (1999) is recommended.

2.6.3 Shear analogy method

From the European Technical Approval Draft (2008), in the analytical Kreuzinger model, all the relevant stiffness of an n-ply beam are systematic applied to two virtual beams A and B (Figure 2-3).

The main part of the bending stiffness is represented by virtual beam A:

$$(EI)_A = \sum_{i=1}^{n} E_i \cdot I_i \tag{2-12}$$

The shear stiffness of virtual beam A is assumed to be infinite.

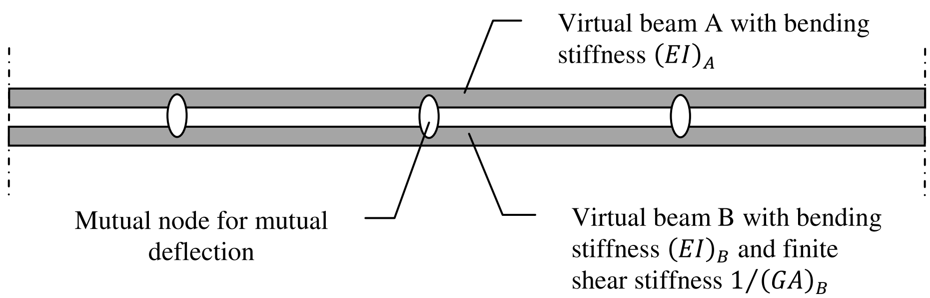

Figure 2-3 Model of the Kreuzinger beam.

The composite action of the n layers is represented by the second part of the bending stiffness (Steiner part) in virtual beam B (Eq. 2-13). The influence of composite action at the interface of neighboring layers and the shear stiffness of each layer are also included in virtual beam B (Eq. 2-14).

$$(EI)_B = \sum_{i=1}^{n} E_i \cdot A_i \cdot \mathrm{z}_\mathrm{i}^2 \tag{2-13}$$

$$\frac{1}{(GA)_B} = \frac{1}{S} = \frac{1}{a^2} \cdot \left(\sum_{i=1}^{n-1} \frac{1}{c_i} + \frac{d_1}{2 \cdot G_1 \cdot b_1} + \sum_{i=2}^{n-1} \frac{d_i}{G_i \cdot b_i} + \frac{d_n}{2 \cdot G_n \cdot b_n} \right) \tag{2-14}$$

where

n number of layers

c_i stiffness of the connection between layer i and $i+1$

d_i thickness of layer i

G_i shear modulus of layer i

a distance between the middle plane of the outmost layers

Because both beam A and B are virtual and actually they belong to the same beam and never separate from each other in reality, it is important to require an equal deflection of them. This can be achieved by placing the beams parallel to each other and connecting them with mutual nodes. The Kreuzinger beam can be loaded by action which results in deflection and internal virtual forces. Then these virtual forces are transferred to the internal forces in each individual layer of the plate. The bending moment M_A and shear force Q_A of virtual beam A contribute to bending ($\sigma_{m,i}$) and shear (τ_{Ai}) stress in each individual layer as shown in Eq. 2-15 and Eq. 2-16.

$$\sigma_{m,i} = \pm E_i \cdot \frac{M_A}{(EI)_A} \cdot \frac{d_i}{2} \tag{2-15}$$

$$\tau_{Ai} = \frac{E_i}{(EI)_A} \cdot Q_A \cdot \frac{d_i^2}{8} \tag{2-16}$$

The bending moment M_B and shear force Q_B of virtual beam B lead to the constant axial stress ($\sigma_{t,i}$) in each layer i and the shear stress distribution ($\tau_{Bi,i+1}$ and $\tau_{Bi-1,i}$) at the interface of adjacent layers (Eq. 2-17 to Eq. 2-19). The total shear stress ($\tau_{max,i}$) in layer i can be calculated using both shear stresses resulting from Q_A and Q_B (Eq. 2-20).

$$\sigma_{t,i} = E_i \cdot \frac{M_B}{(EI)_B} \cdot \mathrm{z_i} \qquad (2\text{-}17)$$

$$\tau_{Bi,i+1} = \frac{Q_B}{(EI)_B} \cdot \frac{\sum_{i=1}^{i} E_i \cdot A_i \cdot z_i}{min\begin{cases} b_i \\ b_{i+1} \end{cases}} \qquad (2\text{-}18)$$

$$\tau_{Bi-1,i} = \frac{Q_B}{(EI)_B} \cdot \frac{\sum_{i=1}^{i-1} E_i \cdot A_i \cdot z_i}{min\begin{cases} b_{i-1} \\ b_i \end{cases}} \qquad (2\text{-}19)$$

$$\tau_{max,i} = \tau_{Ai} + \tau_{1,i} + \frac{\tau_{2,i}}{2} + \frac{\tau_{2,i}^2}{16 \cdot \tau_{Ai}} \quad \text{if} \quad \tau_{Ai} > \frac{\tau_{2,i}}{4}$$

$$\tau_{max,i} = \tau_{1,i} + \tau_{2,i} \quad \text{if} \quad \tau_{Ai} \leq \frac{\tau_{2,i}}{4} \qquad (2\text{-}20)$$

where

$$\tau_{1,i} = min\begin{cases} \tau_{Bi-1,i} \\ \tau_{Bi,i+1} \end{cases}$$

$$\tau_{2,i} = \left|\tau_{Bi-1,i} - \tau_{Bi,i+1}\right|$$

The shear analogy method enables both different modulus of elasticity and shear modulus values to be considered in any plate configuration loaded in the out-of-plane direction. In addition, rolling shear modulus of layers perpendicular to the beam axis is needed for both of these two design methods, i.e. theory of mechanically jointed beams and shear analogy method.

2.7 Vibration

Since the objective of this research is to study behavior of thick laminated wood plate products in floor applications, vibration is an issue that must be considered.

Floor vibration is resulted from dynamic forces acting upon a floor system. Excessive floor vibration can detract the occupants from their sense of comfort and security and even lead to fears about structural safety. The well known deflection criterion (deflection of less than span/360 under distributed live load) has been used for more than 100 years to ensure a certain level of serviceability under static loads. However, nowadays this simple criterion may be insufficient to guarantee acceptable vibration serviceability of floors due to normal human activities and also the wide use of longer span and lighter weight designs. Therefore, several dynamic design criteria have been proposed to improve the vibration serviceability of wood floors (Al-Foqaha'a et al., 1999; Ebrahimpour and Sack, 2005; Kalkert et al., 1995; Foschi, 2005; Foschi et al., 1995; Ohlsson, 1988; Smith and Chui, 1988). Smith and Chui (1988) developed methods to predict dynamic behavior of light weight wood floors. They recommended a root-mean-squared acceleration response of less than 0.45 m/s^2 for a floor under heel drop impact. They also required a floor natural frequency of more than 8 Hz. Ohlsson (1988) presented a design approach for footstep loading in lightweight wood floors with frequencies higher than 8 Hz. Kalkert et al. (1995) evaluated six criteria proposed by other researchers in two different ways. First, a design-deflection factor was determined based on specific floor dimensions and average material properties. Second, the design results of the individual criteria were used to determine the acceptability of selected experimental floors. Al-Foqaha’a et al. (1999) quantified the subjective perception of unwanted vibrations caused by occupant-induced footfalls and developed a complete design procedure which could reduced the number of occupant complaints. The procedure was based on a series of dynamic analyses using a detailed finite element model of wood floors that was validated with experimental testing. Foschi (2005) discussed the utilization of neural networks for representation of structural responses, and the utility and efficiency of such an approach was illustrated with an example on floor vibrations as a serviceability limit state.

To determine a floor's dynamic properties simply and reliably, different test methods were developed. Blakeborough and Williams (2002) presented a technique called the instrumented heel drop test. The floor was excited by a series of heel drops performed on top of a slim load cell placed on the floor. This test gave excellent resolution of natural frequencies between 2 and 15 Hz which corresponded well with the frequency range of interest in floor vibration problems. Foschi et al. (1995) studied experimental results for the dynamic response of light weight floors under occupancy. They measured fundamental natural frequencies of floor specimens from their response to three different types of test, i.e. hammer impact, impulse excitation by dropping a sand bag and heel drop impact.

Assessing vibration properties of existing timber structures required nondestructive evaluations (Cai et al., 2002; Ross et al., 2002; Soltis et al., 2002; Hunt et al., 2007). Soltis et al. (2002) carried out a pilot investigation on the use of transverse vibration testing techniques for inspecting timber structures by evaluating component systems such as floor systems rather than individual members. Cai et al. (2002) reported the transverse vibration response of laboratory-built floor systems with new and salvaged joists. Hunt et al. (2007) conducted transverse vibration test on actual, in-place floor systems in four buildings that varied in age from a little less to a little more than 100 years as well as on laboratory-built floors. They suggested an implementation technique to assess structural quality of in-place, one-way action, wood floor systems. Pedersen (2006) performed tests identifying floor frequency and damping of a human occupied test floor to explore the relationship between floor damping and seated crowds of people.

2.8 Conclusions

Basic theories and models concerning design approaches of thick laminated wood plates were reviewed in this chapter. As span-to-depth ratio of laminated plates decreases, the influence of transverse shear effect is getting more and more important. Since classical composite theory does not take into account the transverse shear, it cannot give precise solutions to plates with a low span-to-depth ratio. Therefore, theory of mechanically jointed beams and shear analogy method were developed to cover the shortcoming of the classical theory. In this way, rolling shear effect, which is very important to low span-to-depth ratio CLT, is included in the design model. In addition, literatures regarding vibration properties, which are critical to floor serviceability, were studied. Several dynamic design criteria were presented to improve the vibration serviceability of wood floors. Different test methods were developed to determine a floor's dynamic properties. This work provides a good understanding of the existing analytical, numerical and experimental methods used in CLT studies and lays a foundation for topics covered in the following chapters.

CHAPTER 3 COMPARISON OF BENDING PERFORMANCE BETWEEN GLUED AND NAILED CLT PLATES

3.1 Introduction

From the previous chapters, it is clear that CLT offers many economic, building-performance and environmental advantages. However, because of the absence of commercial availability and therefore the product familiarization and use, the introduction of CLT to North America is very limited. In addition, the European experience is not directly transferable to North America because European CLT products have been developed as a proprietary product by individual companies aimed at servicing specific markets. Therefore, there is a need to try different ways of making CLT and to define its structural performance in North America. Since glue and nail are two major options to connect neighbouring layers, it would be necessary and essential to study the behaviour of CLT manufactured with these two different methods. The main focus of this chapter is to develop models for predicting the performance of thick laminated wood plates manufactured by gluing or nailing. The computer model will be verified using data developed in an experimental study on thick MPB wood plates.

Comprehensive three dimensional (3-D) finite element models were developed to analyze the behavior of cross laminated wood plates using the commercial software package ANSYS® (version 11.0). With this model, several plate configurations were designed prior to constructing thick MPB panel prototypes to demonstrate the effects of gluing and nailing and for model verification. A three-layer cross laminated plate with nominal dimensions of 1.2 m × 2.4 m × 114 mm (4 feet × 8 feet × 6 inch) was selected for the testing program.

Using the nominal dimensions determined from the 3-D model, six thick MPB wood plate specimens were manufactured at UBC using randomly selected MPB lumber from a package of #2 grade and better material. Selected members were planed, sanded and cut to final sizes. Phenol–resorcinol–formaldehyde resin is widely used in the manufacture of structural, exterior-grade glulam, finger joints, and other exterior timber structures in North America. In order to adapt the existing industry knowledge to the new CLT technology, this type of adhesive was selected and applied between the neighboring layers (wide face) but not between lumber within the same layer (narrow face). Identical specimen configurations were manufactured using aluminum siding nails which were chosen for their flexibility and ease of being cut with ordinary wood working equipments. Bending behavior of the specimens manufactured with different bonding options, i.e. glue and nail, were studied and discussed.

3.2 Finite element model

The configuration of a three-layer cross laminated plate is shown in Figure 3-1. Using the software package ANSYS®, the plate was discretized into 3-D structural brick elements. There are two brick elements options, i.e. SOLID45 and SOLID95 (a higher order version of SOLID45). The geometry, node locations, and the coordinate system for both elements are shown in Figure 3-2. Elements SOLID45 and SOLID95 are defined by eight nodes and twenty nodes having three degrees of freedom at each node: translations in the nodal x, y, and z directions, respectively (ANSYS, 2007). Both elements were tried and numerical results were compared.

Figure 3-1 Layout of a three-layer cross laminated wood plate.

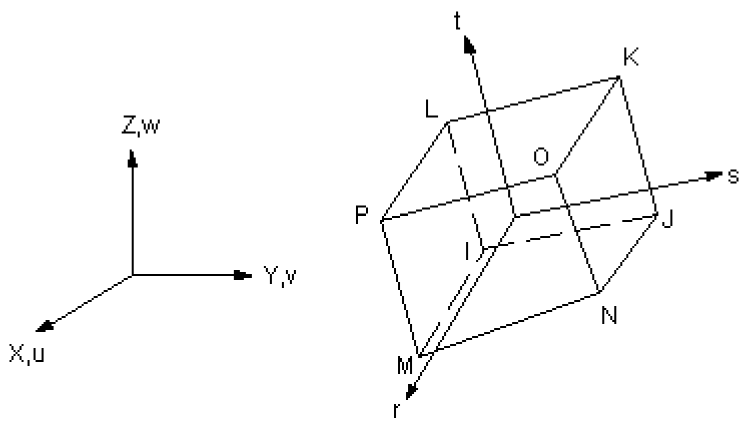

(a)

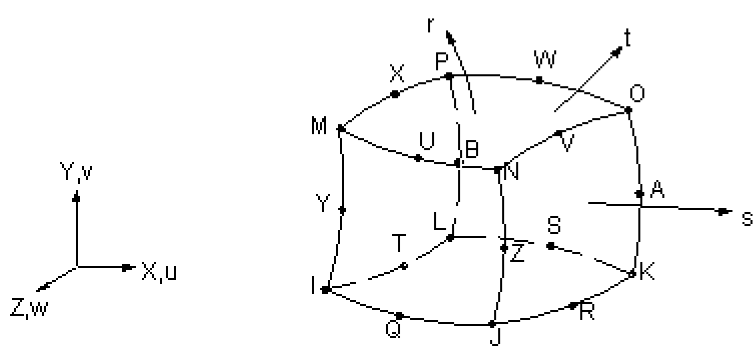

(b)

Figure 3-2 Brick elements (a) SOLID45 and (b) SOLID95 provided by ANSYS®.

The shape functions for element SOLID45 are:

$$
\begin{aligned}
u = \frac{1}{8}\Big(& u_I(1-s)(1-t)(1-r) + u_J(1+s)(1-t)(1-r) + u_K(1+s)(1+t)(1-r) \\
& + u_L(1-s)(1+t)(1-r) + u_M(1-s)(1-t)(1+r) \\
& + u_N(1+s)(1-t)(1+r) + u_O(1+s)(1+t)(1+r) \\
& + u_P(1-s)(1+t)(1+r)\Big) \\
v = \frac{1}{8}\Big(& v_I(1-s)(1-t)(1-r) + v_J(1+s)(1-t)(1-r) + v_K(1+s)(1+t)(1-r) \\
& + v_L(1-s)(1+t)(1-r) + v_M(1-s)(1-t)(1+r) \\
& + v_N(1+s)(1-t)(1+r) + v_O(1+s)(1+t)(1+r) \\
& + v_P(1-s)(1+t)(1+r)\Big) \\
w = \frac{1}{8}\Big(& w_I(1-s)(1-t)(1-r) + w_J(1+s)(1-t)(1-r) + w_K(1+s)(1+t)(1-r) \\
& + w_L(1-s)(1+t)(1-r) + w_M(1-s)(1-t)(1+r) \\
& + w_N(1+s)(1-t)(1+r) + w_O(1+s)(1+t)(1+r) \\
& + w_P(1-s)(1+t)(1+r)\Big)
\end{aligned}
\tag{3-1}
$$

The shape functions for element SOLID45 are:

$$
\begin{aligned}
u = \frac{1}{8}\Big(& u_I(1-s)(1-t)(1-r)(-s-t-r-2) \\
& + u_J(1+s)(1-t)(1-r)(s-t-r-2) \\
& + u_K(1+s)(1+t)(1-r)(s+t-r-2) \\
& + u_L(1-s)(1+t)(1-r)(-s+t-r-2) \\
& + u_M(1-s)(1-t)(1+r)(-s-t+r-2) \\
& + u_N(1+s)(1-t)(1+r)(s-t+r-2) \\
& + u_O(1+s)(1+t)(1+r)(s+t+r-2) \\
& + u_P(1-s)(1+t)(1+r)(-s+t+r-2)\Big) \\
& + \frac{1}{4}\Big(u_Q(1-s^2)(1-t)(1-r) + u_R(1+s)(1-t^2)(1-r) \\
& + u_S(1-s^2)(1+t)(1-r) + u_T(1-s)(1-t^2)(1-r) \\
& + u_U(1-s^2)(1-t)(1+r) + u_V(1+s)(1-t^2)(1+r) \\
& + u_W(1-s^2)(1+t)(1+r) + u_X(1-s)(1-t^2)(1+r) \\
& + u_Y(1-s)(1-t)(1-r^2) + u_Z(1+s)(1-t)(1-r^2) \\
& + u_A(1+s)(1+t)(1-r^2) + u_B(1-s)(1+t)(1-r^2)\Big)
\end{aligned}
$$

$$
\begin{aligned}
v = \frac{1}{8}\Big(& v_I(1-s)(1-t)(1-r)(-s-t-r-2) \\
& + v_J(1+s)(1-t)(1-r)(s-t-r-2) \\
& + v_K(1+s)(1+t)(1-r)(s+t-r-2) \\
& + v_L(1-s)(1+t)(1-r)(-s+t-r-2) \\
& + v_M(1-s)(1-t)(1+r)(-s-t+r-2) \\
& + v_N(1+s)(1-t)(1+r)(s-t+r-2) \\
& + v_O(1+s)(1+t)(1+r)(s+t+r-2) \\
& + v_P(1-s)(1+t)(1+r)(-s+t+r-2)\Big) \\
& + \frac{1}{4}\Big(v_Q(1-s^2)(1-t)(1-r) + v_R(1+s)(1-t^2)(1-r) \\
& + v_S(1-s^2)(1+t)(1-r) + v_T(1-s)(1-t^2)(1-r) \\
& + v_U(1-s^2)(1-t)(1+r) + v_V(1+s)(1-t^2)(1+r) \\
& + v_W(1-s^2)(1+t)(1+r) + v_X(1-s)(1-t^2)(1+r) \\
& + v_Y(1-s)(1-t)(1-r^2) + v_Z(1+s)(1-t)(1-r^2) \\
& + v_A(1+s)(1+t)(1-r^2) + v_B(1-s)(1+t)(1-r^2)\Big)
\end{aligned}
$$

$$
\begin{aligned}
w = \frac{1}{8}\Big(& w_I(1-s)(1-t)(1-r)(-s-t-r-2) \\
& + w_J(1+s)(1-t)(1-r)(s-t-r-2) \\
& + w_K(1+s)(1+t)(1-r)(s+t-r-2) \\
& + w_L(1-s)(1+t)(1-r)(-s+t-r-2) \\
& + w_M(1-s)(1-t)(1+r)(-s-t+r-2) \\
& + w_N(1+s)(1-t)(1+r)(s-t+r-2) \\
& + w_O(1+s)(1+t)(1+r)(s+t+r-2) \\
& + w_P(1-s)(1+t)(1+r)(-s+t+r-2)\Big) \\
& + \frac{1}{4}\Big(w_Q(1-s^2)(1-t)(1-r) + w_R(1+s)(1-t^2)(1-r) \\
& + w_S(1-s^2)(1+t)(1-r) + w_T(1-s)(1-t^2)(1-r) \\
& + w_U(1-s^2)(1-t)(1+r) + w_V(1+s)(1-t^2)(1+r) \\
& + w_W(1-s^2)(1+t)(1+r) + w_X(1-s)(1-t^2)(1+r) \\
& + w_Y(1-s)(1-t)(1-r^2) + w_Z(1+s)(1-t)(1-r^2) \\
& + w_A(1+s)(1+t)(1-r^2) + w_B(1-s)(1+t)(1-r^2)\Big)
\end{aligned}
\tag{3-2}
$$

Regardless of the type of structure or type of material, structural systems can behave as a unit only with proper interconnection of the components and assemblies. Laminated plates with glued connections and mechanical fasteners were studies to compare structural performance of plates with different bonding options. For glued plates, it was assumed that neighboring layers were perfectly bonded meaning no relative movement between the two wide surfaces that were glued together. And for nailed plates, the capacity of each nail was simulated by a group of longitudinal springs (two in the lateral and one in the axial direction). The spring element COMBIN39 with nonlinear generalized force-deflection capability (Figure 3-3) was employed to model nail resistance in the two lateral directions and the spring-damper element COMBIN14 (Figure 3-4) was used in the axial direction. The force-deflection curve of the COMBIN39 element was obtained from experimental studies while joint axial stiffness was assumed to be infinite.

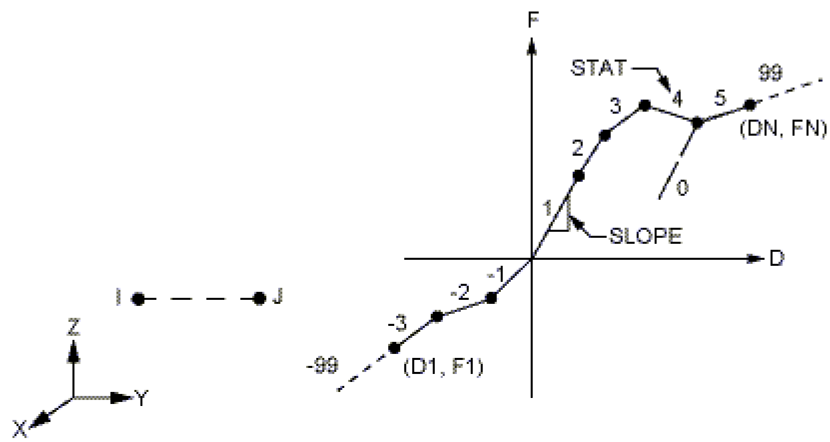

Figure 3-3 Nonlinear spring element COMBIN39 provided by ANSYS®.

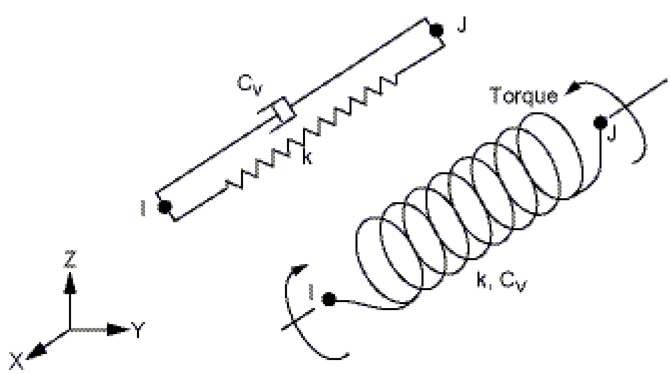

Figure 3-4 -damper element COMBIN14 provided by ANSYS®.

Another factor that had to be considered for nailed plate is the friction between the laminated layers which may occur when the layers are connected with nails. Friction is the resisting force encountered when one surface slides over another; this force acts along the tangent to the contact surfaces. The force necessary to overcome friction depends on the nature of the materials in contact such as the roughness or smoothness of the wood surface and the normal force acting on the layers. It is well known that the friction force is directly proportional to the normal force with a constant of proportionality called the coefficient of friction.

It is very important to note that different locations on the wood surface have different coefficients of friction. This is due to the non-uniform nature of wood. The difference may be slight or very great in a small area. If there is a knot or change in the grain, it may have a significant influence on the coefficient of friction.

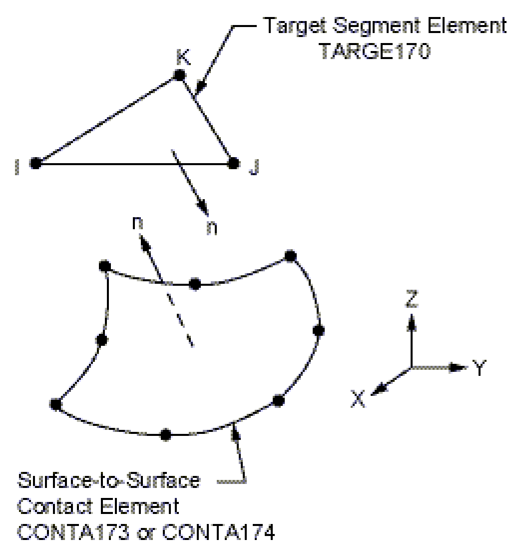

Figure 3-5 3-D target segment element TARGE170 provided by ANSYS®.

In the finite element model, 3-D target segment element TARGE170 (Figure 3-5) was paired with 3-D surface to surface contact element CONTA173/CONTA174 (Figure 3-6) to represent contact and sliding between adjacent wood layers. CONTA173 which is associated with solid element SOLID45 is defined by four nodes and CONTA174 which is related to

SOLID95 is defined by eight nodes. The model was calibrated based on test data to find suitable coefficient of friction for the nailed plates.

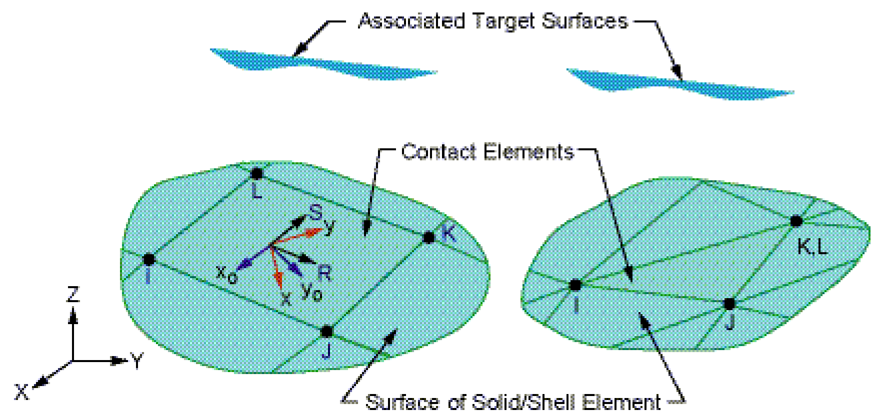

(a)

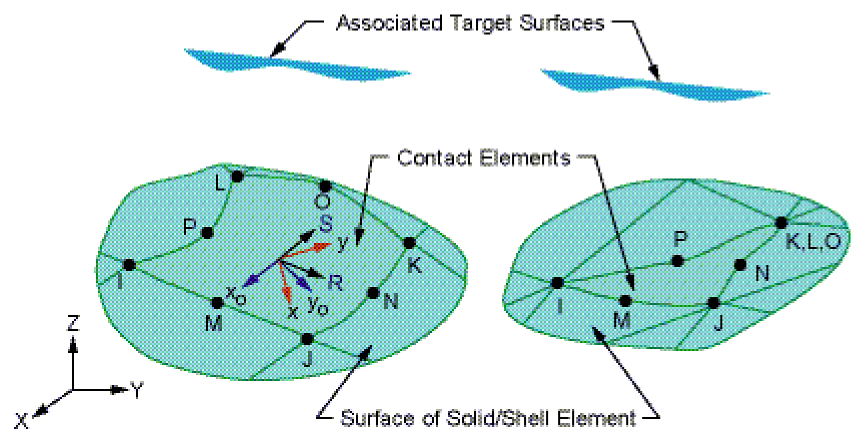

(b)

Figure 3-6 3-D (a) 4-node surface-to-surface contact element CONTA173 and (b) 8-node surface-to-surface contact element CONTA174 provided by ANSYS®.

Figure 3-7 is the finite element model of a three-layer nailed plate. In Figure 3-7 (a), wood materials were modeled with the brick element SOLID45 and the elongated blue lines between each layer were spring elements COMBIN39 and COMBIN14 which were used to simulate nails. Contact pairs between adjacent layers (CONTA173 and TARGE170) are shown in Figure 3-7 (b). Boundary conditions are displayed in Figure 3-8 where the two red rectangles represent the loading area. The element dimensions are 27.7 mm × 27.7 mm × 16.5 mm. Nine material property parameters, which were obtained from test described in session 3.3.2, were assigned to the elements.

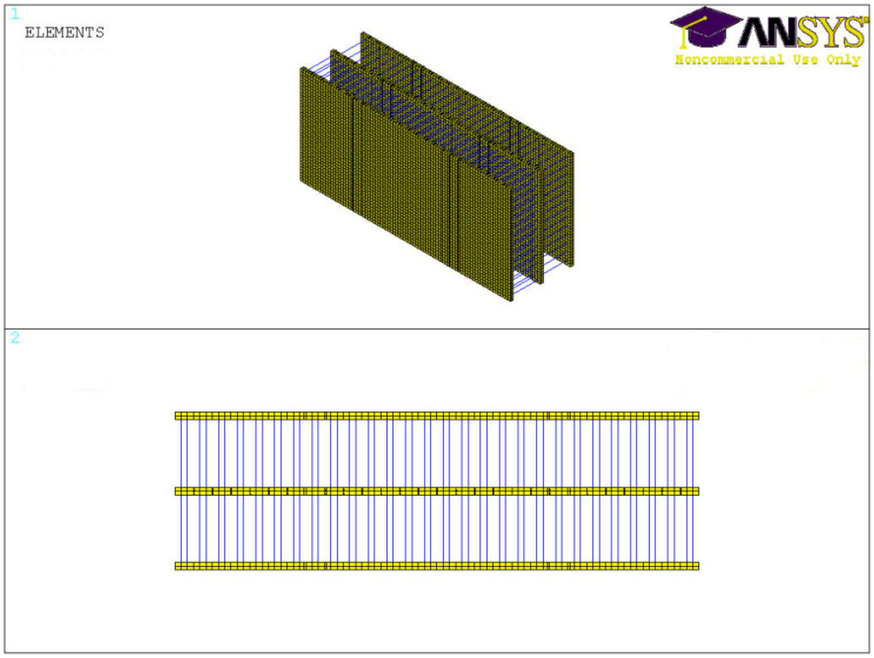

(a)

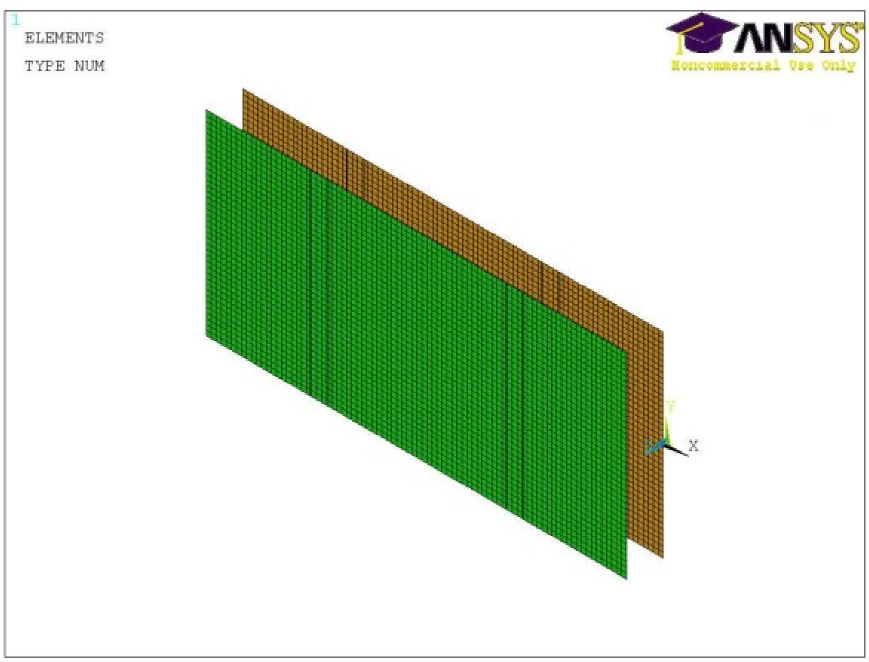

(b)

Figure 3-7 Finite element model of a three-layer nailed plate.

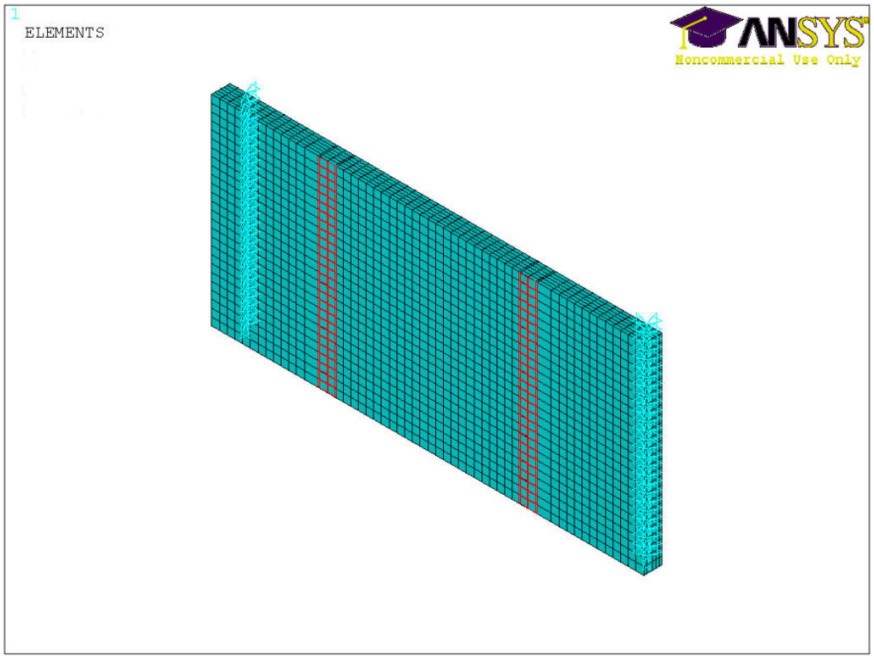

(a)

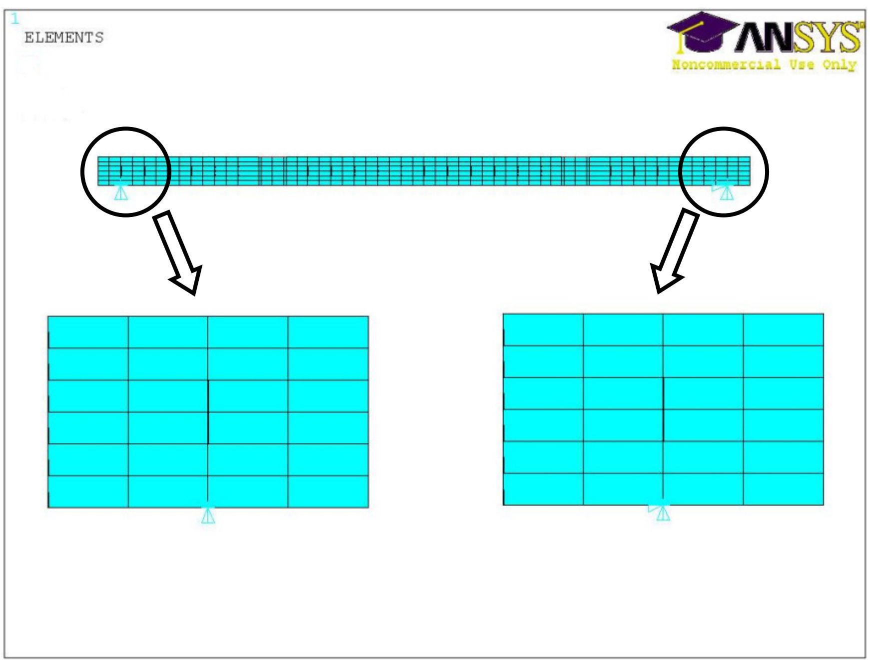

(b)

Figure 3-8 Boundary conditions in the finite element model.

3.3 Experimental studies

3.3.1 Thick laminated plate specimen manufacturing

To verify the finite element model, three specimens of three-layer cross laminated glued plates and three specimens of three-layer cross laminated nailed plates were manufactured. One package of 38 mm × 89 mm (nominal 2 inch × 4 inch) of #2 and better MPB lumber, 4.88 m (16 feet) in length, with a moisture content of about 15% was received courtesy of Canfor Corporation, Canada. The MPB wood came from the beetle pine infested area around Quesnel, British Columbia. The lumber was stored in the laboratory to reach the equilibrium moisture content. The wood members which were used for panel manufacturing were selected randomly from the package in order to get a good representative of the beetle killed wood. After reaching the equilibrium moisture content, selected pieces were planed, sanded and cut into the appropriate sizes for the test specimens (Figure 3-9).

Figure 3-9 A pile of #2 and better MPB lumber.

3.3.1.1 Glued plate

PRF resin was chosen for manufacturing the three-layer glued plates. The Italpresse SCF/6 – Oleodynamic hot press was used to apply a pressure of 0.392 N/mm^2 and a temperature of 90 ^{o}C during glue curing to provide a good bond between the laminas (Figure 3-10). The recommended range of pressure is 0.6 to 1 N/mm^2 according to the Aerodux-500 technical data sheet (DGR Industrial Products Inc., 2010) but the applied pressure was the highest level the machine could reach considering the panel area. In order to guarantee a perfect bonding the panels were kept under the high pressure and temperature for a few hours which were certainly longer than the recommended glue curing period. The panels were trimmed to the target size to get smooth edges of the final test specimens (Figure 3-11).

Figure 3-10 Manufacturing of a three-layer cross laminated glued plate.

Figure 3-11 A product three-layer cross laminated glued plate.

3.3.1.2 Nailed plate

In Europe, threaded aluminum nails, which comply with building license Z-9.1-563, were specially developed for the CLT products (Rondoni Group srl, 2010). Every intersection of CLT is assembled crosswise through the use of two nails which are placed as far as possible from each other. Such nails are not available for evaluation in North America. In this study, 63.5 mm (2 ½ inch) long aluminum siding nails (with head diameter of 9.5 mm (3/8 inch)) was selected because of their market availability in North America. Aluminum was chosen because it is soft and can be cut easily with ordinary shop tools. This characteristic of aluminum would benefit the further processing of nailed plates. A specific nailing pattern (Figure 3-12) was designed to establish enough connection strength between laminas. The values of b, W and L are 83 mm, 1079 mm and 2324 mm, respectively. The circle and cross represent nails driven into and out of the paper plane, respectively.

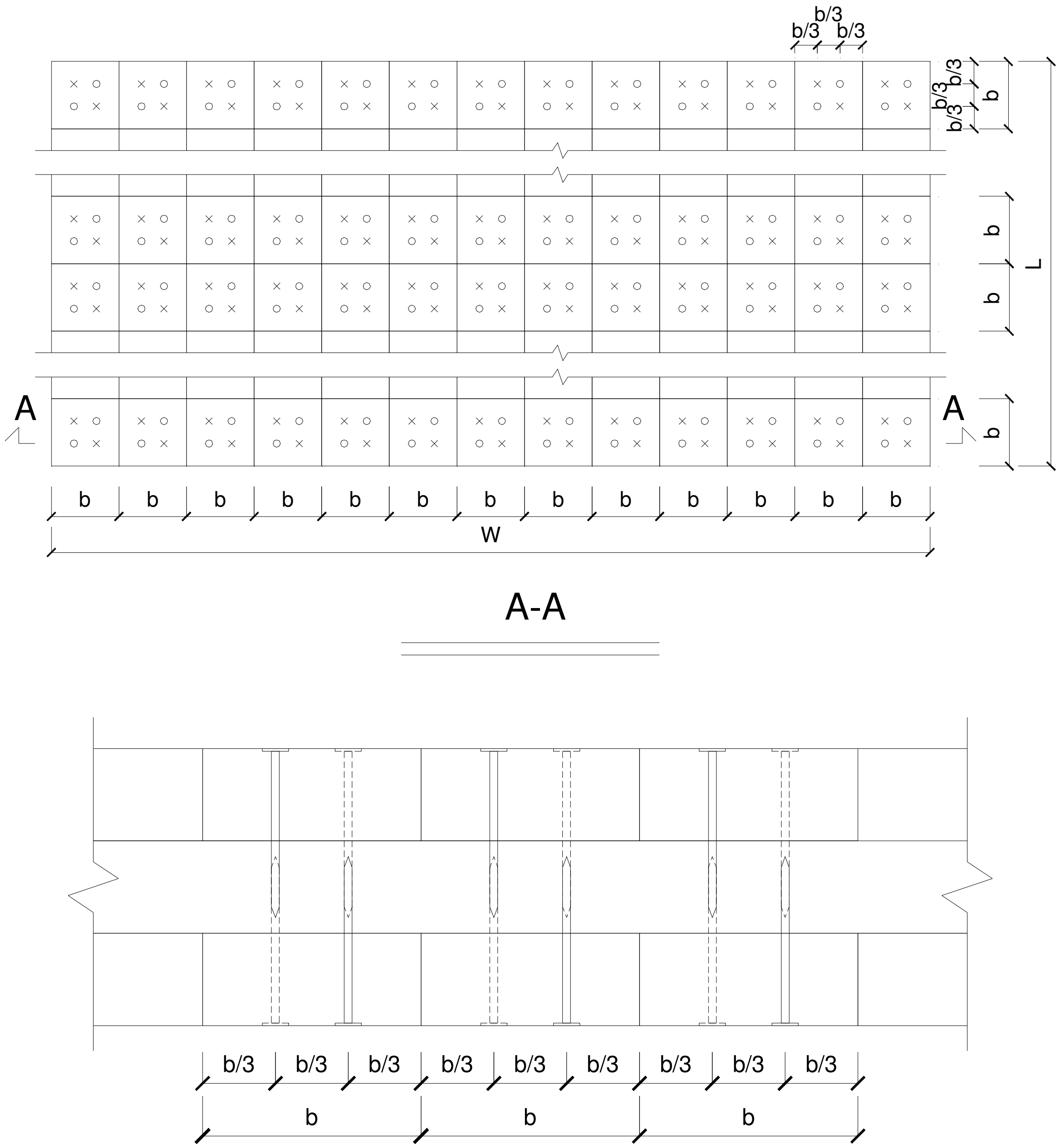

Figure 3-12 Nailing pattern of a three-layer cross laminated nailed plate.

Pencil marks were made on the wood surfaces to locate nail points quickly and accurately. Nails were driven straight down through the top and bottom layers with hammer. Because of their unique characteristics, aluminum nails tended to bend when they hit a hard spot such as a knot. In this case, they were replaced by steel nails to ensure a complete bonding system. The number of steel nails was very small compared to the number of aluminum nails so that their influence on the whole structure was negligible. The nailing process and an end product of three-layer cross laminated nailed plates are shown in Figure 3-13.

Figure 3-13 Manufacturing of a three-layer cross laminated nailed plate.

To establish an accurate numerical model, material properties of MPB wood and aluminum nails were tested as shown in sections 3.3.2 and 3.3.3.

3.3.2 Compression parallel to grain test

According to Wood Handbook (1999), relationships between mechanical properties of lodgepole pine at a moisture content of 12% are listed as follows,

Table 3-1 Elastic ratios for lodgepole pine at approximately 12% moisture content.

E_T/E_L	E_R/E_L	G_{LR}/E_L	G_{LT}/E_L	G_{RT}/E_L	μ_{RL}	μ_{LT}	μ_{RT}
0.068	0.102	0.049	0.046	0.005	0.032	0.347	0.469

where E represents modulus of elasticity; G modulus of rigidity; and μ Poisson's ratio. The longitudinal axis L is parallel to the fiber (grain); the radial axis R is normal to the growth rings (perpendicular to the grain in the radial direction); and the tangential axis T is perpendicular to the grain but tangent to the growth rings. The modulus of elasticity E_L along fiber direction was obtained from compression parallel to grain test.

Thirty compression test specimens with the dimensions of 33 mm × 83 mm × 267 mm were cut from the MPB wood. They were conditioned in a conditioning room maintained at 20 ^{o}C and at 65% relative humidity (RH). Weight, dimensions and moisture content of each piece were recorded at the time of testing (Table 3-2). The compression parallel to grain test was conducted in accordance with ASTM Test Methods D 198 "Standard test methods of static tests of lumber in structural sizes" (ASTM 2004). For measuring load deformation data, a constant rate of head motion of 0.267 mm/min was applied. Deflection under the compression load was measured over a 216 mm gage length with two linear variable displacement transducers (LVDTs) – one on each side of the specimen. Load and displacement signals were collected by a data acquisition system. Figure 3-14 shows the compression test setup. Figure 3-15 is a typical stress-strain relationship observed during compression testing. It was shown that stress increased with strain until the ultimate compressive stress point, and then the stress decreased with increasing strain. The maximum recorded strain was based on an arbitrary stopping point for the test to prevent damage to the test instrumentation.

Table 3-2 Compression parallel to grain test sample.

Sample size	Average dimensions (mm)			Average moisture content (%)	Average weight (g)
	Length	Width	Depth		
30	267	82	32	11.89	326.75

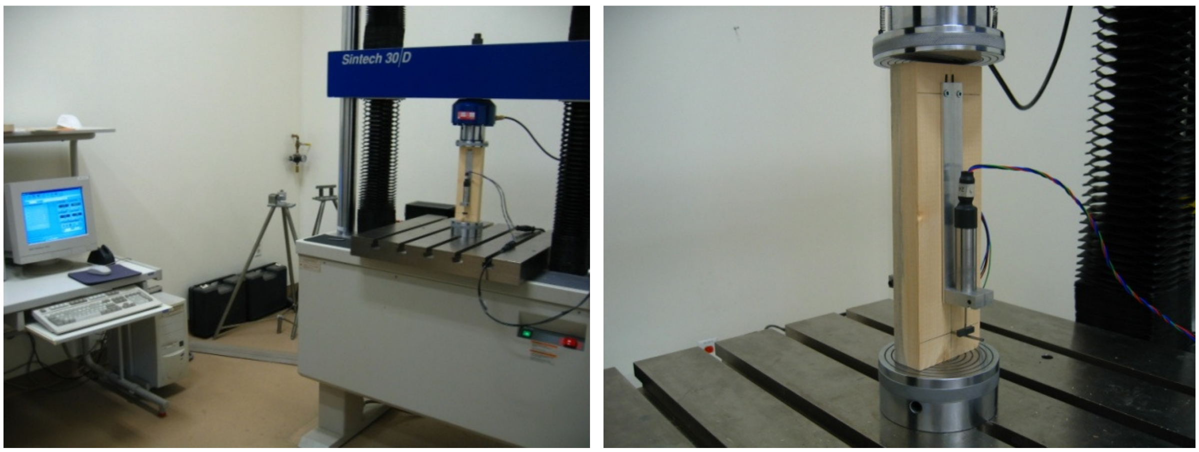

Figure 3-14 Compression parallel to grain test of MPB wood.

For the stress-strain relationship shown in Figure 3-15, the ultimate compression stress was 29.47 MPa, with an associated strain of 0.008569 and 0.008537 by transducer 1 and transducer 2, respectively. In this study, the material constitutive relation was assumed to be linear. So the slope of the up-loading part of the curve (i.e. before the ultimate compression stress point) was used as the modulus of elasticity value. The MOE value of the specimen was obtained by averaging results from the measurements of the two transducers. The average MOE of the thirty specimens was 10.24 GPa with a standard deviation of 1.79 GPa. This MOE value was used as E_L to calculate the other material properties based on the ratios listed in Table 3-1.

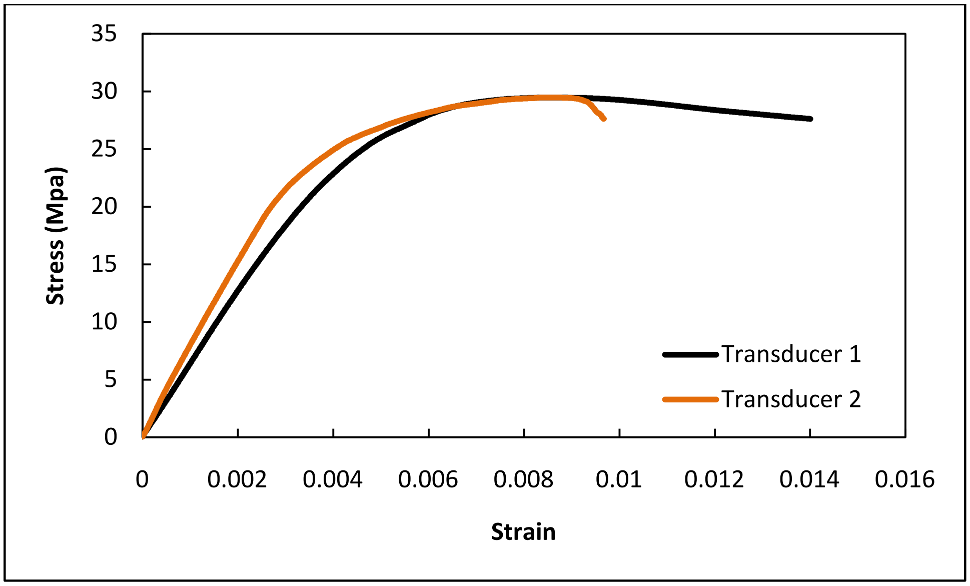

Figure 3-15 Stress-strain relationship of a specimen under compression parallel to grain test.

3.3.3 Nail lateral resistance test

The aluminum nails (Figure 3-16) mainly functioned to provide resistance to slippage between the layers when the plate was subject to out of plane bending loads.

Two types (A and B) of nail connection with nails loaded in single shear were manufactured and ten specimens of each type were tested. The nailing pattern was exactly the same as that of the nailed panels. The test set up is shown in Figure 3-17 and Figure 3-18. Again, the circle and cross represent nails driven into and out of the paper plane, respectively. b and h are 83 mm and 33 mm, respectively. In type A connection, the fiber orientation of the middle member was vertical while that of the two side members was horizontal. Type B connection was assembled in an opposite way meaning that the middle member had horizontal fiber direction and the side members had vertical fiber direction. Nails were inserted into the members using a hammer. Nails were driven as nearly perpendicular to the specimen surface as possible. The top of the nail head was left flush with the wood surface. Two LVDTs, one mounted on each edge of the middle member, were used and the load-displacement relationship of each specimen was recorded by a computer system.

Figure 3-16 A 63.5 mm aluminum siding nail.

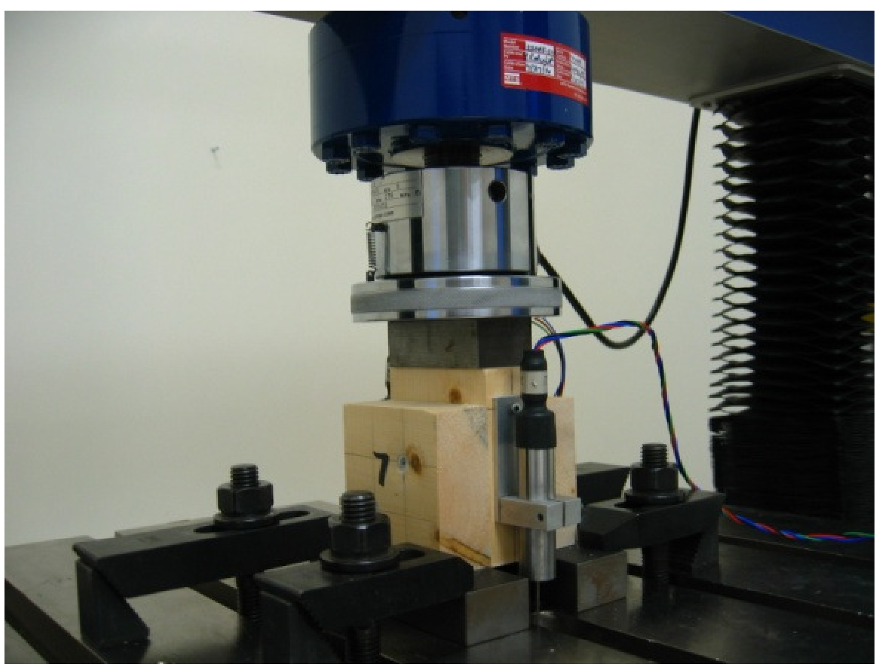

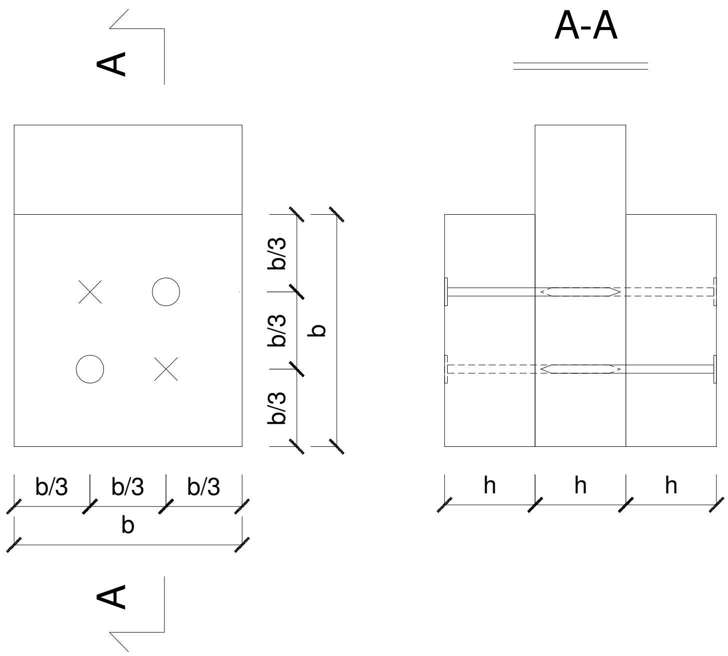

Figure 3-17 Nail lateral resistance test A.

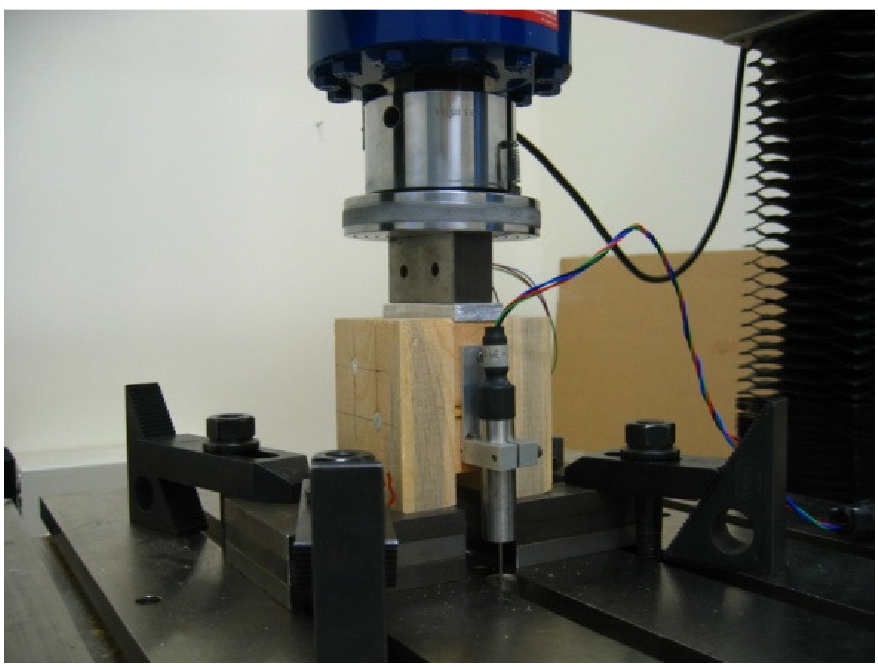

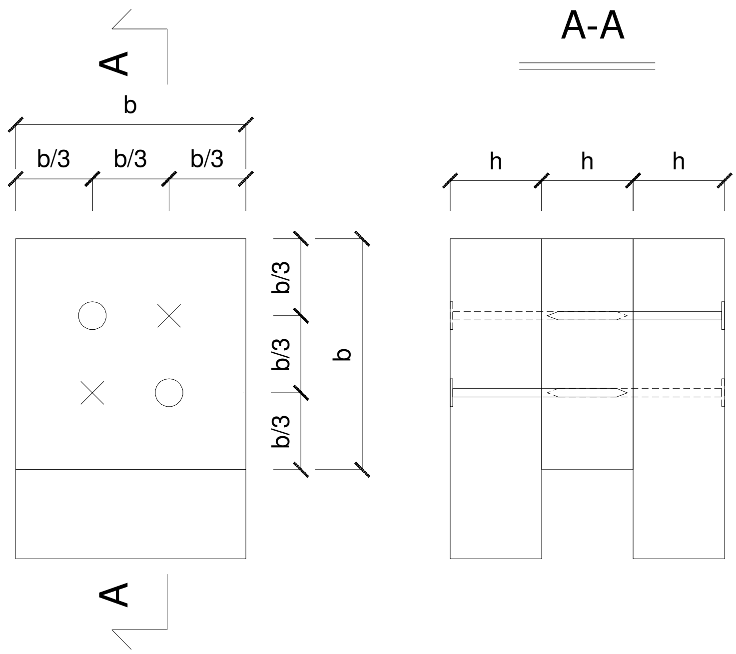

Figure 3-18 Nail lateral resistance test B.

Load-displacement curves for the two types of nail connection tests are shown in Figure 3-19. Load was given on a per nail basis assuming each nail carried one quarter of the total load. The displacement increased with load almost linearly in the beginning, and then it still increased up but with a decreasing slope until the specimen failed. Values from the average load-displacement curve were used to represent lateral resistance of the aluminum siding nails (Figure 3-20).

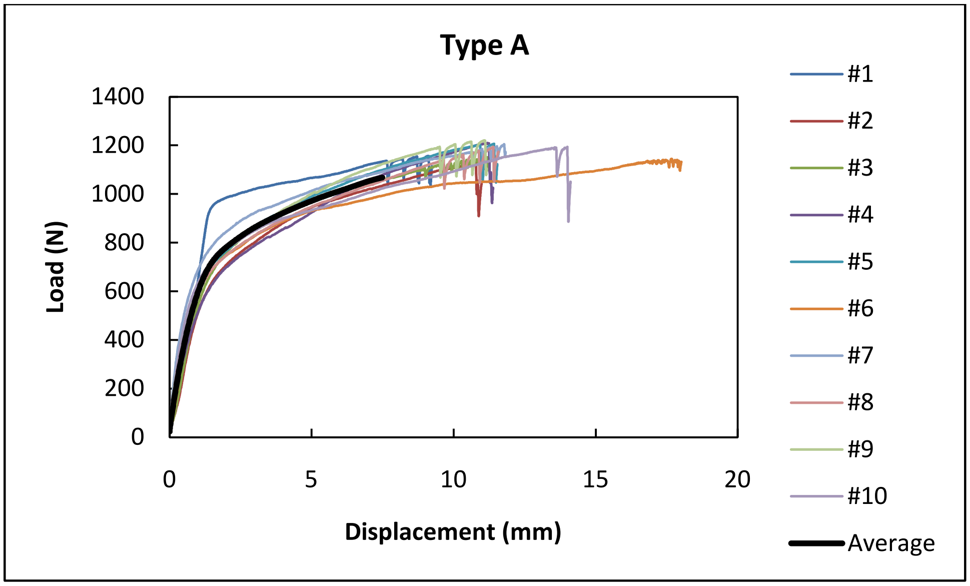

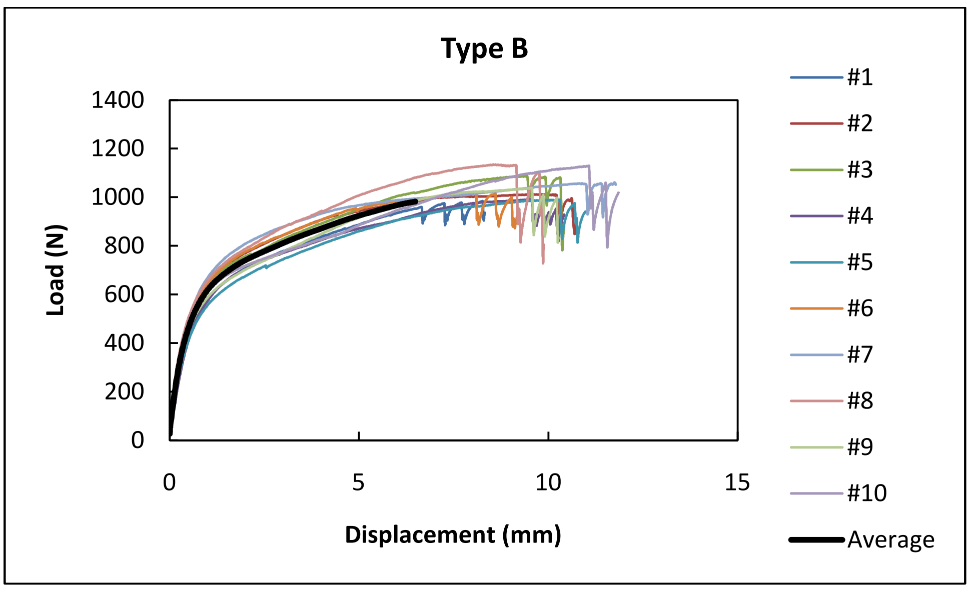

Figure 3-19 Load-displacement relationships of nail connections.

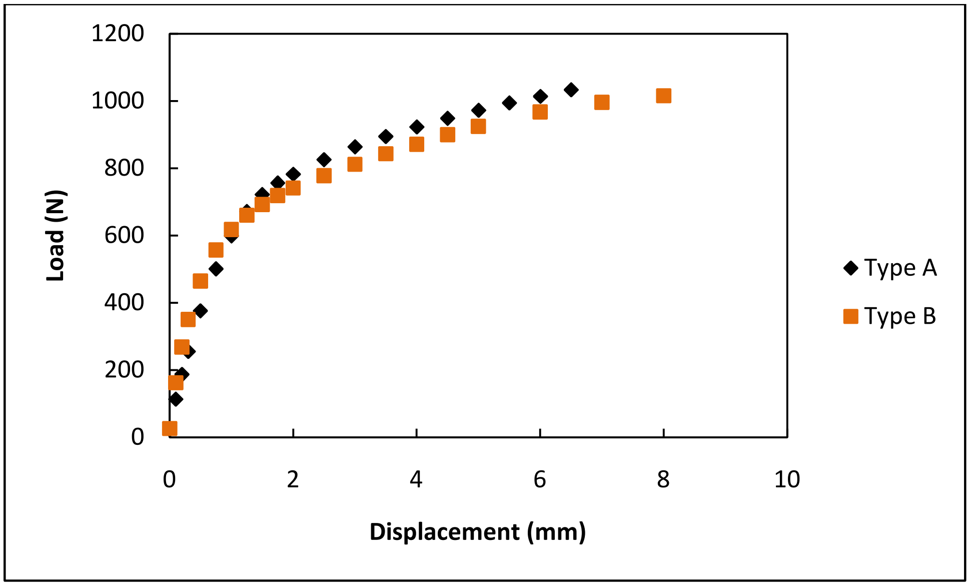

Figure 3-20 Load-displacement relationships used in the nail lateral resistance simulation.

3.3.4 Thick laminated plate bending test

The plate was simply supported at the two opposite ends (Figure 3-21). Two equal loads were applied at the quarter points of the span (2.158 m). The transverse loads were applied to the upper face of the specimens. An aluminum frame was placed on the upper face of the plate in a manner such that the frame would not deform as the plate deformed under load. Two LVDTs, one near each longitudinal edge of the specimen, were attached to the frame at the mid span. The deflection measurement was referenced to the plate deflection at the end supports. The load-deflection data was recorded with a computer system. A loading rate of 5 mm/min was selected to complete the testing.

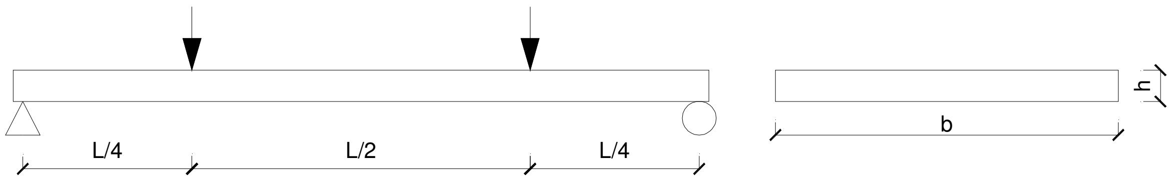

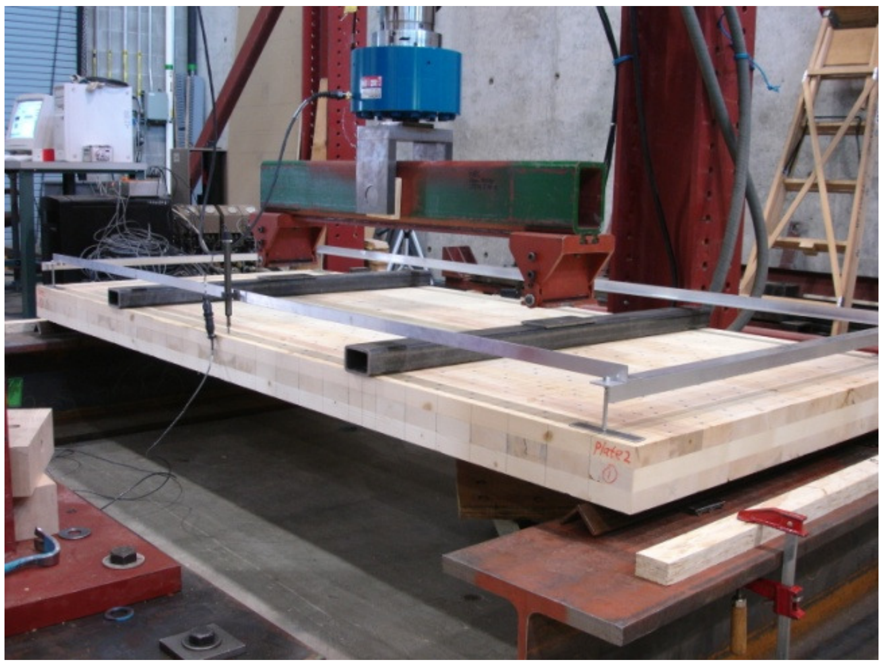

Figure 3-21 Bending test of a cross laminated plate specimen.

3.4 Results and discussion

Table 3-3 lists dimensions of the six cross laminated plate members. Even though they had different lengths, the test span was fixed to 2.158 m for all specimens. Based on section 3.3.2, MOE values of MPB lumber were obtained from compression parallel to grain test at a moisture content of 11.89%. Considering moisture content of the CLT during the experiments, these values were adjusted to different moisture content according to ASTM D 2915 “Standard practice for evaluating allowable properties for grades of structural lumber” (2004) (Table 3-3).

Table 3-3 Dimensions and tested bending properties of plate specimens.

Specimen		Glued plate			Nailed plate		
		1	2	3	1	2	3
Dimension	Length (m)	2.324	2.408	2.408	2.324	2.324	2.324
	Width (m)	1.079	1.118	1.118	1.079	1.079	1.079
	Depth (mm)	99	109.5	109.5	99	99	99
Material properties	Adjusted moisture content (%)	10	8	8	10	10	10
	MOE of MPB lumber (GPa)	10.561	10.902	10.902	10.561	10.561	10.561
Bending behavior	Peak load (kN)	205.39	233.69	249.42	103.01	103.27	107.95
	Max. bending stress at mid span from theory (MPa)	32.52	29.19	31.15	16.31	16.35	17.09
	Max. bending stress at mid span from FE analysis (MPa)	32.74	29.45	31.43	26.36	26.43	27.71

The theoretical maximum bending stress at mid span was calculated using $\sigma = PLh/16I$, where P was the peak load; L span; h depth of the panel; and I moment of inertia of the cross-sectional area of the transformed section. The cross-sectional area transformation of the CLT panels is shown in Figure 3-22.

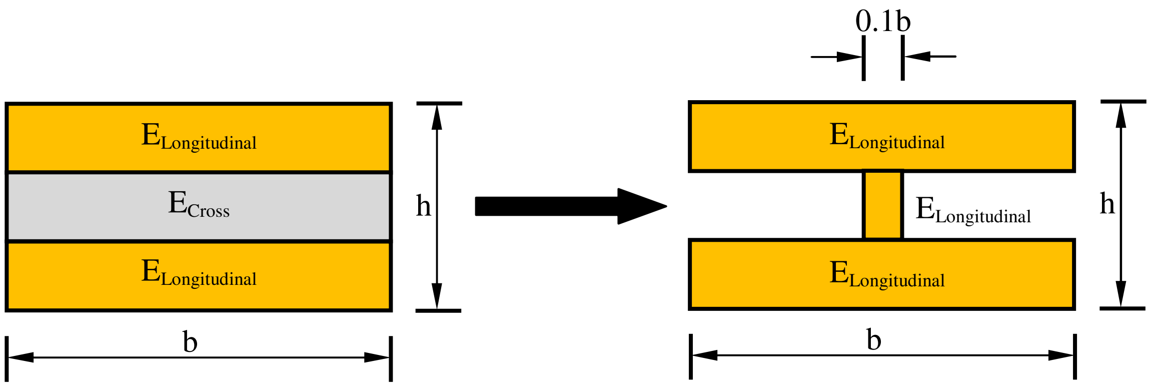

Figure 3-22 Cross-sectional area transformation of the CLT panels.

Here, $E_{Longitudinal}$ and E_{Cross} correspond to E_L and E_R in Table 3-1, respectively. Therefore, the ratio of $E_{Longitudinal}/E_{Cross} = 10$ was used to obtain the moment of inertia of the transformed section. The maximum bending stress of the panel was then calculated to be $45PL/58bh^2$, where b was the width of the panels. It was founded that the theoretical and numerical methods offered very close results for glued plates. But in the case of nailed plates, the theoretical model failed to give good predictions because slipping between neighboring layers, which was an obvious phenomenon, was not considered.

Figure 3-23 shows the computed vertical deflection contour of a glued plate under bending test using element SOLID45. As mentioned in section 3.2, both brick elements SOLID45 and SOLID95 were used in the finite element model and results were compared. Figure 3-24 displays comparisons between the numerical simulations and experimental data of the bending specimens using elements SOLID45 and SOLID95. Legend "G" and "N" represents glued and nailed plate, respectively; 1, 2 and 3 are specimen number. For example, G1 means glued plate #1 and N2 is nailed plate #2.

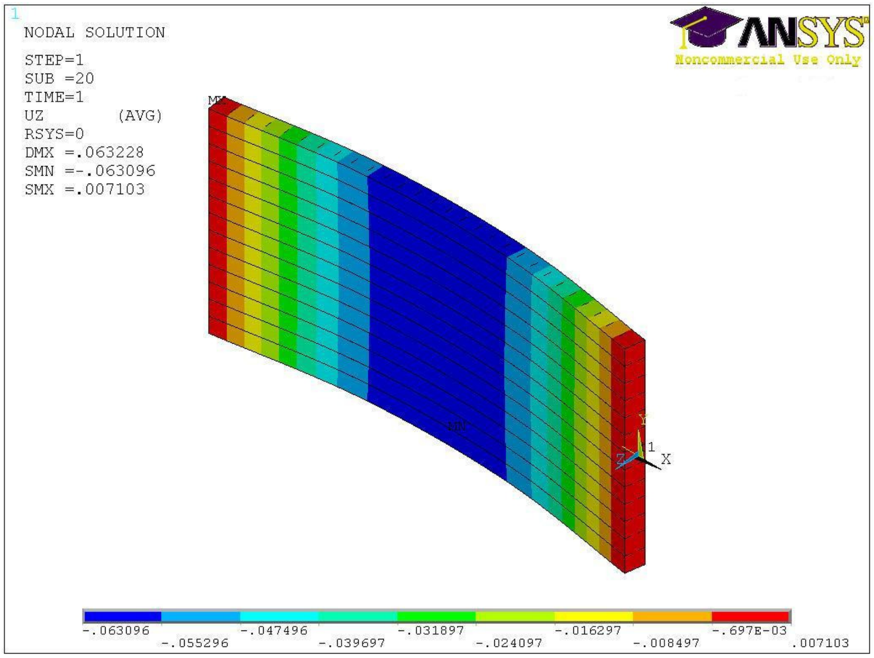

Figure 3-23 Vertical deflection contour of a three-layer glued plate under bending test.

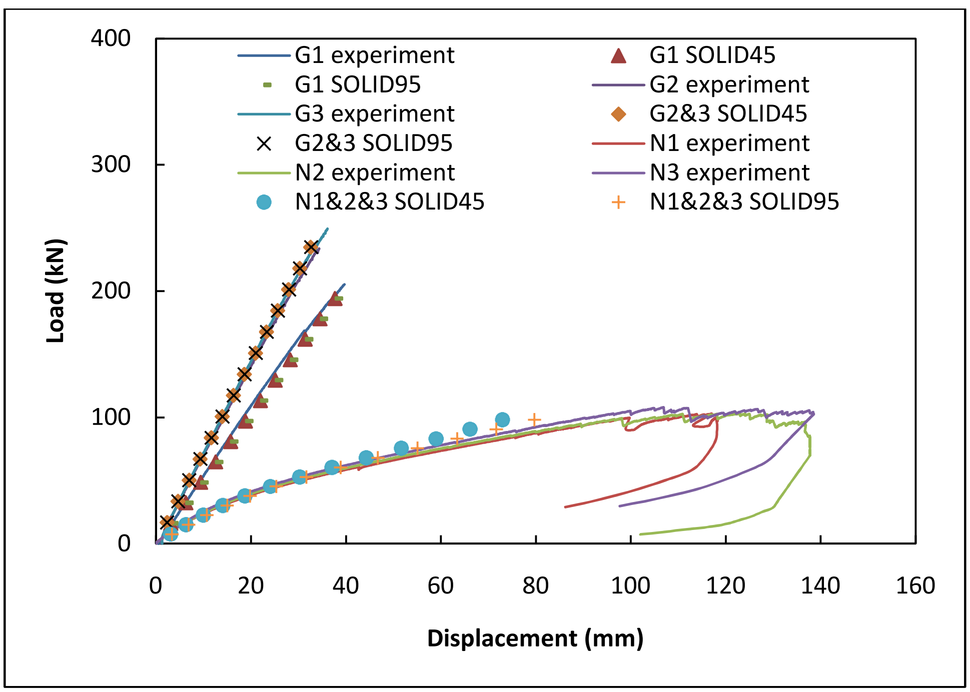

Figure 3-24 Comparison between finite element analysis and test results for plate specimens.

It was found that nailed plates showed a clear nonlinear behavior. Since deflection of the nailed plates was influenced by the coefficient of friction, experimental data was used to calibrate the finite element model and determine the appropriate value which was 0.1 in this case. Glued plates showed a linear load-displacement relationship until failure. It was not surprising to observe much lower peak load and higher deflection values for nailed plates compared to the glued ones because of the flexibility of nails. For more detailed peak load and bending strength information, refer to Table 3-3. The load carrying capacity of glued specimens were approximately twice as those of nailed ones.

Calculated and observed bending stiffness (EI) of glued specimens is given in Table 3-4. Numerical simulations using either element SOLID45 or element SOLID95 lead to an excellent agreement with measured results. Therefore, SOLID45 was chosen to further investigate more complicated plate configurations in the following chapters because of the computer time consumption and greater computational efficiency.

Table 3-4 Bending stiffness of glued specimens.

Specimen		1	2	3
Bending stiffness ($\times 10^6$ N·m^2)	Test	0.7832	1.0127	1.0374
	SOLID45	0.7417	1.0387	1.0387
	Error (%)	-5.30	2.57	0.12
	SOLID95	0.7390	1.0343	1.0343
	Error (%)	-5.65	2.13	-0.30

The classical plate theory is inadequate for the analysis of thick plates as it is based on a linear displacement across the entire thickness with transverse shear deformation neglected. In the case of CLT, transverse shear effect plays a significant role because of the low shear strength across the wood grain (often referred as rolling shear strength), which is only 20% to 30% of that parallel to the grain according to the Wood Handbook (1999). In addition, CLT is a very complicated material because of its inhomogeneosity, orthotropy and discontinuity.

Straight lines were drawn through the panel thickness before testing. It was very clear that the original straight lines did not remain straight between supports and loading points when load was applied for nailed plates (Figure 3-25 (a)). This obvious relative movement between neighboring layers was due to transverse shear effect and also the flexible characteristics of aluminum nails. The glued plates, on the other hand, showed a different phenomenon with lines remaining perfectly straight during testing (Figure 3-25 (b)). This evidence shows that the glue bond was very strong and the assumption of perfect bonding in the computer model was reasonable. The fact that glued plates deformed linearly until brittle failure occurred in wood rather than the adhesive joints could also be explained with this reason. All the specimens were loaded until failure occurred (Figure 3-26).

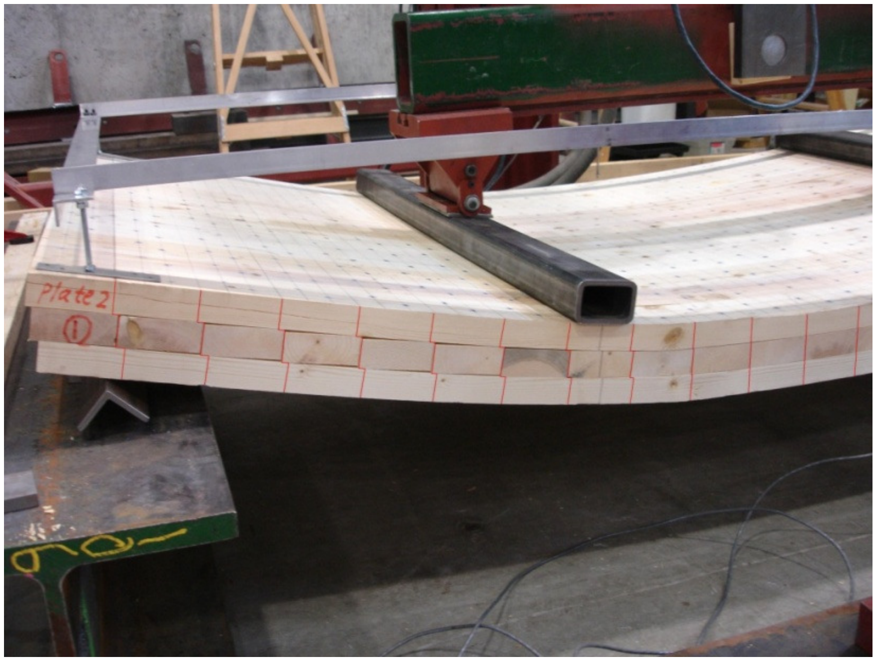

(a)

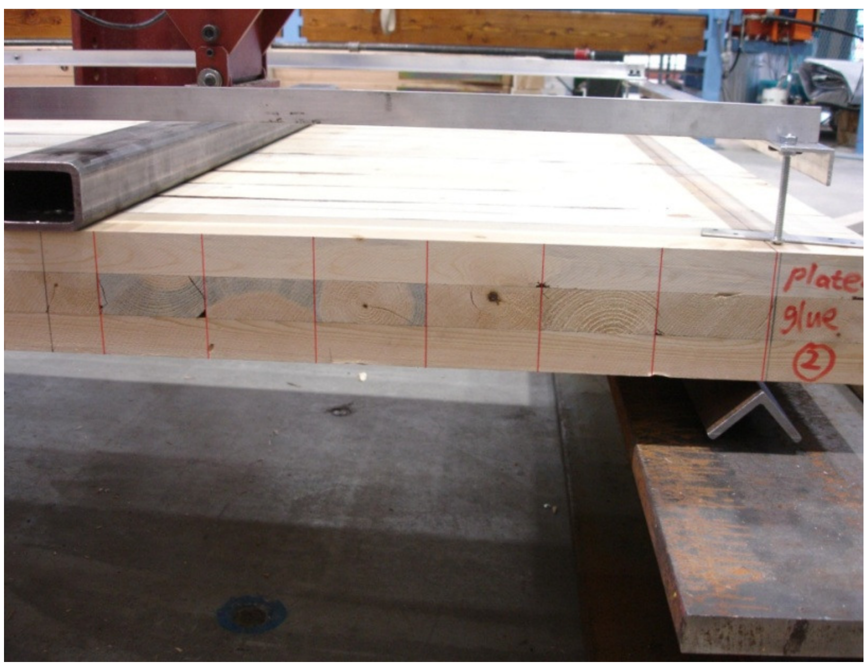

(b)

Figure 3-25 Relative movement between adjacent layers of (a) a nailed plate and (b) a glued plate.

(a)

(b)

Figure 3-26 Failure of (a) glued and (b) nailed plate specimens under bending test.

Two paths were defined in the finite element model to have a better understanding of stress and deflection information in glued structure (Figure 3-27). Here glued plate #1 was taken as an example. Figure 3-28 (a) is the contour of transverse shear stress (σ_{xz}) along path 1 under a total load of 194220 N. Figure 3-28 (b) shows the vertical deflection (U_z) along path 1. In the high shear stress area, obvious wood rolling shear failure was observed (Figure 3-29). Figure 3-30 (a) displays the bending stress (σ_x) along path 2. Because of the complexity of the CLT, e.g. the inner layer having lower MOE values compared to the outer ones, no edge glue, etc, the slope changes at the glue joint surfaces.

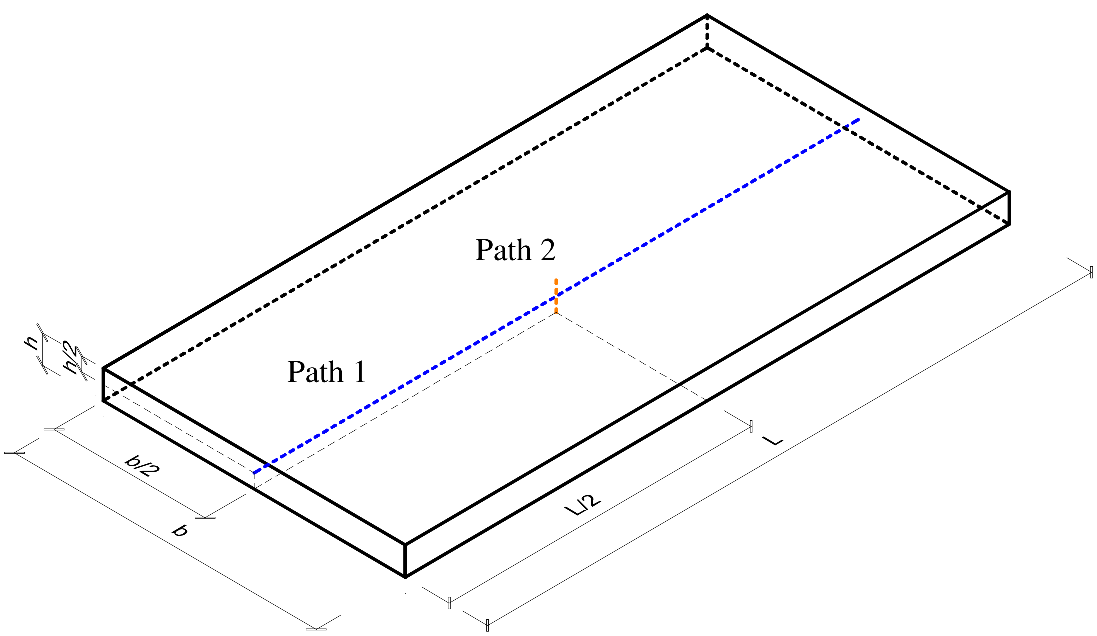

Figure 3-27 Path definition in glued plates.

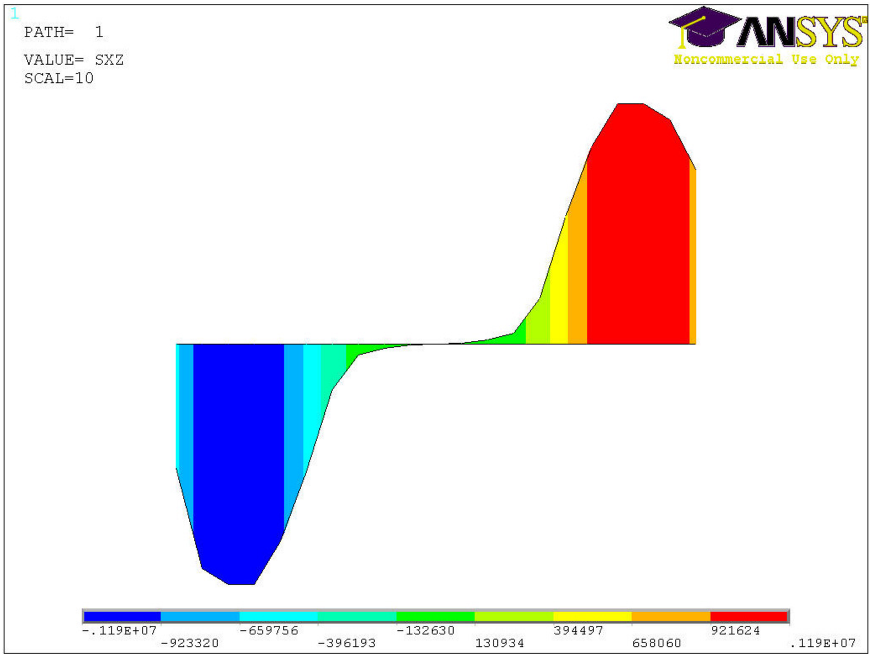

(a)

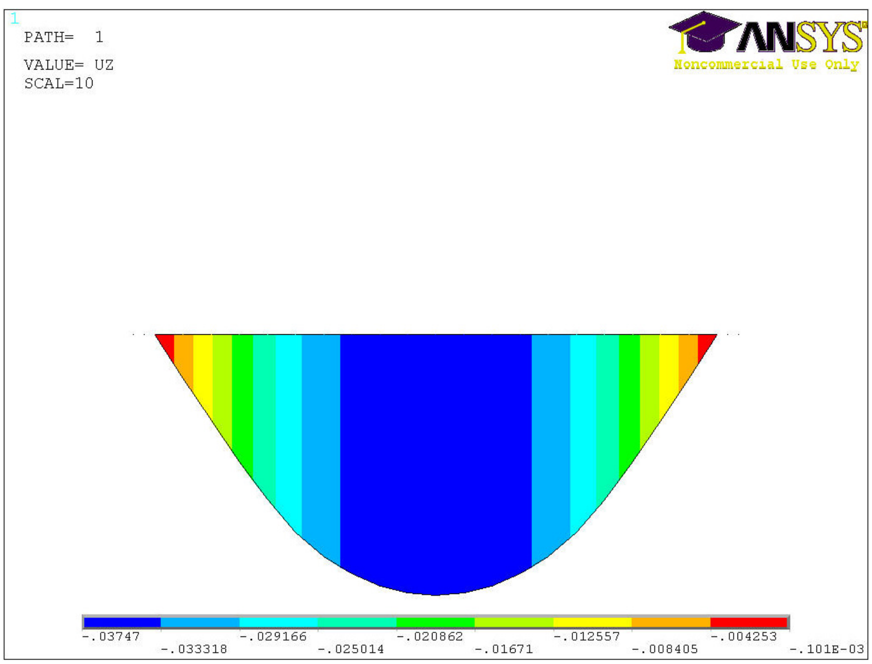

(b)

Figure 3-28 (a) Transverse shear stress and (b) vertical deflection along path 1 of glued plate #1.

Figure 3-29 Wood rolling shear failure in a glued plate.

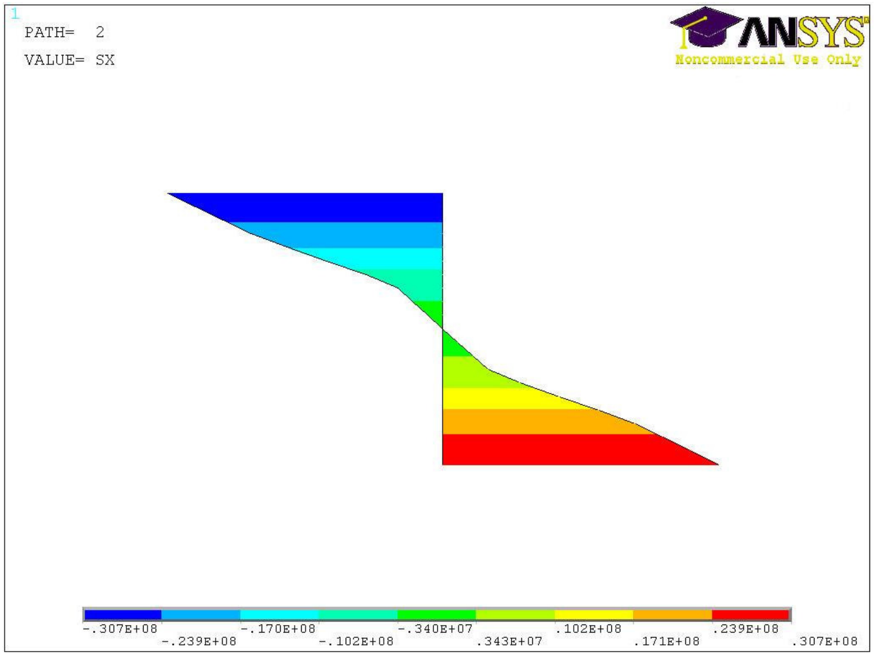

Figure 3-30 Bending stress along path 2 of glued plate #1.

3.5 Conclusions

In this chapter, 3-D finite element models were developed and verified with bending tests of three glued three-layer cross laminated plate specimens and three nailed three-layer cross laminated plate specimens. The numerical predictions agreed with measured data very well in terms of maximum deflection at mid span. Two types of elements, SOLID45 and SOLID95, gave similar results and SOLID45 was chosen for further study because of its computational efficiency. Different bonding methods, i.e. glue and aluminum nail, were also studied and compared. Glued plates performed more linearly compared to nailed ones and failed in a brittle fashion at the peak load. These 3-D models serve as a basis for further investigation on more complicated plate configurations in the next chapters.

CHAPTER 4 STUDY OF LAMINATED WOOD PLATES WITH DIFFERENT CONFIGURATIONS

4.1 Introduction

To expand the fundamental work presented in previous chapters, more complicated experimental scenarios were designed and performed to verify the predictions of the proposed model. Different from the conventional CLT, new laminated wood plate configurations were designed using the computer model verified in Chapter 3. In the new designs, variables such as material properties, number of layers, fiber direction in each individual layer, etc. were varied to investigate the corresponding structural performance of the plate. Four representative designs were constructed for testing.

A total of 1496 pieces of 22 mm × 100 mm × 4.29 m and 374 pieces of 22 mm × 100 mm × 2.45 m sawn lumber were prepared for the manufacturing of laminated plates. Properties such as modulus of elasticity, weight, specific gravity and vibration damping ratio of each individual piece were evaluated using a Metriguard Model 340 Transverse Vibration E-Computer system. The dynamic MOE was converted to static MOE values to be used in the finite element calculations. Moisture content and defect information of wood members were also recorded before the vibration test.

Forty laminated wood plates of four different configurations were manufactured at CST Innovations Ltd. in New Westminster, B.C.. Phenol-resorcinol-formaldehyde resin was employed to face-glue the adjacent layers. Third point bending tests were conducted on all plate specimens in the Timber Engineering and Applied Mechanics (TEAM) Laboratory at

UBC. The plates were proof loaded to produce a maximum deflection of about 15 mm to evaluate the MOE values. Test results were compared with finite element simulations.

4.2 Experimental studies

4.2.1 Materials

- **Lumber**

Kiln dried SPF (Spruce-Pine-Fir) lumber was supplied courtesy of Canfor Corporation, Canada. Some of the pieces came from trees attacked by mountain pine beetle. Detailed information of the lumber sample is listed in Table 4-1.

Table 4-1 Information on the kiln dried SPF lumber.

Dimension		Grade	Count
Nominal	Actual		
22 mm × 100 mm × 4.29 m	22 mm × 95 mm × 4.29 m	STD&BTR 15% UTIL	1496
22 mm × 100 mm × 2.45 m	22 mm × 95 mm × 2.45 m	STD&BTR 15% UTIL	374

- **Adhesive**

A liquid, phenol-resorcinol timber laminating resin Cascophen LT75C from Borden Chemical, Canada was chosen. The setting of this resin was obtained through reaction with a dry powdered hardener, Cascoset FM282. Immediately prior to lumber assembling, the hardener was added to the resin at a resin to hardener weight ratio of 100:12, and stirred until thoroughly dispersed. Specimens were bonded using a glue spread rate of 244 g/m^2 (50 lbs/1000 ft^2). This resin was similar to that used previously. It was selected based on industry recommendations and availability.

4.2.2 Specimen manufacturing

- **Lumber preparation**

All the wood members were numbered as the first step in the process (Figure 4-1). They were visually graded based on the characteristics such as blue stain, red heart, knots, wane, checks, etc.

Figure 4-1 A pile of 22 mm × 100 mm × 4.29 m SPF lumber.

The stiffness of each individual piece was measured directly with a non-destructive method using the Metriguard Model 340 Transverse Vibration E-Computer. The Model 340 E-Computer operated with a personal computer to determine material properties of a simply supported test specimen. MOE, weight and specific gravity were determined by processing the signal from a load cell at one of the supports during specimen vibration (Table 4-2). The vibrations were initiated by gently tapping the specimen by hand near the span center. Moisture content was measured at three points along the length of each specimen using a Delmhorst 2-pin moisture meter. The average value of these three readings was calculated to represent the moisture content of this piece. Figure 4-2 to Figure 4-5 show frequency distributions of moisture content and dynamic MOE values of the lumber specimens.

Table 4-2 Properties of the total tested SPF lumber.

	4.29 m lumber (1494 pieces)			2.45 m lumber (374 pieces)		
	Moisture content (%)	Specific gravity	MOE (GPa)	Moisture content (%)	Specific gravity	MOE (GPa)
Mean	14.98	0.48	8.75	14.81	0.49	9.14
SD*	1.76	0.05	1.67	0.92	0.04	1.73

* SD = standard deviation.

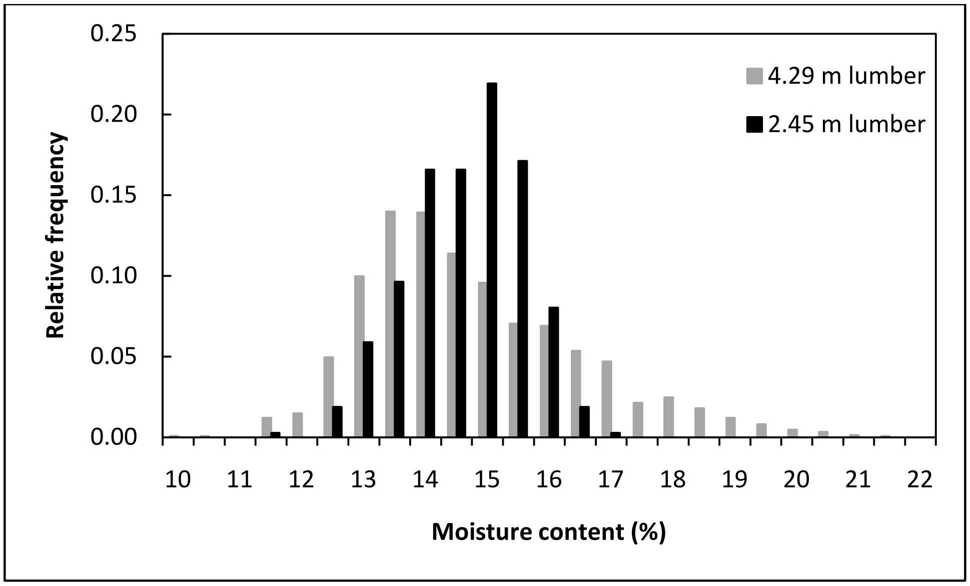

Figure 4-2 Relative frequency distribution of moisture content of the SPF lumber.

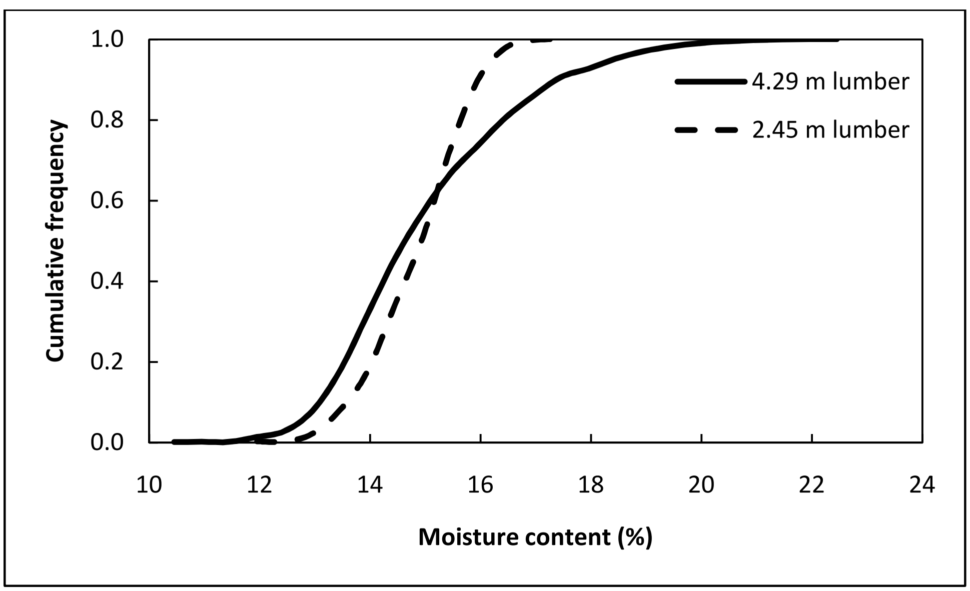

Figure 4-3 Cumulative frequency distribution of moisture content of the SPF lumber.

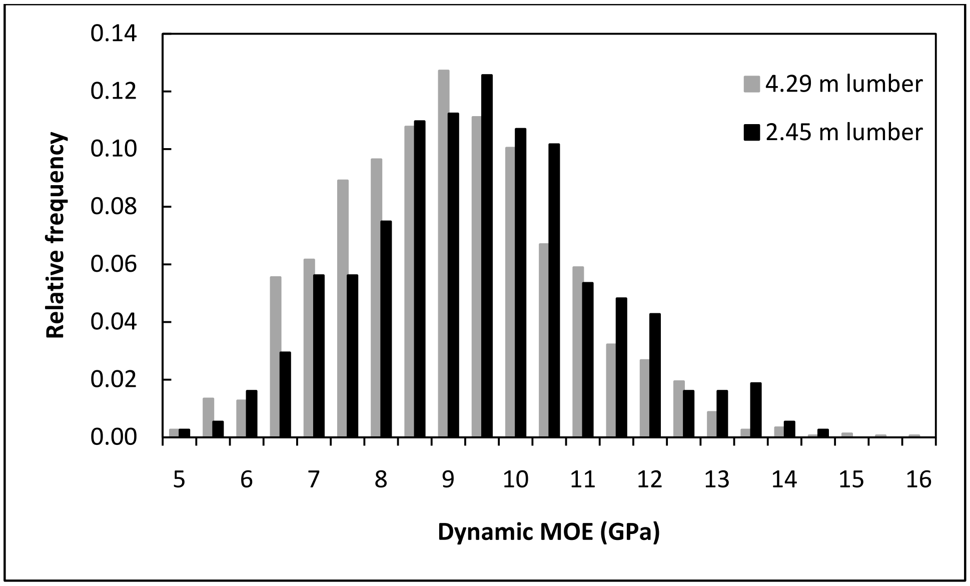

Figure 4-4 Relative frequency distribution of dynamic MOE values of the SPF lumber.

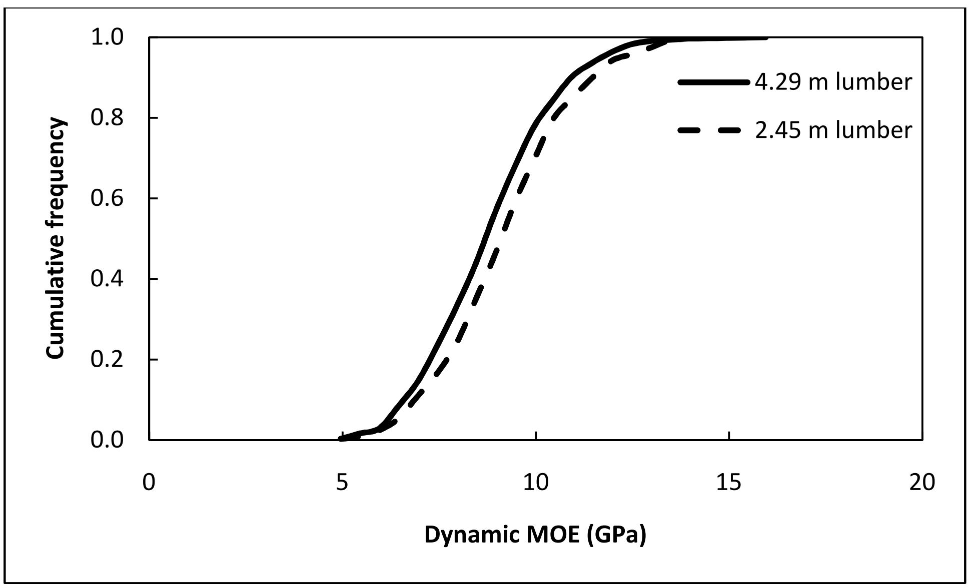

Figure 4-5 Cumulative frequency distribution of dynamic MOE values of the SPF lumber.

- **Plate Manufacturing**

The two wide faces of each piece of lumber were planed just prior to the gluing process to obtain clean, parallel, and gluable surfaces. This procedure ensured that the final assembly would be rectangular and the pressure could be applied evenly. Adhesives were then spread smoothly on the bonding surfaces with paint roller or glue applicator (Figure 4-6).

Figure 4-6 Planing and glue application of a piece of SPF lumber.

Laminations were then assembled into the specified lay-up pattern on the lay-up table without edge gluing. After the assembly was finished, pressure and temperature were applied using the Kallesoe A/S hot press. Specimens were pressed with a top pressure of 0.20 N/mm^2 (28.37 psi) and heated at a temperature of approximately 90^oC for about 120 minutes (Figure 4-7).

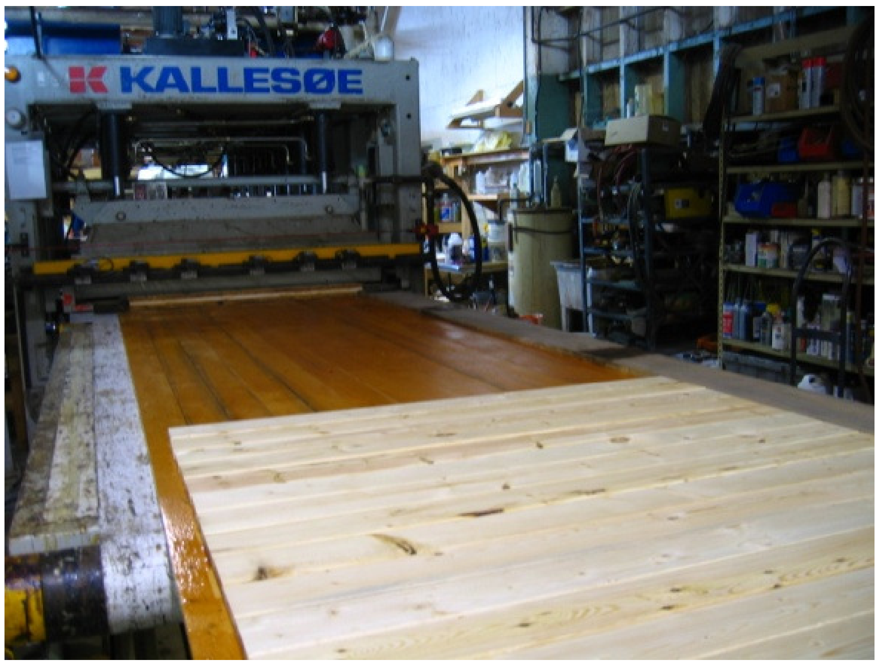

Figure 4-7 Assembling and pressing of a laminated plate specimen.

Detailed information of the four types of laminated plates is shown in Figure 4-8 and Table 4-3.

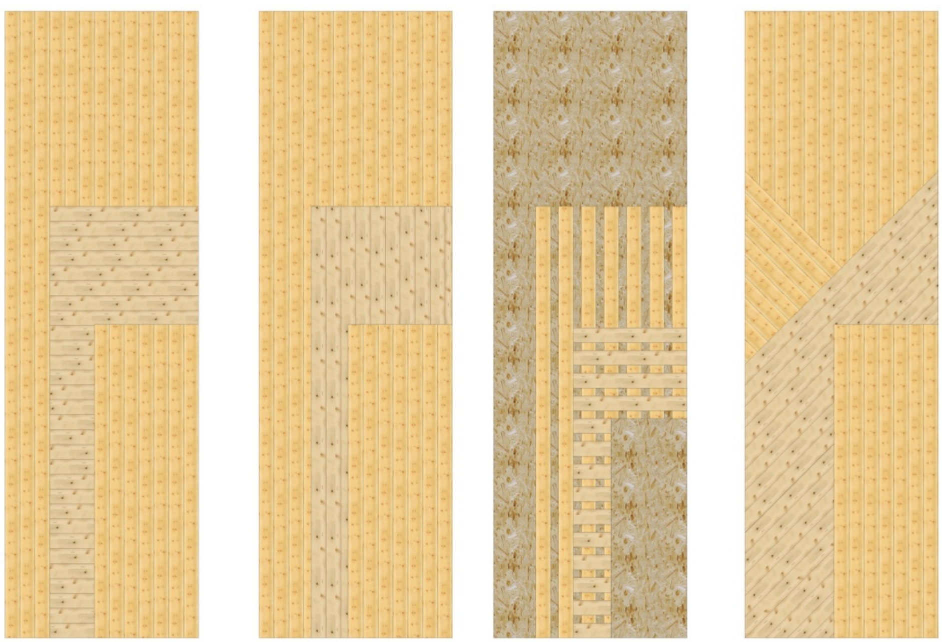

Figure 4-8 Plate configurations of the four types of laminated wood plates.

Table 4-3 Information of four types of laminated wood plates.

Configuration	Count	# of layers
Cross laminated	10	3
Parallel laminated	10	3
Cross laminated with OSB facing	10	4
45^{o} laminated	10	4

I. Three-layer cross laminated plate

This was a typical CLT layout where the fiber direction of the inner layer was perpendicular to that of the surface layers (Figure 4-9). Thirteen pieces of SPF lumber with glue on the top surface were put side by side together to form the bottom layer. Then the cross layer was placed with a layer of glue spread on top of it. Last step was to attach the finish ply which also contained thirteen SPF lumber pieces. Edge gluing was not performed.

Figure 4-9 A three-layer cross laminated plate.

II. Three-layer parallel laminated plate

Different from CLT elements, in this case all three layers were in the longitudinal direction of the plate. Edge gluing was not performed. The parallel layers were staggered with respect to each other so the gaps between wood members did not line up and the entire structure behaved as a unit (Figure 4-10).

Figure 4-10 A three-layer parallel laminated plate.

III. Cross laminated plate with OSB facing

First, two sheets of 1R24/2F16/W24 OSB panel with a thickness of 11 mm (7/16 inch) were placed end to end without any connection in between on the lay-up table to achieve the 4.29 m length. The OSB panels were obtained from Ainsworth Lumber Company. A layer consisting of 9 pieces of SPF lumber with glue applied on the bottom surface was then laminated on top of the OSB panels. These SPF members were also lying in the longitudinal direction of the plate. A 50 mm gap between the lumber pieces was maintained by provision of many precisely cut spacers (95 mm × 50 mm) to avoid movement during manufacturing process. Next, another layer of SPF lumber with glue applied on both wide surfaces was added in the cross direction. Again, spacers were inserted between lumber pieces to maintain the 50 mm gap and stabilize the whole structure. Since the spacers were not connected either to each other or to the surrounding members, they would not contribute to structural behavior of the whole plate and could be ignored in numerical simulations. Lastly, another two pieces of OSB panel were installed on top. At this stage the plate was ready for the pressing (Figure 4-11). Note that interfaces between adjacent OSB panels in the outer layers were staggered to avoid creating a very weak area in the plate.

Figure 4-11 A cross laminated plate with OSB facing.

IV. Four-layer 45^{o} laminated plate

According to the design, in which lumber was laid 45^{o} to the plate span direction in inner layers, lumber was cut at 45^{o} angle to its longitudinal axis at each end to different lengths. These 45^{o} pieces were used to form the inner layers of the plate. The two inner layers were perpendicular to each other, meaning that one was oriented at +45^{o} and the other was at -45^{o} with respect to the plate longitudinal direction. The two outmost layers on top and bottom consisted of thirteen SPF wood members and were parallel to the plate longitudinal axis (Figure 4-12). It was very important to align inner layer pieces carefully to ensure members in the same layer being parallel and oriented at +/-45^{o} to the plate axis. As with the cross laminated and parallel laminated configurations, edge gluing was not applied.

Figure 4-12 A four-layer 45^{o} laminated plate.

4.2.3 Third point bending test

To evaluate bending stiffness of the formed panels, third point bending test was carried out on all the forty specimens (Figure 4-13). The test specimen was simply supported and loaded by two equal, concentrated forces spaced equidistant between the supports. The transverse loads were applied to the upper face of the specimens. Ten LVDTs were attached to the middle plane of the plate at specific locations as shown in Figure 4-14. The span *L* was 4 m and the distance *a* was 0.1 m. Based on finite element analysis, plates were proof loaded to a maximum deflection at mid-span of about 15 mm, in order not to damage any of them. Loading rate was 3 mm/min and the load-deflection data was recorded with a data acquisition system.

Figure 4-13 Third point bending test on a four-layer 45^{o} laminated plate.

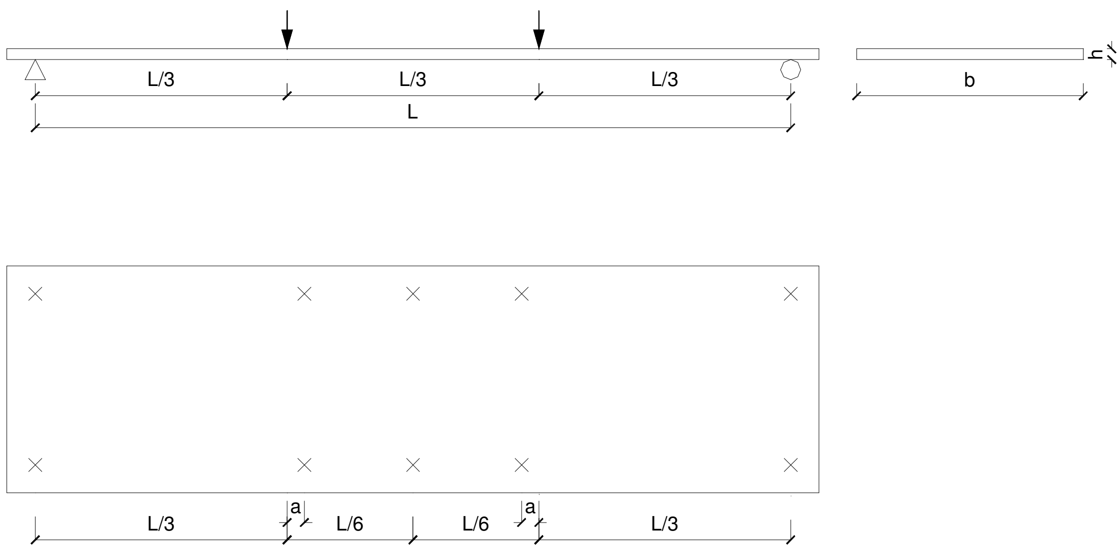

Figure 4-14 Transducer locations during the third point bending test.

4.2.4 Experimental results

Because moisture content has a significant impact on the mechanical properties of wood, the MOE value was adjusted to 10 percent moisture content in the finite element model to match the test condition during the third point bending test (Table 4-4). The adjustment was based on procedures specified in ASTM D 2915-98, "Standard Practice for Evaluating Allowable Properties for Grades of Structural Lumber" (ASTM, 2004).

Table 4-4 Adjusted dynamic MOE values of wood members.

Nominal dimension	Count	Dynamic MOE (GPa)		
		Mean	SD	COV
22 mm × 100 mm × 4.29 m	1494	9.52	1.81	0.19
22 mm × 100 mm × 2.45 m	374	9.92	1.92	0.19

Based on previous research work conducted at UBC, a factor of 0.95 was considered as the influence of the dynamic testing method.

$$E_{stat} \approx 0.95\ E_{dyn} \tag{4-1}$$

As mentioned in Chapter 3, according to Wood handbook, the relations between mechanical properties of Lodgepole pine were used as shown in Table 3-1. Again, E_L was approximated by increasing the static MOE values obtained from Eq. (4-1 by 10%.

In engineering design, the deflection of a structural member under applied loads can often govern the design by reaching the serviceability limit state prescribed by the building code. In theory, the total deflection of a structural member subjected to design loads is composed of the deflections induced by bending and shear stresses,

$$Total\ deflection\ (\delta_T) = Bending\ deflection\ (\delta_b) +\ Shear\ deflection\ (\delta_s) \tag{4-2}$$

Since the bending deflection is calculated separately from the shear deflection, the modulus of elasticity used to calculate the bending component of the total deflection (δ_b)

should be based on a shear-free modulus of elasticity, which is commonly termed "true E" in the wood engineering community. For prismatic bending members with a high span to depth ratio, the shear deflection under design loads is generally small as compared to the bending deflection. Therefore, for simplicity and practicality, it is customary to use the so-called "apparent modulus of elasticity", apparent E, for the calculation of total deflection δ_T. The apparent modulus of elasticity is related to the true modulus of elasticity by the following function,

$$E_{apparent} = \frac{E_{true}}{1+f\ (E_{true}\ ,I,K,L\ )} \tag{4-3}$$

where $f\ (E_{true}\ ,I,K,L\ ) > 0$ and

$I = moment\ of\ inertia$

$K = shear\ deflection\ coefficient$

$L = span\ of\ the\ specimen$

From Eq. 4-3, it is clear that the true modulus of elasticity is greater than the apparent modulus of elasticity. When the span becomes longer for the same bending member, $E_{apparent}$ approaches E_{true}. On the other hand, when the span becomes shorter, the difference between $E_{apparent}$ and E_{true} becomes more significant.

In this study, the apparent bending stiffness and true bending stiffness, which were associated with $E_{apparent}$ and E_{true} respectively, were determined through the above-mentioned third point bending test for all plate specimens. The apparent bending stiffness was determined from the mid-span deflection measured at the neutral axis by referencing to the supports since the shear deflection was already included in the experimental data. The true bending stiffness was determined from the mid-span deflection measured at the neutral axis by referencing to points between the loading points where there were no shear stresses.

Figure 4-15 to Figure 4-18 show all the load-displacement relationships observed from the third point bending test. All specimens deformed linearly with respect to applied load until the test was terminated. For each plate configuration, at the same load level, relative deflections which were used to calculate apparent MOE values were about ten times those used for true MOE calculations. It was also noticed that plates with OSB facing needed much lower load than the other configurations at the same deflection level. This was due to the fact that there was only one layer of lumber in the longitudinal direction to take the bending load in this type of plate.

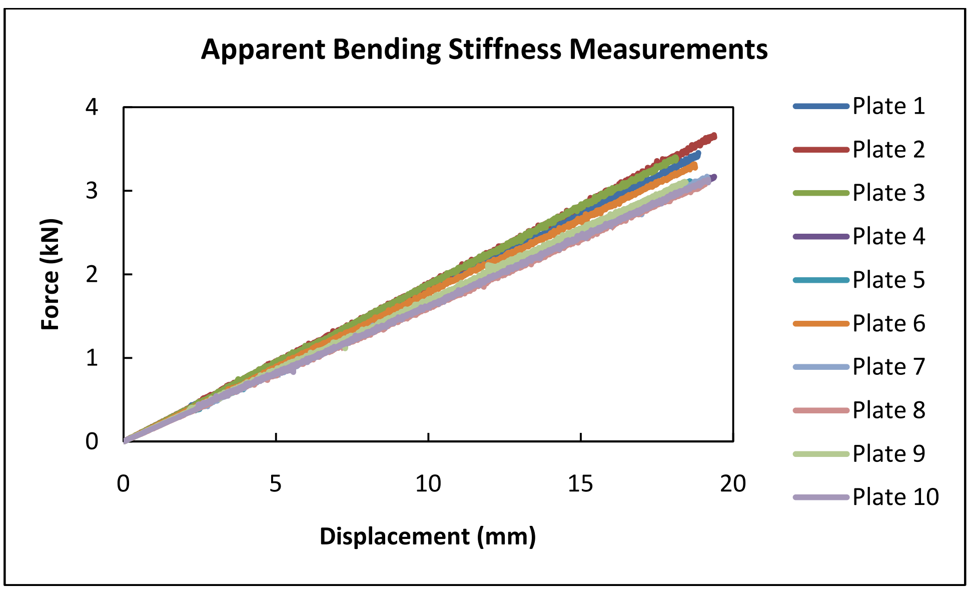

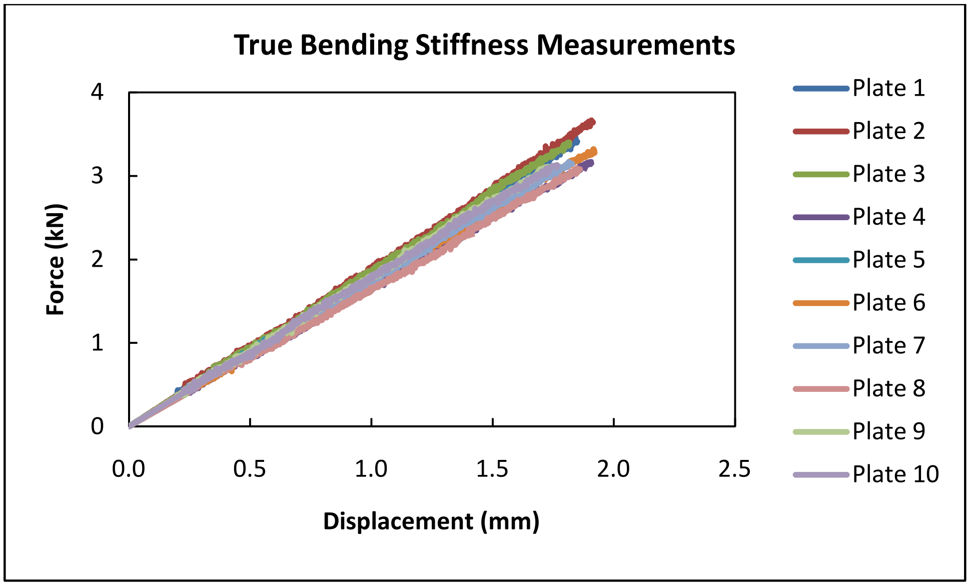

Figure 4-15 Load displacement measurements for apparent and true bending stiffness of cross laminated plates.

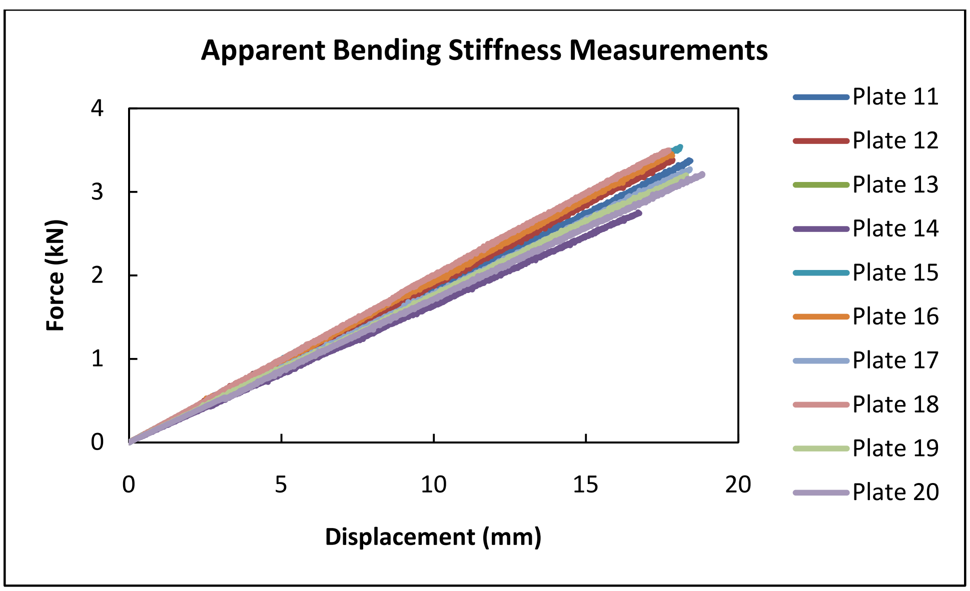

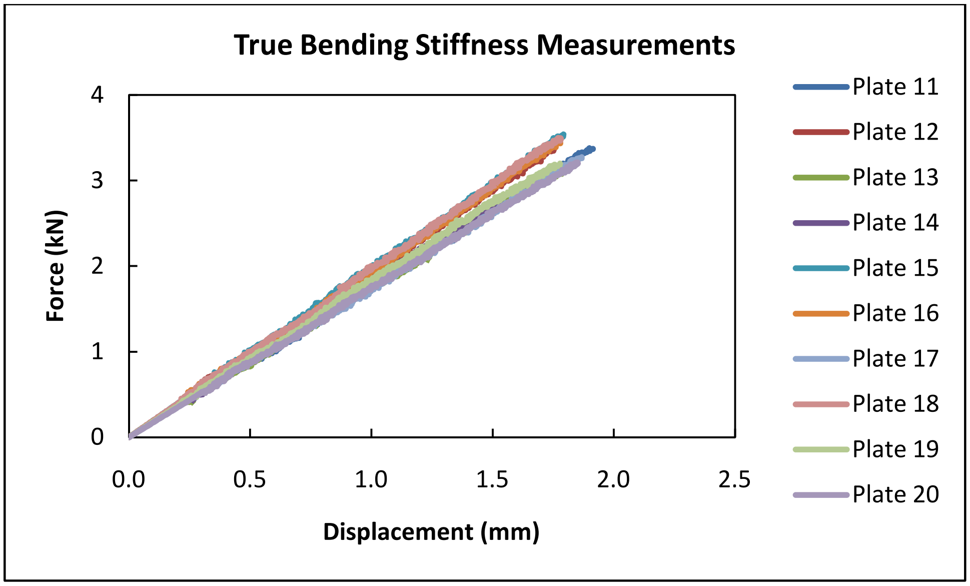

Figure 4-16 Load displacement measurements for apparent and true bending stiffness of parallel laminated plates.

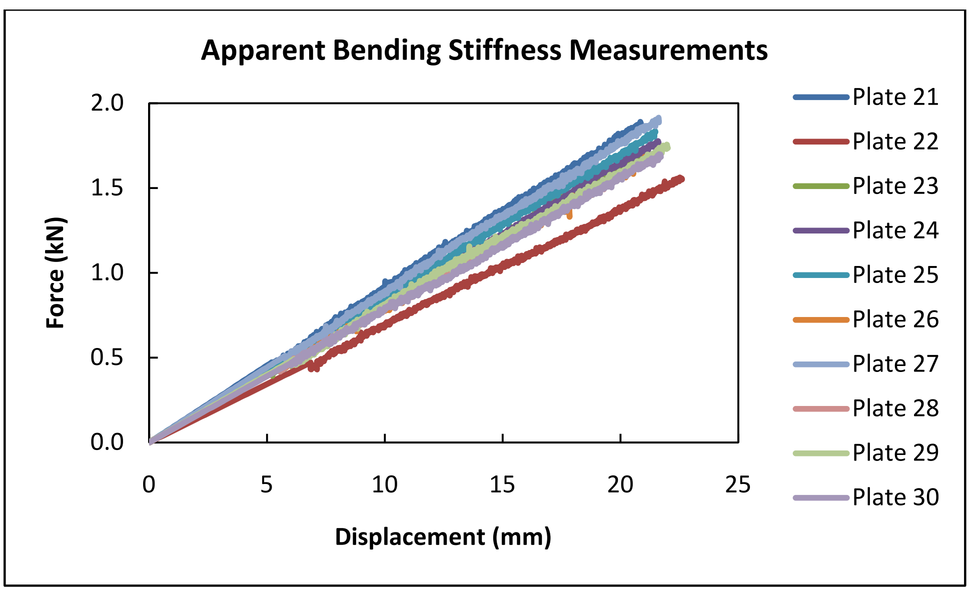

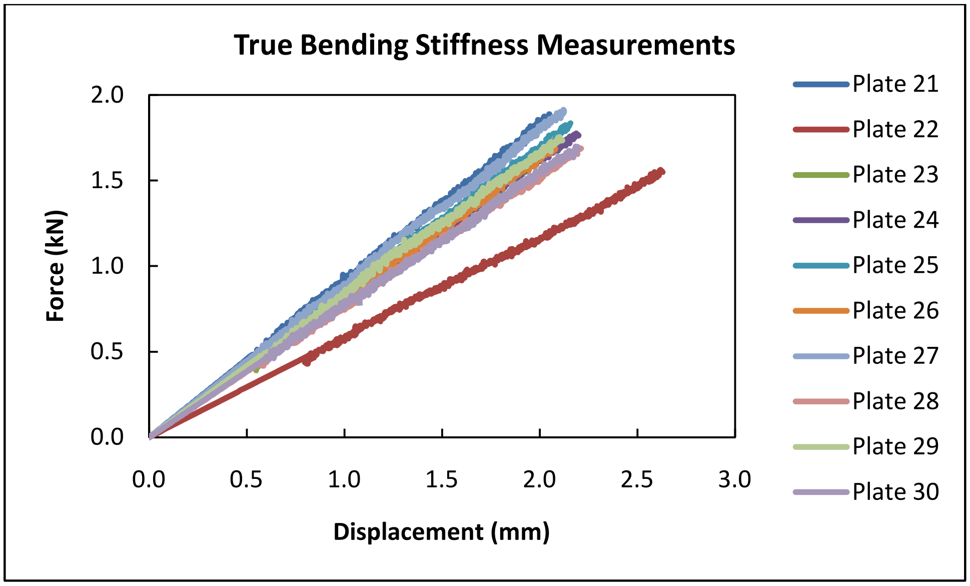

Figure 4-17 Load displacement measurements for apparent and true bending stiffness of cross laminated plates with OSB facing.

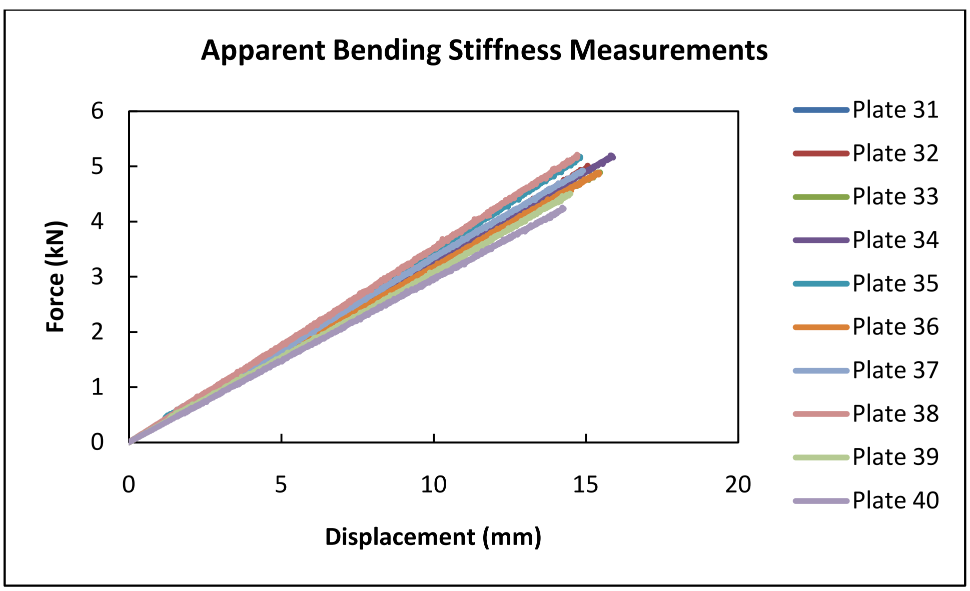

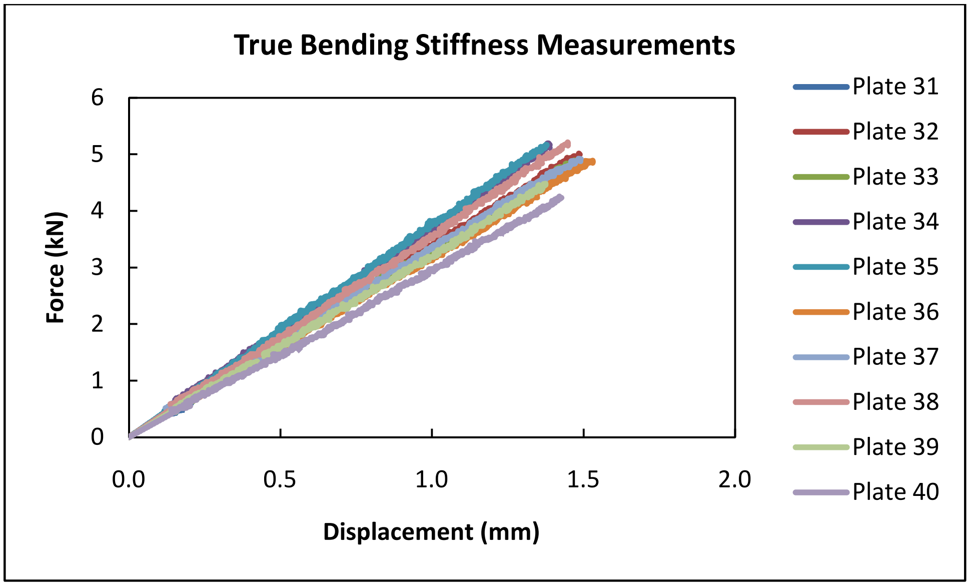

Figure 4-18 Load displacement measurements for apparent and true bending stiffness of 45^{o} laminated plates.

The tested apparent and true bending stiffness values of the forty specimens are listed in Table 4-5. In this case, the apparent bending stiffness should have approached the true bending stiffness because all the plates were very thin, i.e. having high span-to-depth ratio, and shear effect was not a significant issue. From Table 4-5 it can be seen that the mean apparent bending stiffness values were a little greater than the mean true bending stiffness values, which was theoretically not possible. Because of the high span-to-depth ratio and changes of environmental conditions such as air humidity and temperature, specimens could not be guaranteed to be perfectly flat on the large flat surfaces. Actually after nine months in storage due to the availability of testing facilities, warp was observed on some specimens during testing. With warping, one/two corner(s) of the plate could not be fully supported by supports which were arranged horizontally on the floor. Load was needed to achieve a good contact between specimen and supports. Therefore, the mid-span deflection measured at the neutral axis by referencing to the supports decreased and the apparent bending stiffness values were artificially increased. But the true bending stiffness values were not much affected by this issue because all the measurement points were relatively close to the mid-span of the specimen and not influenced by plate warping. For this reason, both of the true and apparent bending stiffness were compared with numerical simulations but the more accurate true bending stiffness was used for the finite element model verification.

Table 4-5 Bending stiffness of laminated wood plates of different configurations.

	Specimen	Cross laminated plates	Parallel laminated plates	Cross Laminated plates with OSB facing	45^{o} laminated plates
Apparent bending stiffness ($\times10^5$ N·m^2)	Mean	1.96	2.08	0.91	3.70
	SD	0.11	0.13	0.07	0.19
True bending stiffness ($\times10^5$ N·m^2)	Mean	1.91	1.99	0.86	3.62
	SD	0.09	0.11	0.10	0.25

4.3 Finite element analysis

Because the finite element modeling procedure was already described in Chapter 3, no more details will be given in this section unless necessary. Forty table sets (one for each plate specimen) were created to locate lumber pieces by recording their label numbers in the proper positions in the tables. The table set for cross laminated plate #9 was taken as an example and shown in Figure 4-19.

Recall that the MOE value of each single piece of SPF lumber was obtained before plate manufacturing, every piece was given its own material properties in the model. Due to glue squeeze-out during the pressing process, labels on some pieces were covered and could not be read. In this case, members with missing labels were given the average MOE value of their original group. For example, wood cut from 2.45 m materials was given mean MOE of the 374 pieces of 2.45 m lumber. However, this phenomenon was very rare, so the influence of missing label pieces was negligible. Figure 4-20 to Figure 4-23 show finite element models of all four plate layouts. The layers were set apart from each other to give a better demonstration of the plate structure. It is very easy to tell the fiber direction of each layer in these models. Figure 4-22 clearly shows the discontinuity of OSB panels on the outer layers.

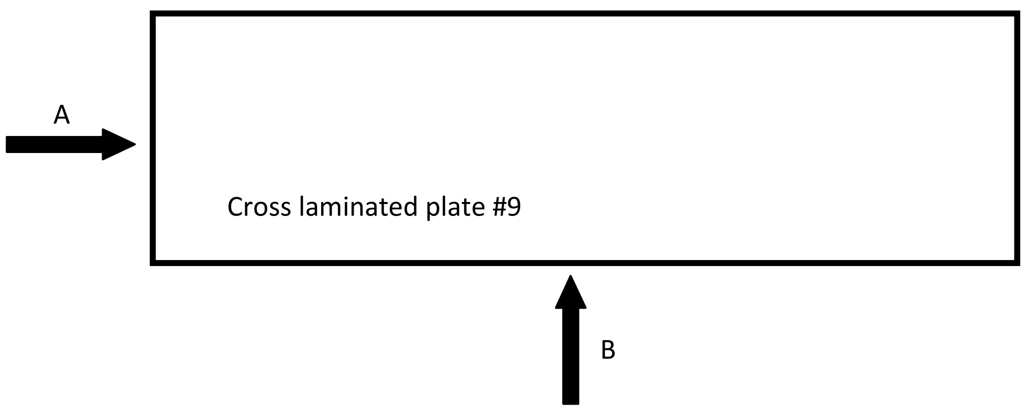

View A

1386	1376	1384	1382	1381	1380	1378	1366	1372	1365	1375	1355	1374
1407	1387	1388	1390	1408	1394	1392	1391	1396	1395	1393	1379	1397

View B

1583	1550	1506	1527	1538	1536	1532	1530	1551	1539	1550	1551	1530	1531	1535	1534	1540	1519	1520	1528	1529	1509	1526	1497	1524	1533	1532	1540	1519	1520	1528	1549	1529	1533	1508	1510	1523	1509	1523	1522	1522	1521	1497	1508	1531

Figure 4-19 Table set for cross laminated plate #9.

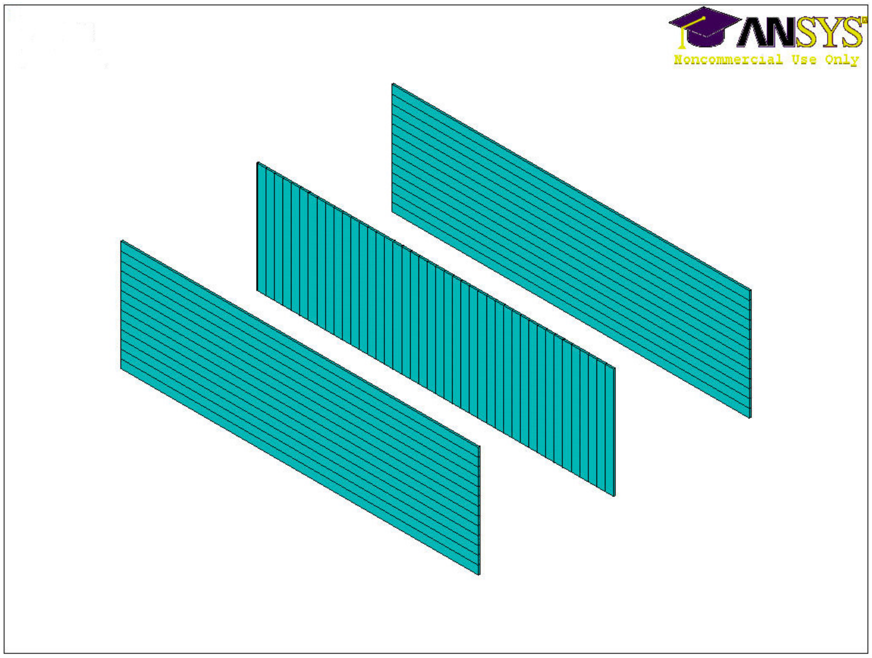

Figure 4-20 Model of a three-layer cross laminated plate.

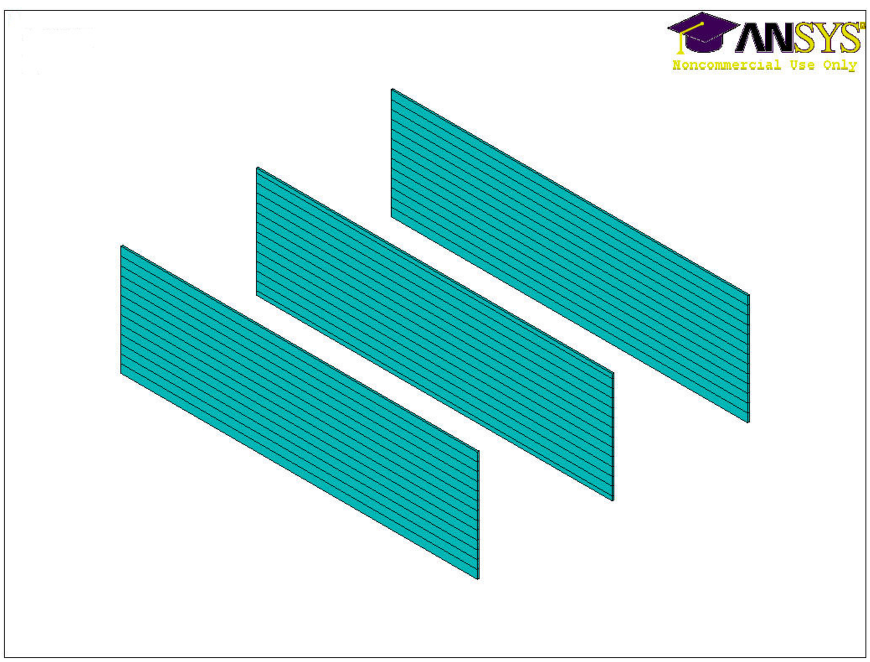

Figure 4-21 Model of a three-layer parallel laminated plate.

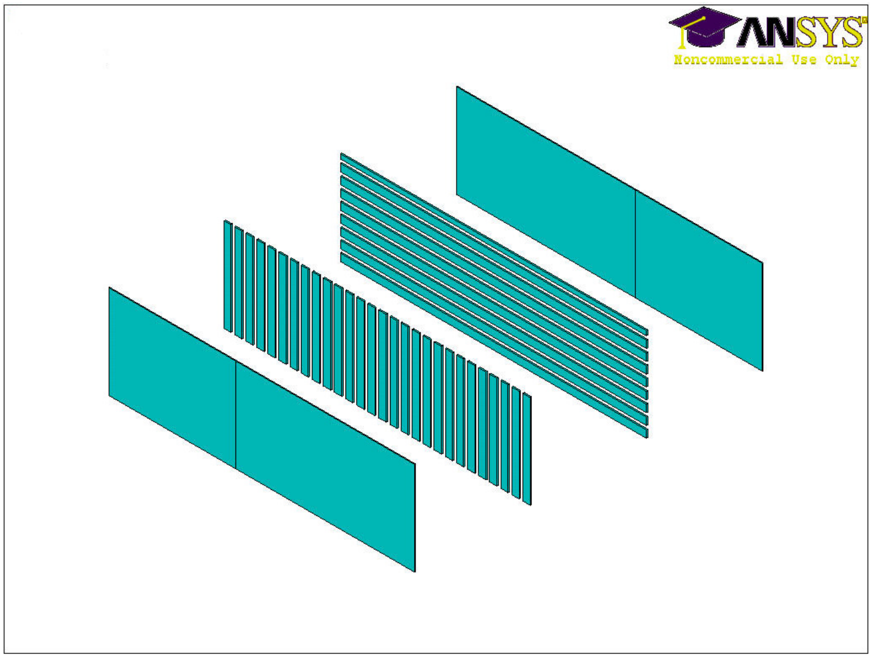

Figure 4-22 Model of a cross laminated plate with OSB facing.

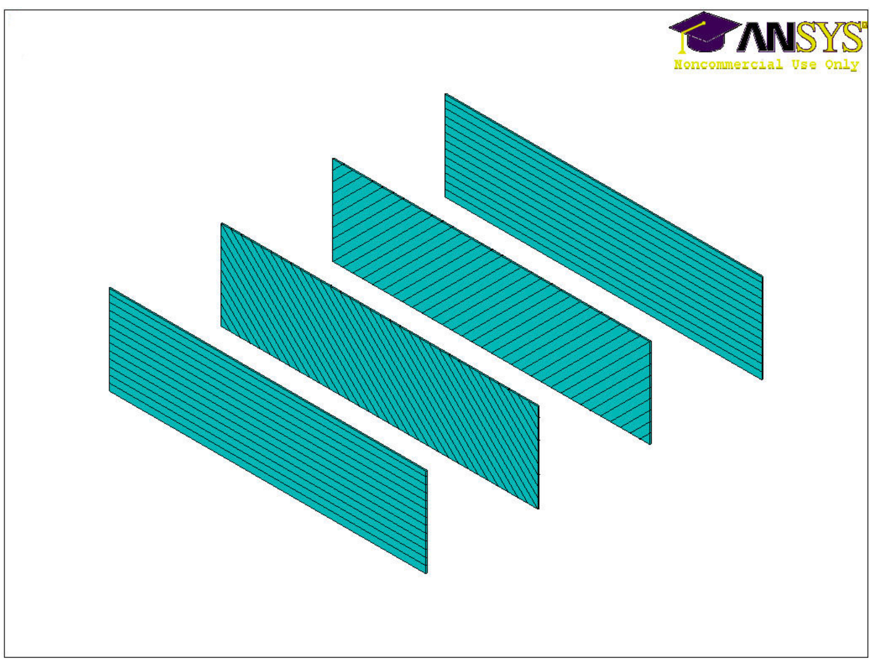

Figure 4-23 Model of a four-layer 45^{o} laminated plate.

The specimen dimensions used in finite element modeling are presented in Table 4-6.

Table 4-6 Specimen dimensions used in finite element modeling.

Configuration	Cross laminated plates	Parallel laminated plates	Cross laminated plates with OSB facing	45^{o} laminated plates
Length (m)	4	4	4	4
Width (m)	1.2350	1.2350	1.2190	1.2065
Thickness (mm)	58.5	58.5	58.0	74.0

The input elastic properties of OSB panels are given in Table 4-7 according to Lam et al. (2004).

Table 4-7 Input elastic properties of OSB panels.

Modulus of elasticity (MPa)			Modulus of rigidity (MPa)			Poisson's ratio		
E_L	E_R	E_T	G_{LR}	G_{LT}	G_{RT}	υ_{LR}	υ_{LT}	υ_{RT}
6359	318	4762	45	454	45	0.50	0.38	0.50

4.4 Analysis using the European design methods

Different analytical CLT design methods were described in Chapter 2. Here the theory of mechanically jointed beams and shear analog method were used to calculate the effective bending stiffness of cross laminated plates and results were compared to the numerical and experimental predictions.

4.4.1 Theory of mechanically jointed beams

According to Eq. 2-7, the effective bending stiffness was taken as

$$(EI)_{ef} = \sum_{i=1}^{2}(E_i I_i + \gamma_i E_i A_i a_i^2) = 1.93 \times 10^5 \ N \cdot m^2 \tag{4-4}$$

Where

$$\gamma_1 = 1/\left(1 + \frac{\pi^2 E_1 A_1 \bar{h}/2}{G_{RT} b l^2}\right) = 0.9780$$

$$\gamma_2 = \gamma_1$$

$$a_1 = \left(\frac{h_1}{2} + \frac{\bar{h}}{2}\right) = 0.0195$$

$$a_2 = \mathrm{a}_1$$

$$I_i = \frac{b h_i^3}{12} \quad (i = 1,2)$$

All the parameters are listed in Table 4-8.

Table 4-8 Parameters for analysis using the theory of mechanically jointed beams.

E_i $(i = 1,2)$ (MPa)	G_{RT} (MPa)	h_i $(i = 1,2)$ (m)	$\bar{h}$ (m)	b (m)	l (m)
9946	51.8	0.0195	0.0195	1.235	4

Note that the top and bottom layers were made of the 4.29 m material and the middle layer was made of the 2.45 m material. E_i $(i = 1, 2)$ were calculated by increasing the average static MOE values of the 4.29 m material by 10%. According to Table 3-1, the rolling shear modulus G_{RT} was obtained using $0.005 \times E'$, where E' was 10% greater than the average static MOE values of the 2.45 m material. Refer Table 4-4 and Eq. 4-1 for details.

4.4.2 Shear analogy method

As described in section 2.6.3, the main part of the effective bending stiffness is

$$(EI)_A = \sum_{i=1}^{3} E_i \cdot I_i = 0.16 \times 10^5 \ N \cdot m^2 \qquad (4\text{-}5)$$

The composite action is represented by

$$(EI)_B = \sum_{i=1}^{3} E_i \cdot A_i \cdot \mathrm{z}_\mathrm{i}^2 = 1.82 \times 10^5 \ N \cdot m^2 \qquad (4\text{-}6)$$

Therefore, the effective bending stiffness is

$$(EI)_{ef} = (EI)_A + (EI)_B = 1.98 \times 10^5 \ N \cdot m^2 \qquad (4\text{-}7)$$

All the parameters are shown in Table 4-9. According to Table 3-1, E_2 was calculated using $0.102 \times E'$, where E' was defined in section 4.4.1.

Table 4-9 Parameters for analysis using the shear analogy method.

$E_i \ (i = 1, 3)$ (MPa)	E_2 (MPa)	$h_i \ (i = 1, 2, 3)$ (m)	$z_i \ (i = 1, 2)$ (m)
9946	1058	0.0195	0.0195

4.5 Results and discussion

From numerical simulations, vertical deflection profiles of all the specimens under third point bending test were very similar. For example, Figure 4-24 shows a contour plot of the vertical deflection of the three-layer parallel laminated plate #11 under a load of 1852.5 N. Graphs of comparisons between tested and model predicted apparent and true bending stiffness were also very similar. Therefore, cross laminated plate #1 was employed as an example as shown in Figure 4-25. The calculation and test data agreed very well.

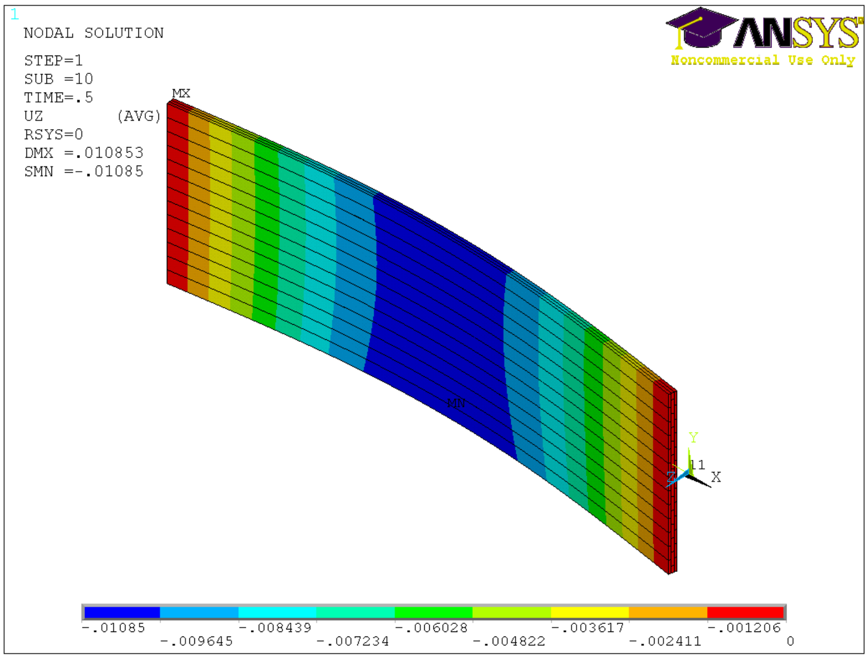

Figure 4-24 Contour plot of the vertical deflection of the three-layer parallel laminated plate #11.

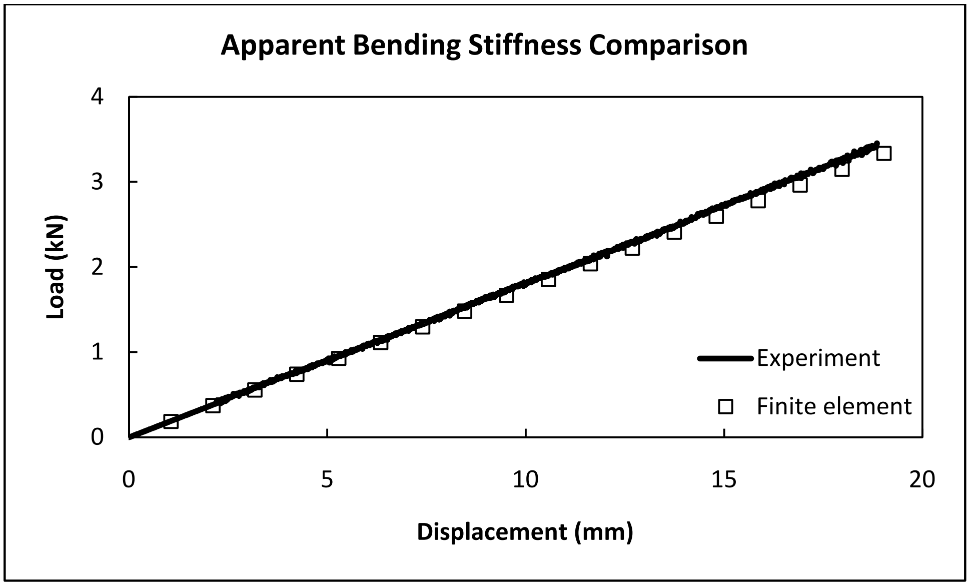

(a)

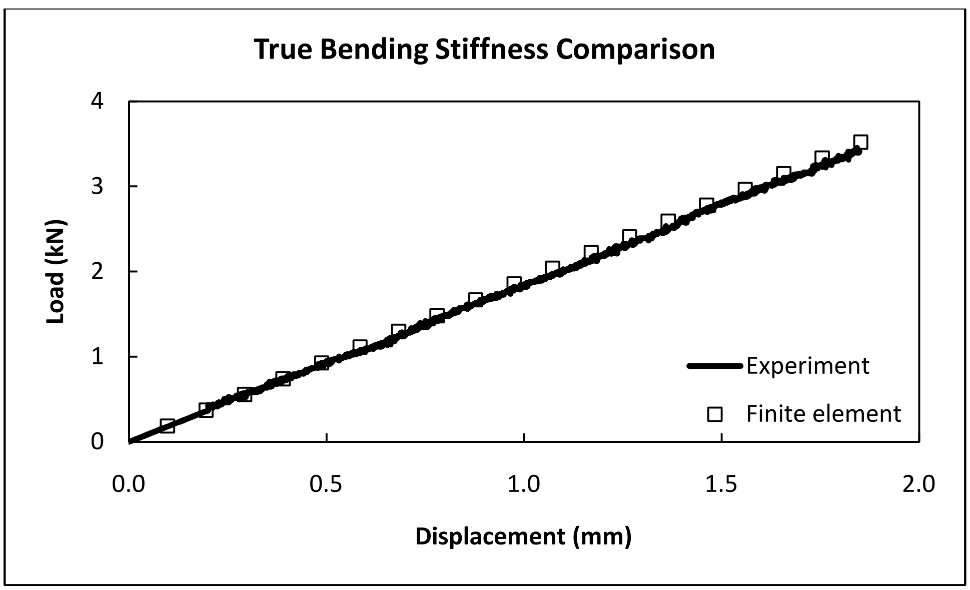

(b)

Figure 4-25 Tested and predicted (a) apparent and (b) true bending stiffness of cross laminated plate #1.

As mentioned in section 4.2.4, the tested true bending stiffness was more accurate because accuracy of the tested apparent bending stiffness was affected by the plate warping during testing. Therefore, the tested true bending stiffness would be used to check the accuracy of numerical solutions.

The tested and predicted apparent and true bending stiffness values of all plates are shown in Table 4-10 to Table 4-13. It was clear that computer model predictions agreed with test results well except for specimen #22 of cross laminated plates with OSB facing which was highlighted in grey in Table 4-12. For that specific specimen, both of the tested true and apparent bending stiffness values were much lower than those of the other specimens in the same category. The dramatic drop of test results could be due to some unpredicted situations during manufacturing or testing operations or unexpected low properties of OSB materials or some other reasons because lumber stiffness in that specimen was not very different from that in the other specimens. Therefore, specimen #22 was culled from the study and did not contribute to the average bending stiffness values used for model verification even though it was still listed in Table 4-12 for the completion of database. From all the comparisons, it was believed that this computer model can be used to calculate laminated wood plates with other material properties and more complicated configurations.

Table 4-10 Tested and predicted apparent and true bending stiffness values of cross laminated plates.

Specimen #	True bending stiffness ($\times 10^5$ N·m^2)			Apparent bending stiffness ($\times 10^5$ N·m^2)		
	Tested	Predicted	Error (%)	Tested	Predicted	Error (%)
1	2.00	2.03	1.54	2.07	1.99	-3.84
2	2.06	2.05	-0.35	2.15	2.00	-6.88
3	2.02	2.02	0.33	2.13	1.98	-6.89

Specimen #	True bending stiffness ($\times10^5$ N·m^2)			Apparent bending stiffness ($\times10^5$ N·m^2)		
	Tested	Predicted	Error (%)	Tested	Predicted	Error (%)
4	1.79	1.86	3.89	1.87	1.83	-2.07
5	1.91	1.92	0.25	1.90	1.88	-0.96
6	1.84	1.94	4.91	2.00	1.89	-5.46
7	1.87	1.84	-1.80	1.88	1.81	-3.51
8	1.80	1.84	2.39	1.85	1.81	-2.15
9	1.93	1.95	0.86	1.93	1.91	-0.88
10	1.91	1.88	-1.63	1.86	1.84	-1.46
Average	1.91	1.93	0.99	1.96	1.89	-3.51

Table 4-11 Tested and predicted apparent and true bending stiffness values of parallel laminated plates.

Specimen #	True bending stiffness ($\times10^5$ N·m^2)			Apparent bending stiffness ($\times10^5$ N·m^2)		
	Tested	Predicted	Error (%)	Tested	Predicted	Error (%)
11	1.92	1.97	2.93	2.10	1.97	-6.12
12	2.08	2.30	10.37	2.17	2.28	5.19
13	1.89	2.05	8.17	1.98	2.04	2.63
14	1.93	2.10	8.47	1.87	2.09	11.54
15	2.11	2.09	-0.91	2.21	2.09	-5.45
16	2.10	2.15	2.21	2.21	2.14	-3.08
17	1.89	2.10	10.79	2.02	2.09	3.20

Specimen #	True bending stiffness ($\times 10^5$ N·m^2)			Apparent bending stiffness ($\times 10^5$ N·m^2)		
	Tested	Predicted	Error (%)	Tested	Predicted	Error (%)
18	2.13	2.10	-1.74	2.26	2.09	-7.30
19	1.96	2.07	5.74	2.00	2.07	3.29
20	1.87	2.07	10.85	1.93	2.06	6.52
Average	1.99	2.10	5.53	2.08	2.09	0.75

Table 4-12 Tested and predicted apparent and true bending stiffness values of cross laminated plates with OSB facing.

Specimen #	True bending stiffness ($\times 10^4$ N·m^2)			Apparent bending stiffness ($\times 10^4$ N·m^2)		
	Tested	Predicted	Error (%)	Tested	Predicted	Error (%)
21	9.69	9.18	-5.28	10.11	9.36	-7.42
22	6.18	9.20	48.80	7.69	9.46	23.04
23	8.66	9.03	4.29	9.20	9.32	1.36
24	8.59	8.99	4.62	9.28	9.27	-0.12
25	9.01	9.07	0.71	9.57	9.37	-2.14
26	8.78	9.12	3.82	8.94	9.35	4.57
27	9.55	9.08	-4.95	9.93	9.30	-6.29
28	8.14	9.01	10.62	8.89	9.29	4.47
29	8.79	8.94	1.63	8.88	9.23	3.96
30	8.26	9.20	11..31	8.85	9.44	6.68
Average	8.83	9.07	2.67	9.29	9.33	0.34

Table 4-13 Tested and predicted apparent and true bending stiffness values of 45° laminated plates.

Specimen #	True bending stiffness ($\times 10^5$ N·m^2)			Apparent bending stiffness ($\times 10^5$ N·m^2)		
	Tested	Predicted	Error (%)	Tested	Predicted	Error (%)
31	3.50	3.53	0.79	3.71	3.41	-7.97
32	3.63	3.39	-6.55	3.74	3.30	-11.90
33	3.52	3.53	0.32	3.58	3.43	-4.15
34	3.93	3.48	-11.51	3.72	3.37	-9.43
35	4.00	3.74	-6.68	3.96	3.52	-11.04
36	3.42	3.54	3.34	3.61	3.44	-4.69
37	3.59	3.76	4.62	3.77	3.64	-3.29
38	3.87	3.85	-0.47	4.02	3.73	-7.21
39	3.48	3.77	8.37	3.54	3.65	3.18
40	3.21	3.66	14.13	3.37	3.55	5.50
Average	3.62	3.62	0.25	3.70	3.50	-5.30

Bending stiffness of cross laminated plates obtained from finite element analysis, theory of mechanically jointed beams, shear analogy method and third point bending test are shown in Table 4-14. The results were very similar because of the high span to depth ratio of the specimens.

Table 4-14 Bending stiffness of cross laminated plate obtained from different methods.

	Finite element analysis	Theory of mechanically joined beams	Shear analogy method	Bending test
Bending stiffness ($\times10^5$	1.93	1.93	1.98	1.91
Error (%)	1.05	1.05	3.66	/

Figure 4-26 gave a better and clearer visualization of comparisons among tested and predicted apparent and true bending stiffness values of all four types of plates. Cross laminated and parallel laminated plates exhibited very similar bending stiffness properties which were more than twice those of specimens with OSB facing. Because of containing one more layer of SPF lumber, 45^{o} laminated plates were much stiffer than the other three configurations. The 45^{o} laminated plates had an average true bending stiffness value at least 72.4% higher than the other lumber based panels. This could be an important consideration for commercial CLT manufacturing operations because bending stiffness often governs many design situations.

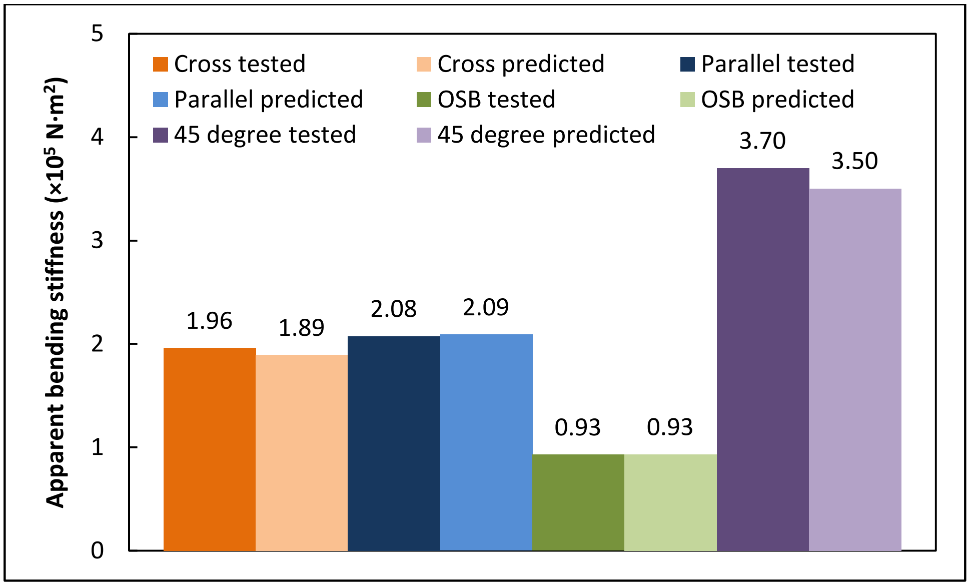

(a)

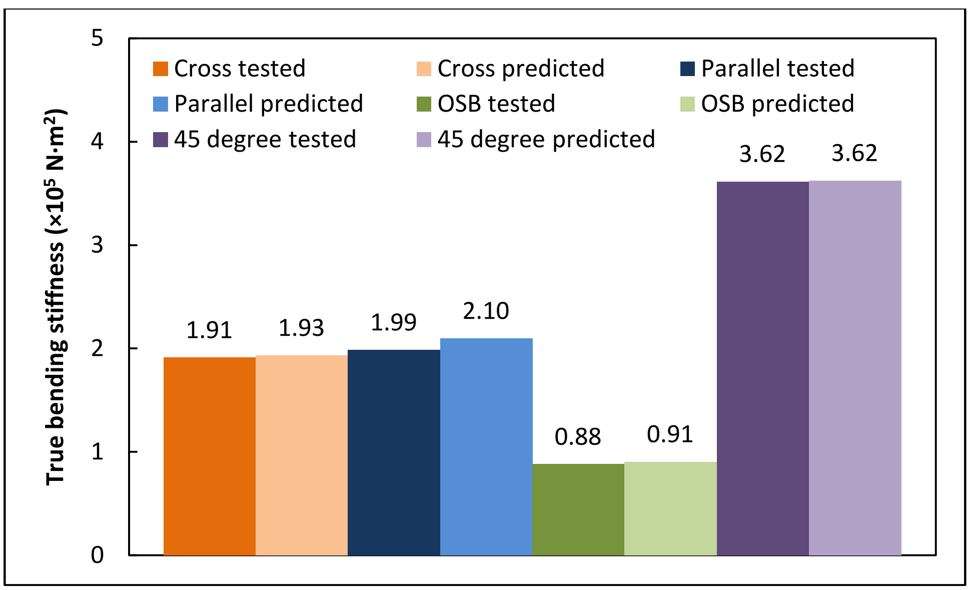

(b)

Figure 4-26 Tested and predicted (a) apparent and (b) true bending stiffness values of four types of laminated plates.

Another interesting issue is the comparison between model predicted apparent and true bending stiffness. The difference between predicted averages of each specimen category is shown in Figure 4-27. Based on reasons explained in section 4.2.4, calculated true bending stiffness was supposed to be higher than the calculated apparent bending stiffness because of the absence of shear effect. This was true for cross laminated, parallel laminated, and 45^{o} laminated specimens. However, panels with OSB facing had an opposite trend that true bending stiffness was about 2.77 percent lower than apparent bending stiffness. In order to find the mechanism behind this interesting phenomenon, transverse shear strain distributions in the middle layer were investigated.

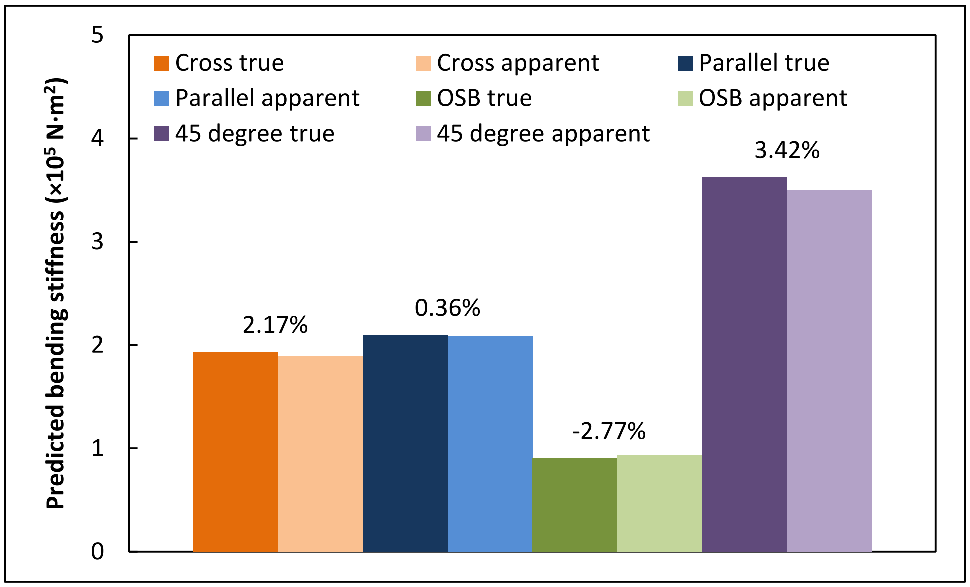

Figure 4-27 Comparison between predicted true and predicted apparent bending stiffness.

Simply supported cross laminated plate with OSB facing #21 under a load P of 975.2 N was taken as an example for this design category. From Figure 4-28 and Figure 4-29, it can be seen that the magnitude of transverse shear strain ϵ_{xz} was significant between the two loading points where the influence of ϵ_{xz} was supposed to be negligible. This caused the inclusion of transverse shear effect in the calculated true bending stiffness which was no longer greater than the calculated apparent bending stiffness. The dramatic change of ϵ_{xz}

around area “A” in Figure 4-28 was a result of the discontinuity of OSB panels on the bottom as shown in Figure 4-22. To support this explanation, an identical plate except for continuous OSB facing was analyzed (Figure 4-30).

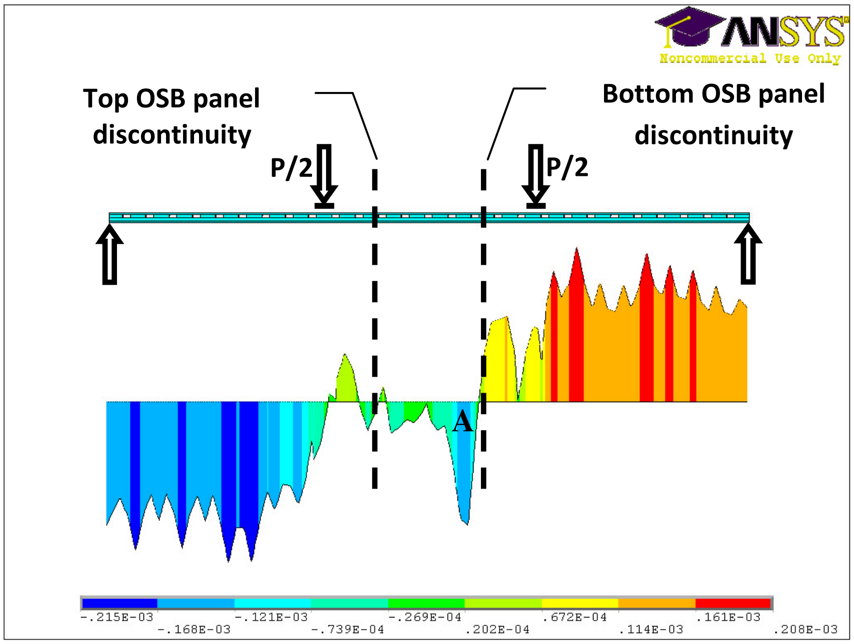

(a)

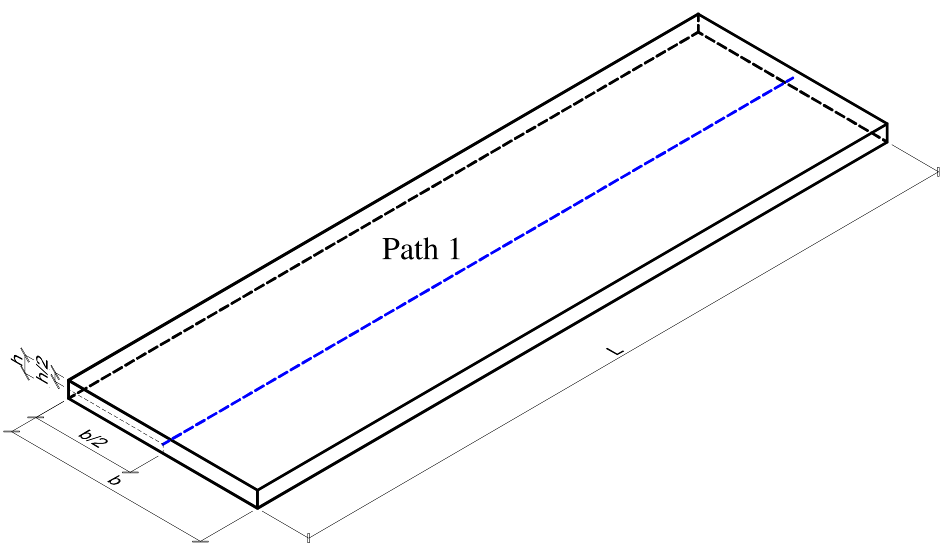

(b)

Figure 4-28 (a) Transverse shear strain ϵ_{xz} along path 1 of plate #21 and (b) path 1 on a cross laminated plate with OSB facing.

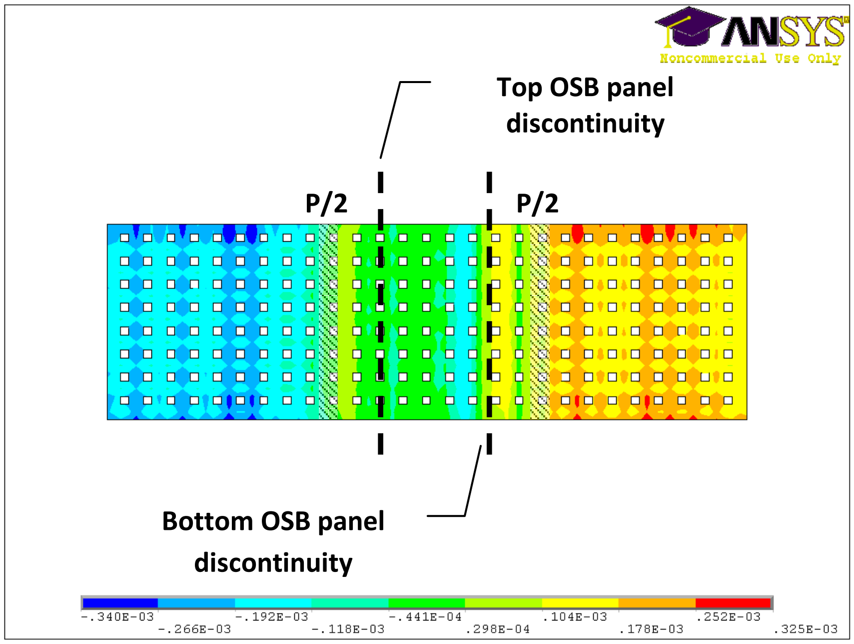

Figure 4-29 Transverse shear strain ϵ_{xz} in the mid-plane of plate #21.

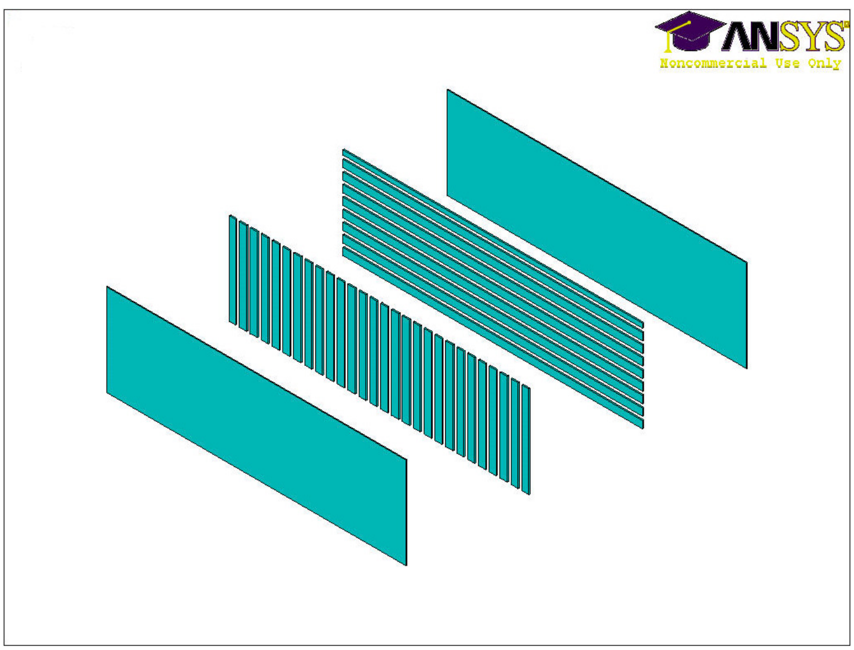

Figure 4-30 Model of a cross laminated plate with continuous OSB facing.

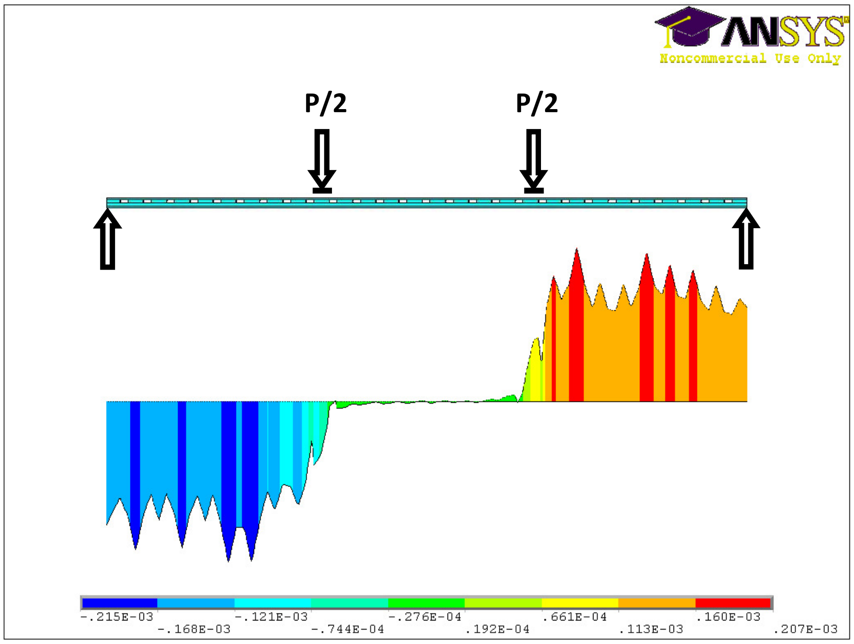

Figure 4-31 Transverse shear strain ϵ_{xz} along path 1 of a plate with continuous OSB facing.

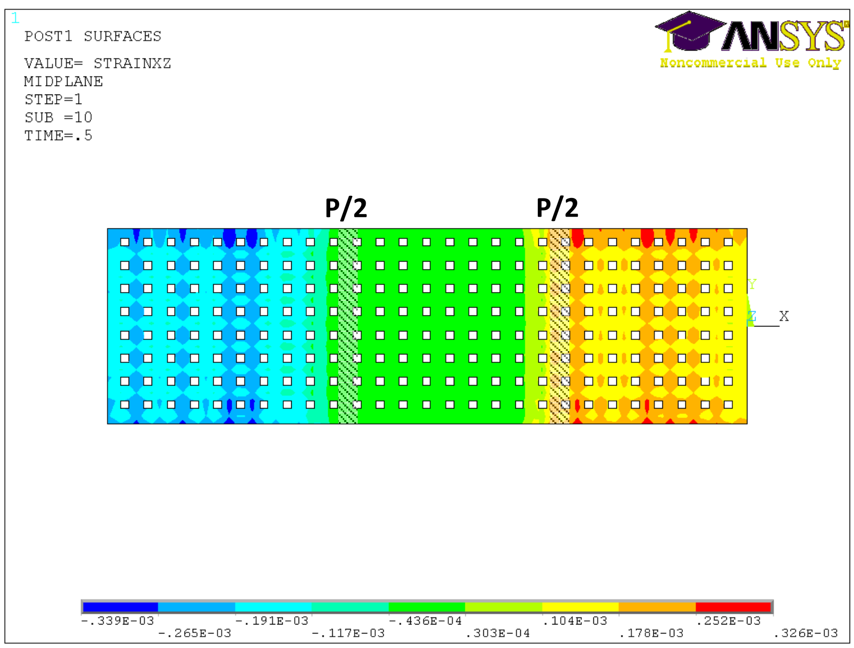

Figure 4-32 Transverse shear strain ϵ_{xz} in the mid-plane of a plate with continuous OSB facing.

Table 4-15 Comparison of calculated bending stiffness values for plates with discontinuous and continuous OSB facing.

	Calculated true bending stiffness ($\times 10^4$ N·m^2)	Calculated apparent bending stiffness ($\times 10^4$ N·m^2)	Difference (%)
Discontinuous OSB facing	9.18	9.36	-1.92
Continuous OSB facing	11.07	10.69	3.54

Path 1 in Figure 4-31 was exactly the same as the one shown in Figure 4-28 (b). As expected, in Figure 4-31 and Figure 4-32, there was no transverse shear strain ϵ_{xz} between loading points. Using specimen #21 as an example, the comparison listed in Table 4-15 approved that the discontinuity of the OSB facing resulted in a large increase of ϵ_{xz} and therefore a negative difference between calculated true and apparent bending stiffness.

Cross laminated and parallel laminated plates had exactly the same geometric design except for fiber direction in the middle layer. However, the calculated true bending stiffness was 2.17 percent higher than the calculated apparent bending stiffness for cross laminated plates while this difference was only 0.36 percent for parallel laminated ones. This was due to all wood members being laid along the plate longitudinal direction and no rolling shear stresses occurred in the parallel laminated panels.

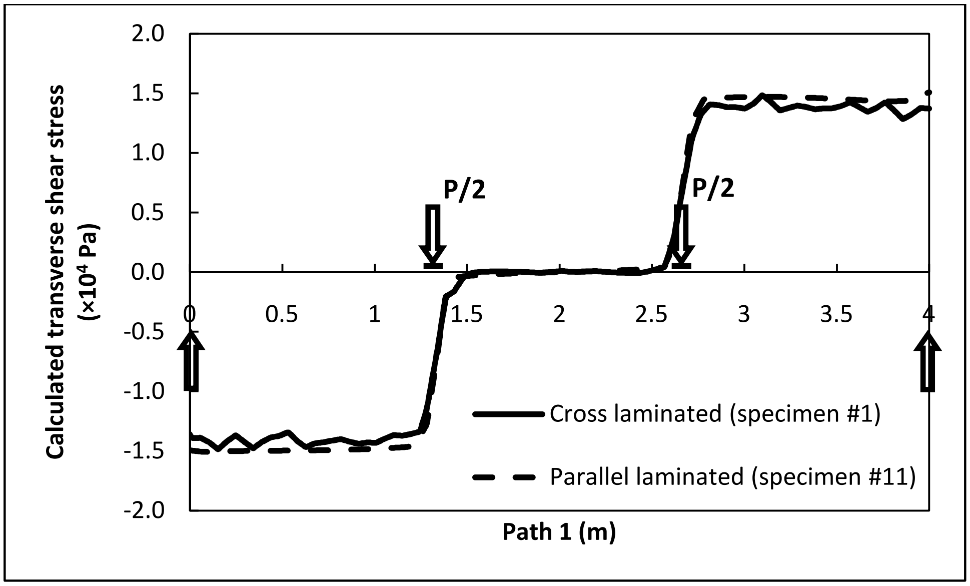

Figure 4-33 Transverse shear stress σ_{xz} along path 1 of a cross laminated (specimen #1) and a parallel laminated plate (specimen #11).

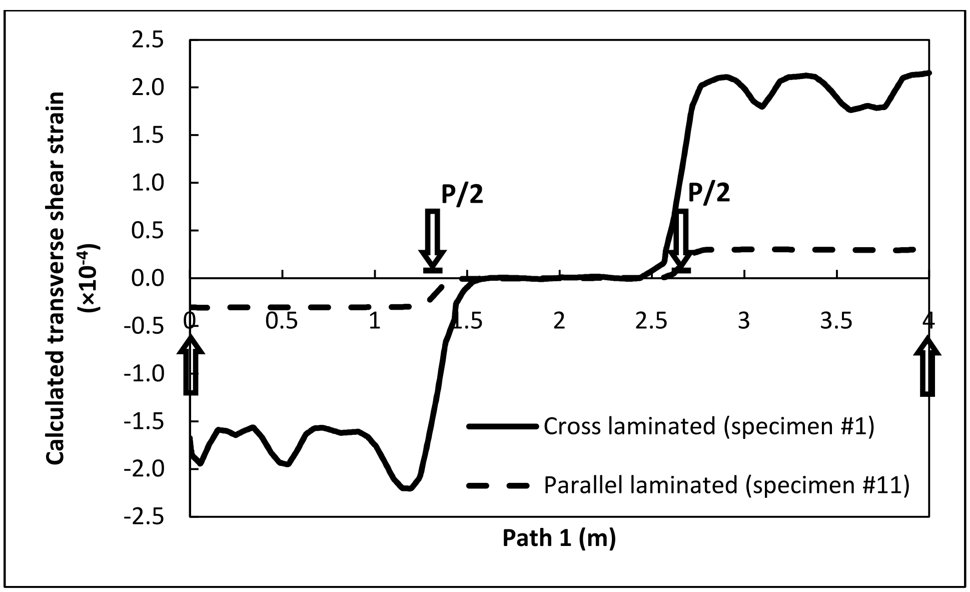

Figure 4-34 Transverse shear strain ϵ_{xz} along path 1 of a cross laminated (specimen #1) and a parallel laminated plate (specimen #11).

Using cross laminated plate #1 and parallel laminated plate #11 as an example, Figure 4-33 and Figure 4-34 exhibit the transverse shear stress σ_{xz} and transverse shear strain ϵ_{xz} along path 1 under a load P of 1852.5 N. Path 1 is the same as shown in Figure 4-28 (b). In both cases, there was no transverse shear effect, i.e. σ_{xz} and ε_{xz}, between loading points, so the calculated true bending stiffness was greater than the calculated apparent bending stiffness. Referring to Figure 4-33, these two specimens generated almost the same transverse shear stress σ_{xz} between supports and loading points. Because the middle layer was cross laminated and rolling shear stresses were introduced, specimen #1 developed higher ϵ_{xz} magnitude between supports and loading points as shown in Figure 4-34, meaning that the influence of transverse shear on plate vertical deflection was larger for this plate configuration. It also provided a better understanding that the difference between predicted true and predicted apparent bending stiffness of cross laminated plates were greater than that of parallel laminated ones.

4.6 Conclusions

Continuing the work from Chapter 3, more complicated laminated wood plates were studied in this chapter. A total of four different configurations with each having ten replicates were manufactured and analyzed. Before manufacturing the specimens, MOE values of all lumber pieces were measured using the vibration MOE test. Third point bending tests were conducted on the plate specimens and deflections at ten different locations on the plate were measured. From the test data, both apparent and true bending stiffness of all forty specimens were obtained. The previous developed finite element models were improved by giving each individual lumber different material properties. The predicted apparent and true bending stiffness are in good match with tested ones. Structural performance of the four plate configurations was also compared. The 45^{o} laminated plates had much higher bending stiffness values than the other lumber based panels and this could be an important consideration for commercial CLT manufacturing operations because bending stiffness often governs many design situations.

CHAPTER 5 BOX STRUCTURES CONSISTING OF LAMINATED WOOD PLATES

5.1 Introduction

The main objective of this chapter is to use the developed finite element models to study more complicated box type structures. Twenty box type structural specimens were assembled and tested at UBC. The box type configurations were chosen based on results from finite element analyses of many different configurations. Two laminated wood plates were connected with ribs to form the box elements. The ribs, which were made of 38 mm × 184 mm (nominal 2 inch × 8 inch) dimension lumber, were cross connected by 10d bright common nails. SFS Befestiger WT-T 6.5 mm × 130 mm self tapping screws were used as connection between plate and rib members (SFS intec, 2007).

In order to accurately predict the behavior of the self tapping screws, eight types of lateral resistance tests were designed and conducted. A total of forty-five connection test specimens were evaluated.

Third point bending tests were performed on all box structures. The specimens were loaded to reach the maximum load level to obtain both of the bending stiffness and bending strength values. However, it was almost impossible to break the specimens completely and get the peak load values before the test facilities' limit was reached. Therefore, only the bending stiffness values were calculated and provided. In conclusion, reasonable agreement between experimental results and numerical predictions has been obtained for bending stiffness.

5.2 Experimental studies

5.2.1 Box elements assembly

In each of the specimen, 38 mm × 184 mm × 4.3 m (nominal 2 inch × 8 inch × 14 feet) dimension lumber was placed parallel along the longitudinal direction at an equal distance from one another. Properly cut short pieces were then inserted between the 4.3 m ribs to stabilize the rectangle frame. Cross connected ribs were toe nailed with four 10d bright common nails (two on each side) (Figure 5-1). Finally, two pieces of laminated wood plates of the same configuration coming from the forty specimens mentioned in Chapter 4 were attached to the frame using WT-T 6.5 mm × 130 mm self tapping screws from SFS intec to form a complete box element. Table 5-1 lists basic information of all the four box configurations.

Table 5-1 Basic information of different box configurations.

		Box consisting of cross laminated plates	Box consisting of parallel laminated plates	Box consisting of cross laminated plates with OSB facing	Box consisting of 45^{o} laminated plates
Count		5	5	5	5
Number of ribs	Longitudinal	3	3	3	4
	Cross-wise	6	6	6	9

Figure 5-1 Toe nail connected ribs.

Figure 5-2 and Figure 5-3 show the assembly process of a box element consisting of 45^{o} laminated plates and a pile of finished box elements.

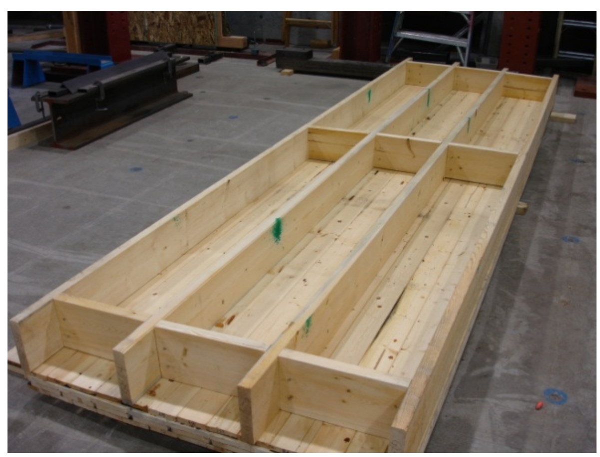

Figure 5-2 Assembly process of a box consisting of 45^{o} laminated plates.

Figure 5-3 A pile of box elements.

Screw patterns for the different box elements are shown in Figure 5-4.

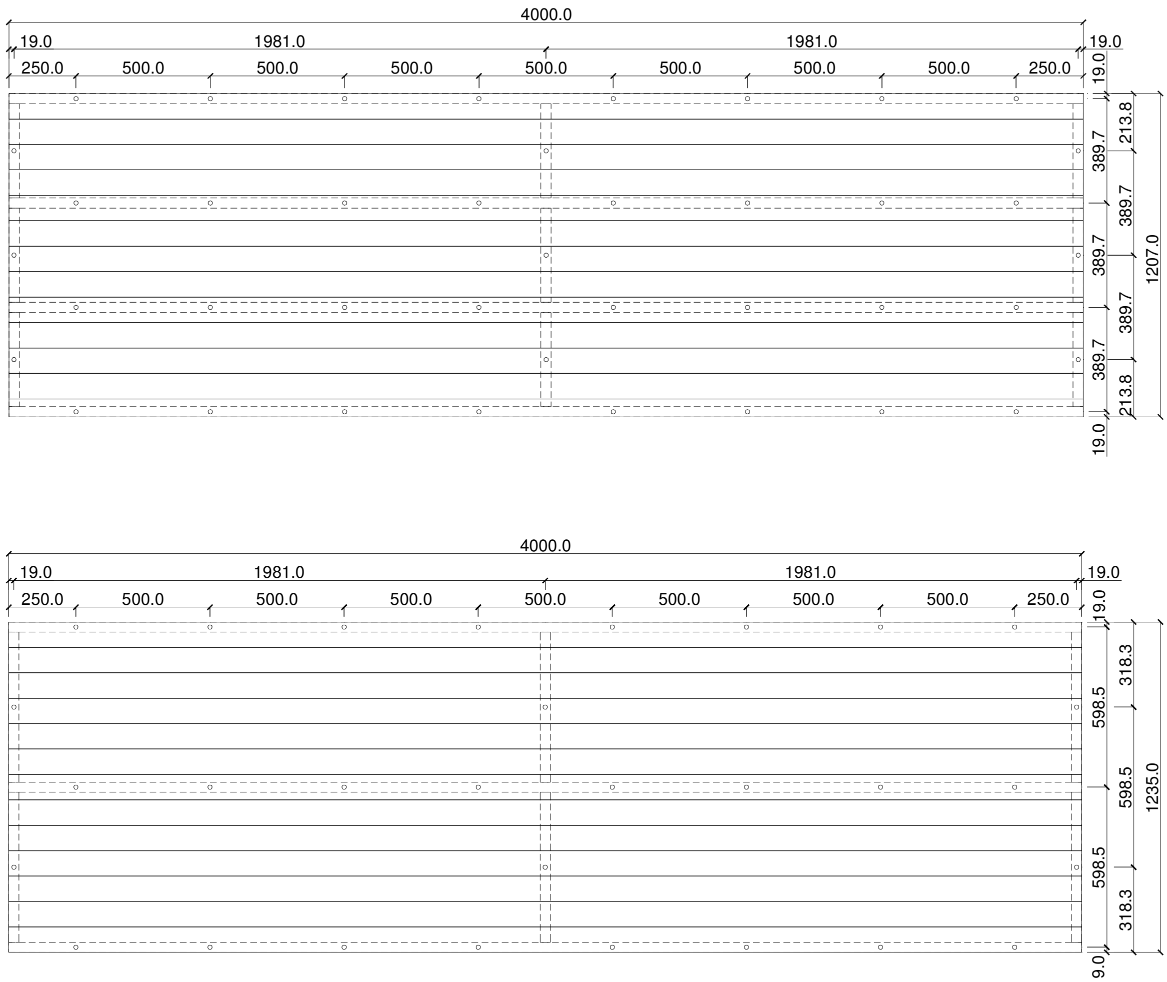

Figure 5-4 Screw patterns for box elements.

Combinations of plate specimens for all box elements are shown in Table 5-2.

Table 5-2 Combinations of plates for box elements.

Box	1	2	3	4	5	6	7	8	9	10	11	12	13	14	15	16	17	18	19	20
Plate	8 & 10	7 & 9	5 & 6	3 & 4	1 & 2	19 & 20	17 & 18	15 & 16	13 & 14	11 & 12	21 & 22	23 & 24	25 & 26	27 & 28	29 & 30	39 & 40	37 & 38	35 & 36	31 & 32	33 & 34

5.2.2 Third point bending test

To evaluate bending properties of the box elements, third point bending tests were conducted on the twenty specimens (Figure 5-5). As described in Chapter 4, the test specimen was simply supported and loaded by two concentrated line forces at 1/3 of the span. The out-of-plane loads were applied by a pair of displacement-controlled hydraulic jacks. Six LVDTs were attached to bottom of the box at specific locations along the longitudinal edges as shown in Figure 5-6. Again, the span L was 4 m and the distance a was 0.1 m. Specimens were initially loaded to the maximum load level available in order to obtain both the bending stiffness and bending strength values. However, even though some failure occurred, it was found that many of these structures could not be completely broken before reaching stroke limit of the test system (Figure 5-7). Hence, it was not possible to establish the load carrying capacity of all the specimens. Therefore, only bending stiffness values were obtained and presented. Loading rate was controlled at 2 mm/min and the load-deflection data was recorded with a data acquisition system and stored on a computer. Table 5-3 presents the maximum load obtained for all the box specimens. Values marked with a star symbol represent the load carrying capacity of the corresponding box. For the rest specimens, there is still large capacity left. Figure 5-8 is load and crosshead displacement relationship curves for specimens #1 to #5 which consist of cross laminated plates. In all cases except box 1, the test was terminated before reaching the maximum load level.

Table 5-3 Maximum load obtained for the box specimens.

Specimen #	Box consisting of cross laminated plates					Box consisting of parallel laminated plates				
	1	2	3	4	5	6	7	8	9	10
max. load obtained (kN)	117*	113	117	89	116	111	122*	28	30	31
Specimen #	Box consisting of cross laminated plates with OSB facing					Box consisting of 45^{o} laminated plates				
	11	12	13	14	15	16	17	18	19	20
max. load obtained (kN)	74*	77*	85*	82*	81*	37	40	188*	39	40

Figure 5-5 Third point bending test of a box element consisting of cross laminated plates with OSB facing.

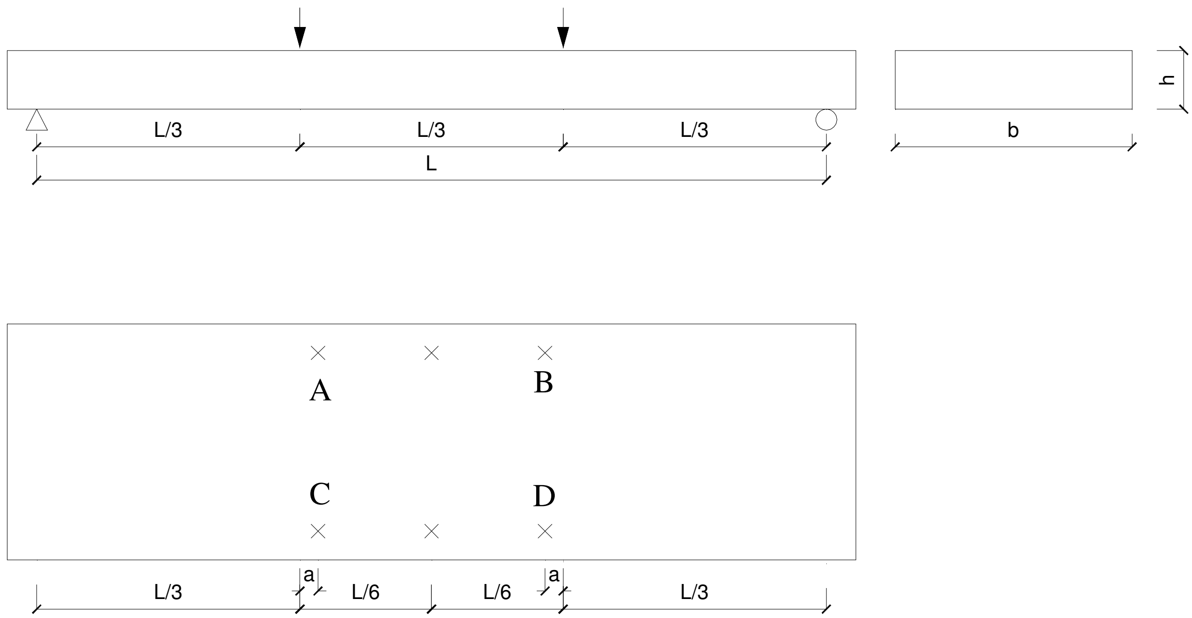

Figure 5-6 Third point bending test of box elements.

Figure 5-7 Third point bending test of a box element consisting of cross laminated plates.

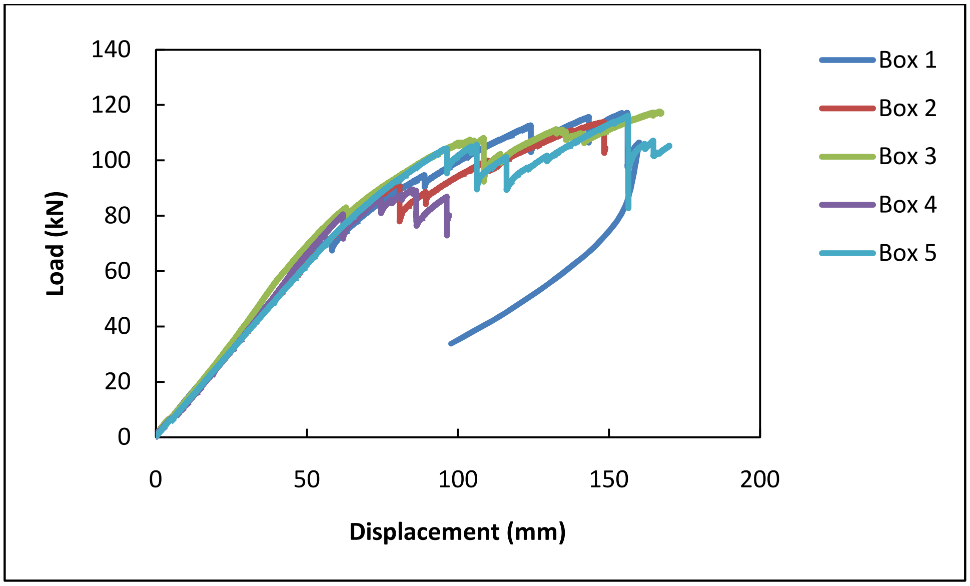

Figure 5-8 Load and crosshead displacement data for boxes consisting of cross laminated plates.

Figure 5-9 to Figure 5-12 exhibit all the load-displacement relationships obtained from the third point bending test.

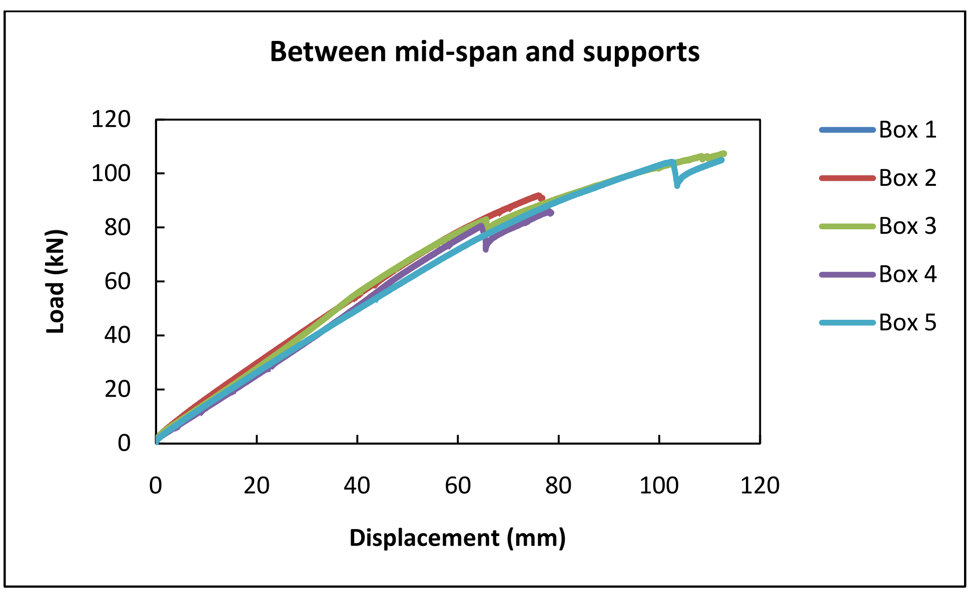

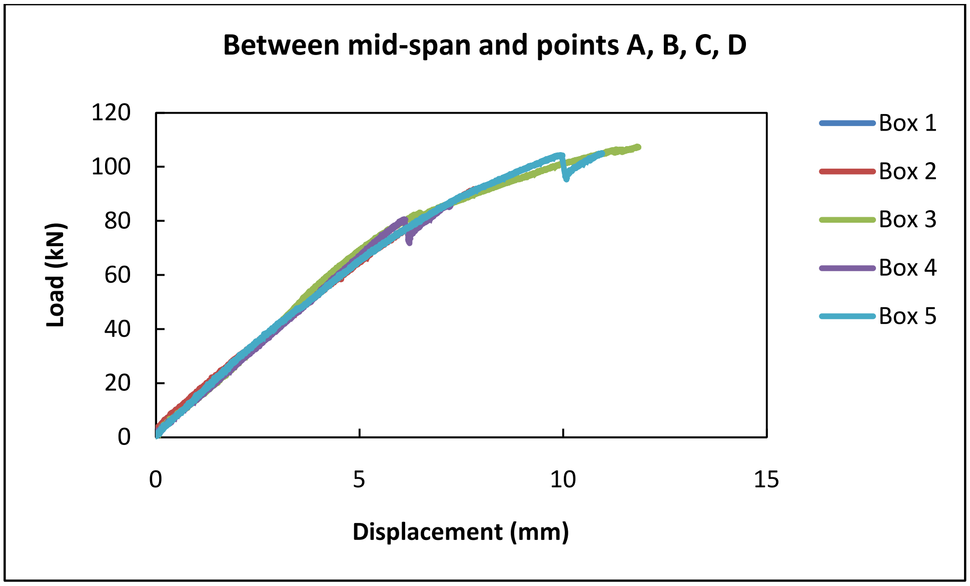

Figure 5-9 Load displacement relationships obtained between mid-span and different points of box structures consisting of cross laminated plates.

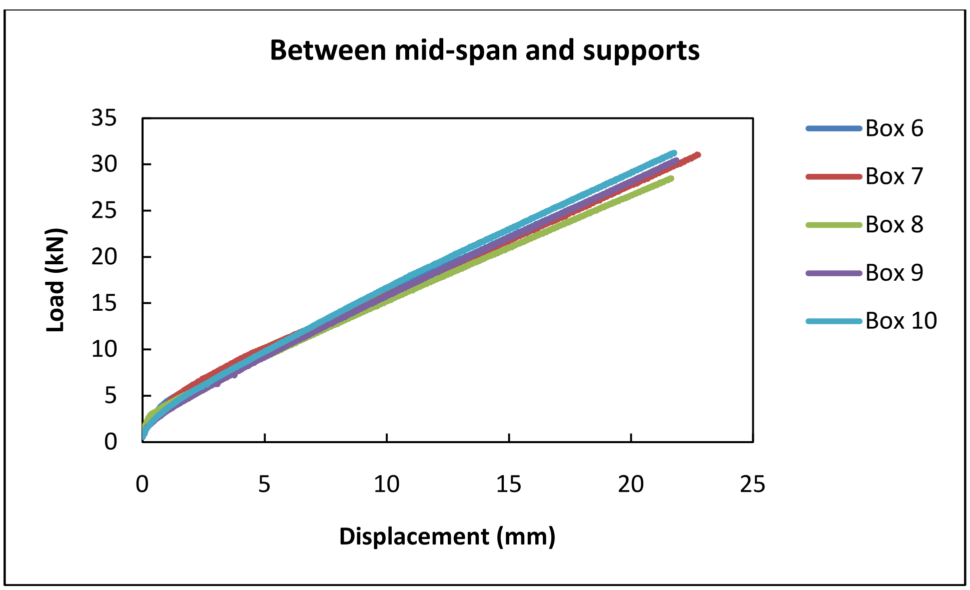

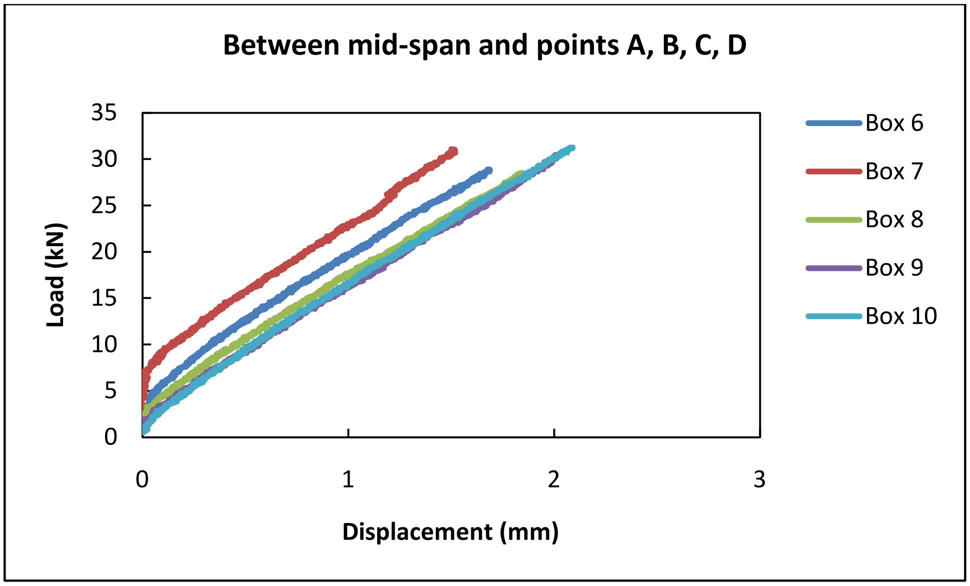

Figure 5-10 Load displacement relationships obtained between mid-span and different points of box structures consisting of parallel laminated plates.

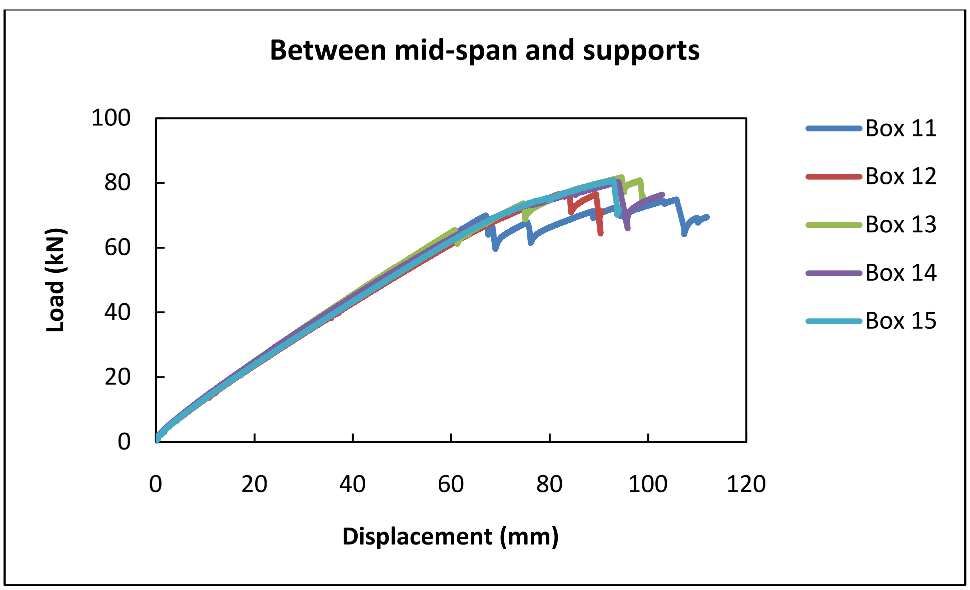

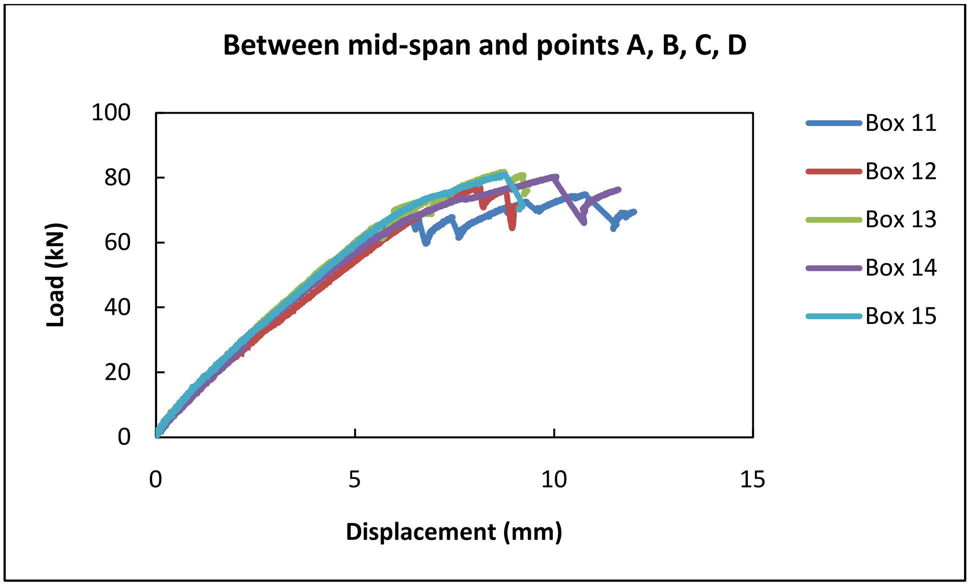

Figure 5-11 Load displacement relationships obtained between mid-span and different points of box structures consisting of cross laminated plates with OSB facing.

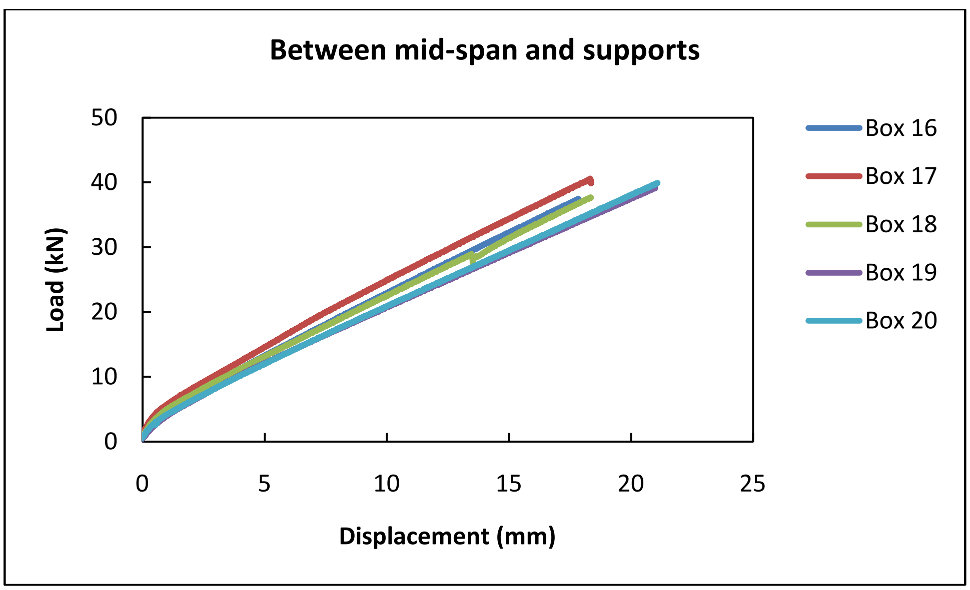

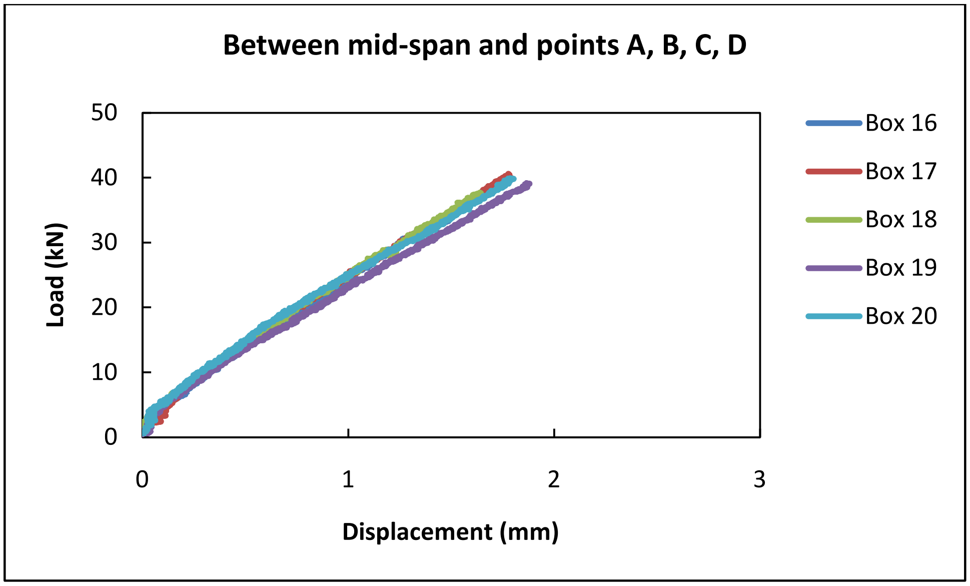

Figure 5-12 Load displacement relationships obtained between mid-span and different points of box structures consisting of 45° laminated plates.

Tested bending stiffness values of the twenty box elements are listed in Table 5-4. As expected, boxes with OSB facing and boxes with 45° laminated plates presented the lowest and highest bending stiffness values, respectively.

Table 5-4 Bending stiffness of box structures consisting of different types of laminated plates.

	Configuration	Box consisting of cross laminated plates	Box consisting of parallel laminated plates	Box consisting of cross laminated plates with OSB facing	Box consisting of 45° laminated plates
Bending stiffness obtained between mid-span and supports ($\times10^6$ N·m^2)	Mean	1.39	1.40	1.12	2.10
	SD	0.08	0.06	0.03	0.14

	Configuration	Box consisting of cross laminated plates	Box consisting of parallel laminated plates	Box consisting of cross laminated plates with OSB facing	Box consisting of 45° laminated plates
Bending stiffness obtained between mid-span and points A, B, C, D ($\times10^6$ N·m^2)	Mean	1.39	1.52	1.13	2.16
	SD	0.09	0.09	0.05	0.12

5.2.3 Self tapping screw lateral resistance test

As mentioned before, WT-T 6.5 mm × 130 mm self tapping screws (Figure 5-13) from SFS intec were used to connect the paired laminated wood plates with middle rib frame. To have a great prediction of the system performance, it was necessary to understand the lateral resistance of the screws and use an accurate load-displacement relationship in the finite element model.

Figure 5-13 A WT-T self tapping screw.

Eight types of specimens were designed to represent typical connection options in box structures. A total of forty-five specimens were assembled and tested to measure the lateral resistance of screws in different box configurations (Table 5-5). The small laminated plates used to make connection test specimens were cut from full sized plates disassembled from box elements after third point bending test. Screw spacing in connection specimens was exactly the same as that in box structures (Figure 5-14).

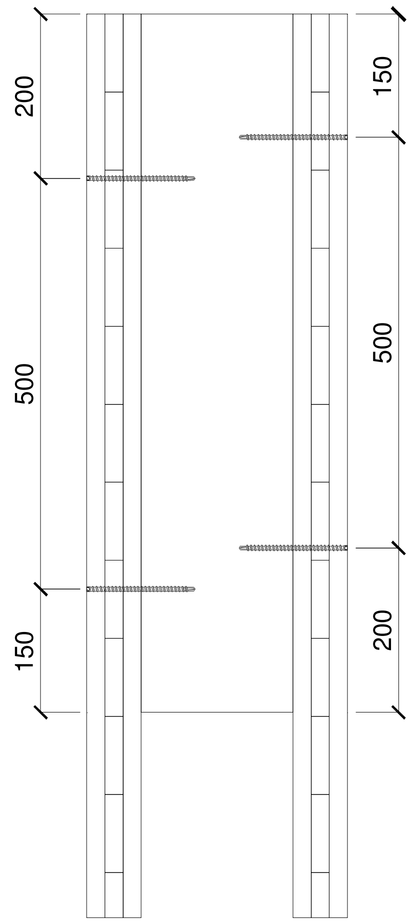

Figure 5-14 Drawing of a screw lateral resistance test specimen.

Table 5-5 Screw lateral resistance test sampling details.

Outer layer plates	Count	Load direction
Cross laminated plates	5	x
	5	y
Parallel laminated plates	6	x
	5	y

Outer layer plates	Count	Load direction
Cross laminated plates with OSB facing	6	x
	6	y
45^{o} laminated plate	7	x
	5	y

Screws were loaded in single shear to get resistance properties in x and y direction, respectively, where x and y represented two directions parallel and perpendicular to the longitudinal direction of laminated plates as shown in Figure 5-15. Loading rate was 1.27 mm/min and 0.762 mm/min for specimens loaded in x and y direction, respectively. Two LVDTs were mounted on the specimen and the load-displacement relationship was recorded by a data acquisition system.

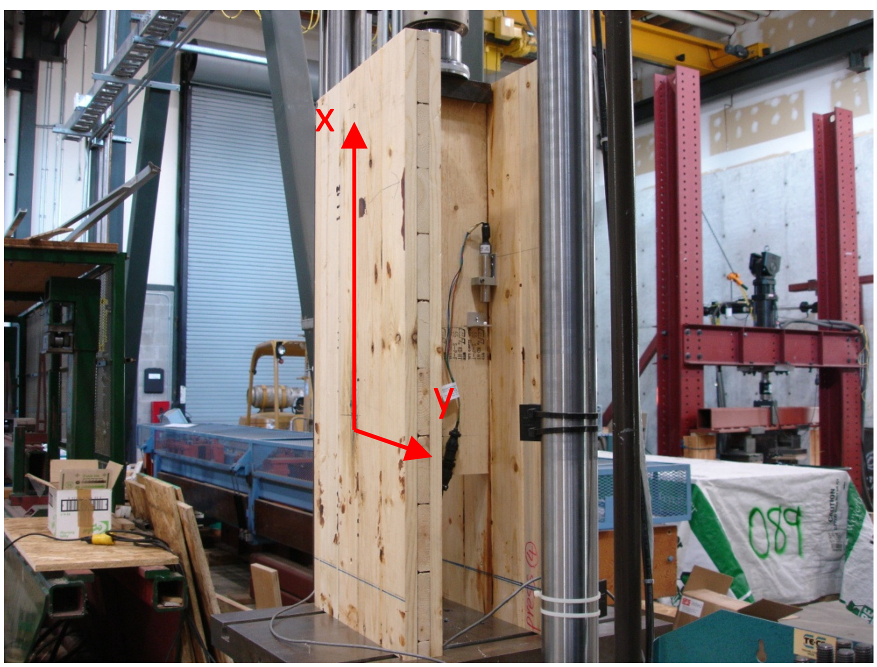

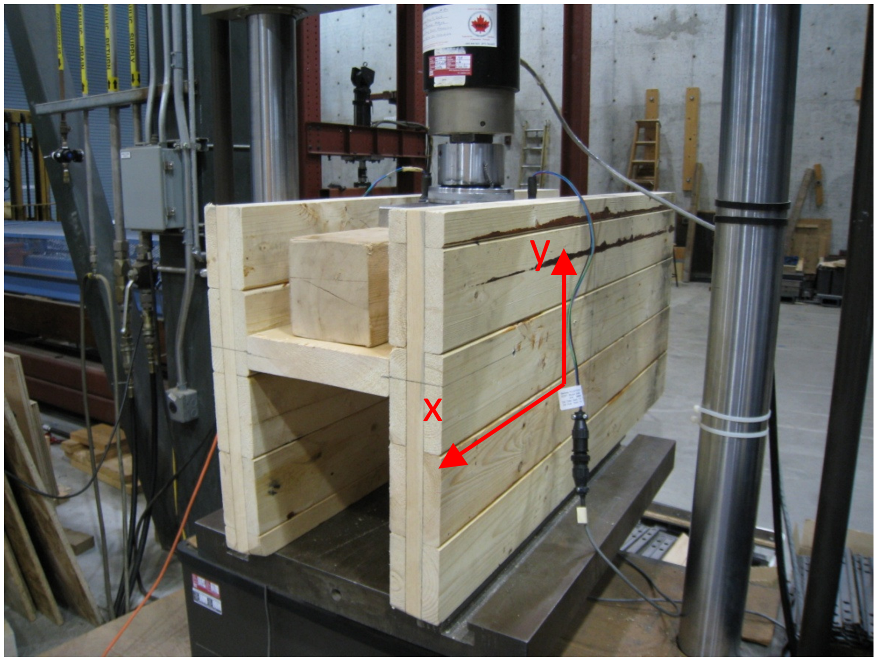

Figure 5-15 Screw lateral resistance test setup.

The load-displacement curves for the eight types of screw connections are displayed in Figure 5-16 to Figure 5-19. Note that these curves represented load carrying ability of all the four screws in each specimen. Properties of each screw were determined by dividing the test values by four.

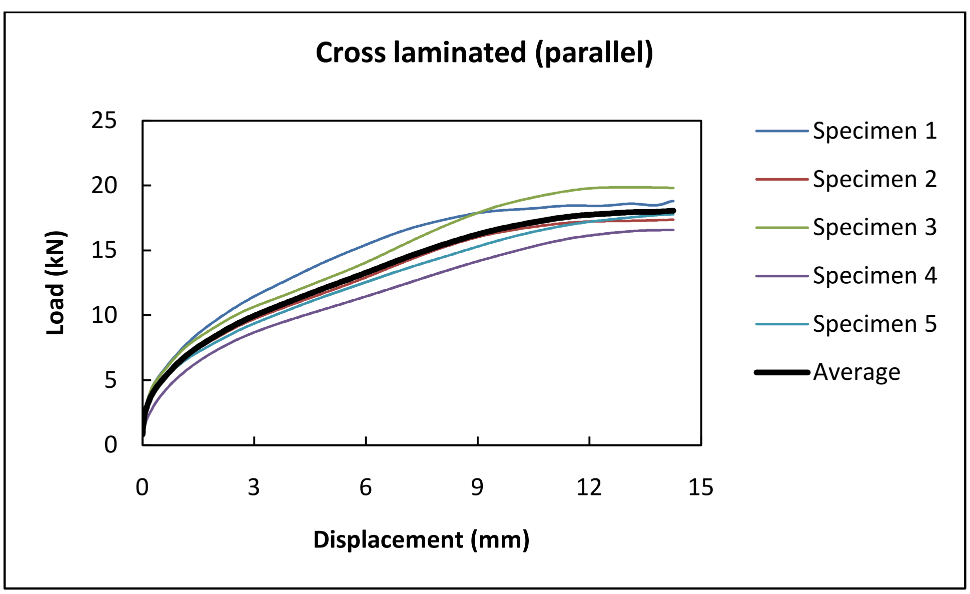

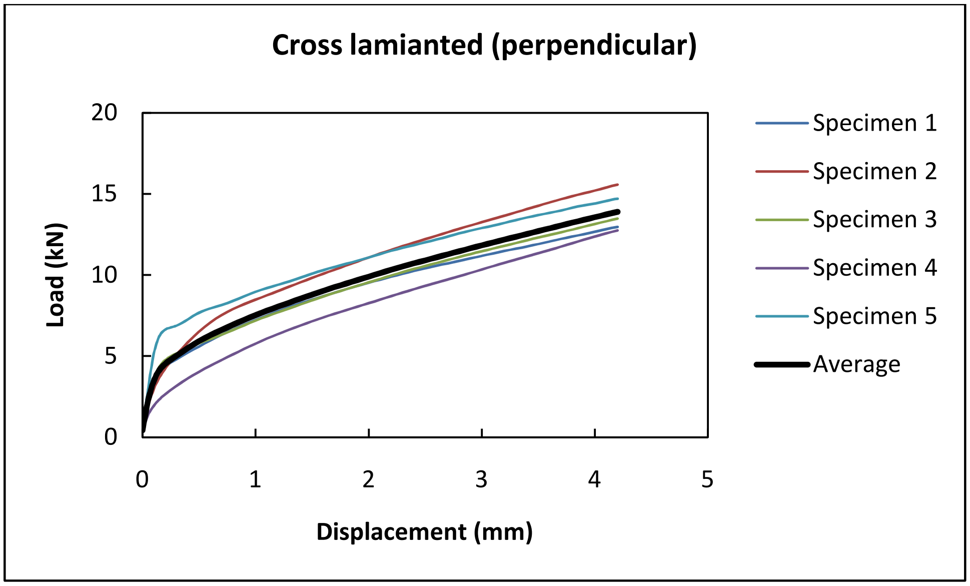

Figure 5-16 Load-displacement relationship for self tapping screws loaded parallel and perpendicular to the longitudinal direction of boxes consisting of cross laminated plates.

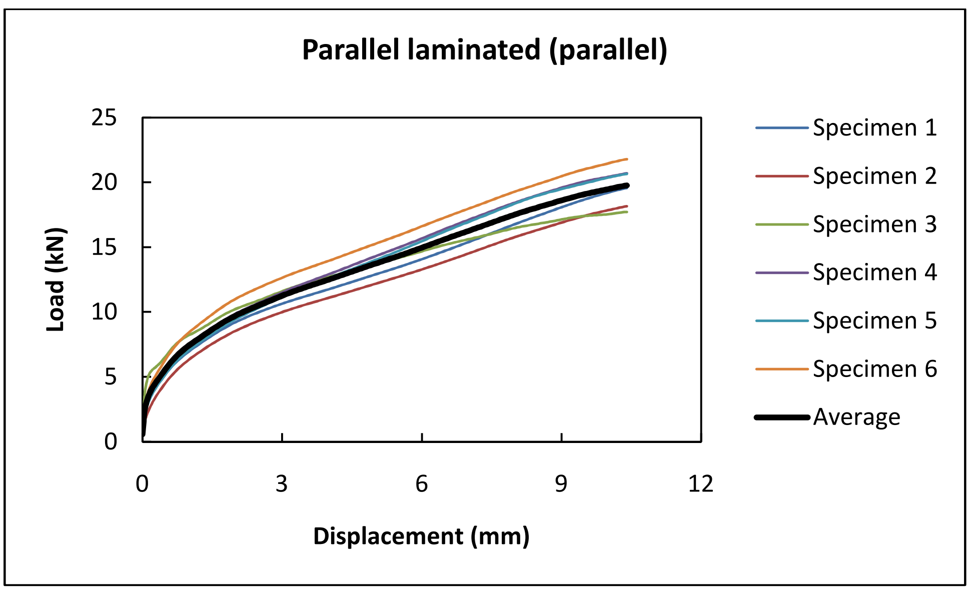

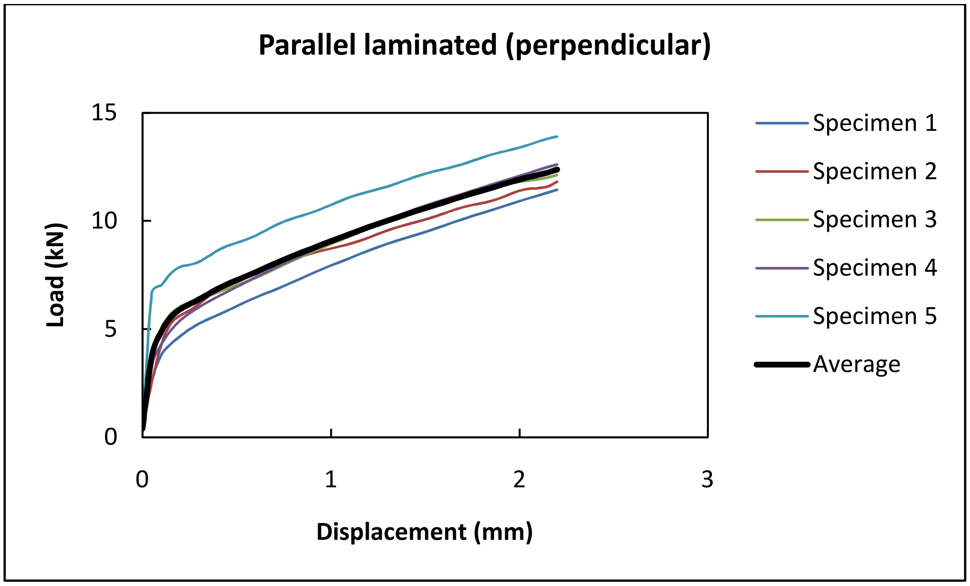

Figure 5-17 Load-displacement relationship for self tapping screws loaded parallel and perpendicular to the longitudinal direction of boxes consisting of parallel laminated plates.

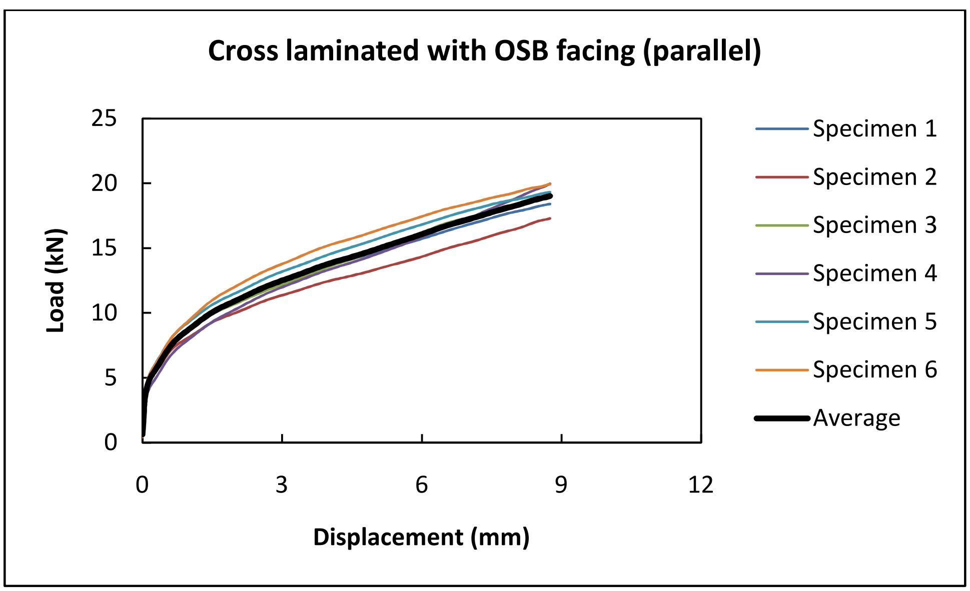

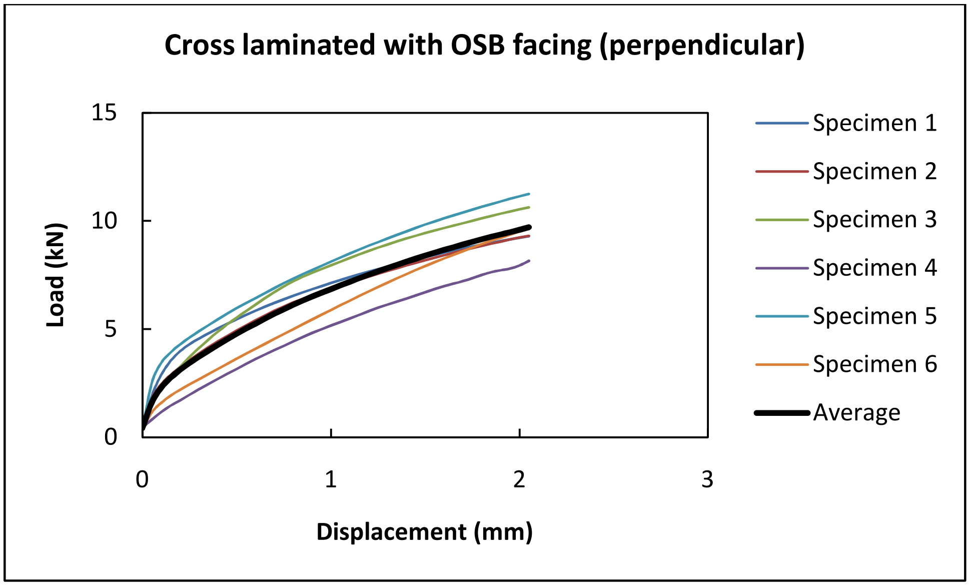

Figure 5-18 Load-displacement relationship for self tapping screws loaded parallel and perpendicular to the longitudinal direction of boxes consisting of cross laminated plates with OSB facing.

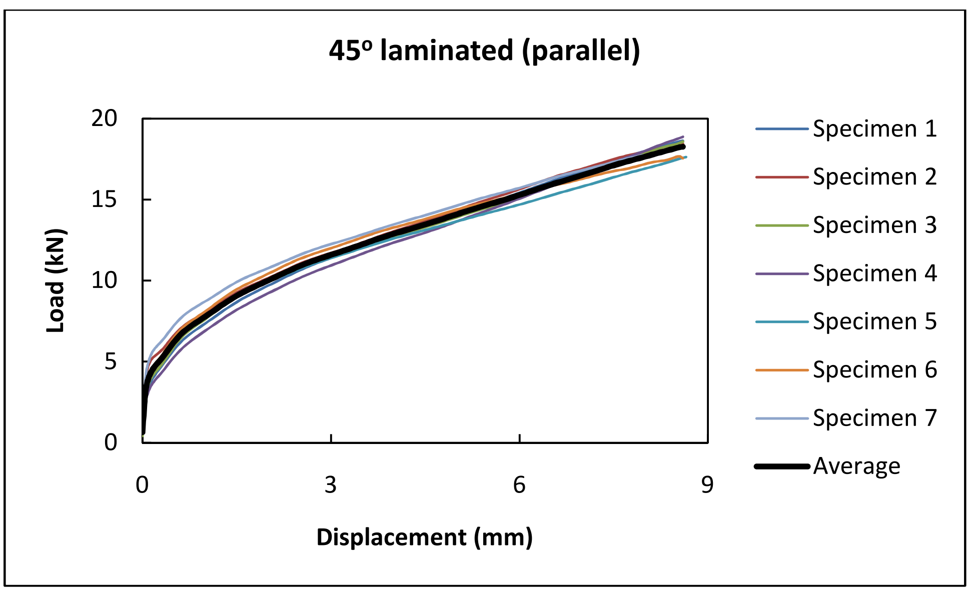

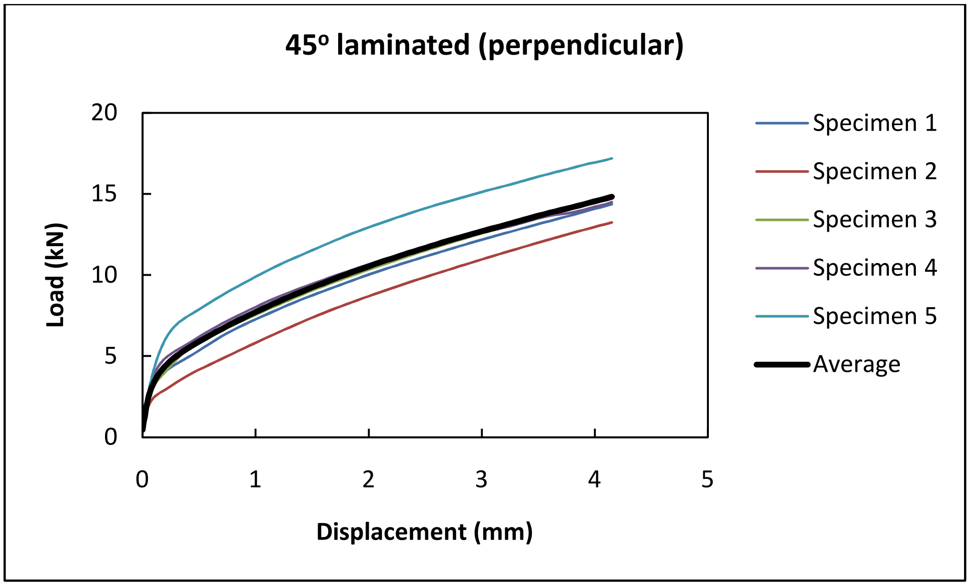

Figure 5-19 Load-displacement relationship for self tapping screws loaded parallel and perpendicular to the longitudinal direction of boxes consisting of 45^{o} laminated plates.

5.2.4 Stress grading of rib materials

Fifty-nine pieces of 38 mm × 184 mm (nominal 2 inch × 8 inch) dimension lumber used for ribs were labeled and marked on both ends. These boards were passed through a Cook-Bolinder SG-AF 100 system, which was a continuous, bending-type, non-destructive stress grading machine, from Tecmach Ltd. (Figure 5-20). The Cook-Bolinder grading machine operates by applying a fixed deflection over a 900 mm span and measuring the loads at 2 mm intervals as the lumber passed flatwise through the machine. MOE values could be calculated by using load-displacement relations obtained from test. In the current study, the magnitude of the fixed deflection was 4.5 mm. Each board was tested twice by being flipped about its longitudinal axis and the MOE value of each piece was calculated from the average of the two test results. The average bending MOE of all fifty-nine specimens was 12.87 GPa.

Figure 5-20 Stress grading of rib materials using a Cook-Bolinder machine.

5.3 Finite element analysis

Since all the single plates were analyzed in Chapter 4, the modeling of screw connections will be the focus of this section.

Separate table sets were utilized to record label and location of each board in the twenty test boxes. Specimen #13 which included two cross laminated plates with OSB facing was employed for illustration (Figure 5-21).

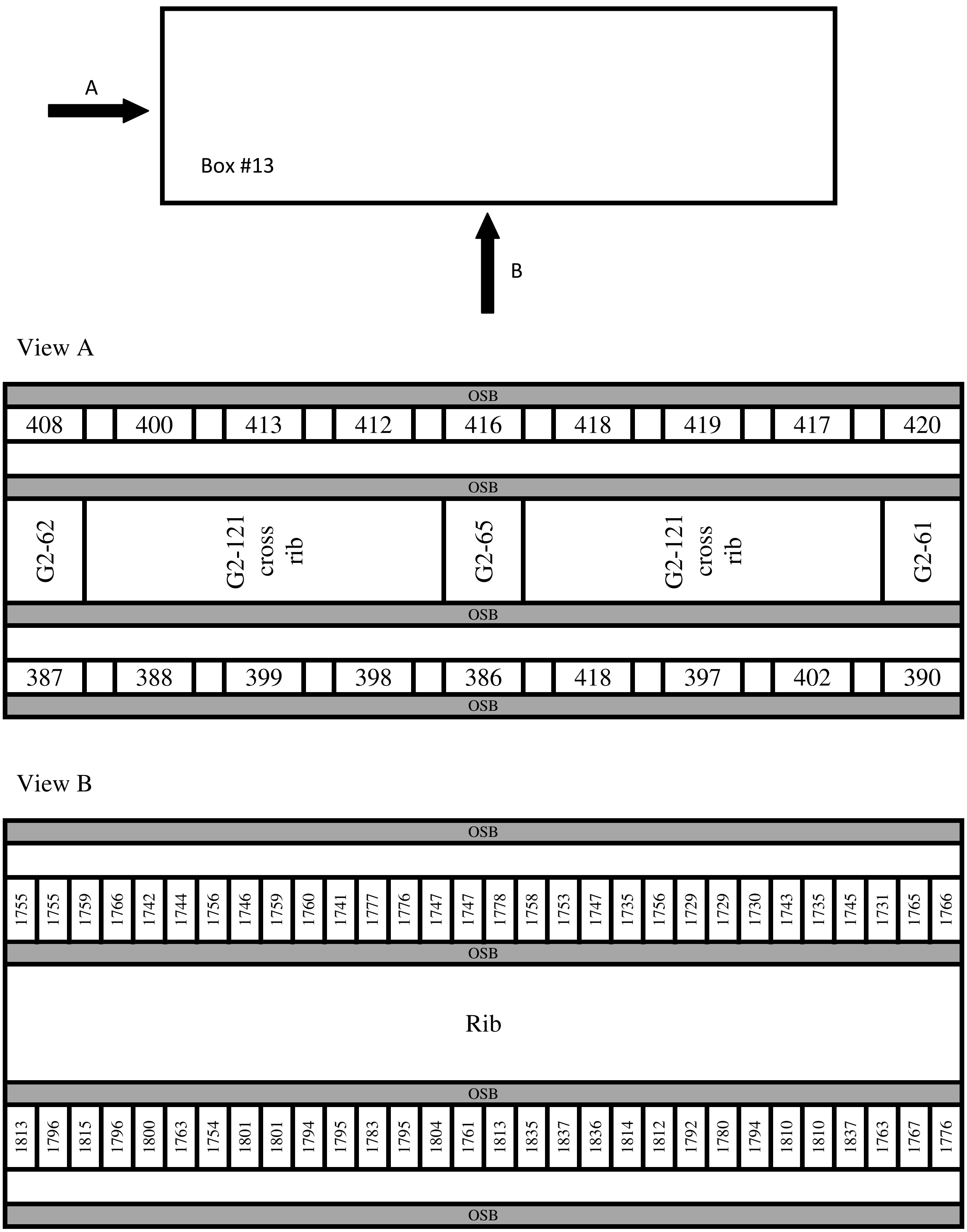

Figure 5-21 Table set for box element #13.

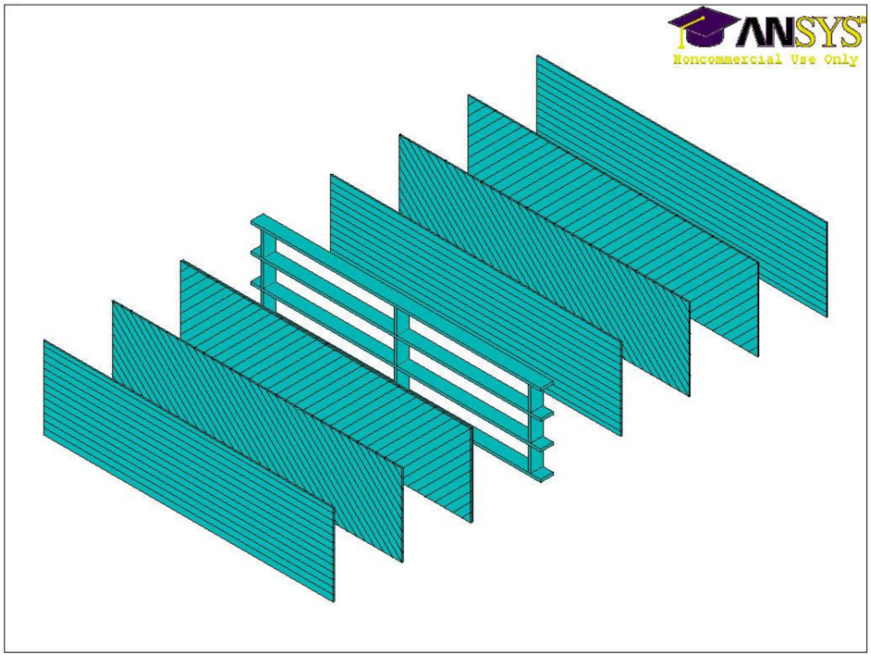

Figure 5-22 Model of a box element consisting of 45° laminated plates.

Figure 5-22 is the computer model of a box element consisting of two 45° laminated plates. Self tapping screws were simulated using elements COMBIN39 (in-plane directions, i.e. x and y) and COMBIN14 (out-of-plane direction, i.e. z). Input data required for the nonlinear spring element COMBIN39 was read from the average of the screw lateral resistance test results presented in section 5.2.3. Withdrawal stiffness of screws which was needed for spring-damper element COMBIN14 was assumed to be infinite. Ribs were considered to be rigid connected with each other by 10d common nails. The surface-to-surface interaction between frame and laminated plates was modeled using contact pairs which were explained in Chapter 3. Models for the other three box configurations were not listed because of their similarity to Figure 5-22 except for only three rib members existing in the structure longitudinal direction. The coefficient of friction between plates and ribs was calibrated to be 0.3 for box elements consisting of cross laminated plates and 0.1 for the rest three cases. Dimensions of box elements are given in Table 5-6.

Table 5-6 Specimen dimensions of box elements used in finite element modeling.

Configuration	Box consisting of cross laminated plates	Box consisting of parallel laminated plates	Box consisting of cross laminated plates with OSB facing	Box consisting of 45^{o} laminated plates
Length (m)	4	4	4	4
Width (m)	1.235	1.235	1.219	1.207
Thickness (mm)	298	298	300	328

5.4 Results and discussion

Stress, strain and deformation of the twenty specimen box elements were calculated using the finite element model. Figure 5-23 and Figure 5-24 show the vertical deflection and normal stress σ_x of box specimen #10 which consists of two parallel laminated plates under a total load of 24.7 kN. All the other specimens are not graphically displayed because of similar performance. It was found that maximum bending stress values occurred at the bottom of the rib members (Figure 5-24). By comparing maximum bending stress to strength ratio of ribs and laminated plates, whether the ribs or the plates are the first part to experience failure can be predicted. This process could not be performed here since the strength of laminated plates was not available. Rib failure was observed from test as shown in Figure 5-25.

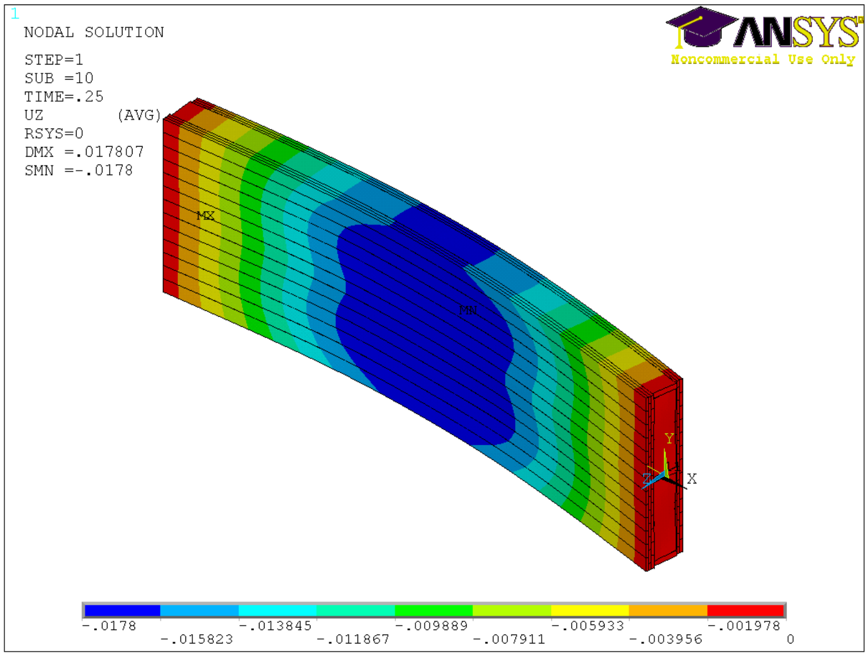

Figure 5-23 Vertical deflection of a box element consisting of parallel laminated plates (specimen #10).

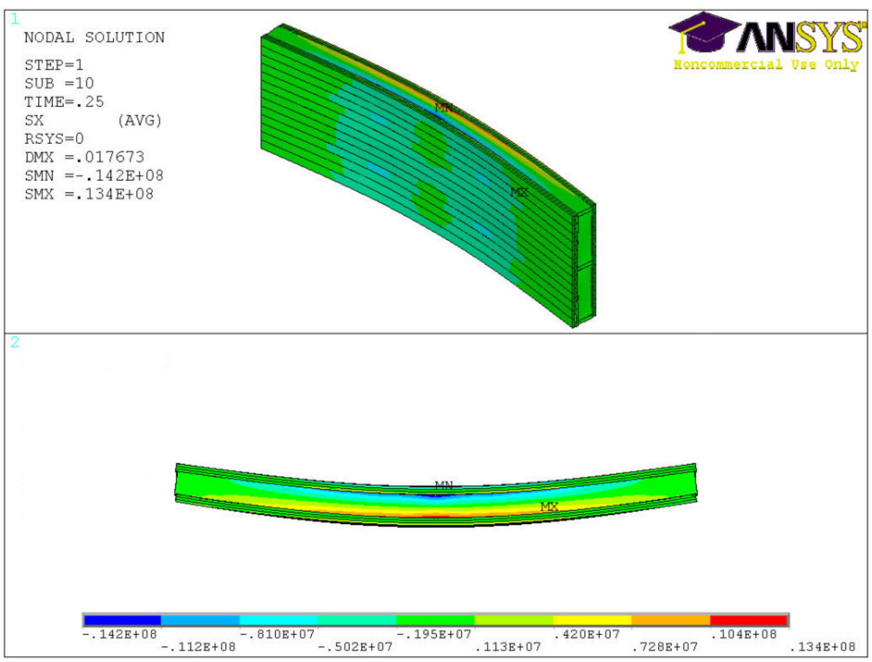

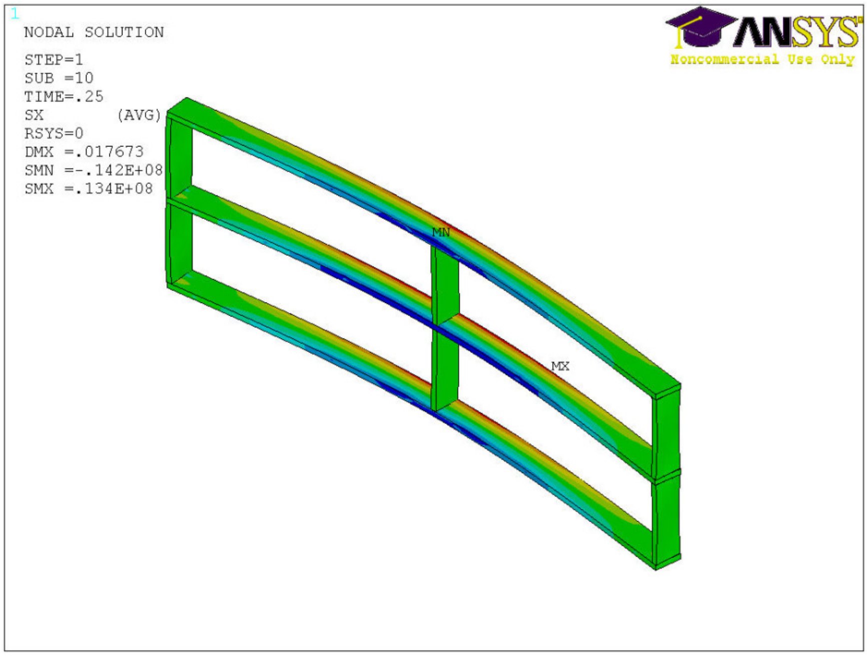

Figure 5-24 Normal stress in longitudinal direction (σ_x) of a box element consisting of parallel laminated plates (specimen #10).

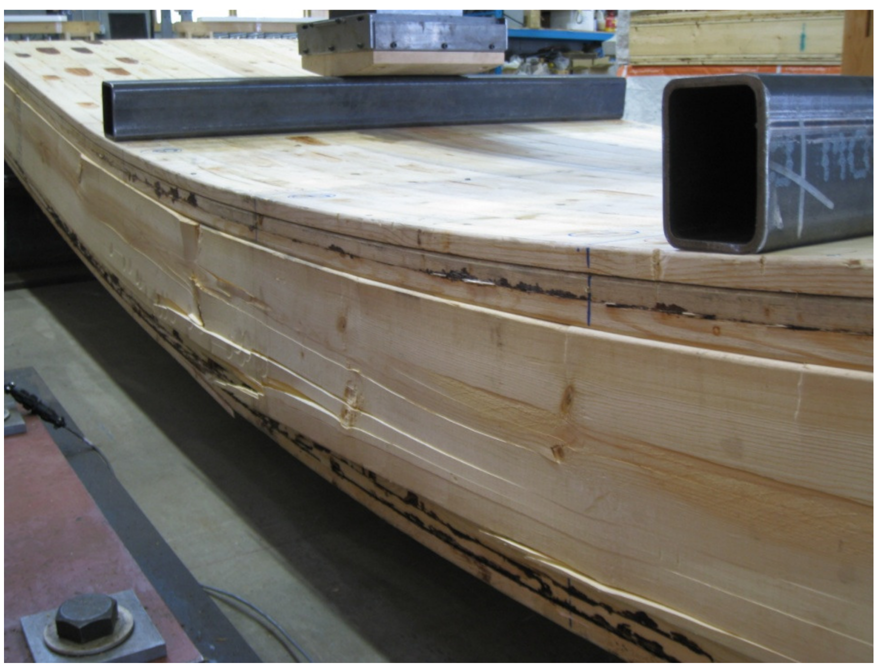

A box element consisting of parallel laminated plates.

A box element consisting of cross laminated plates.

A box element consisting of cross laminated plates with OSB facing.

Figure 5-25 Failure of rib members of different box elements.

Comparisons between tested and predicted bending stiffness values of the twenty box specimens are listed in Table 5-7 to Table 5-10.

Table 5-7 Tested and predicted bending stiffness values of boxes consisting of cross laminated plates.

Specimen #	Bending stiffness obtained between mid-span and supports ($\times 10^6$ N·m^2)			Bending stiffness obtained between mid-span and points A, B, C, D ($\times 10^6$ N·m^2)		
	Tested	Predicted	Error (%)	Tested	Predicted	Error (%)
1	1.41	1.45	3.00	1.46	1.45	-0.56
2	1.30	1.33	2.88	1.28	1.32	2.44
3	1.48	1.40	-5.65	1.46	1.39	-5.18
4	1.45	1.37	-5.65	1.41	1.35	-4.28
5	1.31	1.37	4.59	1.31	1.35	3.09
Average	1.39	1.38	-0.38	1.39	1.37	-1.05

Table 5-8 Tested and predicted bending stiffness values of boxes consisting of parallel laminated plates.

Specimen #	Bending stiffness obtained between mid-span and supports ($\times 10^6$ N·m^2)			Bending stiffness obtained between mid-span and points A, B, C, D ($\times 10^6$ N·m^2)		
	Tested	Predicted	Error (%)	Tested	Predicted	Error (%)
6	1.39	1.50	7.57	1.54	1.51	-1.73
7	1.34	1.52	13.39	1.67	1.53	-8.49
8	1.33	1.53	14.99	1.43	1.51	5.34
9	1.45	1.49	3.03	1.47	1.46	-0.54
10	1.48	1.51	2.07	1.49	1.48	-1.03
Average	1.40	1.51	8.00	1.52	1.50	-1.52

Table 5-9 Tested and predicted bending stiffness values of boxes consisting of cross laminated plates with OSB facing.

Specimen #	Bending stiffness obtained between mid-span and supports ($\times 10^6$ N·m^2)			Bending stiffness obtained between mid-span and points A, B, C, D ($\times 10^6$ N·m^2)		
	Tested	Predicted	Error (%)	Tested	Predicted	Error (%)
11	1.13	1.19	5.22	1.14	1.25	9.36
12	1.08	1.12	3.13	1.06	1.17	10.51
13	1.15	1.16	0.55	1.18	1.21	2.98
14	1.11	1.21	8.39	1.12	1.27	13.46
15	1.10	1.19	7.57	1.16	1.24	6.95
Average	1.12	1.17	4.95	1.13	1.23	8.56

Table 5-10 Tested and predicted bending stiffness values of boxes consisting of 45^o laminated plates.

Specimen #	Bending stiffness obtained between mid-span and supports ($\times 10^6$ N·m^2)			Bending stiffness obtained between mid-span and points A, B, C, D ($\times 10^6$ N·m^2)		
	Tested	Predicted	Error (%)	Tested	Predicted	Error (%)
16	2.16	2.22	2.87	2.22	2.34	5.68
17	2.26	2.25	-0.46	2.22	2.38	7.13
18	2.15	2.32	7.75	2.29	2.48	8.29
19	1.93	2.14	10.81	2.01	2.25	12.37
20	1.97	2.15	9.15	2.07	2.29	10.64
Average	2.10	2.22	5.80	2.16	2.35	8.72

Figure 5-26 is an example of comparison between tested and predicted load-displacement relationship of a box element with OSB facing (specimen #15).

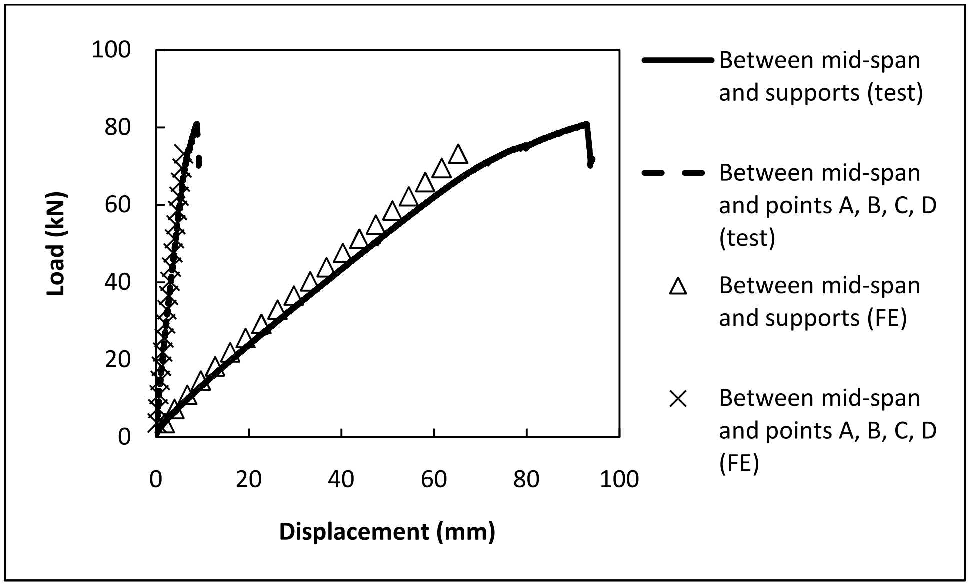

Figure 5-26 Tested and predicted load-displacement relationship of specimen #15.

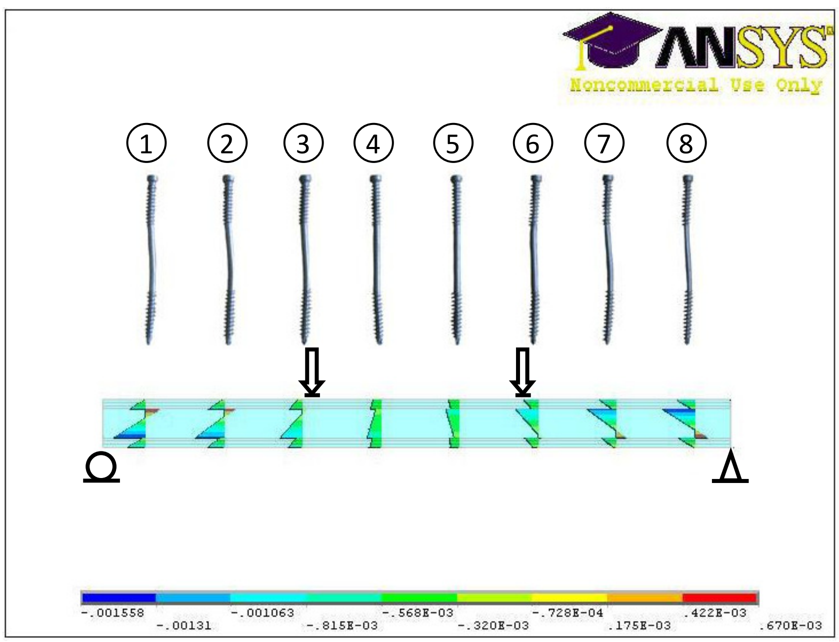

Figure 5-27 Lateral displacement (u_x) along path 1 of box specimen #10.

Lateral displacement u_x at different screw locations along the longitudinal direction of the box specimen #10 which consists of two parallel laminated plates are presented in

Figure 5-27. In this case, the specimen was subjected to a load of 24.7 kN. Because of shear effect, relative movement between wood plates and rib members was much greater in magnitude between supports and loading points, where obvious lateral deformation of screws 1, 2, 3, 6, 7 and 8 was observed.

5.5 Conclusions

This chapter focused on finite element analysis and experimental study of box type structures. Four different types of box elements, each having five replicates, were assembled and loaded under third point bending to examine deflection in the vertical direction. Bending stiffness of each specimen was calculated. Bending failure of ribs was observed from the test. Lateral resistance test of self tapping screws was conducted to obtain load-displacement relationships of screws used in the finite element models. Reasonable agreement was achieved between numerical calculations of the specimen out-of-plane stiffness and third point bending test measurements. These models are able to analyze the structural performance of box systems under out-of-plane loading. Based on these findings, modified models which can be used to study vibration properties of the box structures will be presented in the next chapter.

CHAPTER 6 FLOOR VIBRATION ANALYSIS

6.1 Introduction

Floor vibration is the up and down motion caused by different sources, such as human activities, running of heavy machinery, etc. The forces could be applied directly to the floor or transmitted from other floors or adjacent buildings through columns. When annoying vibrations due to occupant activities are present, a serviceability failure has occurred. While these failures usually do not affect the safety of the occupants, the vibrations definitely affect the comfort of the occupants. The simple floor deflection criterion (deflection of less than span/360 under distributed live load) is not enough when vibration problems become more and more critical because of the use of longer spans, lighter floor systems and so on. Therefore, people must pay much more attention to floor serviceability issues.

In this chapter, the twenty box elements were subjected to vibration tests individually to verify the finite element model and to assess the accuracy of modeled versus measured data comparisons.

6.2 Vibration tests

Box specimens were simply supported as described in the previous chapters. A data acquisition system which included a desktop computer linked to signal analyzers was used to collect and process test data. Three types of excitations listed as follows were conducted to determine the natural frequencies of the structures.

- Hammer impact introduced by a DYTRAN model 5803A sledge hammer (Figure 6-1 (a))

- Human induced impact commonly referred to as a heel drop

- Sand bag drop impact induced by a sand bag with a weight of 10 kg (22.1 lb)

(a) (b)

Figure 6-1 (a) A DYTRAN model 5803A sledge hammer and (b) a PCB Piezotronics model 393A03 accelerometer.

Performing different types of impact test was designed to provide confirmation of the experimental results which would be used to verify the finite element model. Once the impact test was performed, the floor response of the box system was measured with two monoaxial piezoelectric accelerometers (PCB Piezotronics, model 393A03 ICP) (Figure 6-1 (b)). The accelerometers have a sensibility of 1000 mV/g, and a frequency range of 0.5 - 2000 Hz (PCB Piezotronics Inc., 2010). They were joined to a metal disc and mounted on the top surface of the specimen using screws. To simulate vibration response of the box structures under occupant load, a simplified test was designed by adding a 90.8 kg (200 lb) weight on the top surface of the specimen (Figure 6-2).

Locations of impact, accelerometers and the simulated occupant load on the box structure are shown in Figure 6-3. Symbols A and B mean impact locations; C1, C2, E1 and E2 accelerometer locations; S center of the specimen; and W location of the simulated occupant load. Figure 6-3 (a) represents box structures consisting of 45^{o} laminated plates. In Figure 6-3 (b), L1, L2, L3 and L are 0.618 m, 0.299 m, 0.318 m and 1.235 m, respectively, for box structures consisting of cross laminated and parallel laminated plates; L1, L2, L3 and L are 0.603 m, 0.292 m, 0.311 m and 1.207 m, respectively, for box structures consisting of cross laminated plates with OSB facing.

Figure 6-2 A box specimen with simulated occupant loading.

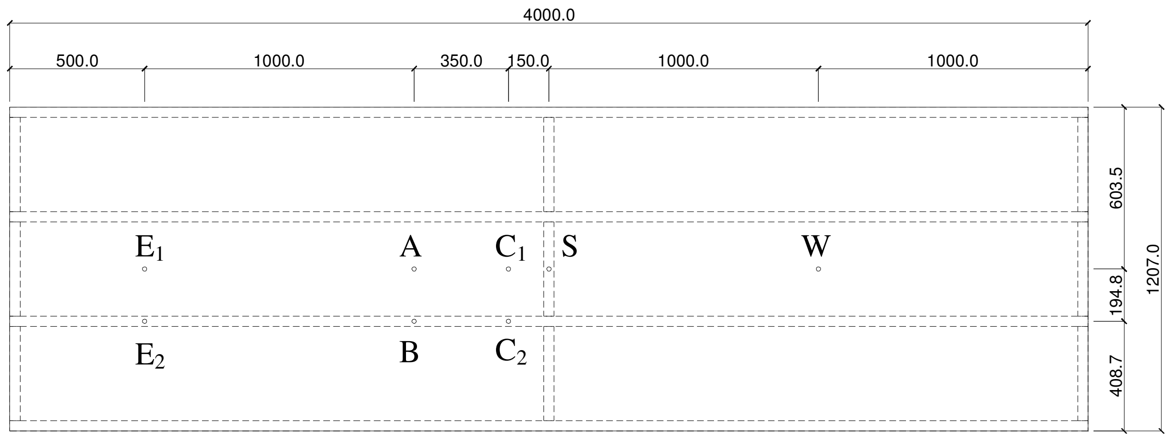

(a)

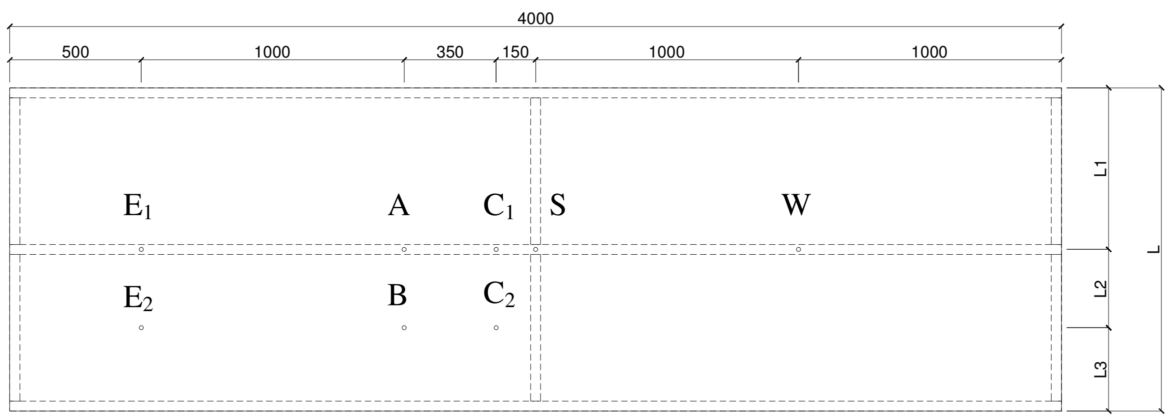

(b)

Figure 6-3 Impact and measuring locations on box specimens consisting of (a) 45^{o} laminated plates and (b) cross/parallel laminated plates or cross laminated plates with OSB facing.

6.2.1 Impulse hammer excitation

DYTRAN model 5803A instrumented impulse hammer is a portable and manually operated device for the application of transient loading on full-scale structures in the low frequency range. The head weight and maximum peak force is 5.4 kg (12 lb) and 22 kN (5000 lb), respectively. It has four polyurethane impact tips, i.e. 1) 6252T impact tip, tough, red, 2) 6252S impact tip, soft, brown, 3) 6252H impact tip, hard, black, and 4) 6252M impact tip, medium, green (Dytran Instruments Inc., 2008). The red impact tip was chosen to create the excitation in this study. This device is usually used in conjunction with portable signal analyzer for quick modal testing of small and medium size Civil Engineering structures.

This modal test was conducted with the cooperation of two people, a hammer operator and a data acquisition operator. Depending on locations of test spots, the hammer operator stood beside the box specimen to use the impulse hammer for the test. The test then progressed with the hammer operator impacting the specimen at the first test point. Meanwhile, the data acquisition operator started data collection which lasted for a duration of 5 seconds. This process should be repeated for a required number of impacts for every box configuration. In the current study, three to five replications were performed. Then the hammer operator hit the second test spot and all the procedures were repeated in the same manner as described above. After the test was finished, values from three trials were reported and the average was regarded as the frequency of the specimen. Figure 6-4 shows typical time history traces when a hammer impact test was performed on a box structure under simulated occupant load.

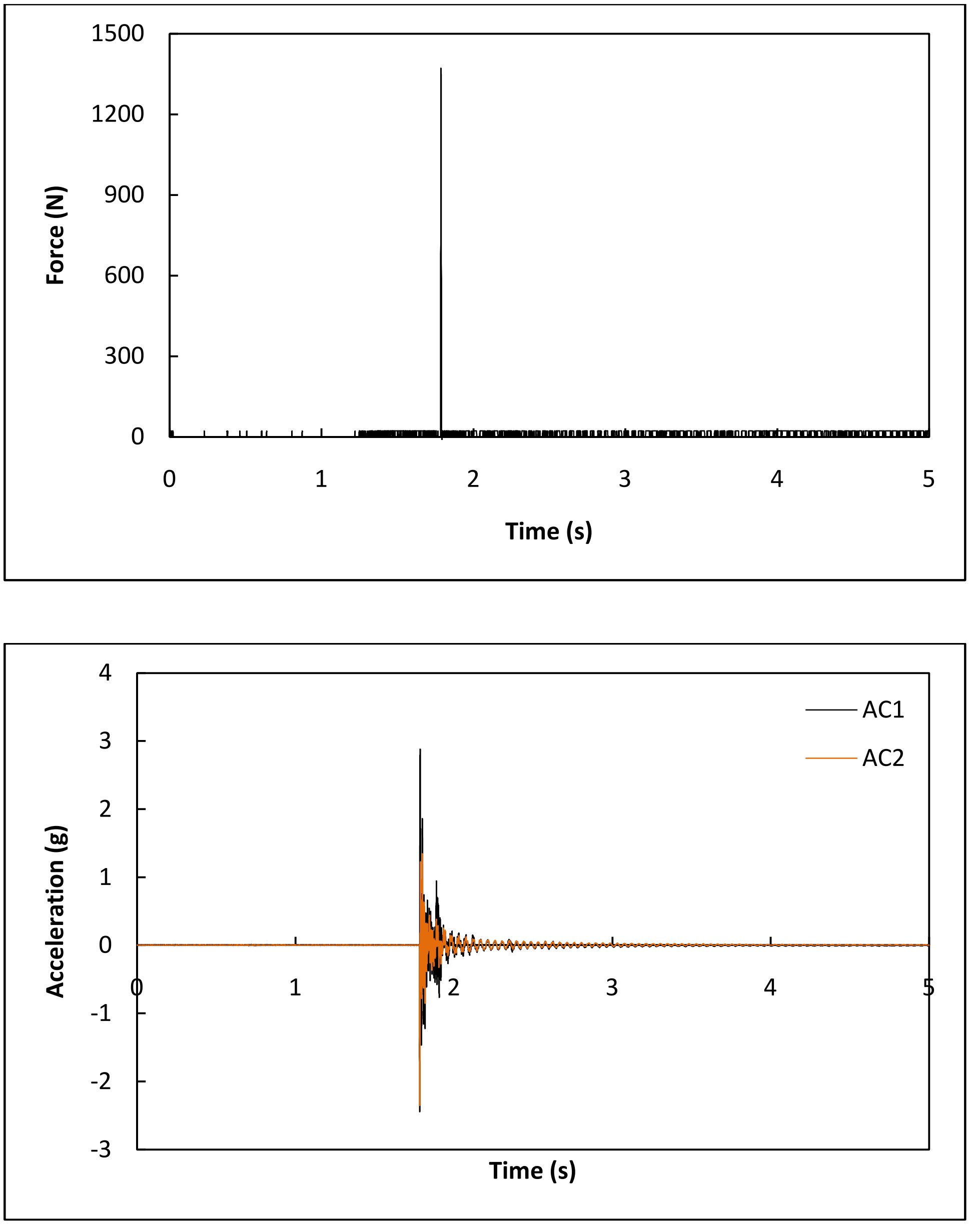

Figure 6-4 Typical hammer impact traces (Specimen #18).

6.2.2 Sandbag drop excitation

A 10 kg (22.1 lb) sandbag was suspended over the center of the specimen at a distance of 200 mm between the sandbag bottom and specimen top surface by a quick release mechanism which was attached to the load head frame (Figure 6-5). Then the sandbag was released by activating the quick release mechanism. At the same time, the data acquisition operator started data recording program and the process of data collection lasted for 5 seconds. The test was repeated for five times before moving the accelerometers to the other measuring spots. Figure 6-6 is a typical acceleration trace of a sandbag drop test on a box structure under simulated occupant load.

Figure 6-5 Sandbag drop test.

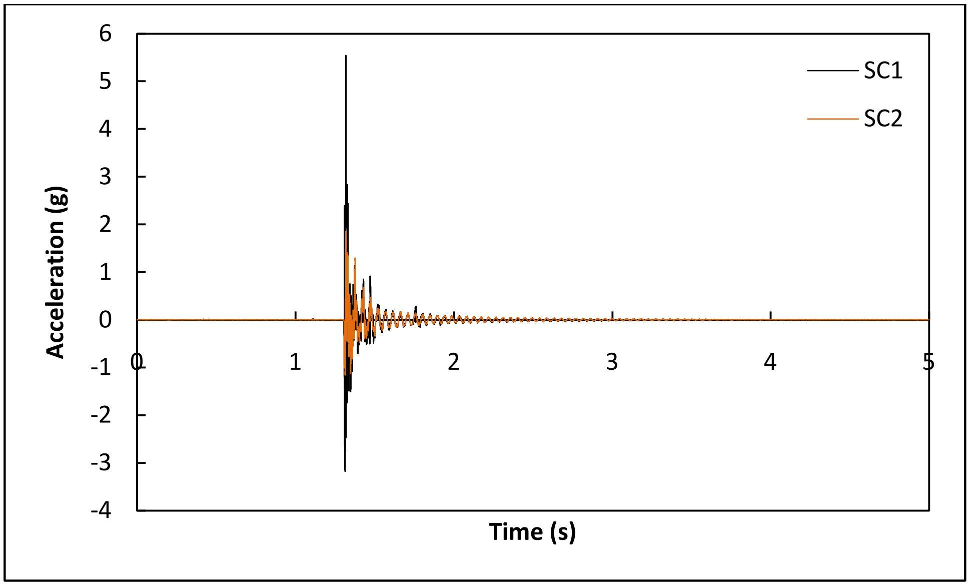

Figure 6-6 Typical sandbag drop acceleration trace (Specimen #18).

6.2.3 Heel drop excitation

The heel drop excitation was performed by a 78 kg (172 lb) person standing at different locations on the box system as shown in Figure 6-7. The person rose onto his toes and then suddenly dropped down so that his heels struck the specimen. Heel drop tests were repeated for at least five times depending on the signal quality. The typical heel drop acceleration signal collected from a box structure under simulated occupant load is displayed in Figure 6-8.

Figure 6-7 Heel drop test.

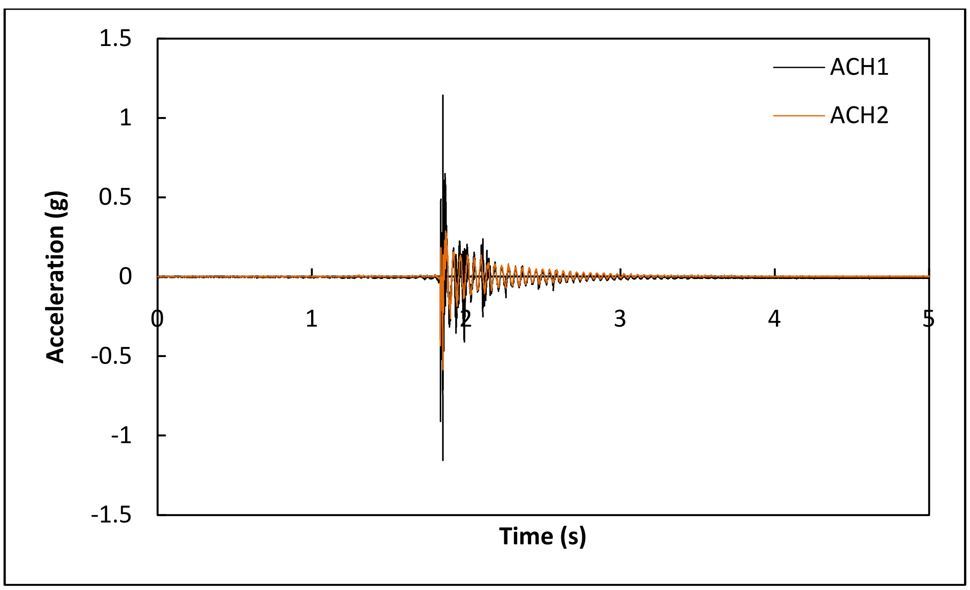

Figure 6-8 Typical heel drop acceleration trace (Specimen #18).

6.3 Determination of specimens' natural frequencies

The Fast Fourier Transform (FFT) technique was used to transform the information recorded in the time domain to the frequency domain. It is a very important and efficient algorithm for calculating the discrete Fourier transform (DFT) and its inverse. Natural frequencies can be identified from peaks in frequency response spectra. Figure 6-9 is typical frequency domain signals obtained by performing FFT. Only frequencies in a range between 0 and 50 Hz were displayed because high frequencies were normally less annoying and not of the same importance as low frequencies for the free vibration of floor system. Usually a floor's lowest three or four frequencies dominate its response. Table A-1 to Table A-8 in the appendix are the measured fundamental frequencies of each specimen with/without simulated occupant loading. Some measurements were not quite accurate due to unexpected test factors. These values, marked with a star symbol, were listed only for the completion of database but not included in the analysis.

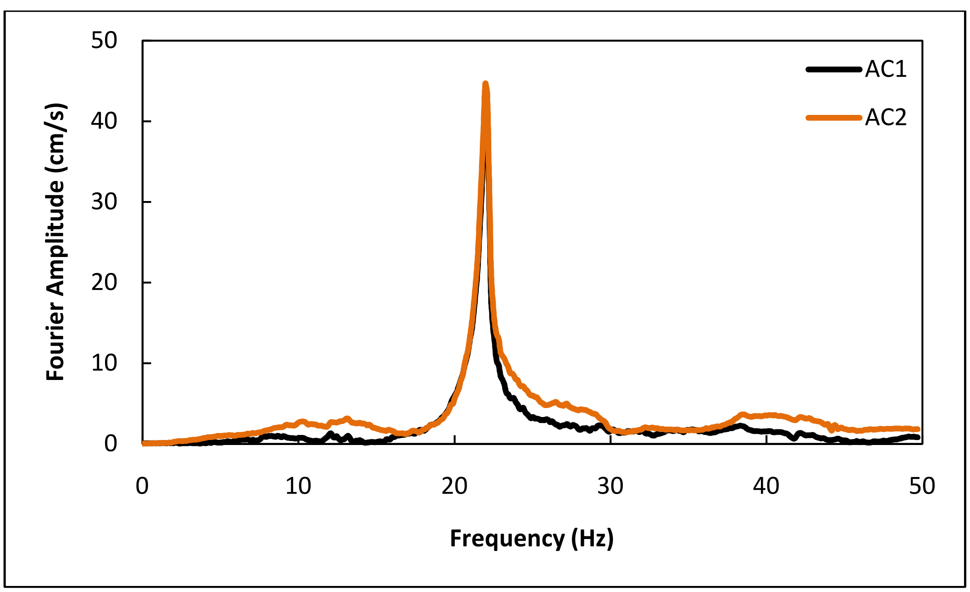

Hammer impact test

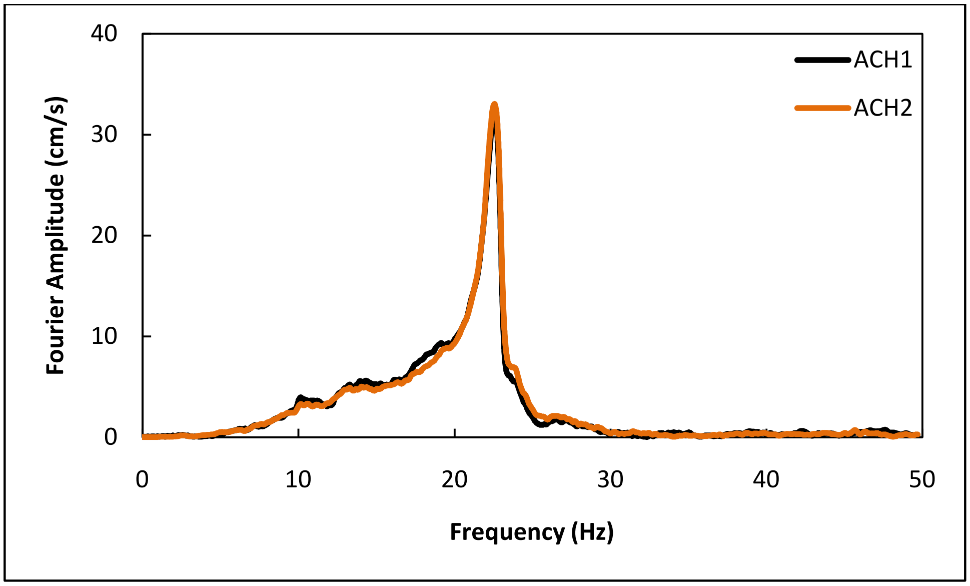

Heel drop test

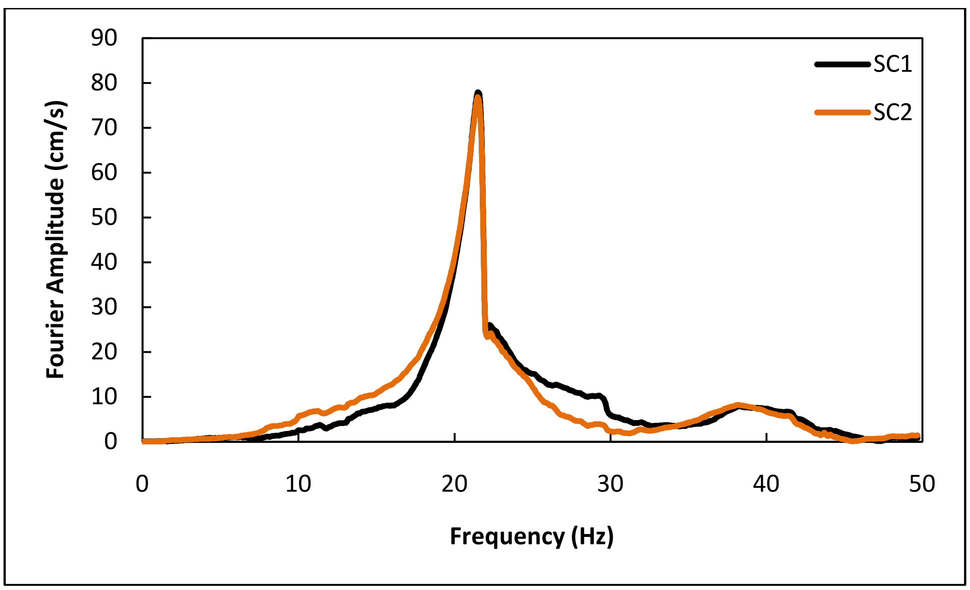

Sandbag drop test

Figure 6-9 Frequency domain signals of specimen #18 under simulated occupant load.

6.4 Finite element modeling and discussion

Modal analysis in ANSYS® is a linear analysis. Any nonlinearities, such as contact elements and plasticity, ANSYS® treats them as linear. Therefore, the contact behavior was very different in dynamic condition compared to static environment which required modifications to the finite element model previously used in the static analysis. Friction between wood plates and rib frame was deleted, meaning that contact surfaces could move relative to each other without resistance against that motion occurring. Removal of friction resulted in free movement between structural components which was not physically realistic. Therefore, screw connections were assumed to be fully rigid by using COMBIN14 element with infinite stiffness in x, y and z directions to simulate the performance of the entire structure.

The 90.8 kg (200 lb) occupant load was modeled to act at nodes within an area of 13.5 mm × 25.5 mm (in red) on the specimen top surface by using a structural mass element MASS21 as shown in Figure 6-10. This element is defined by a single node, concentrate mass components in the element coordinate directions, and rotary inertias about the element coordinate axes.

Weight of the box elements was measured using a precision electronic scale (MTS 458 system) right before testing in order to find out the average material density of each specimen which was required to determine natural frequencies in modal analysis (Figure 6-11). A full detail of weight and density of each box element is given in Table 6-1.

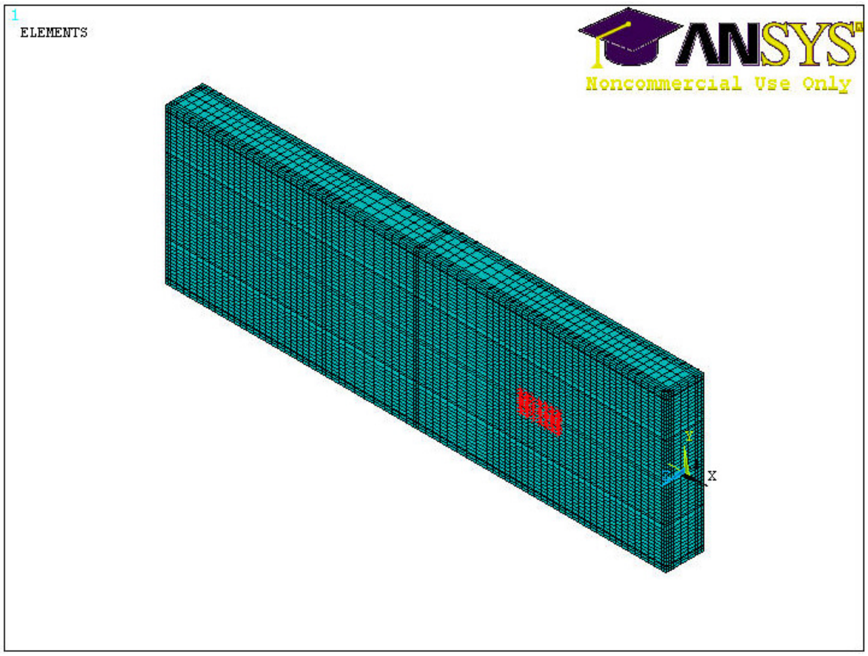

Figure 6-10 Finite element model of a box specimen with occupant load.

Figure 6-11 Weight measuring of a box element consisting of 45^{o} laminated plates.

Table 6-1 Weight and density of box specimens.

	Specimen #	Weight (kg)	Density (kg/m^3)		Specimen #	Weight (kg)	Density (kg/m^3)
Box consisting of cross laminated plates	1	354.57	484.84	Box consisting of parallel laminated plates	6	361.38	494.98
	2	353.21	483.79		7	359.11	491.46
	3	354.12	484.63		8	364.56	498.50
	4	350.49	480.06		9	361.38	494.15
	5	355.48	486.08		10	358.66	490.84
Box consisting of cross laminated plates with OSB facing*	11	355.48	754.21	Box consisting of 45° laminated plates	16**	/	472.44
	12	353.21	744.33		17**	/	472.44
	13	349.58	728.53		18	431.30	476.28
	14	348.22	722.60		19	425.85	471.47
	15	351.85	738.40		20	424.49	469.56

* Densities listed are for OSB panels. Wood density was assumed to be 479.5 kg/m^3 which was the average density value of all lumber pieces determined at dynamic MOE test described in Chapter 4.

** Density value is the average of that of specimens #18, #19 and #20 because weight of specimens #16 and #17 was not measured.

Table A-9 to Table A-16 in the appendix present comparisons of the first natural frequency between predicted and laboratory measured values. As mentioned before, symbols "A" and "B" mean impact locations on the specimen; "C" accelerometer positions close to the center of the specimen; "E" accelerometer positions close to the end of the specimen; "H" heel drop test; "S" sandbag drop test. For example, "AC" represents measurements from accelerometers close to the center of a specimen subjected to hammer impact at point A; "BEH" measurements from accelerometers close to the end of a specimen subjected to heel drop impact at point B; "SC" measurements from accelerometers close to the center of a specimen subjected to sandbag drop impact.

For the same type of specimen, finite element analysis resulted in very similar natural frequency predictions. This is easy to explain because natural frequency is proportional to the square root of stiffness, K, and inversely proportional to the square root of mass, M. Therefore, specimens with similar stiffness and mass properties are theoretically expected to demonstrate similar natural frequencies. For the same reason, specimens gave a lower fundamental frequency under the simulated occupant load. The computer model provided good predictions in most cases except for specimen #7 highlighted in Table A-10. As mentioned before, specimens belonging to the same layout category were expected to have similar vibration performance, but the tested frequency of specimen #7 was 20.09 Hz which was 14.47% lower than the average frequency value (23.49 Hz) of the other four specimens (#6, #8, #9 and #10). Therefore, the difference between calculation and test data was greater than all the other cases.

6.5 Conclusions

Controlling floor vibration is very important because it provides not only comfort for the occupants but also good testing environments for sensitive equipments that might be on the floor, especially in industrial and laboratory settings. In order to study vibration properties of floor system, 3-D finite element models were built based on the static models developed in the previous chapters. To verify the new models, three types of excitation were used to measure the fundamental frequency of the twenty box specimens with/without a 90.8 kg (200 lb) weight which was used to simulate occupant load. Fundamental frequencies were calculated using data collected from different locations on the specimen. Finite element analysis provided good predictions of fundamental frequency values comparing to the experimental results.

In the future, this work can be used as a foundation from which to establish more complicated computer models dealing with different building floor systems. That will be useful in the early stage of floor design to help analyze vibration and improve serviceability of the system.

CHAPTER 7 CASE STUDY: L41 HOME

7.1 Introduction

The L41 home, which rhymes with "all for one" and infers "one for all", was designed as an ultra-compact, sustainable, high-design, high quality and energy-efficient house (Figure 7-1). Constructed of CLT panels which were made of beetle killed timber, the 20.4 m^2 (220 ft^2) structure features built-in storage, living and bedroom space, a kitchen and a bathroom and has been designed as an affordable, fully equipped home with an estimated price of $50,000. The L41home was first displayed during the 2010 Winter Olympics in Vancouver, Canada (Figure 7-2).

Figure 7-1 Wood structure of the L41 home.

Figure 7-2 The L41 home displayed during the 2010 Winter Olympics in Vancouver (www.L41home.com).

7.2 Structural analysis

The main structure of the L41 home includes 5-ply CLT living room floor, 3-ply CLT balcony floor, 5-ply CLT roof and 3-ply CLT walls. Because the object of this dissertation is to investigate CLT type structures used in floor applications, the following sections will focus on structural analysis of the floor and roof systems.

7.2.1 CLT floor

Figure 7-3 shows the main floor system consisting of five CLT panels and two glulam beams.

Figure 7-3 Main floor system.

In Figure 7-4, symbols 1, 2, 3 and 4 represent living room floor which was made of 5-ply CLT panels and symbol 5 represents the balcony floor which was made of 3-ply CLT panels. The longitudinal and cross layers of the 5-ply CLTs were constructed of wood boards with different thicknesses, i.e. 35 - 17.5 - 35 - 17.5 - 35 mm. But for 3-ply CLTs, all layers had the same thickness of 35 mm. The floor was supported by two 215 mm × 342 mm

(8 ½ inch× 13 ½ inch) Douglas-fir glulam beams sitting on four 215 mm × 215 mm posts. Note that the glulam was customized and not commercial type. Würth ASSY® VG plus 6 mm × 250 mm wood screws at a spacing of 300 mm were used to connect the glulam beams and the CLT panels. The adjacent CLTs were toe-screwed at a spacing of 300 mm.

All CLT panels were made of 38 mm × 140 mm (nominal 2 inch × 6 inch) #2 and better SPF lumber. The 38 mm material was re-sawn to get the 17.5 mm members. Elastic properties of SPF and Douglas-fir materials at 12% moisture content were obtained from the Wood Handbook (1999) as shown in Table 7-1.

Table 7-1 Input elastic properties of SPF and Douglas-fir materials.

	Modulus of elasticity (MPa)			Modulus of rigidity (MPa)			Poisson's ratio		
	E_L	E_R	E_T	G_{LR}	G_{LT}	G_{RT}	υ_{LR}	υ_{LT}	υ_{RT}
SPF	11990	1223	815	588	552	60	0.316	0.347	0.469
Douglas-fir	14960	1017	748	957	1167	105	0.292	0.449	0.390

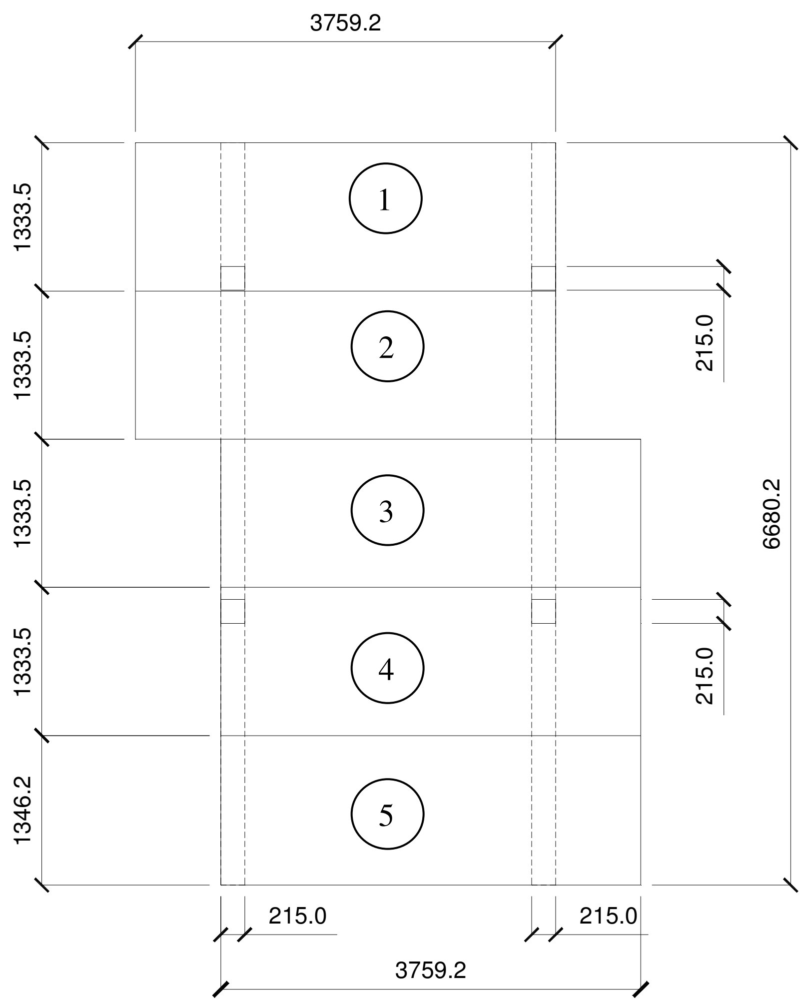

Figure 7-4 Plan of the main floor system.

The lateral stiffness K of the screws can be estimated as 1737.25 N/mm by using the following equation according to the DIN 1052: 2004-08.

$$K = \frac{\rho_k^{1.5}}{25} \cdot d^{0.8} \tag{7-1}$$

where $\rho_k = \sqrt{\rho_{k1} \cdot \rho_{k2}}$.

ρ_{k1} and ρ_{k2} are density of the two materials to be connected. In this case, ρ_{k1} is 448 kg/m^3 for lodgepole pine and ρ_{k2} is 504 kg/m^3 for Douglas-fir according to the Wood Handbook (1999). d is diameter of the screw which is 6 mm.

In the design, the floor was subjected to uniformly distributed load which included a live load of 1915 Pa (40 psf) and a dead load of 479 Pa (10 psf). Therefore, the total specified load was 2394 Pa (50 psf).

Based on the finite element models developed and verified in previous chapters, deflection and stress of the floor system under the total specified loads could be determined as shown in Figure 7-5 to Figure 7-7. Figure 7-5 displays the mesh and boundary conditions of the floor. The maximum deflection allowed for this system is 20.88 mm defined as L/180 based on total load, where L is floor span. From Figure 7-6, the maximum deflection is 3.95 mm which is only 18.92% of the deflection criteria, meaning that the floor structure is much stiffer than the building code requirement. According to Figure 7-7, the maximum deflection of the glulam beams underneath the CLT floor is 3.30 mm. Therefore, total deflection of the system was mainly caused by the beams other than CLT panels. This gave evidence that CLT products have great ability to be used in such floor, especially long span floor applications. From Figure 7-8, the maximum tensile stress occurred at the mid-span of the balcony with a value of 1.31 MPa which is much lower than the tension parallel to grain strength of No.1/No.2 grade SPF lumber (5.5 MPa) in the CSA Standard O86-01 (2001).

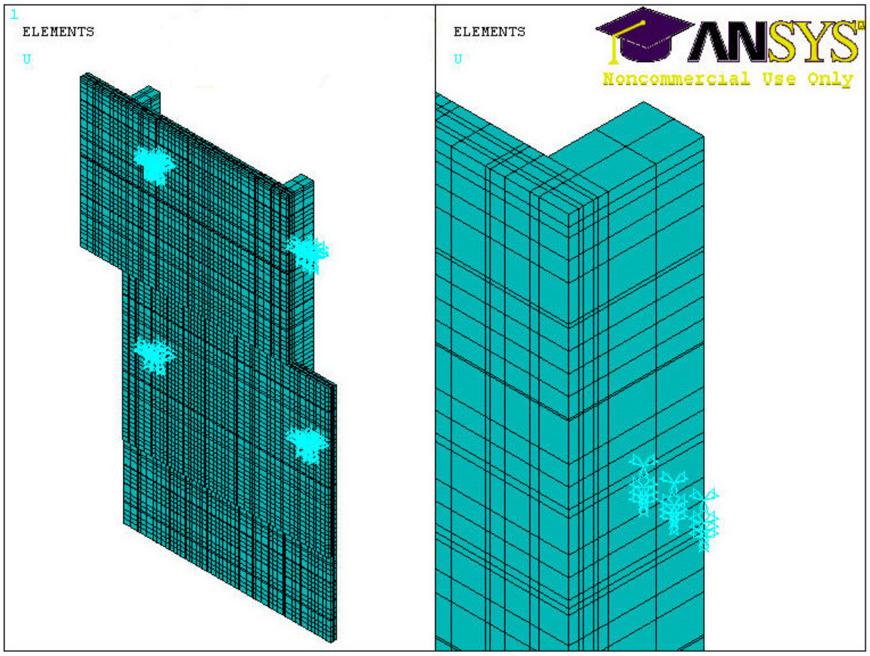

Figure 7-5 Boundary condition of the main floor system.

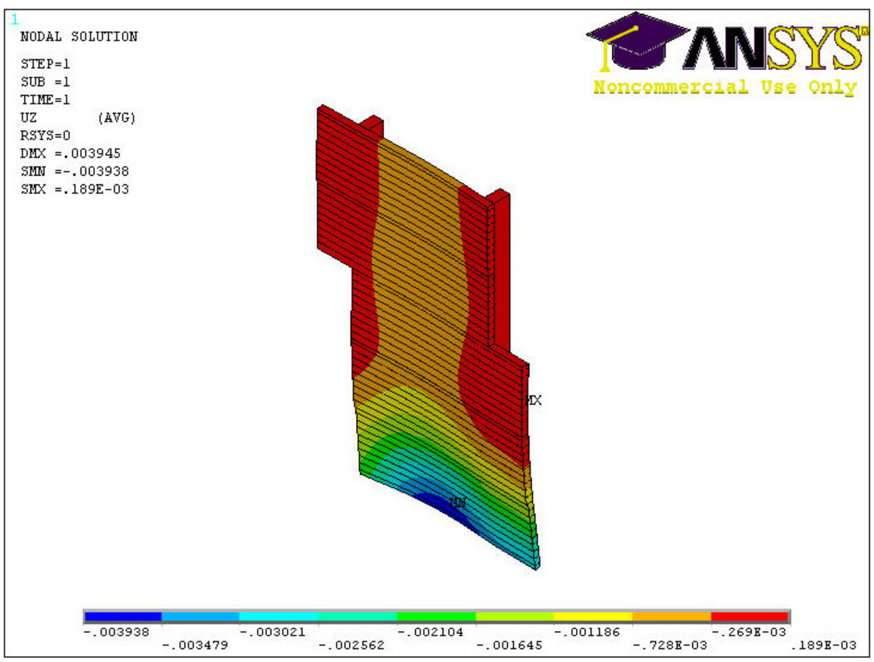

Figure 7-6 Deflection profile of the main floor under a load of 2394 N.

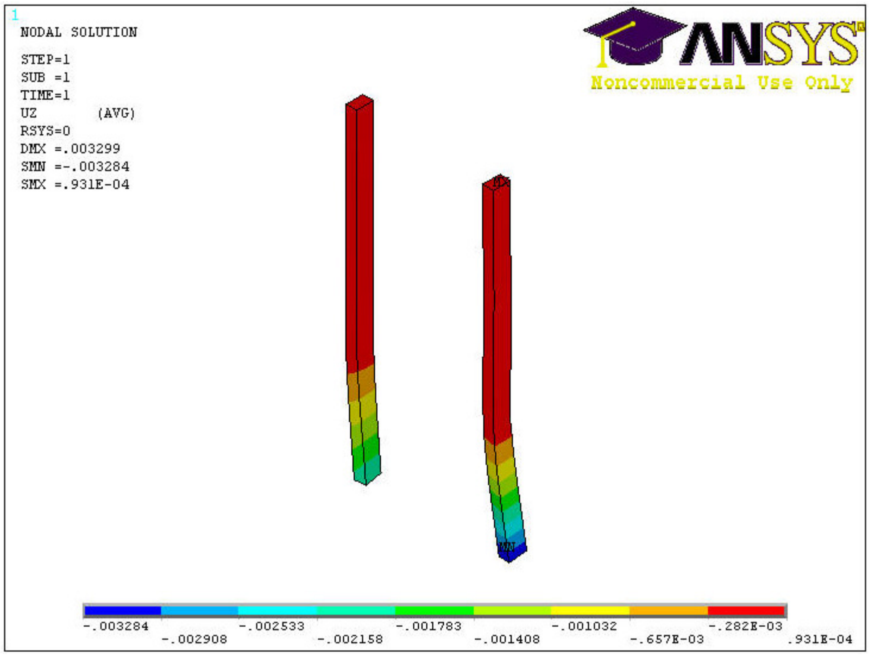

Figure 7-7 Deflection of the glulam beams under a load of 2394 N.

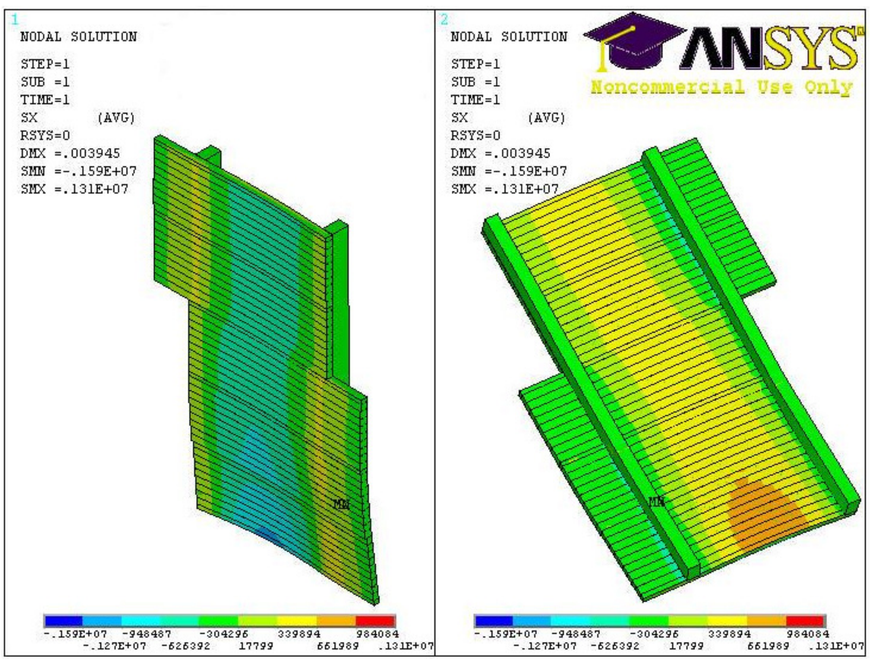

Figure 7-8 Normal stress in floor span direction under a load of 2394 N.

7.2.2 CLT roof

Figure 7-9 is the CLT roof system. The roof is made of five pieces of 5-ply CLT panels (35 - 17.5 - 35 - 17.5 - 35 mm) and there is an 80 mm × 266 mm (3 1/8" × 10 ½") Douglas-fir glulam beam underneath the roof as shown in Figure 7-10. The same as in the floor system, Würth ASSY® VG plus 6 mm × 250 mm wood screws at a spacing of 300 mm were used to connect the glulam beam and CLT panels. The adjacent CLTs were toe-screwed at a spacing of 300 mm.

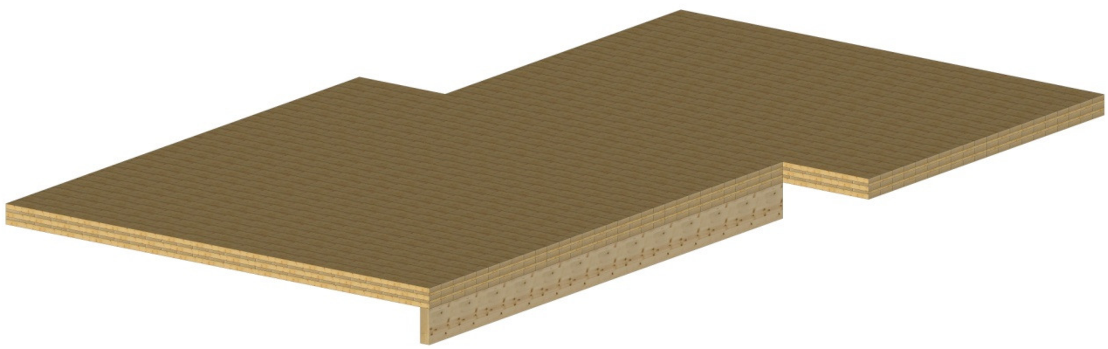

Figure 7-9 CLT roof system.

Figure 7-11 shows the plan of floor and wall systems. The grey areas are CLT walls which serve as supports for the roof structure. This boundary condition was modeled in the finite element analysis as shown in Figure 7-12.

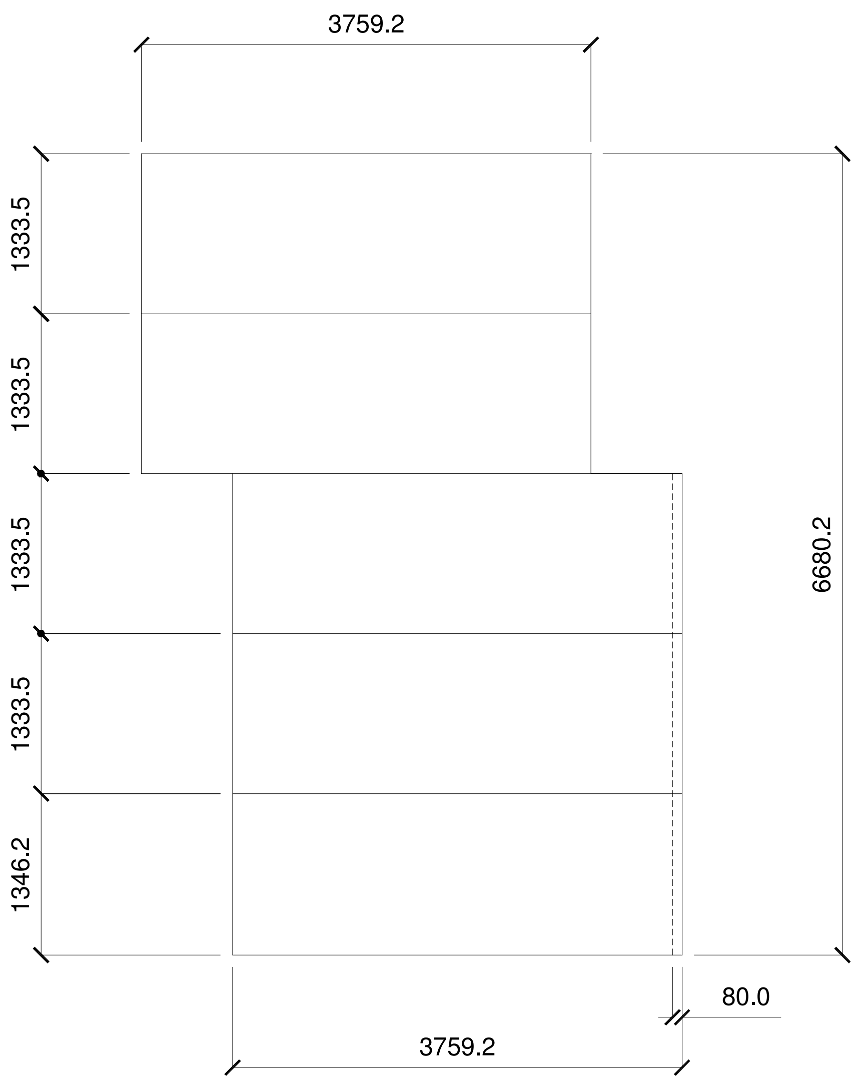

Figure 7-10 Plan of the roof system.

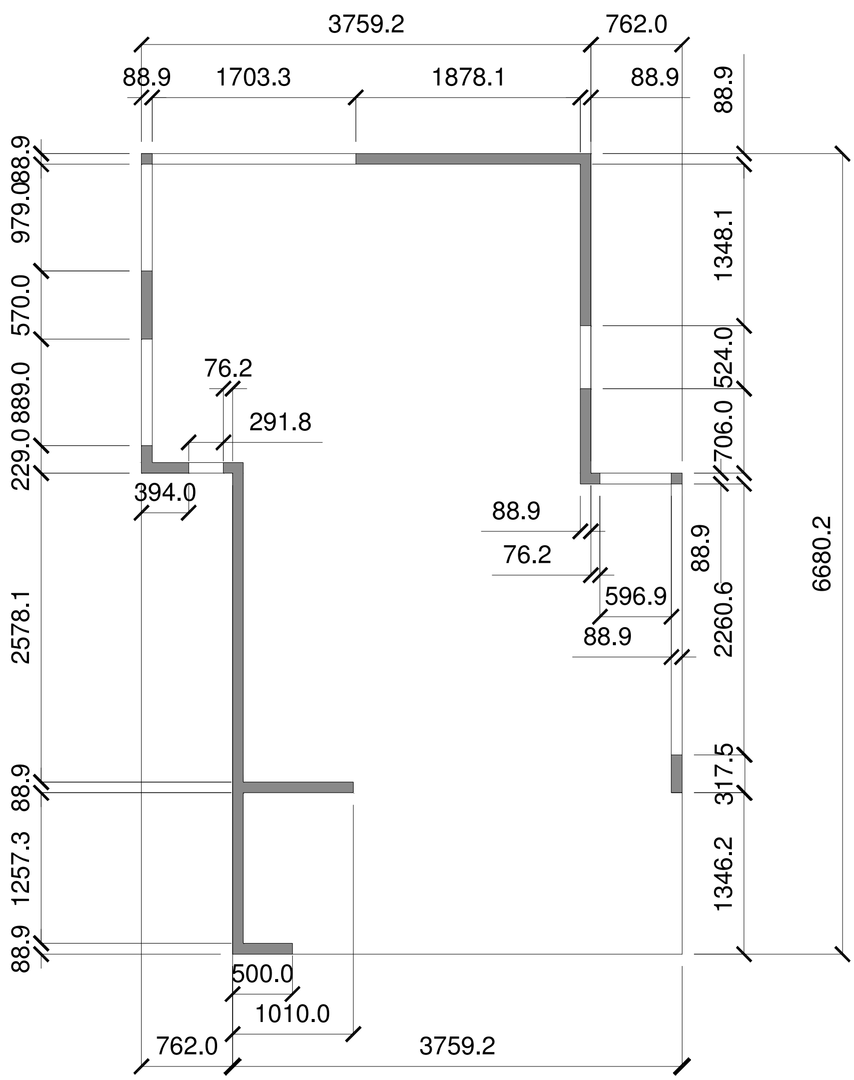

Figure 7-11 Plan of the floor and wall system.

The roof was subjected to uniformly distributed load which included (a) a dead load of 1436 Pa (30 psf) considering a green roof, and (b) a live load of 2001 Pa (41.8 psf) considering a ground snow load of 1800 Pa (37.6 psf) and a rain load of 201 Pa (4.2 psf). Under the total specified load 3437 Pa (71.8 psf), the maximum deflection was 2.68 mm (Figure 7-13) which was very small comparing to the maximum allowed deflection 20.88 mm calculated by using the L/180 criterion. Considering the strength, maximum tensile stress in the roof was 2.95 MPa (Figure 7-14) and much lower than the lumber tension strength, 5.5 MPa, in the standard.

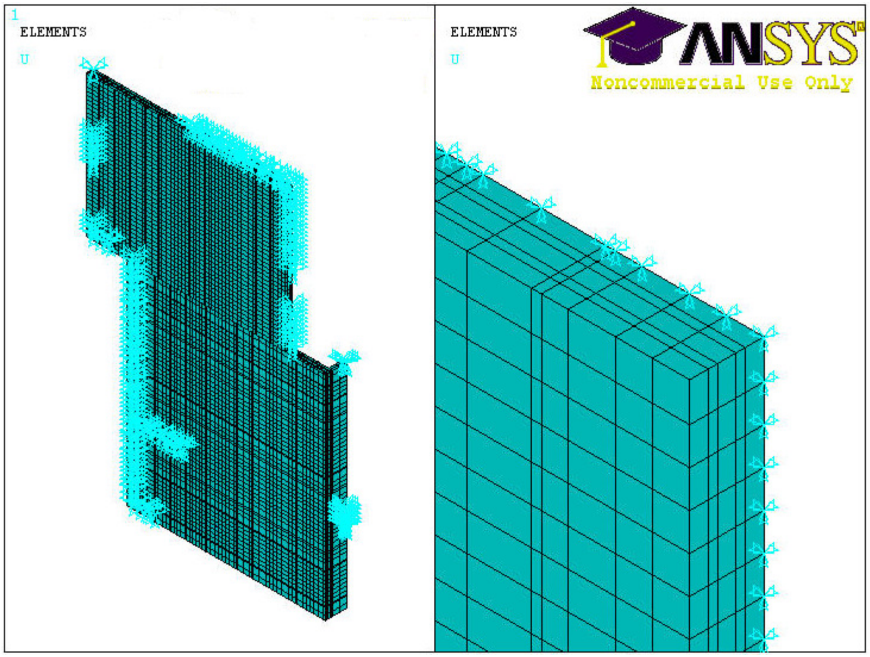

Figure 7-12 Boundary condition of the roof system.

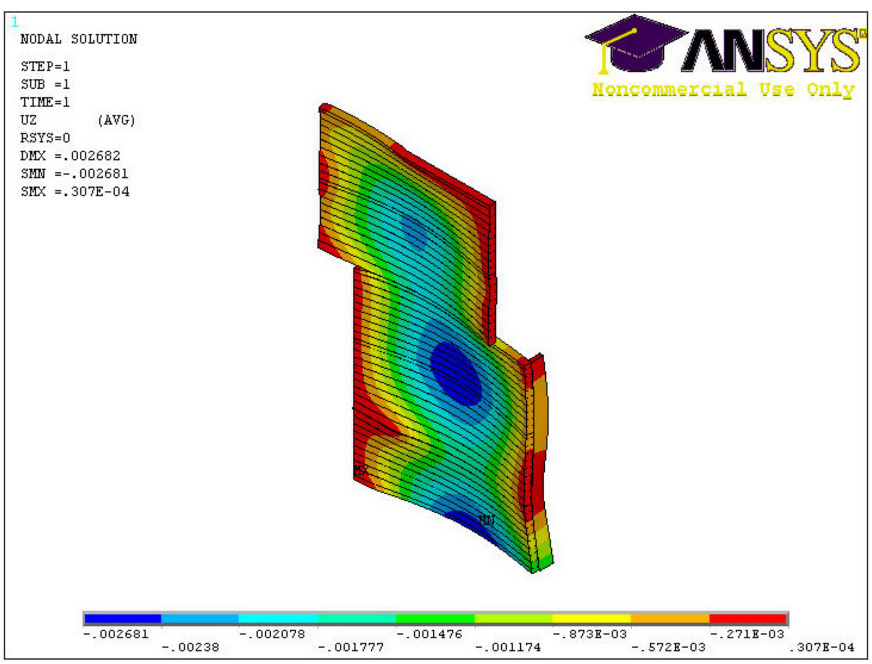

Figure 7-13 Deflection profile of the roof under a load of 3437 N.

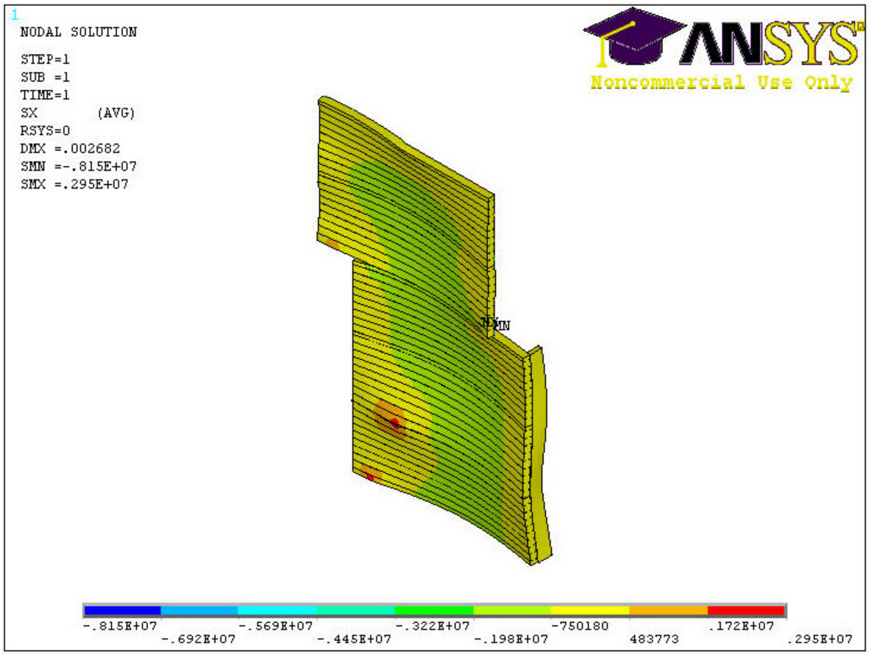

Figure 7-14 Normal stress in roof span direction under a load of 3437 N.

7.3 Conclusions

L41 home, a pre-fabricated demonstration building built with local manufactured CLT panels, was analyzed in this chapter. It is an application example of the previous developed computer models. The bending stress and deflection were calculated for floor and roof systems. Under the total specific load, both of the floor and roof structures demonstrated excellent structural properties and satisfied the design criteria in terms of strength and stiffness.

CHAPTER 8 CONCLUSIONS AND FUTURE WORK

8.1 Conclusions

The focus of this dissertation has been devoted to the investigation of mechanical and vibration characteristics of box-type CLT structures used in floor applications. As a pioneer research of CLT materials in North America, this work has contributed to the understanding of the structural performance of floor systems using CLT panels designed, manufactured and aimed primarily for the commercial and residential applications, particularly in tall and long-span situations where conventional timber framing has limitations. The main achievements can be grouped in the following categories.

8.2 Computer modeling

A comprehensive three-dimensional computational model was developed using the finite element analysis package ANSYS®. Measurable parameters, such as CLT panel layout and dimensions, lumber dimensions and material properties and effect of glue/nail bond between lumber wide faces, were considered as input data for the simulation. This model is capable of predicting mechanical properties, such as deflection, stress, strain, etc., of CLT systems under different load scenarios in static environments.

In the early stage of the model development, structural brick elements SOLID45 and SOLID95 were both used to create the wood lamella. Based on the comparison between numerical results and experimental measurements, element SOLID45 was chosen because of its accuracy and efficiency during the computer simulation process. Spring element

COMBIN39 and spring-damper element COMBIN14 were employed to model the resistance of nails/screws which were used to assemble the CLT systems (i.e. single panel and box-type structure). 3-D target segment element TARGE170 was paired with 3-D surface to surface contact element CONTA173/CONTA174 to represent contact and sliding between components of CLT systems. The static model was verified with bending tests of different CLT structures and provided good agreement between calculated and experimental data.

In dynamic situations, the above mentioned model was modified and then used to estimate the fundamental frequency of the box-type CLT structures. Friction was eliminated and element COMBIN39 was replaced with element COMBIN14 to simulate lateral resistance of the screws. The predicted fundamental frequency values were in good agreement with those obtained from the tests.

8.3 Experimental investigation

In order to verify that the numerical model was sufficiently accurate at predicting the bending and vibration behavior of the CLT system, a series of tests were designed and conducted at the University of British Columbia.

In the first stage of the study, 38 mm × 89 mm (nominal 2 inch × 4 inch) #2 and better MPB wood was used to manufacture the CLT panels which were used to compare bending performance of glued and nailed CLTs. Phenol-resorcinol formaldehyde resin and 63.5 mm (2 ½ inch) aluminum siding nails were chosen. Compression parallel to grain tests were conducted on thirty specimens to evaluate the modulus of elasticity along fiber direction of the lamella. Two types of nail test were performed to measure lateral resistance of aluminum nails. Glued and nailed CLT panels (each with three replicates) were manufactured and tested under out-of-plane bending until failure. The load and deflection relationship was measured and recorded. Bending behavior, such as stiffness and strength, was calculated and reported.

Next, four different CLT panels (each with ten replicates) were designed and produced. Kiln dried SPF lumber of grade standard and better with 15% utility and phenol-resorcinol formaldehyde resin were used. Modulus of elasticity of each piece of lumber was determined by means of a non-destructive vibration method. Third point bending test was conducted on these specimens. Because of the complexity of the manufacturing process, all specimens were proof loaded to a specific load level without failure and then reserved for further experiment and study. Therefore, only bending stiffness was obtained from the test and included in the dissertation. This part of experiment was a preparation for the investigation of the box-type CLT systems.

Four types, twenty box elements were assembled, with each consisting of two CLT panels reserved from the previous experiment. The cross connected frame between CLT panels was made of 38 mm × 184 mm (nominal 2 inch × 8 inch) MSR lumber which was run through a continuous, bending-type, non-destructive stress grading machine to measure the modulus of elasticity value. 10d common nails were used to connect the ribs. 6.5 mm × 130 mm self tapping screws were installed to attach the frame to the CLT panels. Eight types of single shear connection were made to find the lateral resistance of screws in different box elements.

The dynamic characteristics of the box structures were examined using three types of impact test, i.e. impulse hammer excitation, sandbag drop excitation and heel drop excitation. The acceleration trace of each test was measured using two accelerometers mounted on specific locations of the specimen and recorded using a data acquisition system. The measured time domain signals were transformed to the frequency domain using the Fast Fourier Transform technique and then natural frequencies of each specimen could be identified from peaks in frequency response spectra. To simulate vibration effect under occupant load, a 90.8 kg (200 lb) weight was placed on top of the specimen and all the tests were repeated following the same procedures as without occupant load. Again, natural frequencies could be observed from the transformed frequency domain signals.

Finally, third point bending test was conducted on the twenty box structures. It was initially planned to load the specimens to failure in order to establish both bending stiffness and bending strength values. However, it was almost not possible to completely break them before reaching the test facilities' limit because they were very strong and flexible. Hence, only bending stiffness values were presented.

8.4 Future work

The work in this dissertation was a pilot study towards a comprehensive understanding of the structural performance of box-type CLT structures used in floor applications. It provides a strong foundation for future work in developing and manufacturing various CLT products in the North American construction market. A variety of research directions are suggested that need to be pursued to accelerate the scientific breakthroughs required to establish product standards and building codes in North America.

The current model aims at out-of-plane performance of the CLT structures. One future direction would be to investigate the in-plane behavior of box-type CLT floor/ceiling. This knowledge would be critical for seismic design of buildings using CLT elements.

Laminated wood plates and dimension lumber rib frame in the box type elements are connected with self tapping screws. It would be interesting to investigate box systems, where wood plates and rib frame are connected by both adhesives and mechanical fasteners.

Another possibility would be to probe research on connection solutions between CLT elements. As a pioneer project, this work focuses on properties of a single CLT panel/box. However, to form floor/ceiling of different dimensions using pre-fabricated CLT products, connections between these structural components are important and inevitable. It would be very valuable to design connections which had high load transfer capacity and could be applied at CLT construction sites efficiently and effectively.

In addition, concrete topped CLT products which can be used as floor components have a real potential of competitiveness in terms of service life and an environmentally friendly material. This concept is that the combination of CLT plates which have high stiffness and bending strength and concrete which has the advantages of no decay and higher compression strength than wood will yield high performance floor systems for multi-storey wood buildings. The current model could be modified and extended to gain a deeper insight into this hybrid structure.

BIBLIOGRAPHY

- Aicher, S., and Dill-Langer, G. (2000). "Basic considerations to rolling shear modulus in wooden boards." *Otto - Graf - Journal,* 11, 157-165.

- Al-Foqaha'a, A. A., Cofer, W. F., and Fridley, K. J. (1999). "Vibration design criterion for wood floors exposed to normal human activities." *Journal of Structural Engineering,* 125(12), 1401-1406.

- ANSI/ASHRAE 55 (1992). *Thermal environmental conditions for human occupancy.* American Society of Heating, Refrigerating and Air-Conditioning Engineers.

- ANSYS (2007). *Elements reference (release 11.0).* ANSYS Inc., Canonsburg, PA, USA.

- ASCE (American Society of Civil Engineers) (1996). *Mechanical connections in wood structures.* USA.

- ASHRAE (1997). *ASHRAE handbook : Fundamentals.* American Society of Heating, Refrigerating and Air-Conditioning Engineers, Atlanta, GA, USA.

- ASTM International (2004). "D 2915-98 Standard practice for evaluating allowable properties for grades of structural lumber." *Annual Book of ASTM Standards,* West Conshohocken, PA, USA.

- B.C. Ministry of Forests (2010). "Facts about B.C.'s mountain pine beetle." http://www.for.gov.bc.ca/HFP/mountain_pine_beetle/Updated-Beetle-Facts_Mar2010.pdf (March, 2010).

- Bejtka, I., and Lam, F. (2008). "Cross laminated timber as innovative building material." *Proceedings of the CSCE (Canadian Society for Civil Engineering) 2008 Annual Conference,* Quebec City, Canada.

- Blakeborough, A., and Williams, M. S. (2002). "Measurement of floor vibrations using a heel drop test." *Structures & Buildings,* 156(SB4), 367-371.

- Blaß , H. J., and Görlacher, R. (2003). "Brettsperrholz. Berechnungsgrundlagen." *Holzbau Kalender,* Karlsruhe: Bruder, 580-598.

- Blaß, H. J., and Fellmoser, P. (2004). "Design of solid wood panels with cross layers." *Proceedings of the 8th World Conference on Timber Engineering,* Lahti, Finland.

- Bodig, J., and Jayne, B. A. (1982). *Mechanics of wood and wood composites.* Van Nostrand Reinhold, New York, USA.

- BS EN 13017-1 (2001). *Solid wood panels. Classification by surface appearance.* British Standards Institution.

- Cai, Z., Ross, R. J., Hunt, M. O., and Soltis, L. A. (2002). "Pilot study to examine use of transverse vibration nondestructive evaluation for assessing floor systems." *Forest Products Journal,* 52(1), 89-93.

- CEN, E. C. f. S. (2004b). "EN 13986: Wood-based panels for use in construction - characteristics, evaluation of conformity and marking." Brussels, Belgium.

- CEN, E. C. f. S. (2004a). "EN 789: Timber structures - test methods - determination of mechanical properties of wood based panels." Brussels, Belgium.

- CEN, E. C. f. S. (2003b). "EN 13353: Solid wood panels (SWP) - requirements." Brussels, Belgium.

- Chen, Y. (2006). "Development of MPB thick laminated wood plate products (literature review of the structural analysis issues)." Annual report to the Forestry Innovation Investment Ltd., Vancouver, Canada.

- Contemporary Timber Construction (2010). "Cross Laminated Timber Structural Forms." http://www.arealclub.com/node/7 .

- CSA. (2001). *CSA standard: O86-01 engineering design in wood.* Canadian Standards Association, Toronto, ON, Canada.

- DGR Industrial Products Inc. (2010). "Technical data sheet: Aerodux-500 Phenol-Resorcinol-Formaldehyde structural adhesive."

- DIN1052 (2004-2008). *Entwurf, Berechnung und Bemessung von Holzbauwerken - Allgemeine Bemessungsregeln und Bemessungsregeln fuer den Hochbau.* DIN Deutsches Institut fuer Normung e.V., Germany.

- Dröge, G., and Stoy, K. H. (1981). *Grundzüge des neuzeitlichen Holzbaus.* Wilhelm Ernst und Sohn, München, Germany.

- Dynea. "Polyurethane (PUR) adhesives." http://www.dynea.com/solutions/products/pur_adhesives.html (2010).

- Dytran Instruments Inc. (2008). "Impulse Hammer 5803A data sheet." http://www.dytran.com/go.cfm/en-us/content/product/289/SLEDGEHAMMER-5803A/x?SID= (2010).

- Ebrahimpour, A., and Sack, R. L. (2005). "A review of vibration serviceability criteria for floor structures." *Computers and Structures,* 83, 2488-2494.

- European Organisation for Technical Approvals (2009). "Solid wood slab elements to be used as structural elements in buildings." *European Technical Approval ETA-08/0242,* .

- European Organisation for Technical Approvals (2008). "Solid wood slab elements to be used as structural elements in buildings." *European Technical Approval Draft*.

- Forest Products Laboratory (1999). "Chapter 4: Mechanical properties of wood." *Wood handbook - wood as an engineering material,* U.S. Department of Agriculture, Forest Service, Forest Products Laboratory, Madison, WI, USA.

- Foschi, R. O., Neumann, G. A., Yao, F., and Folz, B. (1995). "Floor vibration due to occupants and reliability-based design guidelines." *Canadian Journal of Civil Engineering,* 22, 471-479.

- Foschi, R. O. (2005). "Performance-based design and application of neural networks." *Proceedings of International Conference on Structural Safety and Reliability,* Rome, Italy.

- Görlacher, R. (2002). "Ein Verfahren zur Ermittlung des Rollschubmoduls von Holz." *Holz Als Roh- Und Werkstoff,* 60, 317-322.

- Gsell, D., Feltrin, G., and Motavalli, M. (2008). "Identification of elastic material properties of solid wood panels." *Proceedings of the Fourth International Conference on FRP Composites in Civil Engineering (CICE2008),* Zurich, Switzerland.

- Gsell, D., Feltrin, G., Schubert, S., Steiger, R., and Motavalli, M. (2007). "Cross-laminated timber plates: evaluation and verification of homogenized elastic properties." *Journal of Structural Engineering ASCE,* 133(1), 132-138.

- Guggenberger, W., and Moosbrugger, T. (2006). "Mechanics of cross-laminated timber plates under uniaxial bending." *Proceedings of the 9th World Conference on Timber Engineering,* Portland, USA.

- Hameury, S., and Lundstrom, T. (2004). "Contribution of indoor exposed massive wood to a good indoor climate: in situ measurement campaign." *Energy Build.,* 36(3), 281-292.

- Hoadley, R. B. (2000). *Understanding wood: a craftsman's guide to wood technology.* The Taunton Press, Inc., USA.

- Holz.Bau Forschungs GmbH. (2010). "BSP - Zugriffe auf CLTdesigner|BSPhandbuch|Ideen die gehen|Beitraege und Veranstaltungen." http://www.holzbauforschung.at/index.php?id=198 (04/16, 2010).

- Hunt, M. O., Ross, R. J., Wang, X., Soltis, L. A., Leavitt, R. R., and Cai, Z. (2007). "Assessment of in-place wood floor systems." *Journal of Architectural Engineering,* 13(1), 30-35.

- Jöbstl, R. A., Bogensperger, T., Moosbrugger, T., and Schickhofer, G. (2006). "A contribution to the design and system effect of crlss laminated timber (CLT)." *Proceedings of the 39th Meeting, International Council for Research and Innovation in Building and Construction, Working Commission W18 – Timber Structures, CIB-W18,* Florence, Italy.

- Jöbstl, R. A., Bogensperger, T., Schickhofer, G., and and Jeitler, G. (2004). "Mechanical behaviour of two orthogonally glued boards." *Proceedings of the 8th World Conference on Timber Engineering,* Lahti, Finland.

- Kalkert, R. E., Dolan, J. D., and Woeste, F. E. (1995). "Wood-floor vibration design criteria." *Journal of Structural Engineering,* 121(9), 1294-1297.

- Kolb, J. (2008). *Systems in timber engineering.* Germany.

- Krämer, V. (2004). "Load carrying capacity of nail-laminated timber loaded perpendicular to its plane." *Proceedings of the 8th World Conference on Timber Engineering,* Lahti, Finland.

- Kreuzinger, H. (1999). "Platten, Scheiben und Schalen - ein Berechnungsmodell fur gangie Statikprogramme." *Bauen Mit Holz,* 1, 34-39.

- Lam, F., Lee, G., Yan, H., Gu, J., and Saravi, A. A. (2004). "Structural performance of wood-based stair stringers." *Forest Products Journal,* 54(4), 39-44.

- Malanit, P. (2009). "The suitability of Dendrocalamus asper Backer for oriented strand lumber." PhD thesis, University of Hamburg, Hamburg, Germany.

- Mestek, P., Kreuzinger, H., and Winter, S. (2008). "Design of crlss laminated timber (CLT)." *Proceedings of the 10th World Conference on Timber Engineering,* Miyazaki, Japan.

- Moosbrugger, T. (2010). "Ein Beitrag zur Bemessung von Mehrschichtigen flächenhaften Holzbauteilen am Beispiel von Brettsperrholzplatten." PhD thesis, Technische Universität Graz, Graz, Austria.

- Ohlsson, S. V. (1988). "A design approach for foot-induced floor vibration." *Proceedings of the International Conference on Timber Engineering,* Seattle, USA, 722-729.

- Pagano, N. J. (1970). "Exact solutions for rectangular bidirectional composites and sandwich plates." *Journal of Composite Materials,* 4, 20-34.

- Pagano, N. J. (1970). "Influence of shear coupling in cylindrical bending of anisotropic laminates." *Journal of Composite Materials,* 4, 330-343.

- Pagano, N. J. (1969). "Exact solutions for composite laminates in cylindrical bending." *Journal of Composite Materials,* 3, 398-411.

- PCB Piezotronics Inc. (2010). "Model 393A03 data sheet." http://www.pcb.com/spec_sheet.asp?model=393A03 (2010).

- Pedersen, L. (2006). "Damping added to floors by seated crowds of people." *SPIE's Proceeding of 13th Annual Conference on Smart Structures and Materials, Damping and Isolation,* San Diego, USA.

- Rodriguez, E., Baalina, A., Molina, M., Santaballa, J., Torres, E., and Infante, C. (2000). "Relationship between humidity, temperature and biological pollution in domestic buildings in a Coruna (Spain)." *Proceedings of healthy buildings conference,* Helsinski, Finland, 353-358.

- Rodriguez, E., Baalina, A., Molina, M., Santaballa, J. A., Vazquez, A., Castellanos, L. R., and Infante, C. (2000). "Indoor/outdoor humidity in mild climate domestic buildings in a Coruna (Spain)." *Proceedings of healthy buildings conference,* Helsinski, Finland, 119-124.

- Rondoni Group srl. (2010). "Presentation MHM system." http://www.rondonigroup.it/eng/metodi-costruttivi.php (2010).

- Ross, R. J., Wang, X., Hunt, M. O., and Soltis, L. A. (2002). "Transverse vibration technique to identify deteriorated wood floor systems." *Techniques,* 26(4), 28-30.

- Schickhofer, G. (1994). "Starrer und nachgiebiger Verbund bei geschichteten flächenhaften Holzstrukturen." PhD thesis, Technischen Universität Graz, Graz, Austria.

- Schickhofer, G., and Guggenberger, W. (1996). "Elastic analysis of flexibly jointed laminated timber plates." *Holzforschung Und Holzverwertung,* 48(1), 15-19.

- Schickhofer, G. (2009). ""Cross Laminated Timber" - an innovative product for the "European timber massive construction"." *Building with Wood seminar,* PowerPoint presentation.

- Schickhofer, G., Bogensperger, T., and Moosbrugger, T. (2009). *BSPhandbuch.* Technischen Universität Graz, Graz, Austria.

- Schickhofer, G., and Hasewend, B. (2000). "Solid timber construction: A construction system for residential houses, office and industrial buildings." Technischen Universität Graz, Lignum Research Graz, Graz, Austria.

- SFS intec. (2007). *WT data sheet No. 01: Principles of design - WT system.* Switzerland.

- Smith, I., and Chui, Y. H. (1988). "Design of lightweight wooden floors to avoid human discomfort." *Canadian Journal of Civil Engineering,* 15, 254-262.

- Soltis, L. A., Wang, X., Ross, R. J., and Hunt, M. O. (2002). "Vibration testing of timber floor systems." *Forest Products Journal,* 52(10), 75-81.

- Steiger, R., Guelzow, A., and Gsell, D. (2008). "Non destructive evaluation of elastic material properties of cross-laminated timber (CLT)." *Proceedings of COST E53 Conference on "End user's needs for wood material and products,* Delft, The Netherlands, 171-182.

- Thiel, A., and Schickhofer, G. (2010). "CLTdesigner - A software tool for designing cross laminated timber elements: 1D-plate-design." *Proceedings of the 11th World Conference on Timber Engineering,* Trentino, Italy.

- Toftum, J., Jorgensen, A. S., and Fanger, P. O. (1998). "Upper limits of air humidity for preventing warm respiratory discomfort." *Energy and Buildings,* 28(1), 15-23.

- TRADA Timber Research and Development Association (2009). "Case studies and timber solutions: Eight storeys of apartments featuring cross-laminated timber panels." http://eoinc.weebly.com/uploads/3/0/5/1/3051016/murray_grove_case_study.pdf .

APPENDIX

Table A-1 Vibration response (Hz) of box specimens consisting of cross laminated plates.

Specimen #1									
	Impact location	A		B		A		B	
	Measurement location	C1	C2	C1	C2	E1	E2	E1	E2
Hammer impact	1	24.41	24.41	24.41	24.41	24.66	24.66	24.66	24.66
	2	24.41	24.41	24.41	24.41	24.78	24.66	24.66	24.66
	3	24.29	24.41	24.41	24.41	24.66	24.66	24.66	24.66
	Average	24.39		24.41		24.68		24.66	
Heel drop impact	1	24.90	25.02	25.02	25.88	20.02	24.78	19.53*	25.27
	2	25.39	25.51	26.12	26.00	20.14	25.76	19.65*	25.64
	3	25.64	25.64	25.15	24.90	20.14	25.39	19.53*	25.27
	Average	25.35		25.51		25.31		25.39	
	Impact location	Center of the specimen							
	Measurement location	C1		C2		E1		E2	
Sandbag drop impact	1	23.80		23.80		23.56		23.19	
	2	23.80		23.44		23.32		23.56	
	3	23.93		23.93		23.07		23.44	
	Average	23.78				23.36			

Specimen #2									
	Impact location	A		B		A		B	
	Measurement location	C1	C2	C1	C2	E1	E2	E1	E2
Hammer impact	1	22.22	22.22	22.10	22.10	22.10	22.10	22.22	22.22
	2	21.97	21.97	22.10	22.10	22.10	22.10	22.10	22.22
	3	22.10	21.97	22.10	22.10	22.22	22.22	22.22	22.22
	Average	22.07		22.10		22.14		22.20	
Heel drop impact	1	19.04*	22.71	19.04*	23.44	20.02*	23.44	19.53*	23.68
	2	18.68*	23.44	18.68*	22.46	20.14*	23.07	19.41*	25.88
	3	18.80*	23.44	19.29*	24.66	20.14*	23.56	19.41*	26.49
	Average	23.19		23.52		23.36		25.35	
	Impact location	Center of the specimen							
	Measurement location	C1		C2		E1		E2	
Sandbag drop impact	1	22.83		22.83		22.95		22.71	
	2	22.71		22.58		22.95		22.71	
	3	22.71		22.58		22.83		22.71	
	Average	22.71				22.81			

Specimen #3									
	Impact location	A		B		A		B	
	Measurement location	C1	C2	C1	C2	E1	E2	E1	E2
Hammer impact	1	23.19	23.32	23.19	23.07	23.19	23.19	23.32	23.32
	2	23.07	23.19	23.07	23.19	23.07	23.07	23.32	23.32
	3	23.07	23.07	23.07	23.19	23.07	22.58	23.32	23.32
	Average	23.15		23.13		23.03		23.32	
Heel drop impact	1	22.95	16.97*	21.36	21.36	22.34	16.85*	21.85	21.61
	2	22.34	16.60*	21.36	21.24	23.19	16.97*	21.61	21.73
	3	22.95	16.60*	21.24	21.12	23.19	16.85*	21.24	21.61
	Average	22.75		21.28		22.91		21.61	
	Impact location	Center of the specimen							
	Measurement location	C1		C2		E1		E2	
Sandbag drop impact	1	20.75		20.63		21.24		21.48	
	2	21.12		20.14		21.12		21.00	
	3	21.12		21.00		21.00		20.87	
	Average	20.79				21.12			

Specimen #4									
	Impact location	A		B		A		B	
	Measurement location	C1	C2	C1	C2	E1	E2	E1	E2
Hammer impact	1	21.85	21.97	22.10	22.10	21.61	21.48	21.97	21.73
	2	20.02	21.85	22.10	22.10	21.61	21.61	21.85	21.85
	3	20.02	21.85	22.10	21.97	21.73	21.61	21.97	21.85
	Average	21.26		22.07		21.61		21.87	
Heel drop impact	1	21.12	21.73	18.92*	22.83	20.75	21.73	20.02	22.22
	2	21.73	21.85	19.04*	22.22	22.10	22.22	20.14	21.73
	3	22.10	22.10	19.17*	21.85	21.73	22.10	20.26	22.46
	Average	21.77		22.30		21.77		21.14	
	Impact location	Center of the specimen							
	Measurement location	C1		C2		E1		E2	
Sandbag drop impact	1	20.14		21.61		20.14		20.14	
	2	20.26		20.14		20.14		20.14	
	3	20.14		20.02		20.14		20.14	
	Average	20.39				20.14			

Specimen #5									
	Impact location	A		B		A		B	
	Measurement location	C1	C2	C1	C2	E1	E2	E1	E2
Hammer impact	1	23.07	23.07	23.19	23.19	22.95	22.95	22.95	22.95
	2	23.07	22.95	23.07	23.19	22.95	22.95	22.95	22.95
	3	23.07	23.07	23.07	23.19	22.95	22.95	22.95	22.95
	Average	23.05		23.15		22.95		22.95	
Heel drop impact	1	23.93	23.68	24.66	23.68*	24.17	24.17	23.56	27.95*
	2	23.80	23.93	24.66	27.95*	23.44	23.93	22.71	27.71*
	3	23.93	24.05	22.22	19.04*	23.44	23.93	23.68	28.56*
	Average	23.89		23.84		23.84		23.32	
	Impact location	Center of the specimen							
	Measurement location	C1		C2		E1		E2	
Sandbag drop impact	1	21.73		21.48		21.97		22.22	
	2	21.48		21.48		21.85		22.22	
	3	22.34		21.97		21.97		22.10	
	Average	21.75				22.05			

Table A-2 Vibration response (Hz) of box specimens consisting of parallel laminated plates.

Specimen #6									
	Impact location	A		B		A		B	
	Measurement location	C1	C2	C1	C2	E1	E2	E1	E2
Hammer impact	1	22.83	22.83	22.83	22.83	23.07	23.07	23.07	23.07
	2	22.83	22.95	22.83	22.83	23.07	23.07	23.19	23.07
	3	22.83	22.83	22.83	22.83	23.07	23.07	23.07	23.07
	Average	22.85		22.83		23.07		23.09	
Heel drop impact	1	24.54	24.54	25.64	25.27	24.66	24.78	25.64	25.15
	2	24.54	24.54	25.64	25.64	25.02	24.90	25.51	24.78
	3	24.54	24.54	25.88	25.27	24.78	25.02	25.76	25.15
	Average	24.54		25.55		24.86		25.33	
	Impact location	Center of the specimen							
	Measurement location	C1		C2		E1		E2	
Sandbag drop impact	1	22.22		22.46		21.85		22.10	
	2	22.10		22.34		21.97		22.10	
	3	22.10		22.22		21.73		22.10	
	Average	22.24				21.97			

Specimen #7									
	Impact location	A		B		A		B	
	Measurement location	C1	C2	C1	C2	E1	E2	E1	E2
Hammer impact	1	19.65	19.53	19.65	19.65	19.65	19.65	19.65	19.65
	2	19.53	19.53	19.65	19.65	19.78	19.78	19.65	19.65
	3	19.53	19.53	19.65	19.65	19.53	19.65	19.65	19.65
	Average	19.55		19.65		19.67		19.65	
Heel drop impact	1	20.87	20.87	21.97	21.36	20.14	19.78	22.58	21.97
	2	21.00	21.00	21.48	21.24	20.63	20.51	21.97	21.97
	3	20.63	20.87	21.36	21.48	20.02	19.78	21.85	21.73
	Average	20.87		21.48		20.14		22.01	
	Impact location	Center of the specimen							
	Measurement location	C1		C2		E1		E2	
Sandbag drop impact	1	18.92		19.04		18.92		18.92	
	2	19.04		19.04		18.68		18.92	
	3	18.80		18.92		18.80		18.92	
	Average	18.96				18.86			

Specimen #8									
	Impact location	A		B		A		B	
	Measurement location	C1	C2	C1	C2	E1	E2	E1	E2
Hammer impact	1	26.37	26.25	26.49	26.61	26.61	26.73	26.86	26.86
	2	26.49	26.61	26.49	26.61	26.86	26.61	26.73	26.73
	3	26.25	26.37	26.61	26.49	26.61	26.73	26.86	26.86
	Average	26.39		26.55		26.69		26.81	
Heel drop impact	1	23.07	22.71	22.10	21.97	22.58	22.83	22.22	22.10
	2	22.22	22.83	22.22	21.97	22.83	22.71	22.22	21.97
	3	22.71	22.71	22.22	22.10	23.80	24.05	21.97	21.85
	Average	22.71		22.10		23.13		22.05	
	Impact location	Center of the specimen							
	Measurement location	C1		C2		E1		E2	
Sandbag drop impact	1	21.61		22.71		21.12		20.87	
	2	21.36		22.71		21.00		21.12	
	3	21.48		21.36		21.24		21.36	
	Average	21.87				21.12			

Specimen #9									
	Impact location	A		B		A		B	
	Measurement location	C1	C2	C1	C2	E1	E2	E1	E2
Hammer impact	1	22.58	22.58	22.71	22.71	22.71	22.71	22.83	22.83
	2	22.58	22.58	22.71	22.71	22.58	22.58	22.71	22.71
	3	22.58	22.58	22.71	22.71	22.46	22.58	22.71	22.71
	Average	22.58		22.71		22.60		22.75	
Heel drop impact	1	24.54	24.54	22.83	22.22	24.29	24.54	22.95	21.97
	2	24.66	24.54	22.95	22.58	24.78	24.54	22.95	22.34
	3	24.78	24.29	23.07	22.22	24.54	24.29	23.07	22.34
	Average	24.56		22.64		24.50		22.60	
	Impact location	Center of the specimen							
	Measurement location	C1		C2		E1		E2	
Sandbag drop impact	1	22.10		22.10		21.85		21.85	
	2	22.10		22.10		21.85		21.85	
	3	21.97		22.10		21.85		21.85	
	Average	22.07				21.85			

Specimen #10									
	Impact location	A		B		A		B	
	Measurement location	C1	C2	C1	C2	E1	E2	E1	E2
Hammer impact	1	23.68	23.68	23.68	23.68	23.80	23.80	23.68	23.68
	2	23.56	23.56	23.68	23.68	23.68	23.56	23.68	23.56
	3	23.56	23.56	23.56	23.56	23.68	23.56	23.68	23.68
	Average	23.60		23.64		23.68		23.66	
Heel drop impact	1	23.56	23.56	23.68	22.46	24.17	24.41	24.41	23.80
	2	23.56	23.68	23.93	21.48	24.17	24.17	24.29	24.17
	3	23.93	23.68	23.68	21.61	24.41	24.41	24.54	24.29
	Average	23.66		22.81		24.29		24.25	
	Impact location	Center of the specimen							
	Measurement location	C1		C2		E1		E2	
Sandbag drop impact	1	22.83		22.83		22.46		22.46	
	2	22.71		22.71		22.58		22.58	
	3	22.58		22.58		22.46		22.46	
	Average	22.71				22.50			

Table A-3 Vibration response (Hz) of box specimens consisting of cross laminated plates with OSB facing.

Specimen #11									
	Impact location	A		B		A		B	
	Measurement location	C1	C2	C1	C2	E1	E2	E1	E2
Hammer impact	1	21.36	21.36	21.36	21.36	21.85	21.48	21.48	21.48
	2	21.36	21.36	21.24	21.24	21.73	21.48	21.61	21.48
	3	21.24	21.24	21.36	21.36	21.73	21.48	21.48	21.61
	Average	21.32		21.32		21.63		21.52	
Heel drop impact	1	21.97	21.97	22.34	20.26	22.34	/	21.48	19.41
	2	21.73	21.73	21.97	21.97	22.22	22.10	21.85	21.97
	3	22.58	22.34	22.22	21.97	21.36	21.73	22.58	22.58
	Average	22.05		21.79		21.95		21.65	
	Impact location	Center of the specimen							
	Measurement location	C1		C2		E1		E2	
Sandbag drop impact	1	19.41		19.41		19.78		19.17	
	2	19.41		19.29		19.90		19.17	
	3	19.29		19.29		19.41		19.41	
	Average	19.35				19.47			

Specimen #12										
	Impact location	A		B		A		B		
	Measurement location	C1	C2	C1	C2	E1	E2	E1	E2	
Hammer impact	1	20.02	20.02	20.02	19.90	20.26	20.26	20.14	20.14	
	2	20.02	20.02	19.90	19.90	20.26	20.14	20.26	20.26	
	3	20.02	20.02	20.02	20.02	20.26	20.14	20.26	20.14	
	Average	20.02		19.96		20.22		20.20		
Heel drop impact	1	20.75	20.75	19.41	19.17	22.71	22.58	19.41	19.29	
	2	22.71	22.58	19.78	19.78	22.46	22.83	19.29	19.17	
	3	22.34	22.10	21.24	21.36	22.10	21.85	19.17	19.29	
	Average	21.87		20.12		22.42		19.27		
	Impact location	Center of the specimen								
	Measurement location	C1		C2		E1		E2		
Sandbag drop impact	1	19.29		19.17		19.90		19.78		
	2	19.78		19.17		19.65		19.41		
	3	19.53		19.41		20.02		19.65		
	Average	19.39				19.73				

Specimen #13									
	Impact location	A		B		A		B	
	Measurement location	C1	C2	C1	C2	E1	E2	E1	E2
Hammer impact	1	21.61	21.48	21.97	21.85	21.97	21.97	21.97	22.10
	2	21.73	21.73	21.85	21.97	22.10	21.97	22.10	21.97
	3	21.85	21.48	21.97	21.85	22.10	21.97	22.10	21.97
	Average	21.65		21.91		22.01		22.03	
Heel drop impact	1	21.00	20.87	21.85	19.90	21.61	21.36	19.29	20.87
	2	21.48	21.48	22.22	19.65	21.36	21.36	21.12	19.17
	3	21.36	21.36	21.00	20.87	21.85	22.10	21.36	19.41
	Average	21.26		20.91		21.61		20.20	
	Impact location	Center of the specimen							
	Measurement location	C1		C2		E1		E2	
Sandbag drop impact	1	19.53		19.41		20.14		20.14	
	2	20.02		19.41		21.00		20.14	
	3	20.26		19.41		21.12		20.02	
	Average	19.67				20.43			

Specimen #14									
	Impact location	A		B		A		B	
	Measurement location	C1	C2	C1	C2	E1	E2	E1	E2
Hammer impact	1	22.22	22.10	22.22	22.22	22.71	22.34	22.46	22.22
	2	22.22	22.10	22.22	22.22	22.71	22.46	22.46	22.34
	3	22.22	22.22	22.22	22.22	22.58	22.46	22.46	22.34
	Average	22.18		22.22		22.54		22.38	
Heel drop impact	1	21.00	20.63	21.85	19.29	22.83	22.46	20.02	19.41
	2	22.58	22.46	22.46	22.58	21.85	21.97	22.71	20.63
	3	23.44	21.24	20.14	19.41	22.71	22.95	23.07	21.12
	Average	21.89		20.96		22.46		21.16	
	Impact location	Center of the specimen							
	Measurement location	C1		C2		E1		E2	
Sandbag drop impact	1	21.36		20.87		22.10		20.75	
	2	21.36		20.87		21.97		20.39	
	3	21.36		20.75		21.85		21.00	
	Average	21.10				21.34			

Specimen #15									
	Impact location	A		B		A		B	
	Measurement location	C1	C2	C1	C2	E1	E2	E1	E2
Hammer impact	1	20.75	20.75	20.75	20.75	20.87	20.75	20.87	20.87
	2	20.75	20.75	20.75	20.75	20.87	20.87	20.87	20.87
	3	20.75	20.51	20.75	20.75	20.87	20.87	20.75	20.87
	Average	20.71		20.75		20.85		20.85	
Heel drop impact	1	19.29	21.12	21.24	19.17	20.02	20.02	19.17	19.17
	2	21.12	21.12	20.14	20.14	19.41	21.61	19.29	23.07*
	3	19.29	19.41	21.24	19.17	19.17	19.17	19.17	22.71*
	Average	20.22		20.18		19.90		19.20	
	Impact location	Center of the specimen							
	Measurement location	C1		C2		E1		E2	
Sandbag drop impact	1	19.90		19.78		20.14		20.14	
	2	20.02		19.78		20.14		19.90	
	3	20.02		19.41		20.26		20.14	
	Average	19.82				20.12			

Table A-4 Vibration response (Hz) of box specimens consisting of 45^{o} laminated plates.

Specimen #16									
	Impact location	A		B		A		B	
	Measurement location	C1	C2	C1	C2	E1	E2	E1	E2
Hammer impact	1	24.66	24.66	24.05	24.05	24.54	24.41	24.54	23.80
	2	24.54	24.41	24.29	24.66	24.29	23.80	24.78	18.43*
	3	24.17	24.05	24.05	23.80	24.29	24.05	24.05	18.43*
	Average	24.41		24.15		24.23		24.29	
Heel drop impact	1	21.97	21.24	22.34	22.22	21.24	20.63	22.34	21.97
	2	22.95	21.24	22.46	22.46	20.26	19.78*	22.83	22.34
	3	22.95	20.02	22.58	22.34	21.61	21.73	22.22	21.97
	Average	21.73		22.40		21.09		22.28	
	Impact location	Center of the specimen							
	Measurement location	C1		C2		E1		E2	
Sandbag drop impact	1	22.46		22.34		22.22		22.22	
	2	22.71		22.58		22.83		22.58	
	3	22.71		22.46		22.10		22.10	
	Average	22.54				22.34			

Specimen #17									
	Impact location	A		B		A		B	
	Measurement location	C1	C2	C1	C2	E1	E2	E1	E2
Hammer impact	1	22.71	22.71	22.71	22.71	24.66	24.66	24.78	24.66
	2	22.71	22.71	22.71	22.71	24.78	24.78	24.66	24.78
	3	22.71	22.71	22.58	22.71	24.66	24.78	24.78	24.78
	Average	22.71		22.68		24.72		24.74	
Heel drop impact	1	24.17	24.05	24.29	24.29	24.17	19.17*	24.17	24.17
	2	24.17	24.54	24.05	24.29	23.68	19.17*	24.29	24.29
	3	24.29	24.54	24.78	24.78	23.93	19.17*	24.90	24.78
	Average	24.29		24.41		23.93		24.43	
	Impact location	Center of the specimen							
	Measurement location	C1		C2		E1		E2	
Sandbag drop impact	1	22.34		22.46		22.83		22.83	
	2	22.46		22.22		22.95		22.71	
	3	22.46		22.46		22.83		22.71	
	Average	22.40				22.81			

Specimen #18									
	Impact location	A		B		A		B	
	Measurement location	C1	C2	C1	C2	E1	E2	E1	E2
Hammer impact	1	24.17	24.17	24.17	24.17	23.68	23.80	23.80	23.80
	2	24.17	24.17	24.17	24.17	23.68	23.80	23.80	23.80
	3	24.17	24.17	24.17	24.17	23.80	23.80	23.80	23.80
	Average	24.17		24.17		23.76		23.80	
Heel drop impact	1	24.17	24.54	24.41	24.29	24.54	24.66	24.29	23.44
	2	24.66	24.66	24.54	24.41	24.41	24.41	24.29	24.41
	3	24.66	24.66	24.41	24.29	24.54	24.78	24.54	24.41
	Average	24.56		24.39		24.56		24.23	
	Impact location	Center of the specimen							
	Measurement location	C1		C2		E1		E2	
Sandbag drop impact	1	23.19		23.19		22.95		22.95	
	2	23.07		23.07		22.83		22.71	
	3	22.83		22.95		22.46		22.71	
	Average	23.05				22.77			

Specimen #19									
	Impact location	A		B		A		B	
	Measurement location	C1	C2	C1	C2	E1	E2	E1	E2
Hammer impact	1	21.85	21.61	21.48	21.48	21.61	21.48	21.61	21.61
	2	21.61	21.61	21.48	21.48	21.61	21.61	21.61	21.61
	3	21.48	21.61	21.61	21.48	21.61	21.48	21.61	21.48
	Average	21.63		21.50		21.57		21.59	
Heel drop impact	1	21.00	21.12	22.10	21.97	21.48	21.73	21.24	20.02
	2	21.36	21.36	21.97	21.97	21.36	21.61	21.61	20.26
	3	20.39	20.63	19.29	21.61	21.61	21.73	19.41	20.14
	Average	20.98		21.48		21.59		20.45	
	Impact location	Center of the specimen							
	Measurement location	C1		C2		E1		E2	
Sandbag drop impact	1	20.87		20.87		20.87		20.87	
	2	20.63		20.63		21.00		20.87	
	3	19.90		20.26		20.63		20.75	
	Average	20.53				20.83			

Specimen #20									
	Impact location	A		B		A		B	
	Measurement location	C1	C2	C1	C2	E1	E2	E1	E2
Hammer impact	1	21.36	21.00	21.36	21.12	20.63	20.87	20.75	20.87
	2	21.61	21.24	21.48	21.24	20.75	20.87	20.75	20.75
	3	21.61	21.48	21.12	21.12	21.24	21.24	21.12	21.12
	Average	21.38		21.24		20.94		20.89	
Heel drop impact	1	22.71	22.83	22.71	22.83	22.10	22.58	22.46	22.58
	2	22.58	22.71	22.83	22.10	22.10	22.58	22.46	22.34
	3	22.71	22.58	22.71	22.46	22.22	22.22	21.97	21.73
	Average	22.68		22.60		22.30		22.26	
	Impact location	Center of the specimen							
	Measurement location	C1		C2		E1		E2	
Sandbag drop impact	1	20.02		20.02		19.78		19.90	
	2	19.78		19.78		19.90		19.78	
	3	19.65		19.90		19.78		19.90	
	Average	19.86				19.84			

Table A-5 Vibration response (Hz) of box specimens consisting of cross laminated plates under simulated occupant load.

Specimen #1									
	Impact location	A		B		A		B	
	Measurement location	C1	C2	C1	C2	E1	E2	E1	E2
Hammer impact	1	19.17	19.04	19.04	19.17	19.17	19.04	19.29	19.29
	2	19.04	19.17	19.17	19.17	19.17	19.04	19.29	19.29
	3	19.04	19.04	19.17	19.17	19.04	19.04	19.17	19.17
	Average	19.08		19.14		19.08		19.25	
Heel drop impact	1	19.29	19.17	19.04	18.92	19.65	19.04	19.53	18.43
	2	19.41	19.29	19.17	18.80	19.41	19.04	19.17	18.68
	3	19.41	19.17	19.17	18.80	19.78	19.65	19.29	18.43
	Average	19.29		18.98		19.43		18.92	
	Impact location	Center of the specimen							
	Measurement location	C1		C2		E1		E2	
Sandbag drop impact	1	18.80		18.80		18.80		18.92	
	2	18.80		18.80		18.92		20.51	
	3	18.80		18.80		18.80		18.80	
	Average	18.80				19.12			

Specimen #2									
	Impact location	A		B		A		B	
	Measurement location	C1	C2	C1	C2	E1	E2	E1	E2
Hammer impact	1	18.56	18.56	18.56	18.43	18.43	18.56	18.68	18.68
	2	18.56	18.56	18.56	18.56	18.56	18.68	18.68	18.68
	3	18.56	18.56	18.56	18.68	18.56	18.68	18.68	18.56
	Average	18.56		18.56		18.58		18.66	
Heel drop impact	1	18.68	18.43	18.43	17.94	18.68	18.56	18.92	18.43
	2	18.07	18.07	18.31	17.58	18.56	18.56	18.92	18.80
	3	18.56	18.43	18.31	17.82	18.43	18.43	18.92	18.43
	Average	18.37		18.07		18.53		18.74	
	Impact location	Center of the specimen							
	Measurement location	C1		C2		E1		E2	
Sandbag drop impact	1	18.19		18.07		18.56		18.43	
	2	18.31		17.70		18.56		17.82	
	3	18.19		17.58		18.56		17.70	
	Average	18.01				18.27			

Specimen #3									
	Impact location	A		B		A		B	
	Measurement location	C1	C2	C1	C2	E1	E2	E1	E2
Hammer impact	1	20.51	18.80	19.29	19.53	20.02	20.51	19.78	19.53
	2	20.51	18.56	19.41	19.65	19.53	18.68	19.90	20.63
	3	20.51	18.31	19.65	19.41	19.53	20.02	20.02	19.78
	Average	19.53		19.49		19.71		19.94	
Heel drop impact	1	19.90	17.70	18.43	19.41	20.63	17.94	18.31	19.53
	2	20.02	17.70	19.53	19.17	20.39	17.58	20.26	20.02
	3	/	/	18.56	18.68	20.02	17.70	18.56	19.53
	Average	18.83		18.96		19.04		19.37	
	Impact location	Center of the specimen							
	Measurement location	C1		C2		E1		E2	
Sandbag drop impact	1	20.14		16.48*		20.02		16.24*	
	2	20.39		16.24*		20.02		16.24*	
	3	20.02		16.11*		20.14		16.11*	
	Average	20.18				20.06			

Specimen #4									
	Impact location	A		B		A		B	
	Measurement location	C1	C2	C1	C2	E1	E2	E1	E2
Hammer impact	1	19.65	19.53	19.65	19.65	19.65	19.53	19.65	19.65
	2	19.53	19.65	19.53	19.41	19.65	19.65	19.65	19.53
	3	19.53	19.53	19.65	19.65	19.65	19.53	19.53	19.41
	Average	19.57		19.59		19.61		19.57	
Heel drop impact	1	19.41	19.41	19.29	19.17	19.41	19.41	20.02	19.41
	2	19.04	19.04	20.02	19.78	19.78	19.78	19.78	19.53
	3	19.53	19.53	20.02	20.02	18.56	18.92	19.17	18.80
	Average	19.33		19.71		19.31		19.45	
	Impact location	Center of the specimen							
	Measurement location	C1		C2		E1		E2	
Sandbag drop impact	1	17.82		17.46		18.19		18.19	
	2	18.07		17.82		18.07		18.19	
	3	18.19		17.21		18.43		17.21	
	Average	17.76				18.05			

Specimen #5									
	Impact location	A		B		A		B	
	Measurement location	C1	C2	C1	C2	E1	E2	E1	E2
Hammer impact	1	20.87	20.26	20.87	20.87	20.87	20.75	20.87	20.87
	2	20.63	20.51	20.87	20.39	20.63	21.00	20.87	20.87
	3	20.75	20.75	20.87	20.75	21.00	20.75	20.87	21.00
	Average	20.63		20.77		20.83		20.89	
Heel drop impact	1	20.51	20.39	20.75	20.63	20.39	20.51	20.39	20.26
	2	19.17	19.04	21.00	20.75	21.00	20.87	21.00	20.02
	3	18.68	19.17	21.00	19.17	20.51	20.51	/	/
	Average	19.49		20.55		20.63		20.42	
	Impact location	Center of the specimen							
	Measurement location	C1		C2		E1		E2	
Sandbag drop impact	1	19.04		18.19		19.29		18.43	
	2	19.04		18.19		18.68		18.80	
	3	19.04		18.07		18.68		18.43	
	Average	18.60				18.72			

Table A-6 Vibration response (Hz) of box specimens consisting of parallel laminated plates under simulated occupant load.

Specimen #6									
	Impact location	A		B		A		B	
	Measurement location	C1	C2	C1	C2	E1	E2	E1	E2
Hammer impact	1	22.10	21.97	22.10	22.10	22.10	22.10	22.22	22.22
	2	22.10	22.10	22.10	22.10	22.10	22.10	22.22	22.22
	3	21.85	21.97	22.10	22.10	22.10	22.10	22.22	22.22
	Average	22.01		22.10		22.10		22.22	
Heel drop impact	1	21.97	21.61	22.34	22.22	21.12	21.00	22.71	22.10
	2	22.22	21.24	22.58	22.46	22.34	22.10	22.58	22.34
	3	22.22	22.34	22.71	21.97	22.22	22.71	22.58	22.34
	Average	21.93		22.38		21.91		22.44	
	Impact location	Center of the specimen							
	Measurement location	C1		C2		E1		E2	
Sandbag drop impact	1	20.87		21.00		21.12		21.12	
	2	20.75		21.00		21.00		20.87	
	3	20.87		21.00		20.75		20.75	
	Average	20.91				20.94			

Specimen #7									
	Impact location	A		B		A		B	
	Measurement location	C1	C2	C1	C2	E1	E2	E1	E2
Hammer impact	1	19.29	19.17	19.41	19.41	19.29	19.29	19.41	19.41
	2	19.29	19.29	19.41	19.41	19.29	19.17	19.29	19.41
	3	19.29	19.29	19.41	19.41	19.29	19.17	19.41	19.29
	Average	19.27		19.41		19.25		19.37	
Heel drop impact	1	19.65	19.65	20.39	20.02	18.92	19.04	21.00	19.78
	2	19.41	19.41	20.39	20.26	19.41	18.92	20.63	20.26
	3	19.17	19.17	19.90	19.53	19.29	18.92	20.75	20.39
	Average	19.41		20.08		19.08		20.47	
	Impact location	Center of the specimen							
	Measurement location	C1		C2		E1		E2	
Sandbag drop impact	1	19.04		19.04		18.56		18.31	
	2	18.68		18.68		18.92		19.04	
	3	18.56		18.68		18.68		18.43	
	Average	18.78				18.66			

Specimen #8									
	Impact location	A		B		A		B	
	Measurement location	C1	C2	C1	C2	E1	E2	E1	E2
Hammer impact	1	21.48	21.48	21.73	21.61	21.12	21.85	21.73	21.73
	2	21.36	21.36	21.61	21.61	21.36	21.85	21.73	21.73
	3	21.48	21.48	21.73	21.73	21.36	21.73	21.85	21.85
	Average	21.44		21.67		21.55		21.77	
Heel drop impact	1	20.75	20.87	21.97	21.48	21.61	20.87	21.24	20.63
	2	21.24	21.48	21.73	21.00	21.12	20.39	21.12	20.51
	3	21.48	21.36	21.97	21.61	21.48	21.00	21.24	20.51
	Average	21.20		21.63		21.08		20.87	
	Impact location	Center of the specimen							
	Measurement location	C1		C2		E1		E2	
Sandbag drop impact	1	20.02		20.14		20.26		19.90	
	2	20.26		20.02		20.39		20.14	
	3	20.14		20.26		20.26		20.39	
	Average	20.14				20.22			

Specimen #9									
	Impact location	A		B		A		B	
	Measurement location	C1	C2	C1	C2	E1	E2	E1	E2
Hammer impact	1	21.97	21.97	21.97	21.85	22.22	22.22	22.34	22.34
	2	21.97	21.97	21.97	21.85	22.22	22.22	22.34	22.34
	3	21.97	21.85	21.97	21.97	22.10	22.10	22.34	22.34
	Average	21.95		21.93		22.18		22.34	
Heel drop impact	1	22.83	22.83	22.58	22.22	22.22	22.71	22.71	21.61
	2	22.83	22.95	22.71	22.10	21.36	22.58	22.58	20.75
	3	22.71	22.83	22.71	21.85	22.58	21.24	22.46	21.97
	Average	22.83		22.36		22.12		22.01	
	Impact location	Center of the specimen							
	Measurement location	C1		C2		E1		E2	
Sandbag drop impact	1	21.48		21.36		21.36		21.36	
	2	21.36		21.36		21.48		21.36	
	3	21.48		21.24		21.36		21.61	
	Average	21.38				21.42			

Specimen #10									
	Impact location	A		B		A		B	
	Measurement location	C1	C2	C1	C2	E1	E2	E1	E2
Hammer impact	1	21.48	21.48	21.48	21.48	21.61	21.61	21.61	21.73
	2	21.48	21.48	21.48	21.48	21.61	21.61	21.73	21.24
	3	21.36	21.36	21.48	21.48	21.61	21.61	21.73	21.73
	Average	21.44		21.4821.61		21.61		21.63	
Heel drop impact	1	21.48	21.48	22.10	21.61	21.61	21.48	21.85	21.61
	2	21.85	21.61	21.97	21.85	21.24	21.36	22.10	21.00
	3	21.73	21.73	22.10	21.73	21.61	21.85	22.10	21.36
	Average	21.65		21.89		21.52		21.67	
	Impact location	Center of the specimen							
	Measurement location	C1		C2		E1		E2	
Sandbag drop impact	1	20.75		20.87		21.00		20.87	
	2	20.75		20.75		20.75		21.00	
	3	20.75		20.75		21.00		20.87	
	Average	20.77				20.91			

Table A-7 Vibration response (Hz) of box specimens consisting of cross laminated plates with OSB facing under simulated occupant load.

Specimen #11									
	Impact location	A		B		A		B	
	Measurement location	C1	C2	C1	C2	E1	E2	E1	E2
Hammer impact	1	19.90	19.90	19.90	19.90	20.02	19.90	19.90	19.78
	2	19.90	19.90	19.90	19.90	20.02	20.02	19.90	19.90
	3	19.90	19.90	19.90	19.90	20.02	20.02	19.90	19.90
	Average	19.90		19.90		20.00		19.88	
Heel drop impact	1	19.41	19.41	20.14	20.02	19.78	20.02	19.90	19.65
	2	20.14	20.26	20.02	19.78	20.26	20.26	19.65	19.65
	3	19.65	20.63	20.51	19.53	20.39	20.39	20.51	19.41
	Average	19.92		20.00		20.18		19.80	
	Impact location	Center of the specimen							
	Measurement location	C1		C2		E1		E2	
Sandbag drop impact	1	18.19		17.46		18.92		17.21	
	2	18.19		17.33		19.04		17.58	
	3	18.43		17.21		19.17		17.46	
	Average	17.80				18.23			

Specimen #12										
	Impact location	A		B		A		B		
	Measurement location	C1	C2	C1	C2	E1	E2	E1	E2	
Hammer impact	1	19.41	19.41	19.53	19.41	19.65	19.53	19.65	19.53	
	2	19.41	19.41	19.41	19.53	19.65	19.65	19.65	19.65	
	3	19.41	19.29	19.53	19.41	19.78	19.65	19.65	19.53	
	Average	19.39		19.47		19.65		19.61		
Heel drop impact	1	20.02	20.14	17.82	17.94	19.65	20.14	18.43	18.31	
	2	21.48	21.61	18.92	16.97	19.04	18.92	17.70	17.70	
	3	20.63	20.75	18.19	18.56	19.65	21.61	18.56	18.31	
	Average	20.77		18.07		19.84		18.17		
	Impact location	Center of the specimen								
	Measurement location	C1		C2		E1		E2		
Sandbag drop impact	1	18.68		18.19		19.65		18.56		
	2	18.92		18.43		19.78		18.07		
	3	19.17		16.85		20.02		20.14		
	Average	18.37				19.37				

Specimen #13									
	Impact location	A		B		A		B	
	Measurement location	C1	C2	C1	C2	E1	E2	E1	E2
Hammer impact	1	20.14	20.14	20.26	20.14	20.39	20.26	20.39	20.39
	2	20.14	20.14	20.26	20.26	20.26	20.14	20.26	19.65
	3	20.14	20.02	20.26	20.14	20.39	20.26	20.39	20.14
	Average	20.12		20.22		20.28		20.20	
Heel drop impact	1	19.53	19.78	20.63	19.53	19.53	20.87	21.00	19.17
	2	19.65	19.65	19.78	19.78	20.14	20.26	20.87	19.04
	3	20.26	19.41	19.29	19.41	20.51	20.51	20.02	20.14
	Average	19.71		19.73		20.30		20.04	
	Impact location	Center of the specimen							
	Measurement location	C1		C2		E1		E2	
Sandbag drop impact	1	19.53		19.17		19.78		19.41	
	2	19.65		19.41		19.17		18.31	
	3	19.41		17.70		19.78		19.29	
	Average	19.14				19.29			

Specimen #14									
	Impact location	A		B		A		B	
	Measurement location	C1	C2	C1	C2	E1	E2	E1	E2
Hammer impact	1	20.51	20.51	20.51	20.51	20.63	20.51	20.63	20.51
	2	20.51	20.51	20.51	20.51	20.63	20.63	20.63	20.51
	3	20.51	20.39	20.51	20.51	20.63	20.63	20.63	20.51
	Average	20.49		20.51		20.61		20.57	
Heel drop impact	1	19.90	19.90	19.53	19.29	19.29	20.02	19.29	19.29
	2	20.02	19.78	20.39	18.92	20.26	20.26	20.14	19.78
	3	19.04	19.04	19.78	19.65	18.56	18.19	20.14	18.31
	Average	19.61		19.59		19.43		19.49	
	Impact location	Center of the specimen							
	Measurement location	C1		C2		E1		E2	
Sandbag drop impact	1	19.65		16.85*		19.53		18.19	
	2	19.90		17.58		19.90		17.70	
	3	19.90		19.17		19.29		18.31	
	Average	19.24				18.82			

Specimen #15									
	Impact location	A		B		A		B	
	Measurement location	C1	C2	C1	C2	E1	E2	E1	E2
Hammer impact	1	18.80	18.80	18.68	18.80	18.56	18.80	18.92	18.80
	2	18.80	18.80	18.92	18.92	18.92	18.92	18.92	18.92
	3	18.80	18.80	18.80	18.80	18.92	18.92	18.31	18.80
	Average	18.80		18.82		18.84		18.78	
Heel drop impact	1	19.29	19.17	18.56	17.70	17.58	19.29	18.43	17.70
	2	18.31	18.43	18.56	18.68	18.43	18.31	19.17	17.33
	3	18.56	18.80	18.92	18.80	18.31	18.80	17.46	19.90
	Average	18.76		18.53		18.45		18.33	
	Impact location	Center of the specimen							
	Measurement location	C1		C2		E1		E2	
Sandbag drop impact	1	18.19		16.97		17.94		16.97	
	2	17.82		16.97		18.43		17.94	
	3	18.07		17.33		18.56		17.58	
	Average	17.56				17.90			

Table A-8 Vibration response (Hz) of box specimens consisting of 45^{o} laminated plates under simulated occupant load.

Specimen #16									
	Impact location	A		B		A		B	
	Measurement location	C1	C2	C1	C2	E1	E2	E1	E2
Hammer impact	1	19.41	19.53	19.53	19.53	19.78	19.78	20.02	19.90
	2	19.53	19.29	19.53	19.53	20.14	20.14	20.26	20.02
	3	19.29	19.41	19.53	19.53	20.14	20.14	19.53	19.90
	Average	19.41		19.53		20.02		19.94	
Heel drop impact	1	21.12	21.12	21.61	21.48	21.12	21.24	21.00	21.24
	2	21.48	21.36	21.85	21.61	21.48	21.48	21.48	21.36
	3	21.36	21.48	21.48	21.24	21.36	21.00	21.36	21.00
	Average	21.32		21.55		21.28		21.24	
	Impact location	Center of the specimen							
	Measurement location	C1		C2		E1		E2	
Sandbag drop impact	1	20.14		20.14		20.14		20.02	
	2	20.26		20.02		20.39		20.26	
	3	20.39		20.14		20.14		20.02	
	Average	20.18				20.16			

Specimen #17									
	Impact location	A		B		A		B	
	Measurement location	C1	C2	C1	C2	E1	E2	E1	E2
Hammer impact	1	22.46	22.46	22.46	22.46	19.41	22.83	19.41	19.41
	2	22.46	22.46	22.46	22.46	22.83	19.29	19.53	19.53
	3	22.34	22.22	22.58	22.58	19.53	19.65	19.53	19.53
	Average	22.40		22.50		20.59		19.49	
Heel drop impact	1	21.97	20.14	22.34	22.34	20.02	20.39	21.00	21.00
	2	20.51	19.29	22.71	22.71	20.39	20.39	22.95	19.65
	3	20.39	20.75	22.58	22.58	20.63	20.51	22.83	20.02
	Average	20.51		22.54		20.39		21.24	
	Impact location	Center of the specimen							
	Measurement location	C1		C2		E1		E2	
Sandbag drop impact	1	21.36		21.12		21.97		19.17*	
	2	21.48		21.12		22.10		19.04*	
	3	21.61		21.36		22.10		19.17*	
	Average	21.34				22.05			

Specimen #18										
	Impact location	A		B		A		B		
	Measurement location	C1	C2	C1	C2	E1	E2	E1	E2
Hammer impact	1	21.97	21.97	21.97	21.97	21.97	21.97	21.97	21.97
	2	21.97	21.97	21.97	21.97	21.97	21.97	21.97	21.97
	3	21.97	21.97	21.97	21.97	21.97	21.97	21.97	21.97
	Average	21.97		21.97		21.97		21.97	
Heel drop impact	1	22.58	22.58	22.58	22.46	22.46	22.46	22.34	22.22
	2	22.46	22.46	22.46	22.46	22.46	22.58	22.46	22.58
	3	22.58	22.71	22.46	22.46	22.58	22.71	22.46	22.34
	Average	22.56		22.48		22.54		22.40	
	Impact location	Center of the specimen							
	Measurement location	C1		C2		E1		E2	
Sandbag drop impact	1	21.48		21.48		21.36		21.36	
	2	21.48		21.48		21.48		21.48	
	3	21.48		21.48		21.48		21.48	
	Average	21.48				21.44			

Specimen #19									
	Impact location	A		B		A		B	
	Measurement location	C1	C2	C1	C2	E1	E2	E1	E2
Hammer impact	1	20.02	20.02	20.02	20.02	20.14	20.14	20.14	20.14
	2	20.02	20.02	20.02	20.02	20.14	20.14	20.14	20.14
	3	20.02	20.02	20.02	20.02	20.14	20.14	20.14	20.14
	Average	20.02		20.02		20.14		20.14	
Heel drop impact	1	19.78	19.65	19.04	18.92	19.29	19.29	18.56	18.56
	2	19.90	20.02	18.80	19.04	19.29	19.65	18.43	18.31
	3	19.90	19.90	19.65	19.04	19.78	19.29	18.43	18.07
	Average	19.86		19.08		19.43		18.39	
	Impact location	Center of the specimen							
	Measurement location	C1		C2		E1		E2	
Sandbag drop impact	1	19.17		19.04		19.29		19.29	
	2	19.04		19.04		19.29		19.04	
	3	19.17		19.04		19.04		19.04	
	Average	19.08				19.17			

Specimen #20										
	Impact location	A		B		A		B		
	Measurement location	C1	C2	C1	C2	E1	E2	E1	E2
Hammer impact	1	20.51	20.51	20.51	20.63	21.00	21.24	21.00	21.00
	2	20.51	20.63	20.51	20.63	21.00	21.24	20.75	20.87
	3	20.51	20.63	20.63	20.63	20.87	20.87	21.00	21.00
	Average	20.55		20.59		21.04		20.94	
Heel drop impact	1	20.26	20.39	21.48	20.63	20.51	20.63	20.51	20.02
	2	20.26	20.51	21.00	21.12	21.00	21.24	20.63	20.63
	3	20.51	20.75	20.75	20.87	20.75	20.63	20.75	20.39
	Average	20.45		20.98		20.79		20.49	
	Impact location	Center of the specimen							
	Measurement location	C1		C2		E1		E2	
Sandbag drop impact	1	19.53		19.78		19.90		20.02	
	2	19.90		19.90		19.78		20.26	
	3	19.53		19.65		20.02		20.02	
	Average	19.71				20.00			

Table A-9 Predicted and tested fundamental frequency (Hz) of box specimens consisting of cross laminated plates.

Specimen #		AC	BC	AE	BE	ACH	BCH	AEH	BEH	SC	SE	Average
1	Predicted	23.04										
	Tested	24.39	24.41	24.68	24.66	25.35	25.51	25.31	25.39	23.78	23.36	24.68
	Error (%)	-5.55	-5.62	-6.63	-6.56	-9.11	-9.69	-8.96	-9.26	-3.12	-1.35	-6.66
2	Predicted	23.52										
	Tested	22.07	22.10	22.14	22.20	23.19	23.52	23.36	25.35	22.71	22.81	22.94
	Error (%)	6.55	6.45	6.25	5.96	1.41	0.01	0.70	-7.22	3.59	3.13	2.51
3	Predicted	23.63										
	Tested	23.15	23.13	23.03	23.32	22.75	21.28	22.91	21.61	20.79	21.12	22.31
	Error (%)	2.07	2.16	2.61	1.36	3.89	11.04	3.15	9.37	13.65	11.90	5.93
4	Predicted	23.38										
	Tested	21.26	22.07	21.61	21.87	21.77	22.30	21.77	21.14	20.39	20.14	21.43
	Error (%)	9.95	5.90	8.19	6.88	7.38	4.83	7.38	10.58	14.67	16.06	9.07
5	Predicted	24.03										
	Tested	23.05	23.15	22.95	22.95	23.89	23.84	23.84	23.32	21.75	22.05	23.08
	Error (%)	4.26	3.80	4.72	4.72	0.62	0.79	0.79	3.08	10.50	8.97	4.13

Table A-10 Predicted and tested fundamental frequency (Hz) of box specimens consisting of parallel laminated plates.

Specimen #		AC	BC	AE	BE	ACH	BCH	AEH	BEH	SC	SE	Average
6	Predicted	24.05										
	Tested	22.85	22.83	23.07	23.09	24.54	25.55	24.86	25.33	22.24	21.97	23.63
	Error (%)	5.26	5.35	4.23	4.14	-1.99	-5.89	-3.27	-5.06	8.14	9.44	1.76
7	Predicted	24.35										
	Tested	19.55	19.65	19.67	19.65	20.87	21.48	20.14	22.01	18.96	18.86	20.09
	Error (%)	24.56	23.91	23.79	23.91	16.67	13.35	20.91	10.63	28.43	29.13	21.24
8	Predicted	24.60										
	Tested	26.39	26.55	26.69	26.81	22.71	22.10	23.13	22.05	21.87	21.12	23.94
	Error (%)	-6.76	-7.33	-7.82	-8.24	8.36	11.36	6.36	11.56	12.50	16.51	2.77
9	Predicted	23.86										
	Tested	22.58	22.71	22.60	22.75	24.56	22.64	24.50	22.60	22.07	21.85	22.89
	Error (%)	5.66	5.10	5.57	4.91	-2.83	5.38	-2.59	5.57	8.10	9.20	4.26
10	Predicted	24.57										
	Tested	23.60	23.64	23.68	23.66	23.66	22.81	24.29	24.25	22.71	22.50	23.48
	Error (%)	4.10	3.92	3.74	3.83	3.83	7.72	1.14	1.31	8.21	9.18	4.63

Table A-11 Predicted and tested fundamental frequency (Hz) of box specimens consisting of cross laminated plates with OSB facing.

Specimen #		AC	BC	AE	BE	ACH	BCH	AEH	BEH	SC	SE	Average
11	Predicted	19.91										
	Tested	21.32	21.32	21.63	21.52	22.05	21.79	21.95	21.65	19.35	19.47	21.21
	Error (%)	-6.63	-6.63	-7.95	-7.51	-9.73	-8.64	-9.30	-8.03	2.89	2.25	-6.12
12	Predicted	19.62										
	Tested	20.02	19.96	20.22	20.20	21.87	20.12	22.42	19.27	19.39	19.73	20.32
	Error (%)	-2.00	-1.70	-2.98	-2.89	-10.29	-2.49	-12.49	1.83	1.19	-0.58	-3.45
13	Predicted	19.89										
	Tested	21.65	21.91	22.01	22.03	21.26	20.91	21.61	20.20	19.67	20.43	21.17
	Error (%)	-8.13	-9.24	-9.66	-9.74	-6.45	-4.91	-7.95	-1.56	1.09	-2.64	-6.05
14	Predicted	20.07										
	Tested	22.18	22.22	22.54	22.38	21.89	20.96	22.46	21.16	21.10	21.34	21.82
	Error (%)	-9.49	-9.66	-10.96	-10.32	-8.31	-4.22	-10.64	-5.14	-4.87	-5.96	-8.02
15	Predicted	19.91										
	Tested	20.71	20.75	20.85	20.85	20.22	20.18	19.90	19.21	19.82	20.12	20.26
	Error (%)	-3.88	-4.07	-4.53	-4.53	-1.56	-1.36	0.05	3.6669	0.46	-1.06	-1.7574

Table A-12 Predicted and tested fundamental frequency (Hz) of box specimens consisting of 45° laminated plates.

Specimen #		AC	BC	AE	BE	ACH	BCH	AEH	BEH	SC	SE	Average
16	Predicted	24.67										
	Tested	24.41	24.15	24.23	24.29	21.73	22.40	21.09	22.28	22.54	22.34	22.95
	Error (%)	1.06	2.17	1.82	1.57	13.55	10.15	16.97	10.75	9.45	10.45	7.52
17	Predicted	24.73										
	Tested	22.71	22.68	24.72	24.74	24.29	24.41	23.93	24.43	22.40	22.81	23.71
	Error (%)	8.92	9.02	0.05	-0.03	1.81	1.30	3.36	1.21	10.41	8.44	4.30
18	Predicted	24.18										
	Tested	24.17	24.17	23.76	23.80	24.56	24.39	24.56	24.23	23.05	22.77	23.95
	Error (%)	0.05	0.05	1.76	1.59	-1.52	-0.87	-1.52	-0.20	4.91	6.22	0.99
19	Predicted	23.98										
	Tested	21.63	21.50	21.57	21.59	20.98	21.48	21.59	20.45	20.53	20.83	21.21
	Error (%)	10.90	11.53	11.21	11.11	14.34	11.63	11.10	17.29	16.83	15.12	13.05
20	Predicted	24.28										
	Tested	21.38	21.24	20.94	20.89	22.68	22.60	22.30	22.26	19.86	19.84	21.40
	Error (%)	13.57	14.33	15.99	16.22	7.05	7.43	8.90	9.10	22.29	22.42	13.48

Table A-13 Predicted and tested fundamental frequency (Hz) of box specimens consisting of cross laminated plates under simulated occupant load.

Specimen #		AC	BC	AE	BE	ACH	BCH	AEH	BEH	SC	SE	Average
	Predicted						19.46					
1	Tested	19.08	19.14	19.08	19.25	19.29	18.98	19.43	18.92	18.80	19.12	19.11
	Error (%)	1.95	1.62	1.95	1.08	0.87	2.49	0.13	2.82	3.49	1.73	1.80
	Predicted						19.85					
2	Tested	18.56	18.56	18.58	18.66	18.37	18.07	18.53	18.74	18.01	18.27	18.43
	Error (%)	6.96	6.96	6.84	6.37	8.03	9.85	7.08	5.91	10.22	8.63	7.67
	Predicted						19.94					
3	Tested	19.53	19.49	19.71	19.94	18.83	18.96	19.04	19.37	20.18	20.06	19.51
	Error (%)	2.07	2.29	1.12	-0.01	5.88	5.14	4.69	2.93	-1.22	-0.62	2.17
	Predicted						19.65					
4	Tested	19.57	19.59	19.61	19.57	19.33	19.71	19.31	19.45	17.76	18.05	19.20
	Error (%)	0.41	0.31	0.20	0.41	1.68	-0.32	1.79	1.04	10.65	8.90	2.38
	Predicted						20.10					
5	Tested	20.63	20.77	20.83	20.89	19.49	20.55	20.63	20.42	18.60	18.72	20.15
	Error (%)	-2.57	-3.24	-3.52	-3.80	3.13	-2.18	-2.57	-1.55	8.09	7.39	-0.26

Table A-14 Predicted and tested fundamental frequency (Hz) of box specimens consisting of parallel laminated plates under simulated occupant load.

Specimen #		AC	BC	AE	BE	ACH	BCH	AEH	BEH	SC	SE	Average
	Predicted						20.30					
6	Tested	22.01	22.10	22.10	22.22	21.93	22.38	21.91	22.44	20.91	20.94	21.89
	Error (%)	-7.79	-8.13	-8.13	-8.63	-7.45	-9.30	-7.36	-9.54	-2.94	-3.04	-7.28
	Predicted						20.60					
7	Tested	19.27	19.41	19.25	19.37	19.41	20.08	19.08	20.47	18.78	18.66	19.38
	Error (%)	6.93	6.15	7.04	6.37	6.15	2.60	7.96	0.66	9.71	10.43	6.32
	Predicted						20.67					
8	Tested	21.44	21.67	21.55	21.77	21.20	21.63	21.08	20.87	20.14	20.22	21.16
	Error (%)	-3.63	-4.62	-4.08	-5.07	-2.52	-4.44	-1.95	-1.00	2.60	2.19	-2.32
	Predicted						20.17					
9	Tested	21.95	21.93	22.18	22.34	22.83	22.36	22.12	22.01	21.38	21.42	22.05
	Error (%)	-8.04	-8.06	-9.07	-9.73	-11.66	-9.81	-8.82	-8.40	-5.69	-5.87	-8.56
	Predicted						20.70					
10	Tested	21.44	21.48	21.61	21.63	21.65	21.89	21.52	21.67	20.77	20.91	21.46
	Error (%)	-3.48	-3.66	-4.21	-4.30	-4.39	-5.46	-3.85	-4.48	-0.36	-1.04	-3.55

Table A-15 Predicted and tested fundamental frequency (Hz) of box specimens consisting of cross laminated plates with OSB facing under simulated occupant load.

Specimen #		AC	BC	AE	BE	ACH	BCH	AEH	BEH	SC	SE	Average
	Predicted						17.33					
11	Tested	19.90	19.90	20.00	19.88	19.92	20.00	20.18	19.80	17.80	18.23	19.56
	Error (%)	-12.89	-12.89	-13.33	-12.80	-12.98	-13.33	-14.12	-12.44	-2.63	-4.92	-11.38
	Predicted						17.07					
12	Tested	19.39	19.47	19.65	19.61	20.77	18.07	19.84	18.17	18.37	19.37	19.27
	Error (%)	-11.98	-12.35	-13.16	-12.98	-17.84	-5.54	-13.97	-6.07	-7.11	-11.89	-11.44
	Predicted						17.27					
13	Tested	20.12	20.22	20.28	20.20	19.71	19.73	20.30	20.04	19.14	19.29	19.91
	Error (%)	-14.15	-14.58	-14.84	-14.50	-12.38	-12.47	-14.93	-13.80	-9.77	-10.44	-13.22
	Predicted						17.43					
14	Tested	20.49	20.51	20.61	20.57	19.61	19.59	19.43	19.49	19.24	18.82	19.84
	Error (%)	-14.94	-15.03	-15.45	-15.28	-11.15	-11.06	-10.31	-10.59	-9.42	-7.40	-12.15
	Predicted						17.31					
15	Tested	18.80	18.82	18.84	18.78	18.76	18.53	18.45	18.33	17.56	17.90	18.48
	Error (%)	-7.92	-8.02	-8.12	-7.82	-7.72	-6.61	-6.19	-5.57	-1.41	-3.32	-6.32

Table A-16 Predicted and tested fundamental frequency (Hz) of box specimens consisting of 45^{o} laminated plates under simulated occupant load.

Specimen #		AC	BC	AE	BE	ACH	BCH	AEH	BEH	SC	SE	Average
	Predicted						20.95					
16	Tested	19.41	19.53	20.02	19.94	21.32	21.55	21.28	21.24	20.18	20.16	20.46
	Error (%)	9.76	9.07	6.41	6.85	-0.09	-1.12	0.10	0.30	5.55	5.66	4.10
	Predicted						21.36					
17	Tested	22.40	22.50	20.59	19.49	20.51	22.54	20.39	21.24	21.34	22.05	21.31
	Error (%)	-4.64	-5.07	3.74	9.59	4.15	-5.24	4.78	0.56	0.09	-3.15	0.26
	Predicted						20.86					
18	Tested	21.97	21.97	21.97	21.97	22.56	22.48	22.54	22.40	21.48	21.44	22.08
	Error (%)	-5.05	-5.05	-5.05	-5.05	-7.53	-7.20	-7.45	-6.86	-2.89	-2.71	-5.51
	Predicted						20.62					
19	Tested	20.02	20.02	20.14	20.14	19.86	19.08	19.43	18.39	19.08	19.17	19.53
	Error (%)	3.01	3.01	2.38	2.38	3.86	8.06	6.14	12.12	8.06	7.60	5.57
	Predicted						20.91					
20	Tested	20.55	20.59	21.04	20.94	20.45	20.98	20.79	20.49	19.71	20.00	20.55
	Error (%)	1.75	1.55	-0.61	-0.13	2.25	-0.32	0.55	2.05	6.06	4.54	1.73